Mathematical Problems in Engineering

New Challenges in Fractional Systems 2014

Guest Editors: Guido Maione, Raoul R. Nigmatullin, José A. Tenreiro Machado, and Jocelyn Sabatier

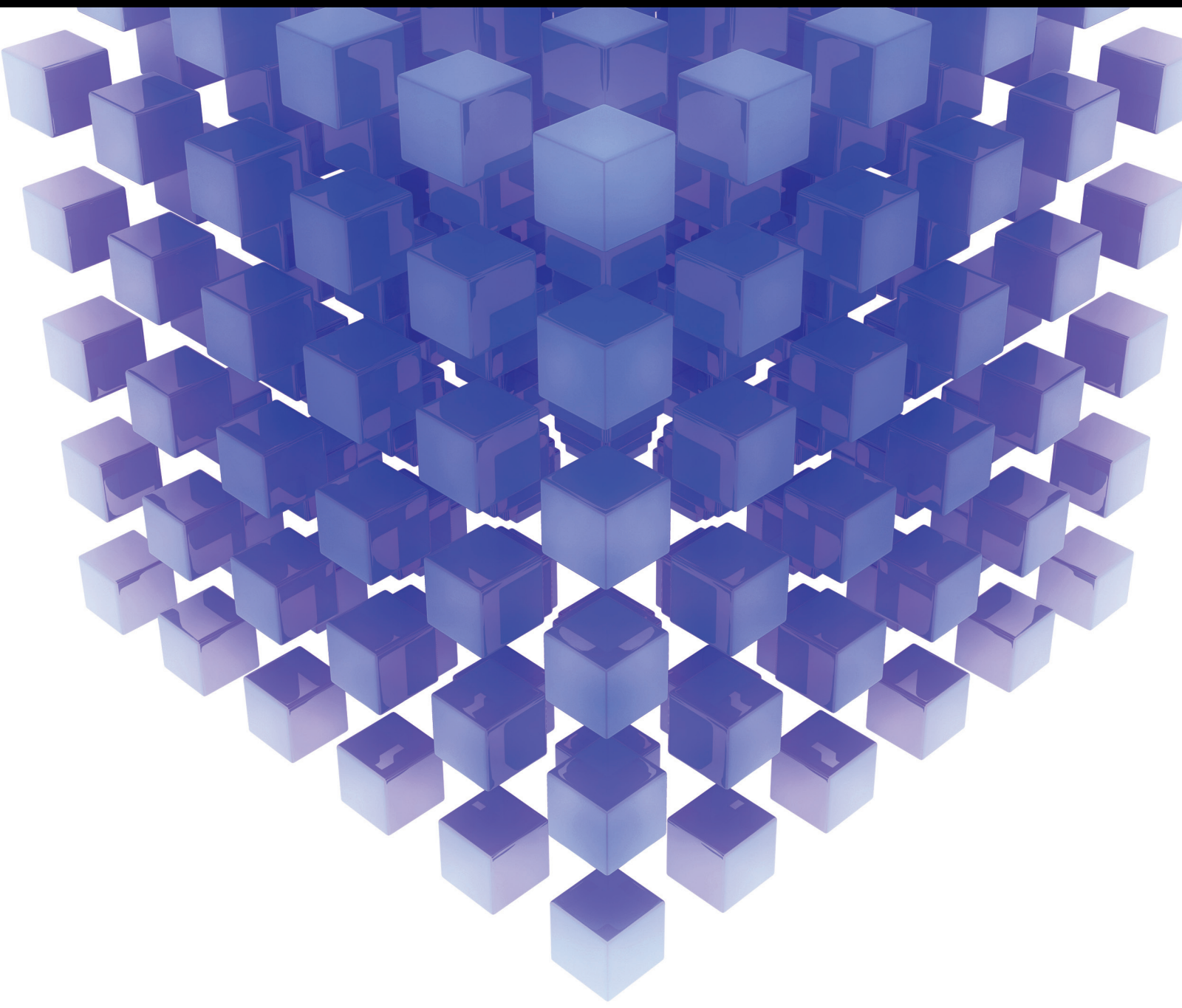

New Challenges in Fractional Systems 2014

Mathematical Problems in Engineering

New Challenges in Fractional Systems 2014

Guest Editors: Guido Maione, Raoul R. Nigmatullin, José A. Tenreiro Machado, and Jocelyn Sabatier

Copyright © 2015 Hindawi Publishing Corporation. All rights reserved.

This is a special issue published in "Mathematical Problems in Engineering." All articles are open access articles distributed under the Creative Commons Attribution License, which permits unrestricted use, distribution, and reproduction in any medium, provided the original work is properly cited.

Editorial Board

Mohamed Abd El Aziz, Egypt
Silvia Abrahão, Spain
Ramesh Agarwal, USA
Juan C. Agüero, Australia
Ricardo Aguilar-López, Mexico
Tarek Ahmed-Ali, France
Hamid Akbarzadeh, Canada
Muhammad N. Akram, Norway
Salvatore Alfonzetti, Italy
Tofigh Allahviranloo, Iran
Christian B. Allen, UK
Lionel Amodeo, France
Igor Andrianov, Germany
Sebastian Anita, Romania
Felice Arena, Italy
Sabri Arik, Turkey
Fumihiro Ashida, Japan
Seungik Baek, USA
Ezzat G. Bakhoum, USA
Laurent Bako, France
Stefan Balint, Romania
José M. Balthazar, Brazil
Alfonso Banos, Spain
Roberto Baratti, Italy
Abdel-Hakim Bendada, Canada
Rasajit K. Bera, India
Simone Bianco, Italy
Jonathan N. Blakely, USA
Daniela Boso, Italy
Taha Boukhobza, France
Francesco Braghin, Italy
Reyolando M. Brasil, Brazil
Michael J. Brennan, UK
Javier Buldufh, Spain
Salvatore Caddemi, Italy
Jose E. Capilla, Spain
Carlo Cattani, Italy
Marcelo M. Cavalcanti, Brazil
Mohammed Chadli, France
Shuenn-Yih Chang, Taiwan
Ching-Ter Chang, Taiwan
Michael J. Chappell, UK
Kacem Chehdi, France
Kui Fu Chen, China
Xinkai Chen, Japan
Jianbing Chen, China
Xuefeng Chen, China
Chunlin Chen, China
Zhang Chen, China
Singa W. Chiu, Taiwan
Jyh-Hong Chou, Taiwan
Slim Choura, Tunisia
Hung-Yuan Chung, Taiwan
Marcelo J. Colao, Brazil
Carlo Cosentino, Italy
Erik Cuevas, Mexico
Weizhong Dai, USA
Binxiang Dai, China
Purushothaman Damodaran, USA
Farhang Daneshmand, Canada
Swagatam Das, India
Fabio De Angelis, Italy
Filippo de Monte, Italy
Yannis Dimakopoulos, Greece
Baocang Ding, China
Zhengtao Ding, UK
Mohamed Djemai, France
Joao B. R. Do Val, Brazil
Alexandre B. Dolgui, France
Rodrigo W. dos Santos, Brazil
Alexander N. Dudin, Belarus
George S. Dulikravich, USA
Horst Ecker, Austria
Mehmet Onder Efe, Turkey
Karen Egiazarian, Finland
Elmetwally Elabbasy, Egypt
Alex E.-Zúñiga, Mexico
Fouad Erchiqui, Canada
Anders Eriksson, Sweden
Vedat S. Erturk, Turkey
Hua Fan, China
Ricardo Femat, Mexico
Jose R. Fernandez, Spain
Thierry Floquet, France
George Flowers, USA
Tomonari Furukawa, USA
Zoran Gajic, USA
Ugo Galvanetto, Italy
Xin-Lin Gao, USA
Zhong-Ke Gao, China
Laura Gardini, Italy
Alessandro Gasparetto, Italy
Oleg V. Gendelman, Israel
Paulo Batista Gonalves, Brazil
Rama S. R. Gorla, USA
Oded Gottlieb, Israel
Quang Phuc Ha, Australia
Masoud Hajarian, Iran
Zhen-Lai Han, China
Thomas Hanne, Switzerland
Xiao-Qiao He, China
Katica R. Hedrih, Serbia
M. Isabel Herreros, Spain
Wei-Chiang Hong, Taiwan
Jaromir Horacek, Czech Republic
Muneo Hori, Japan
Feng-Hsiag Hsiao, Taiwan
Fu-Shiung Hsieh, Taiwan
Changchun Hua, China
Zhenkun Huang, China
Chiung-Shiann Huang, Taiwan
Chuangxia Huang, China
Gordon Huang, Canada
Huabing Huang, China
Hai-Feng Huo, China
Asier Ibeas, Spain
Giacomo Innocenti, Italy
Nazrul Islam, USA
Reza Jazar, Australia
Khalide Jbilou, France
Linni Jian, China
Bin Jiang, China
Zhongping Jiang, USA
Jun Jiang, China
Jianjun Jiao, China
Ningde Jin, China
J. Joao Judice, Portugal
Tadeusz Kaczorek, Poland
T. Kalmar-Nagy, Hungary
T. Kapitaniak, Poland
Haranath Kar, India
C. Masood Khalique, South Africa
Do Wan Kim, Korea
Nam-Il Kim, Korea
Kyung Y. Kim, Republic of Korea

Manfred Krafczyk, Germany
V. Kravchenko, Mexico
Jurgen Kurths, Germany
Kyandoghere Kyamakya, Austria
Hak-Keung Lam, UK
Wen-Chiung Lee, Taiwan
Marek Lefik, Poland
Yaguo Lei, China
Valter J. S. Leite, Brazil
Stefano Lenci, Italy
Roman Lewandowski, Poland
Ming Li, China
Jian Li, China
Qing Q. Liang, Australia
Yan Liang, China
Teh-Lu Liao, Taiwan
Panos Liatsis, UK
Kim M. Liew, Hong Kong
Yi-Kuei Lin, Taiwan
Shueei M. Lin, Taiwan
Jui-Sheng Lin, Taiwan
Wanquan Liu, Australia
Yan-Jun Liu, China
Yuji Liu, China
Xian Liu, China
Peter Liu, Taiwan
Peide Liu, China
Paolo Lonetti, Italy
Vassilios C. Loukopoulos, Greece
Junguo Lu, China
Chien-Yu Lu, Taiwan
Jianquan Lu, China
Jinhu Lü, China
Tiedong Ma, China
Nazim I. Mahmudov, Turkey
Fazal M. Mahomed, South Africa
O. Daniel Makinde, South Africa
Didier Maquin, France
Rafael Martínez-Guerra, Mexico
Gefhrard A. Maugin, France
Driss Mehdi, France
Khaled Saad Mekheimer, Egypt
Roderick Melnik, Canada
Pasquale Memmolo, Italy
Xiangyu Meng, Canada
Xinzhu Meng, China
Jose Merodio, Spain
Y. V. Mikhlin, Ukraine
Hiroyuki Mino, Japan
Pablo Mira, Spain
Nenad Mladenovic, Serbia
Ebrahim Momoniat, South Africa
Gisele Mophou, France
Rafael M. Morales, Spain
Giuseppe Muscolino, Italy
N. Bhujappa Naduvinamani, India
Trung Nguyen-Thoi, Vietnam
Hung Nguyen-Xuan, Vietnam
Ben T. Nohara, Japan
Sotiris K. Ntouyas, Greece
Maxim A. Olshanskii, Russia
Alejandro Ortega-Moñux, Spain
Erika Ottaviano, Italy
Alkiviadis Paipetis, Greece
Alessandro Palmeri, UK
Bijaya Ketan Panigrahi, India
Manuel Pastor, Spain
Pubudu N. Pathirana, Australia
Francesco Pellicano, Italy
Mingshu Peng, China
Zhike Peng, China
Haipeng Peng, China
Matjaz Perc, Slovenia
Maria do Rosário Pinho, Portugal
José R. C. Piqueira, Brazil
Antonina Pirrotta, Italy
Javier Plaza, Spain
Stanislav Potapenko, Canada
Sergio Preidikman, USA
Carsten Proppe, Germany
Hector Puebla, Mexico
Yuming Qin, China
Dane Quinn, USA
Jose Ragot, France
K. Ramamani Rajagopal, USA
Sellakkutti Rajendran, Singapore
Gianluca Ranzi, Australia
Bhairavavajjula N. Rao, India
Sivaguru Ravindran, USA
Alessandro Reali, Italy
Giuseppe Rega, Italy
Ricardo Riaza, Spain
Gerasimos Rigatos, Greece
José Rodellar, Spain
Rosana Rodriguez-Lopez, Spain
Ignacio Rojas, Spain
Carla Roque, Portugal
Debasish Roy, India
Rubén Ruiz García, Spain
Antonio Ruiz-Cortes, Spain
Ivan D. Rukhlenko, Australia
Abbas Saadatmandi, Iran
Kishin Sadarangani, Spain
Mehrdad Saif, Canada
Roque J. Saltarén, Spain
Miguel A. F. Sanjuan, Spain
Juan F. San-Juan, Spain
Ilmar Ferreira Santos, Denmark
Nickolas S. Sapidis, Greece
Evangelos J. Sapountzakis, Greece
Themistoklis P. Sapsis, USA
Andrey V. Savkin, Australia
Valery Sbitnev, Russia
Massimo Scalia, Italy
Mohammed Seaid, UK
Mohamed A. Seddeek, Egypt
Mathieu Sellier, New Zealand
Leonid Shaikhet, Ukraine
Cheng Shao, China
Sanjay K. Sharma, India
Bo Shen, Germany
Zhan Shu, UK
Dan Simon, USA
Luciano Simoni, Italy
Christos H. Skiadas, Greece
Delfim Soares Jr., Brazil
Davide Spinello, Canada
Victor Sreeram, Australia
Sri Sridharan, USA
Hari M. Srivastava, Canada
Ivanka Stamova, USA
Rolf Stenberg, Finland
Yuangong Sun, China
Xi-Ming Sun, China
Jitao Sun, China
Zhongkui Sun, China
Andrzej Swierniak, Poland
Wai Yuen Szeto, Hong Kong
Yang Tang, Germany
Alexander Timokha, Norway
Cristian Toma, Romania
Francesco Tornabene, Italy
Antonio Tornambe, Italy
Irina N. Trendafilova, UK

Jung-Fa Tsai, Taiwan
Chia-Cheng Tsai, Taiwan
George Tsiatas, Greece
Efstratios Tzirtzilakis, Greece
Francesco Ubertini, Italy
Kuppalapalle Vajravelu, USA
Robertt A. Valente, Portugal
Alain Vande Wouwer, Belgium
Pandian Vasant, Malaysia
Josep Vehi, Spain
Kalyana C. Veluvolu, Korea
Georgios Veronis, USA
Michael Vynnycky, Ireland
Cheng C. Wang, Taiwan
Yijing Wang, China
Qing-Wen Wang, China
Junwu Wang, China
Shuming Wang, Singapore
Yan-Wu Wang, China
Youqing Wang, China
Yongqi Wang, Germany
Moran Wang, China
Gerhard-Wilhelm Weber, Turkey
Hung-Yu Wei, Taiwan
J. A. S. Witteveen, Netherlands
Kwok-Wo Wong, Hong Kong
Zheng-Guang Wu, China
Yuqiang Wu, China
Dash Desheng Wu, Canada
Huang Xia, China
Gongnan Xie, China
Xuejun Xie, China
Guangming Xie, China
Lianglin Xiong, China
Hang Xu, China
Gen Qi Xu, China
Jun-Juh Yan, Taiwan
Xinggang Yan, UK
Chunyu Yang, China
Dan Ye, China
Peng-Yeng Yin, Taiwan
Mohammad I. Younis, USA
Bo Yu, China
Simin Yu, China
Jianming Zhan, China
Hongbin Zhang, China
Xu Zhang, China
Huaguang Zhang, China
Hong Zhang, China
Qingling Zhang, China
Hongyong Zhao, China
Lu Zhen, China
Jian Guo Zhou, UK
Quanxin Zhu, China
Zexuan Zhu, China
Mustapha Zidi, France
Alessandro Zona, Italy

Contents

Editorial

New Challenges in Fractional Systems 2014

Guido Maione,[1] Raoul R. Nigmatullin,[2] José A. Tenreiro Machado,[3] and Jocelyn Sabatier[4]

[1]*Department of Electrical and Information Engineering (DEI), Technical University of Bari, Via E. Orabona 4, 70125 Bari, Italy*
[2]*Radio-Electronic and Information & Measuring Technology Department, Kazan National Research Technical University (KNRTU-KAI), Karl Marx Street 10, Kazan, Tatarstan 420111, Russia*
[3]*Department of Electrical Engineering, Institute of Engineering (ISEP), Polytechnic of Porto, Rua Dr. Antonio Bernardino de Almeida 431, 4200-072 Porto, Portugal*
[4]*IMS Laboratory, Bordeaux 1 University, 351 Cours de la Liberation, 33400 Talence, France*

Correspondence should be addressed to Guido Maione; guido.maione@poliba.it

Received 17 November 2014; Accepted 17 November 2014

Copyright © 2015 Guido Maione et al. This is an open access article distributed under the Creative Commons Attribution License, which permits unrestricted use, distribution, and reproduction in any medium, provided the original work is properly cited.

In many fields, theoretical and applied researches have strengthened the belief that fractional calculus is not only a branch of the mathematical analysis, but also a useful and powerful tool for engineers. Namely, fractional calculus allows both a better modeling of a wide class of systems with anomalous dynamic behavior and a better understanding of the facets of both physical phenomena and artificial processes. Hence the mathematical models derived from differential equations with noninteger/fractional order derivatives or integrals are becoming a fundamental research issue for scientists and engineers. In particular, fractional models are successful when describing power-law long-term memory or hereditary properties. They are also successful when anomalous diffusion, transport phenomena, and waves propagation in complex media require nonlocal operators, or when fractal-like properties are evident in some processes. These potentialities and the related benefits have attracted many experts and practitioners of different fields to reconsider mathematical models and engineering methods both for linear and for nonlinear systems.

To synthesize, many different areas of science and engineering invest on fractional order modeling and systems by now [1–7]. Moreover, in the last years, many researchers are becoming aware of the interdisciplinary aspects of complex engineering problems that require knowledge from different fields. At the same time, inspiration is often taken from theories or applications of different areas and sometimes it is necessary to combine scientific methodologies that are developed for different problems. To cite a recent example, achieving good results in delivering a high-quality multimedia service through wireless networks not only is a matter of advanced communication technologies and protocols, but also requires to build a proper transmission scheduler that employs classical or innovative control systems. Namely, a feedback control technique may schedule the transmission in advance [8, 9], but can also consider the fractional nature of the data traffic [10] and the fractional modeling of the streams [11].

The above remarks justify the interest in fractional modeling and fractional order systems that may represent a communication language to integrate expertise, results, and new ideas of researchers coming from different areas. The consequences could have a great impact on everyday life, services, technology, industrial processes, and environmental issues. However, fractional calculus and fractional order systems are not a panacea. Namely, many potentialities of fractional order systems are still unexplored or under investigation so that there are many challenges. The contributions gathered in this special issue offer a snapshot of different interesting researches, problems, and solutions.

In detail, the papers of this special issue cover topics in the fields of control systems, electric circuits, and image and signal processing, concern some aspects of mathematical modeling for biological and physical phenomena, and consider some applications of numerical and computational methods to engineering and finance. In the following, we briefly highlight these topics and synthesize the content of each paper.

The paper "*Fractional dynamics of computer virus propagation*," by C. M. A. Pinto and J. A. Tenreiro Machado, introduces a fractional order model to describe the propagation and spread of computer viruses due to dynamical interactions between computing and removable devices. The fractional order system is inspired by mathematical models for biological epidemics and extends an integer order model taken from the literature by using fractional order differentiation. Numerical results show that fractional modeling can serve to describe and capture very fast dynamics or long-term memory effects that cannot be represented by classical integer order models. The investigation is therefore interesting for antivirus development and for studying effective protective measures for applications based on internet connections that are exposed to computer viruses.

The paper "*On fractional order dengue epidemic model*," by H. Al-Sulamia et al., applies fractional calculus to model the spread of the tropical fever and considers memory effects. The model is very sensitive to the fractional order of differentiation. Moreover, the authors study the stability of the equilibrium points of the fractional order system describing the epidemic model. Numerical simulation of the fractional order system is based on the generalized Adams-Bashforth-Moulton method that provides an approximate solution, which converges to the fixed point after a longer time than with an integer order model.

The paper "*Algorithms of finite difference for pricing american options under fractional diffusion models*," by J. Xi et al., regards the application of fractional calculus tools to a financial topic, namely, developing accurate and effective algorithms for the price of American options. The authors start from fractional order partial differential equations used under fractional diffusion models to develop a first-order approximation. This is obtained by an iterative algorithm that avoids singularities in the integral part of partial integrodifferential equations and computes the numerical estimates by combining a fractional difference approach and a penalty method. Then the authors employ a spatial extrapolation for a second-order accurate estimate. The numerical results in the paper are intended to show the effectiveness and feasibility of the approach.

The paper "*Adaptive sliding control for a class of fractional commensurate order chaotic systems*," by J. Yuan and B. Shi, is in the framework of control methodologies developed for nonlinear fractional dynamic systems. The authors take advantage of fractional calculus tools and nonlinear control theory. They propose adaptive sliding mode control design for a class of commensurate fractional order chaotic systems. The authors first introduce a fractional integral sliding manifold for the nominal systems. Next, they prove the stability of the corresponding fractional sliding dynamics. Then, they obtain the desired sliding control law by using a Lyapunov candidate function and the Mittag-Leffler stability theory. The proposed sliding manifold is also adapted by a fractional adaptation law for perturbed systems because of uncertainties and external disturbances. Simulation tests are provided to show the performance of the designed controllers.

The paper "*Approximated fractional-order chebyshev lowpass filters*," by T. Freeborn et al., is in the field of research studies devoted to design of fractional order filters for analog signal processing. The authors use a nonlinear least squares optimization method to determine the coefficients of the fractional order transfer function that approximates the passband ripple characteristics of traditional Chebyshev lowpass filters. Matlab and SPICE simulation tests are used to verify the implementation of the fractional order filters.

The paper "*Computational challenge of fractional differential equations and the potential solutions: a survey*," by C. Gong et al., surveys computational costs of numerical methods to solve fractional differential equations. The authors analyze the computational complexity to solve time fractional, space fractional, and space-time fractional equations, with respect to the case of integer order partial differential equations solved by finite difference methods. The investigation aims at giving a useful guide for solving problems that are mathematically represented by complex fractional differential equations, also with variable fractional orders, and then requires numerical techniques with many time steps and many space grid points.

The paper "*On a time-fractional integrodifferential equation via three-point boundary value conditions*," by D. Baleanu et al., considers fractional differential equations useful to model physical processes that exhibit a fractional order behavior that varies with time and space. The complex, nonlinear fractional differential equations can be solved numerically but it is important to prove existence and uniqueness of the solution. To this aim, the authors investigate and prove the existence of solutions for a time-fractional integrodifferential equation via three-point boundary value conditions.

The paper "*Hybrid prediction and fractal hyperspectral image compression*," by S. Zhu et al., presents a method for hyperspectral image compression based on the combination of a prediction and a modified fractal coding technique. Hyperspectral images are important in remote sensing applications. The key point is to take advantage of the local self-similarity that exist between adjacent bands in the considered images to obtain a high compression ratio at low bitrate, resolution independence, and a fast decoding speed. The authors implement a hybrid algorithm that first carries out an intraband prediction and then applies an interband fractal encoding. The authors show the reduced encoding complexity, enhanced decoding quality, and higher peak signal-to-noise performance.

The paper "*A novel high efficiency fractal multiview video codec*," by S. Zhu et al., proposes a fractal multiview video codec for compressing three-dimensional video signals. The contribution can be considered in the context of research efforts devoted to improving transmission and reproduction of high-quality multimedia over broadband communication channels, for example, wireless networks of last generation. These processes are very important in streaming, videoconferencing, interactive videos, and other similar applications in delivery of multimedia digital services. In particular, the authors propose a compression algorithm that exploits temporal and spatial correlations and a disparity estimation to increase the codec efficiency for encoding and/or decoding a digital data stream or signal. Improvements are shown

in encoding performance (lower time and bitrate, higher compression ratio) and in quality of decoding.

Guido Maione
José A. Tenreiro Machado
Raoul R. Nigmatullin
Jocelyn Sabatier

References

[1] R. Caponetto, G. Dongola, L. Fortuna, and I. Petráš, *Fractional Order Systems: Modeling and Control Application*, vol. 72 of *World Scientific Series on Nonlinear Science Series A*, World Scientific Publishing, Singapore, 2010.

[2] R. Hilfer, *Applications of Fractional Calculus in Physics*, Academic Press, Orlando, Fla, USA, 1999.

[3] F. Mainardi, *Fractional Calculus and Waves in Linear Viscoelasticity: An Introduction to Mathematical Models*, Imperial College Press, London, UK, 2010.

[4] C. A. Monje, Y. Q. Chen, B. M. Vinagre, D. Xue, and V. Feliu, *Fractional-Order Systems and Controls: Fundamentals and Applications*, Springer, London, UK, 2010.

[5] I. Podlubny, *Fractional Differential Equations. An Introduction to Fractional Derivatives, Fractional Differential Equations, Some Methods of Their Solution and Some of Their Applications*, vol. 198 of *Mathematics in Science and Engineering*, Academic Press, San Diego, Calif, USA, 1999.

[6] J. Sabatier, O. P. Agrawal, and J. A. Tenreiro Machado, *Advances in Fractional Calculus: Theoretical Developments and Applications in Physics and Engineering*, Springer, 2007.

[7] S. G. Samko, A. A. Kilbas, and O. I. Marichev, *Fractional Integrals and Derivatives: Theory and Applications*, Gordon and Breach Science, Amsterdam, The Netherlands, 1993.

[8] C. Ceglie, G. Maione, and D. Striccoli, "Periodic feedback control for streaming 3D videos in last-generation cellular networks," in *Proceedings of the 5th IFAC International Workshop on Periodic Control Systems (PSYCO '13)*, F. Giri and V. van Assche, Eds., vol. 5, part 1, pp. 23–28, IFAC Proceedings Online, Caen, France, July 2013.

[9] G. Maione and D. Striccoli, "Transmission control of Variable-Bit-Rate video streaming in UMTS networks," *Control Engineering Practice*, vol. 20, no. 12, pp. 1366–1373, 2012.

[10] C. Ceglie, G. Maione, and D. Striccoli, "Statistical analysis of long-range dependence in three-dimensional video traffic," in *Proceedings of the Mathematical Methods in Engineering International Conference (MME '13)*, Porto, Portugal, July 2013.

[11] R. R. Nigmatullin, C. Ceglie, G. Maione, and D. Striccoli, "Reduced fractional modeling of 3-D video streams: the FERMA approach," *Nonlinear Dynamics*, 2014.

Research Article

Adaptive Sliding Control for a Class of Fractional Commensurate Order Chaotic Systems

Jian Yuan,[1] Bao Shi,[1] and Zhentao Yu[2]

[1]*Institute of System Science and Mathematics, Naval Aeronautical and Astronautical University, Yantai 264001, China*
[2]*Department of Navigation, Naval Submarine Academy, Qingdao 266001, China*

Correspondence should be addressed to Jian Yuan; yuanjianscar@gmail.com

Received 13 June 2014; Accepted 22 September 2014

Academic Editor: Jocelyn Sabatier

Copyright © 2015 Jian Yuan et al. This is an open access article distributed under the Creative Commons Attribution License, which permits unrestricted use, distribution, and reproduction in any medium, provided the original work is properly cited.

This paper proposes adaptive sliding mode control design for a class of fractional commensurate order chaotic systems. We firstly introduce a fractional integral sliding manifold for the nominal systems. Secondly we prove the stability of the corresponding fractional sliding dynamics. Then, by introducing a Lyapunov candidate function and using the Mittag-Leffler stability theory we derive the desired sliding control law. Furthermore, we prove that the proposed sliding manifold is also adapted for the fractional systems in the presence of uncertainties and external disturbances. At last, we design a fractional adaptation law for the perturbed fractional systems. To verify the viability and efficiency of the proposed fractional controllers, numerical simulations of fractional Lorenz's system and Chen's system are presented.

1. Introduction

In recent years, fractional calculus has attracted an increasing interest not only among mathematicians, but also among physicists and engineers. Fractional calculus is a generalization of the traditional integer order integration and differentiation to arbitrary noninteger (real or complex) order. In comparison with classical calculus, fractional-order derivatives and integrals provide more accurate modeling of dynamical systems possessing memory and hereditary properties [1, 2]. Various fractional dynamic models have been developed in rheology, viscoelasticity, electrochemistry, electromagnetism, and so forth [3].

To propose more efficient control design for fractional dynamic systems, fractional control provides a suitable way [2]. Fractional control has attracted interest in the control community since the first fractional controller, the CRONE controller, has been introduced and applied in various fields of control systems [4]. Other pioneering contributions on fractional control methodologies have been made, such as the TID controller, the fractional $PI^{\lambda}D^{\mu}$ controller [5], and the fractional lead-lag compensator [6]. Basic ideas and comparisons between the above four fractional control schemes have been addressed in [7]. More recently, several control methodologies for nonlinear fractional dynamic systems have been developed by combining fractional calculus and nonlinear control theory, such as the fractional sliding control [8–10], the fractional adaptive control [11–13], and the fractional optimal control [1, 14–16].

The works on fractional control go hand in hand with the stability of fractional differential equations (FDEs) and rely largely on their results [17]. Broad surveys in the stability issue involving fractional dynamic systems have been published. A complete and systematic picture of the state of the art in the stability of FDEs is provided in [18]. This review article covers the stability results in linear FDEs, nonlinear FDEs, and time delayed FDEs. There are two most important approaches to analyze the stability of nonlinear FDEs: one is to use the frequent distributed fractional integrator model [19], and the other is to use the Mittag-Leffler stability theorem [20]. The first approach relies on the concept of a fractional integration operator characterized by a continuous frequency distributed model. It involves two steps: firstly converting FDEs into exactly equivalent infinite dimensional ODEs, secondly applying the traditional indirect Lyapunov approach. Utilizing this approach, the stability of sliding

dynamics and a fractional sliding control law for a novel class of fractional chaotic systems have been investigated in [21]. The stability and tracking convergence of fractional model reference adaptive control systems are analyzed in [13].

Analyzing the stability of nonlinear FDEs by using the second approach is usually a complicated task, because it is difficult to calculate the fractional-order derivative of the commonly used Lyapunov candidate function. Fortunately, a new property for Caputo fractional derivative is obtained in [22], providing an easy way to derive an inequality for the fractional-order derivative of the Lyapunov candidate function in the quadratic form, instead of directly calculating its fractional-order derivative. So it is potentially a convenient way to propose the stability analysis for nonlinear FDEs.

In this paper, our main objective is to propose adaptive sliding control design for a class of commensurate fractional-order chaotic systems based on the newly discovered property of Caputo operator. For this end, we firstly introduce a fractional integral sliding manifold for these nominal systems. Next we prove the stability of the corresponding fractional sliding dynamics. Then, by introducing a quadratic Lyapunov control function and using the Mittag-Leffler stability theory we derive the desired control law. Furthermore, we prove that the proposed sliding manifold is also adapted for these fractional systems in the presence of uncertainties and external disturbances. At last, we investigate adaptive sliding control design for these perturbed systems.

The main contributions of this paper include the following: (1) a fractional integral sliding manifold is designed which is adapted not only for the nominal fractional systems but also for the perturbed systems; (2) the stability of the sliding dynamics corresponding to the nominal systems and the perturbed systems is proved; (3) a sliding control law and an adaptive law are designed, respectively, for the nominal systems and the perturbed systems.

The rest of the paper is organized as follows. Section 2 presents some basic definitions and theorems about fractional calculus and stability of fractional differential equations. Section 3 introduces a fractional integral sliding manifold and proposes the sliding control design for a class of nominal fractional-order chaotic systems. Section 4 investigates adaptive sliding control design for perturbed systems. In Section 5, numerical simulations of fractional Lorenz's system and Chen's system are presented to show the viability and efficiency of the proposed fractional controllers. Finally, the paper is concluded in Section 6.

2. Basic Definitions and Preliminaries

In this section we recall the definitions and several theorems in the fractional calculus. The most commonly used definitions of fractional derivatives are Grünwald-Letnikov, Riemann-Liouville, and Caputo definitions.

Definition 1. The Grünwald-Letnikov derivative definition of order α is described as

$$ {}_aD_t^{\alpha} f(t) = \lim_{h \to 0} \frac{1}{h^{\alpha}} \sum_{j=0}^{[(t-a)/h]} (-1)^j \binom{\alpha}{j} f(t - jh), \quad (1) $$

where h is the time step.

Definition 2. The Riemann-Liouville derivative of order α is defined as

$$ {}_aD_t^{\alpha} f(t) = \frac{1}{\Gamma(n-\alpha)} \frac{d^n}{dt^n} \int_a^t \frac{f(\tau)\, d\tau}{(t-\tau)^{\alpha-n+1}} \quad (2) $$

for $n-1 < \alpha < n$, where $\Gamma(\cdot)$ is Euler's Gamma function.

Definition 3. The Caputo definition of fractional derivative can be written as

$$ {}_aD_t^{\alpha} f(t) = \frac{1}{\Gamma(n-\alpha)} \int_a^t \frac{f^{(n)}(\tau)\, d\tau}{(t-\tau)^{\alpha-n+1}} \quad (3) $$

for $n-1 < \alpha < n$.

Lemma 4 (fractional comparison principle [20]). *Let $x(0) = y(0)$ and $D^{\alpha}x(t) \geq D^{\alpha}y(t)$, where $0 < \alpha < 1$; then $x(t) \geq y(t)$.*

Lemma 5 (Mittag-Leffler stability [20]). *Let $x_{eq} = 0$ be an equilibrium point of a fractional nonlinear system and a domain containing the origin. Let $V(t, x(t)) : [0, \infty) \times D \to R^+$ be a continuously differentiable function satisfying*

$$ \begin{aligned} V(t, x(t)) &\geq \alpha(\|x\|), \\ D^q V(t, x(t)) &\leq 0, \end{aligned} \quad (4) $$

where $\alpha(\cdot)$ is the class-K function, $x \in D$, and $0 < q < 1$. Then $x = 0$ is globally stable.

Lemma 6 (see [22]). *Let $x(t) \in R$ be a continuous and derivable function. Then, for any time instant $t \geq t_0$,*

$$ \frac{1}{2} {}_{t_0}^{C}D_t^q x^2(t) \leq x(t) {}_{t_0}^{C}D_t^q x(t), \quad \forall q \in (0,1). \quad (5) $$

3. Sliding Control for the Nominal Fractional Chaotic Systems

Consider a class of fractional-order chaotic systems described by the following fractional differential equations:

$$ \begin{aligned} D^{q_1} x &= f(x, y, z) - \alpha x, \\ D^{q_2} y &= x g(x, y, z) - \beta y, \\ D^{q_3} z &= x h(x, y, z) - \gamma z, \end{aligned} \quad (6) $$

where $q_1, q_2, q_3 \in (0, 1)$ are fractional-orders, x, y, and z are state variables, and α, β, and γ are nonnegative known constants.

The above fractional system (6) is introduced by Yuan et al. [21]. It consists of 6 fractional chaotic systems, including the fractional-order Lorenz system, the fractional-order Chen system, the fractional-order Lü system, the fractional-order Liu system, the fractional-order Lotka-Volterra system, and the fractional-order Rucklidge system.

In this paper, our main purpose is to propose the sliding control design for the commensurate ordered chaotic system, that is, the case when $q_1 = q_2 = q_3 = q \in (0, 1)$. Firstly, we introduce a fractional integral sliding surface which is different from the one in [21] and design sliding control law for the nominal fractional system (6) using the Mittag-Leffler stability theorem. Secondly, we consider system with uncertainties and external disturbances and propose adaptive sliding control design.

3.1. Sliding Surface Design. To propose the sliding control design for the nominal system (6), we introduce the following fractional integral sliding surface:

$$s(t) = x(t) + {}_0I_t^q \varphi(t), \tag{7}$$

where $\varphi(t) = yg(x, y, z) + zh(x, y, z) + \alpha x$.

Taking its qth order fractional derivative with respect to time leads to the following:

$$D^q s(t) = D^q x(t) + \varphi(t). \tag{8}$$

3.2. Stability Analysis of Sliding Dynamics. Now we are about to prove that the system motion on the sliding manifold (i.e., sliding dynamics) satisfies our desired specifications; that is, once the trajectory of system (6) is steered to the sliding surface (7), the three state variables x, y, and z will converge to zero asymptotically.

Let $D^q s(t) = 0$; then we derive the following fractional sliding dynamics for the nominal system:

$$\begin{aligned} D^q x &= -yg(x, y, z) - zh(x, y, z) - \alpha x, \\ D^q y &= xg(x, y, z) - \beta y, \\ D^q z &= xh(x, y, z) - \gamma z. \end{aligned} \tag{9}$$

For the sliding dynamics (9) a Lyapunov function is chosen as

$$V_1(x, y, z) = \frac{1}{2}x^2 + \frac{1}{2}y^2 + \frac{1}{2}z^2. \tag{10}$$

By taking its qth order fractional derivative with respect to time, using Lemma 6, and inserting the three equations of system (9) into (10), one derives

$$\begin{aligned} D^q V_1 &\le xD^q x + yD^q y + zD^q z \\ &= x(-yg - zh - \alpha x) + y(xg - \beta y) + z(xh - \gamma z) \\ &= -\left(\alpha x^2 + \beta y^2 + \gamma z^2\right). \end{aligned} \tag{11}$$

Denoting $\eta = \min\{\alpha, \beta, \gamma\}$, then inequality (11) becomes

$$D^q V_1 \le -\eta V_1. \tag{12}$$

Inequality (12) satisfies the Mittag-Leffler stability theorem. This implies that the three state variables x, y, and z tend to zero asymptotically. Up to this point, we come to the following statement.

Theorem 7. *The fractional sliding dynamics (9) of the nominal fractional system (6) is asymptotically stable.*

3.3. Sliding Control Design. To propose the sliding control design for the nominal system (6), we introduce the following control Lyapunov function:

$$V_2(s) = \frac{1}{2}s^2. \tag{13}$$

Taking its qth order fractional derivative with respect to time and inserting the first equation of system (6), one derives

$$\begin{aligned} D^q V_2 &\le sD^q s \\ &= s\left(D^q x + \varphi\right) \\ &= s\left[f(x, y, z) - \alpha x + u(t) + yg(x, y, z) \right. \\ &\qquad \left. + zh(x, y, z) + \alpha x\right]. \end{aligned} \tag{14}$$

Then the control law is constructed as

$$\begin{aligned} u(t) = &-f(x, y, z) - yg(x, y, z) \\ &- zh(x, y, z) - k_1 \operatorname{sgn}(s) - k_2 s. \end{aligned} \tag{15}$$

Substituting the control law (15) into (14) yields

$$\begin{aligned} D^q V_2 &\le s\left[-k_1 \operatorname{sgn}(s) - k_2 s\right] \\ &= -k_1 |s| - k_2 s^2 \\ &\le -k_2 V_2. \end{aligned} \tag{16}$$

In terms of the Mittag-Leffler stability theorem, we obtain that $s \to 0$ and $x, y, z \to 0$.

Up to this point, we arrive at the following conclusion.

Theorem 8. *The nominal fractional chaotic system (6) is asymptotically stabilized under the proposed sliding control law (15).*

4. Adaptive Sliding Control for the Perturbed System

In this section, we are about to go further by considering the commensurate ordered chaotic system (6) in the presence

of systematic uncertainties and external disturbances. It is described by the following fractional differential equations:

$$\begin{aligned} D^q x &= f(x,y,z) - \alpha x + \Delta f_1(x,y,z) + d_1(t), \\ D^q y &= xg(x,y,z) - \beta y + \Delta f_2(x,y,z) + d_2(t), \\ D^q z &= xh(x,y,z) - \gamma z + \Delta f_3(x,y,z) + d_3(t). \end{aligned} \tag{17}$$

We assume that all the uncertainties and external disturbances are bounded; that is, $|\Delta f_1(x,y,z)| < \theta_1$, $|d_1(t)| < \theta_2$, $|\Delta f_2(x,y,z)| < F_2$, $|d_2(t)| < D_2$, $|\Delta f_3(x,y,z)| < F_3$, and $|d_3(t)| < D_3$, where θ_1, θ_2, F_2, D_2, F_3, and D_3 are unknown nonnegative constants.

4.1. Stability Analysis of Sliding Dynamics of Perturbed Systems. Proceeding as before, we introduce the fractional integral sliding surface as in (7) and derive the following sliding dynamics:

$$\begin{aligned} D^q x &= -yg(x,y,z) - zh(x,y,z) - \alpha x, \\ D^q y &= xg(x,y,z) - \beta y + \Delta f_2(x,y,z) + d_2(t), \\ D^q z &= xh(x,y,z) - \gamma z + \Delta f_3(x,y,z) + d_3(t). \end{aligned} \tag{18}$$

To analyze the stability of the sliding dynamics (18), we introduce the following Lyapunov function:

$$V_3(x,y,z) = \frac{1}{2}x^2 + \frac{1}{2}y^2 + \frac{1}{2}z^2. \tag{19}$$

Taking its qth order fractional derivative with respect to time, using Lemma 6, and inserting the three equations of system (18) into (19), one derives

$$\begin{aligned} D^q V_3 &\le xD^q x + yD^q y + zD^q z \\ &= x(-yg - zh - \alpha x) + y(xg - \beta y + \Delta f_2 + d_2) \\ &\quad + z(xh - \gamma z + \Delta f_3 + d_3) \\ &= -\left(\alpha x^2 + \beta y^2 + \gamma z^2\right) + y(\Delta_2 + D_2) + z(\Delta_3 + D_3). \end{aligned} \tag{20}$$

We denote

$$\rho = y(\Delta_2 + D_2) + z(\Delta_3 + D_3). \tag{21}$$

It is observed that ρ is also bounded, since all the state variables of chaotic system have bounded amplitude [23]. As a result, we ultimately derive the following inequality:

$$D^q V_3 \le -\eta V_3 + \rho. \tag{22}$$

Following the proof of Theorem 2 in [23], we conclude that the sliding dynamics (18) is globally stable.

Up to this point, we come to the following conclusion.

Theorem 9. *The fractional sliding dynamics (18) of the fractional system (17) in the presence of system uncertainties and external disturbances is globally stable.*

4.2. Adaptive Sliding Control Design. To propose the sliding control design for the perturbed system (17), we introduce the following Lyapunov function:

$$V_4\left(x,y,z,\widehat{\theta}_1,\widehat{\theta}_2\right) = \frac{1}{2}\left[s^2 + \frac{1}{\mu_1}\left(\widehat{\theta}_1 - \theta_1\right)^2 + \frac{1}{\mu_2}\left(\widehat{\theta}_2 - \theta_2\right)^2\right]. \tag{23}$$

Taking its qth order fractional derivative with respect to time and inserting the first equation of system (17) into (23), one obtains

$$\begin{aligned} D^q V_4 &\le sD^q s + \frac{1}{\mu_1}\left(\widehat{\theta}_1 - \theta_1\right)D^q\widehat{\theta}_1 + \frac{1}{\mu_2}\left(\widehat{\theta}_2 - \theta_2\right)D^q\widehat{\theta}_2 \\ &= s\left(D^q x + \varphi\right) + \frac{1}{\mu_1}\left(\widehat{\theta}_1 - \theta_1\right)D^q\widehat{\theta}_1 \\ &\quad + \frac{1}{\mu_2}\left(\widehat{\theta}_2 - \theta_2\right)D^q\widehat{\theta}_2 \\ &= s\left[f - \alpha x + \Delta f_1 + d_1 + u(t) + yg + zh + \alpha x\right] \\ &\quad + \frac{1}{\mu_1}\left(\widehat{\theta}_1 - \theta_1\right)D^q\widehat{\theta}_1 + \frac{1}{\mu_2}\left(\widehat{\theta}_2 - \theta_2\right)D^q\widehat{\theta}_2. \end{aligned} \tag{24}$$

If we chose the control law as

$$\begin{aligned} u(t) = &-f(x,y,z) - yg(x,y,z) - zh(x,y,z) \\ &-\left(\widehat{\theta}_1 + \widehat{\theta}_2 + k_1\right)\operatorname{sgn}(s) - k_2 s \end{aligned} \tag{25}$$

and the fractional adaptive law as

$$\begin{aligned} D^q\widehat{\theta}_1 &= \mu_1 |s|, \\ D^q\widehat{\theta}_2 &= \mu_2 |s|, \end{aligned} \tag{26}$$

then inequality (24) becomes

$$\begin{aligned} D^q V_4 &\le s\left[\Delta f_1 + d_1 - \left(\widehat{\theta}_1 + \widehat{\theta}_2 + k_1\right)\operatorname{sgn}(s) - k_2 s\right] \\ &\quad + \left(\widehat{\theta}_1 - \theta_1\right)|s| + \left(\widehat{\theta}_2 - \theta_2\right)|s| \\ &= (\Delta f_1 + d_1)s - \left(\widehat{\theta}_1 + \widehat{\theta}_2 + k_1\right)|s| \\ &\quad + \left(\widehat{\theta}_1 - \theta_1\right)|s| + \left(\widehat{\theta}_2 - \theta_2\right)|s| - k_2 s^2 \\ &\le (\theta_1 + \theta_2)|s| - \left(\widehat{\theta}_1 + \widehat{\theta}_2 + k_1\right)|s| + \left(\widehat{\theta}_1 - \theta_1\right)|s| \\ &\quad + \left(\widehat{\theta}_2 - \theta_2\right)|s| - k_2 s^2 \\ &= -k_1|s| - k_2 s^2 \le 0. \end{aligned} \tag{27}$$

It is obvious that $D^q V_4(x, y, z, \widehat{\theta}_1, \widehat{\theta}_2) = 0$ if and only if $s = 0$. So we can conclude that $x, y, z \to 0$, $\widehat{\theta}_1 \to \theta_1$, and $\widehat{\theta}_2 \to \theta_2$.

Up to this point, we arrive at the following theorem.

Theorem 10. *The fractional system (17) in the presence of system uncertainties and external disturbances is asymptotically stabilized under the proposed sliding control law (24) and the fractional adaptive law (25).*

Remark 11. The control design proposed in this paper is different from those in [9, 21]. Firstly, the fractional sliding surfaces are of different forms. Secondly, the stability of the fractional sliding dynamics is analyzed using the Mittag-Leffler stability theorem, instead of the continuous frequency distributed model (see [21]) or the traditional Lyapunov method (see [9]). More importantly, a stability analysis for the fractional sliding dynamics of the perturbed systems is given in this paper.

5. Numerical Simulations

To show the viability and efficiency of the proposed control design, we give two illustrative examples, fractional-order Lorenz's system and fractional-order Chen's system. We utilize the proposed fractional integral sliding control technique to control the two nominal fractional chaotic systems. Furthermore, we apply the adaptive sliding control approach to control the fractional systems in the presence of system uncertainties and external disturbances.

Numerical simulations are implemented using the MATLAB software. We utilize the algorithm for numerical calculation of fractional derivatives, which is introduced by Petráš in [24]. This algorithm takes advantage of the "Short-Memory" principle and derived from Grünwald-Letnikov Definition (1) based on the fact that three Definitions (1), (2), and (3) are equivalent for a wide class of functions.

5.1. Control of Fractional-Order Lorenz's System. Fractional Lorenz's system is described as

$$\begin{aligned} D^q x &= -a(x - y), \\ D^q y &= rx - y - xz, \\ D^q z &= -bz + xy, \end{aligned} \tag{28}$$

where $a = 10$, $r = 28$, and $b = 8/3$.

In terms of (7), the sliding surface is

$$s(t) = x(t) + {}_0I_t^q \varphi(t), \tag{29}$$

where $\varphi(t) = ax(t) + ry(t)$.

Following (15), the control law is

$$u(t) = -(a + r)\, y(t) - k_1 \operatorname{sgn}(s) - k_2 s. \tag{30}$$

The performances of nominal closed-loop fractional-order Lorenz's system are shown in Figures 1 and 2, under the proposed fractional integral sliding surface (29) and the sliding control law (30). Figure 1 shows the time response of the three state variables and the control input (30). Figure 2 shows the corresponding fractional integral sliding surface (29).

Parameters for the numerical simulations are specified, respectively, as follows: the fractional-order $q = 0.993$ and the coefficients of control law $k_1 = 0.02$, $k_2 = 0.02$.

Next we investigate the control design for fractional-order Lorenz's system in the presence of system uncertainties and external disturbances

$$\begin{aligned} D^q x &= -a(x - y) + \Delta f_1 + d_1 + u(t), \\ D^q y &= rx - y - xz + \Delta f_2 + d_2, \\ D^q z &= -bz + xy + \Delta f_3 + d_3. \end{aligned} \tag{31}$$

To carry out numerical simulations, the system uncertainties and external disturbances in the above perturbed system are assumed, respectively, to be $\Delta f_1(x, y, z) = 0.1 + 0.1 \sin(\pi x)$, $d_1(t) = 0.1 \cos t$, $\Delta f_2(x, y, z) = 0.1 - 0.2 \sin(\pi y)$, $d_2(t) = 0.2 \sin(2t)$, $\Delta f_3(x, y, z) = 0.1x \cos(\pi z)$, and $d_3(t) = 0.1 \cos(\pi t)$.

In view of (25) and (26), the control law and the fractional adaptive law are, respectively,

$$u(t) = -(a + r)\, y - \left(\widehat{\theta}_1 + \widehat{\theta}_2 + k_1\right) \operatorname{sgn}(s) - k_2 s, \tag{32}$$

$$\begin{aligned} D^q \widehat{\theta}_1 &= \mu_1 |s|, \\ D^q \widehat{\theta}_2 &= \mu_2 |s|. \end{aligned} \tag{33}$$

Figures 3 and 4 illustrate the performances of controlled fractional Lorenz's system with uncertainties and external disturbances, under the proposed fractional integral sliding surface (29), the sliding control law (32), and the fractional adaptive law (33). The time responses of the state variables, the control input, and the estimation of uncertainties/external disturbances are depicted in Figure 3. The corresponding fractional integral sliding surface (29) is illustrated in Figure 4.

Parameters for the numerical simulations are specified, respectively, as follows: the fractional-order $q = 0.993$, the coefficients of control law $k_1 = 0.02$, $k_2 = 0.02$, the coefficients of adaptive law $\mu_1 = 0.03$, $\mu_2 = 0.02$, and the initial conditions of the adaptive parameters $\theta_1(0) = \theta_2(0) = 0.2$.

5.2. Control of Fractional-Order Chen's System. Fractional-order Chen's system is described as

$$\begin{aligned} D^{q_1} x &= a(y - x), \\ D^{q_2} y &= (c - a)\, x - xz + cy + u, \\ D^{q_3} z &= xy - bz. \end{aligned} \tag{34}$$

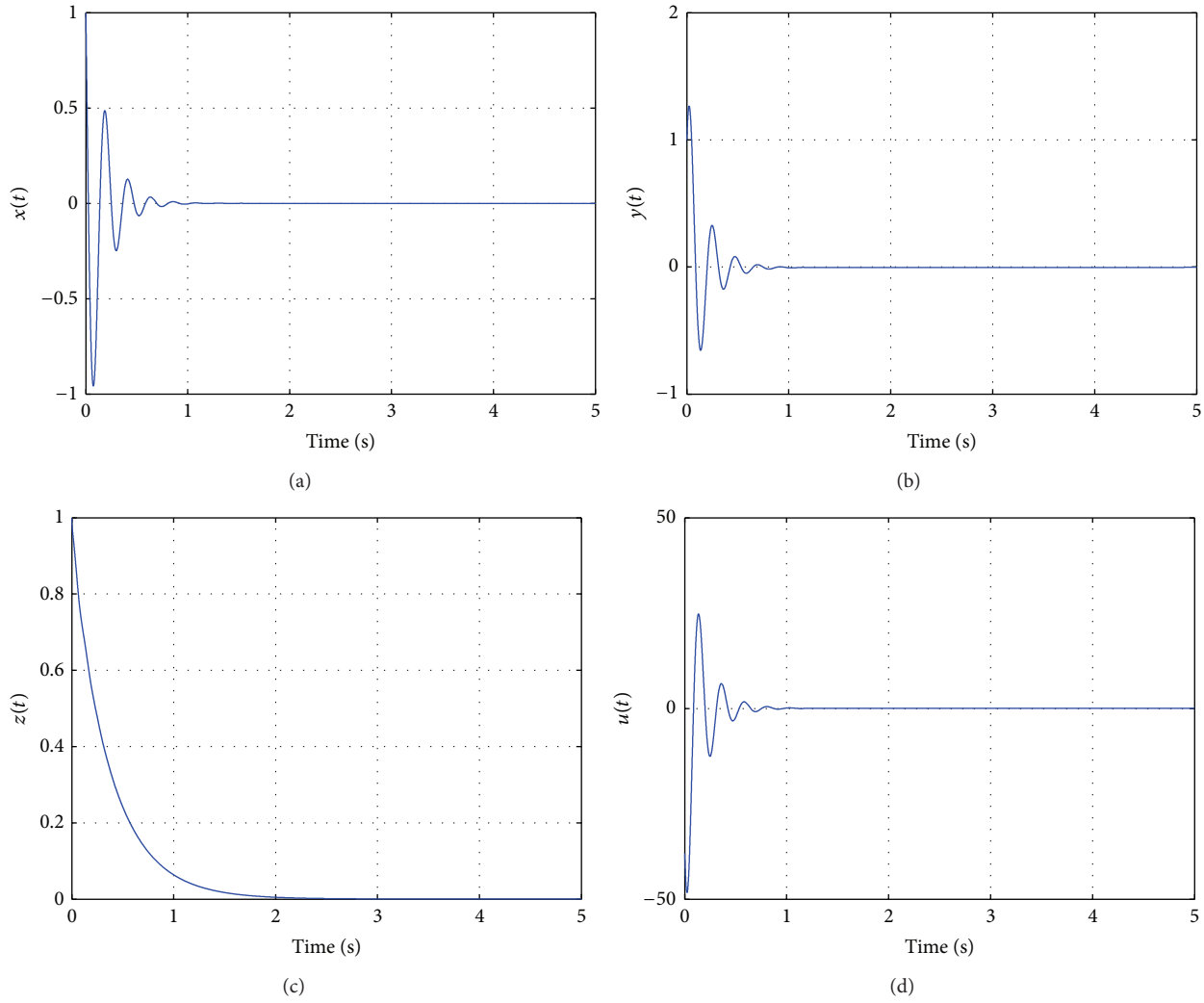

Figure 1: Fractional sliding control of nominal fractional-order Loren's system with time step $h = 0.0005$: (a) the x-t space; (b) the y-t space; (c) the z-t space; (d) the u-t space.

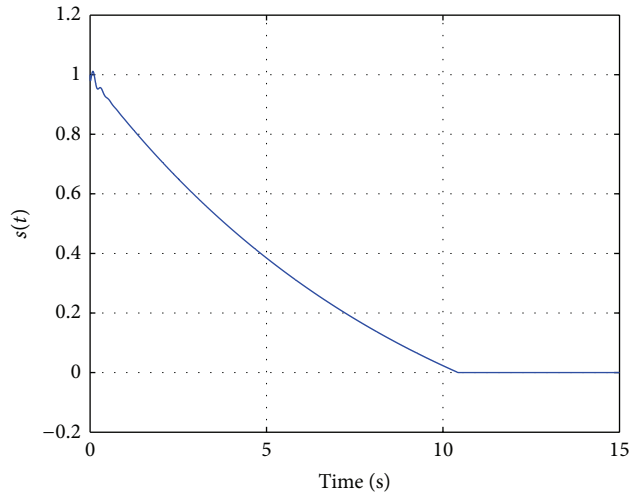

Figure 2: The time response of the sliding manifold (29).

In terms of (7), the sliding surface is

$$s(t) = y(t) + {}_0I_t^q \varphi(t), \tag{35}$$

where $\varphi(t) = ax(t) + cy(t) + x(t)z(t)$.

Following (15), the control law is

$$u(t) = -cx - 2cy - k_1 \operatorname{sgn}(s) - k_2 s. \tag{36}$$

The performances of nominal closed-loop fractional-order Chen's system are shown in Figures 5 and 6, under the proposed fractional integral sliding surface (35) and the sliding control law (36). Figure 5 shows the time response of the three state variables and the control input (36). Figure 6 shows the corresponding fractional integral sliding surface (35).

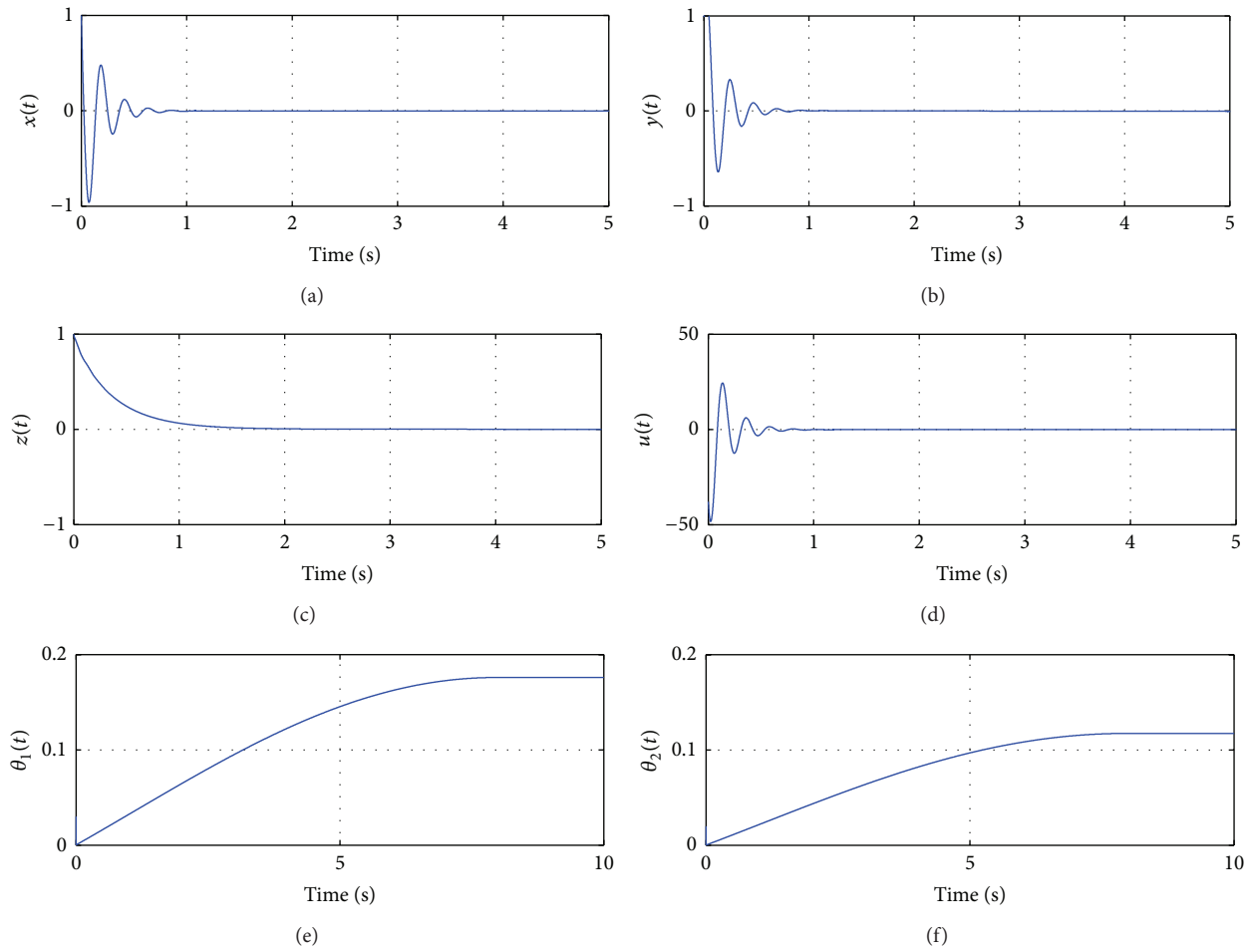

Figure 3: Adaptive sliding control of fractional-order Loren's system with dynamics uncertainties and external disturbances: (a) the x-t space; (b) the y-t space; (c) the z-t space; (d) the u-t space; (e) online estimate of θ_1; (f) online estimate of θ_2.

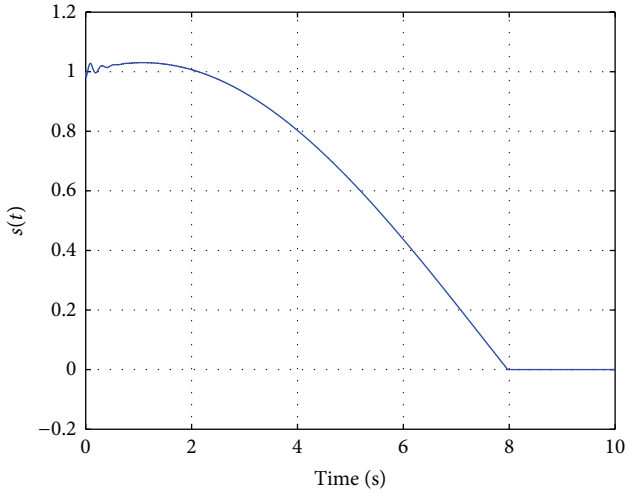

Figure 4: The time response of the sliding manifold (29).

Parameters for the numerical simulations are specified, respectively, as follows: the fractional-order $q = 0.9$ and the coefficients of control law $k_1 = 0.1$, $k_2 = 0.1$.

Next we propose the adaptive sliding control design for fractional-order Chen's system in the presence of uncertainties and external disturbances which are added to the three equations. The control input is added to the second equation. Then the perturbed system to be controlled reads as

$$\begin{aligned} D^{q_1} x &= a(y - x) + \Delta f_1 + d_1, \\ D^{q_2} y &= (c - a)x - xz + cy + \Delta f_2 + d_2 + u(t), \\ D^{q_3} z &= xy - bz + \Delta f_3 + d_3. \end{aligned} \tag{37}$$

To carry out numerical simulations, the system uncertainties and external disturbances in the above perturbed system are assumed, respectively, as $\Delta f_1(x, y, z) = 0.1\cos(xy)$, $d_1(t) = 0.2\sin(3t)$, $\Delta f_2(x, y, z) = 0.2 - 0.1\sin(\pi x)$, $d_2(t) = 0.1\cos t$, $\Delta f_3(x, y, z) = 0.1\sin(xy)$, and $d_3(t) = -0.1\cos(5t)$.

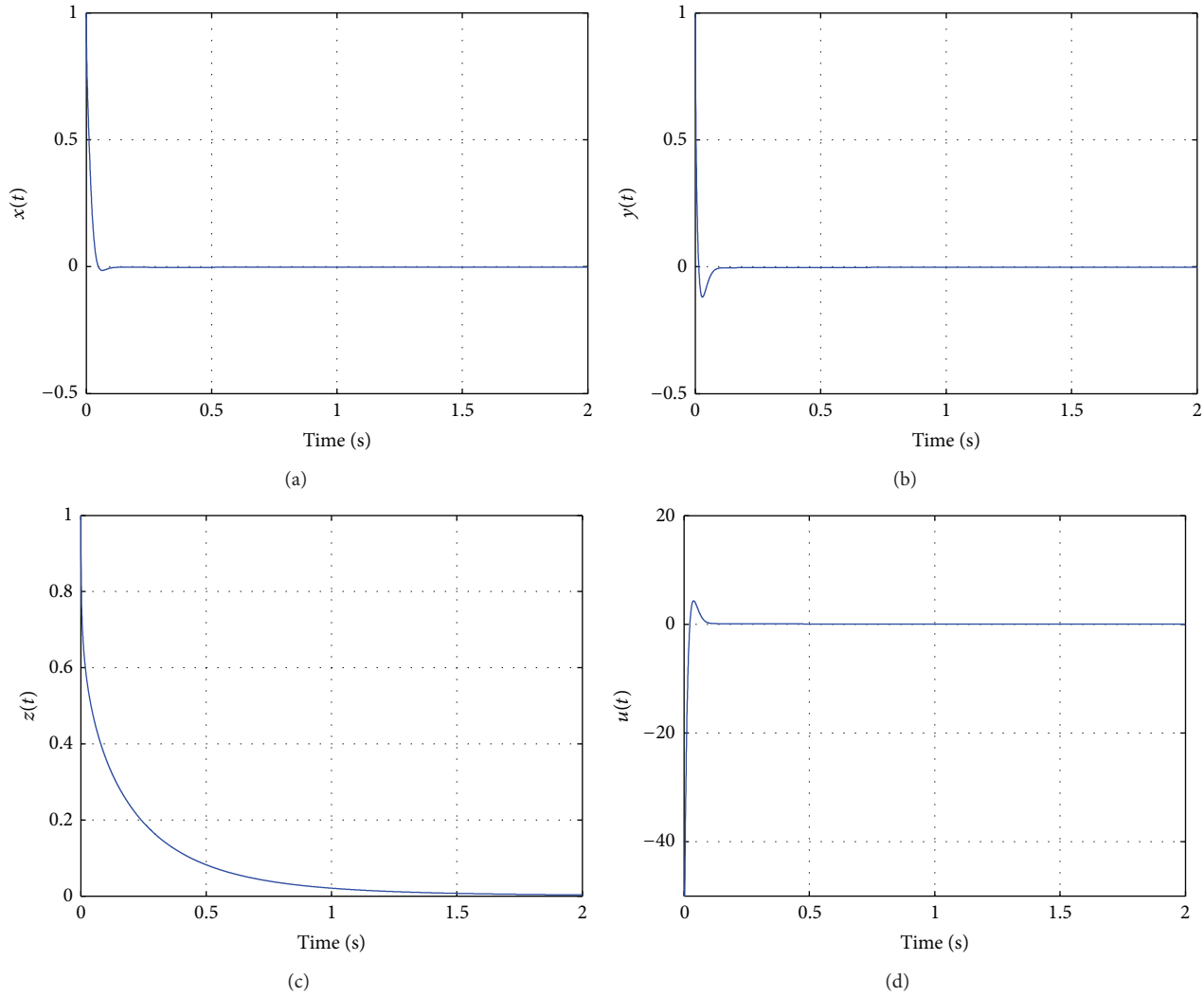

Figure 5: Sliding control of nominal fractional-order Chen's system: (a) the x-t space; (b) the y-t space; (c) the z-t space; (d) the u-t space.

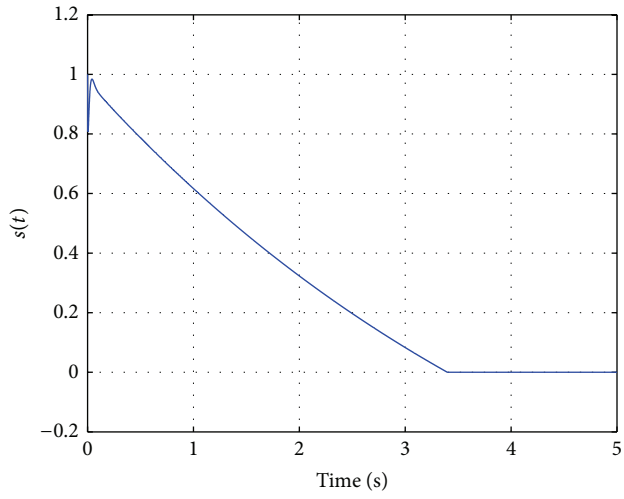

Figure 6: The time response of the sliding manifold (35).

In terms of (25) and (26), the control law and factional adaptive law are selected, respectively, as

$$u(t) = -cx - 2cy - \left(\widehat{\theta}_1 + \widehat{\theta}_2 + k_1\right) \operatorname{sgn}(s) - k_2 s, \tag{38}$$

$$\begin{aligned} D^q \widehat{\theta}_1 &= \mu_1 |s|, \\ D^q \widehat{\theta}_2 &= \mu_2 |s|. \end{aligned} \tag{39}$$

Figures 7 and 8 illustrate the performances of controlled fractional-order Chen's system with uncertainties and external disturbances, under the proposed fractional integral sliding surface (35), the sliding control law (38), and the fractional adaptive law (39). The time responses of the state variables, the control input (38), and the estimation of uncertainties/external disturbances are depicted in Figure 7; the corresponding fractional integral sliding surface (35) is illustrated in Figure 8.

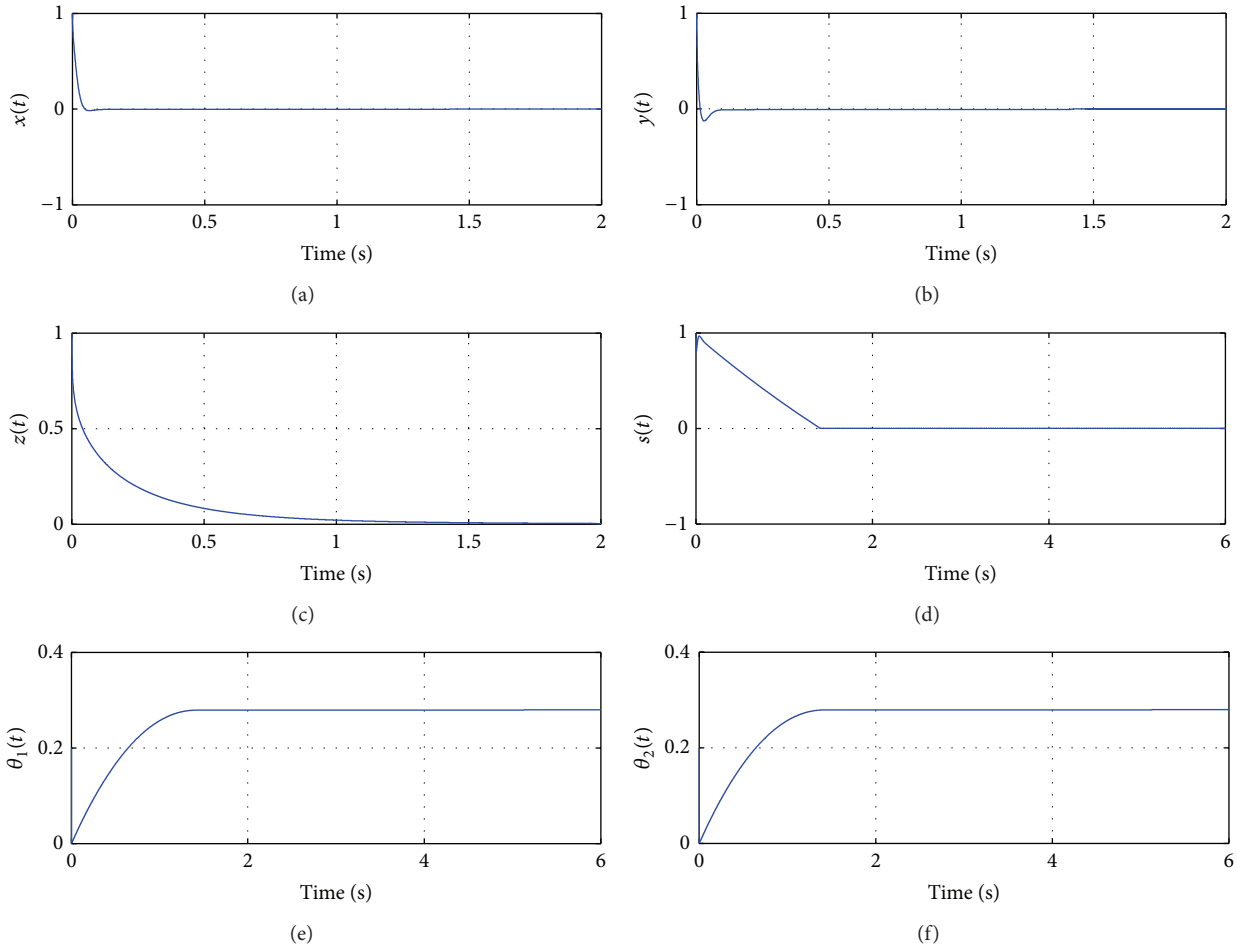

Figure 7: Adaptive sliding control of fractional-order Chen's system with dynamics uncertainties and external disturbances: (a) the x-t space; (b) the y-t space; (c) the z-t space; (d) the u-t space; (e) online estimate of θ_1; (f) online estimate of θ_2.

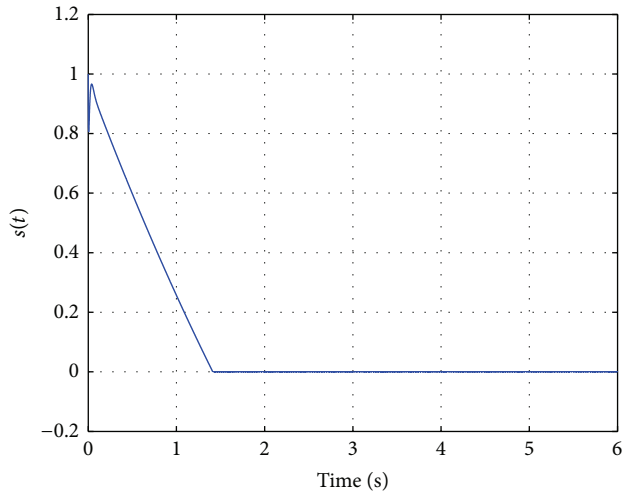

Figure 8: The time response of the sliding manifold (35).

Parameters for the numerical simulations are specified, respectively, as follows: the fractional-order $q = 0.9$, the coefficients of control law $k_1 = 0.5$, $k_2 = 0.1$, the coefficients of adaptive law $\mu_1 = 0.2$, $\mu_2 = 0.2$, and the initial conditions of the adaptive parameters $\theta_1(0) = \theta_2(0) = 0.2$.

6. Conclusions

In this paper, a fractional sliding controller and an adaptive sliding controller have been, respectively, designed for a class of commensurate fractional-order chaotic systems and the perturbed ones. Firstly, a fractional integral sliding manifold for the nominal systems has been introduced. Secondly, the stability of the corresponding fractional sliding dynamics has been proved. Then, by introducing a Lyapunov candidate function and using the Mittag-Leffler stability theory, a desired sliding control law has been obtained. Furthermore, the proposed sliding manifold has been proved to be adapted for the fractional systems in the presence of uncertainties and external disturbances. At last, an adaptation law for the perturbed fractional systems has been designed. Numerical simulations of fractional Lorenz's system and Chen's system are presented to verify the viability and efficiency of the proposed fractional controllers.

Conflict of Interests

The authors do not have any possible conflict of interests.

Acknowledgment

This study was supported by a grant from the Natural Science Foundation of the Province Shandong of China (ZR2014AM006).

References

[1] O. P. Agrawal, "A general formulation and solution scheme for fractional optimal control problems," *Nonlinear Dynamics*, vol. 38, no. 1–4, pp. 323–337, 2004.

[2] I. Podlubny, *Fractional Differential Equations: An Introduction to Fractional Derivatives, Fractional Differential Equations, to Methods of Their Solution and Some of Their Applications*, Academic Press, 1998.

[3] K. Diethelm, *The Analysis of Fractional Differential Equations: An Application-Oriented Exposition Using Differential Operators of Caputo Type*, vol. 2004 of *Lecture Notes in Mathematics*, Springer, Berlin, Germany, 2010.

[4] A. Oustaloup, X. Moreau, and M. Nouillant, "The CRONE suspension," *Control Engineering Practice*, vol. 4, no. 8, pp. 1101–1108, 1996.

[5] I. Podlubny, "Fractional-order systems and $PI^{\lambda}D^{\mu}$-controllers," *IEEE Transactions on Automatic Control*, vol. 44, no. 1, pp. 208–214, 1999.

[6] H.-F. Raynaud and A. Zergaïnoh, "State-space representation for fractional order controllers," *Automatica*, vol. 36, no. 7, pp. 1017–1021, 2000.

[7] D. Xue and Y. Q. Chen, "A comparative introduction of four fractional order controllers," in *Proceedings of the 4th World Congress on Intelligent Control and Automation*, pp. 3228–3235, Shanghai, China, June 2002.

[8] A. Razminia and D. Baleanu, "Complete synchronization of commensurate fractional order chaotic systems using sliding mode control," *Mechatronics*, vol. 23, no. 7, pp. 873–879, 2013.

[9] C. Yin, S. Dadras, S.-M. Zhong, and Y. Chen, "Control of a novel class of fractional-order chaotic systems via adaptive sliding mode control approach," *Applied Mathematical Modelling*, vol. 37, no. 4, pp. 2469–2483, 2013.

[10] S. Dadras and H. R. Momeni, "Fractional terminal sliding mode control design for a class of dynamical systems with uncertainty," *Communications in Nonlinear Science and Numerical Simulation*, vol. 17, no. 1, pp. 367–377, 2012.

[11] B. M. Vinagre, I. Petráš, I. Podlubny, and Y. Q. Chen, "Using fractional order adjustment rules and fractional order reference models in model-reference adaptive control," *Nonlinear Dynamics*, vol. 29, no. 1–4, pp. 269–279, 2002.

[12] S. Ladaci and A. Charef, "On fractional adaptive control," *Nonlinear Dynamics*, vol. 43, no. 4, pp. 365–378, 2006.

[13] B. Shi, J. Yuan, and C. Dong, "On fractional model reference adaptive control," *The Scientific World Journal*, vol. 2014, Article ID 521625, 8 pages, 2014.

[14] Z. D. Jelicic and N. Petrovacki, "Optimality conditions and a solution scheme for fractional optimal control problems," *Structural and Multidisciplinary Optimization*, vol. 38, no. 6, pp. 571–581, 2009.

[15] R. Kamocki, "On the existence of optimal solutions to fractional optimal control problems," *Applied Mathematics and Computation*, vol. 235, pp. 94–104, 2014.

[16] A. B. Malinowska and D. F. Torres, *Introduction to the Fractional Calculus of Variations*, Imperial College Press, London, UK, 2012.

[17] A. G. Butkovskii, S. S. Postnov, and E. A. Postnova, "Fractional integro-differential calculus and its control-theoretical applications. II. Fractional dynamic systems: modeling and hardware implementation," *Automation and Remote Control*, vol. 74, no. 5, pp. 725–749, 2013.

[18] C. P. Li and F. R. Zhang, "A survey on the stability of fractional differential equations," *European Physical Journal: Special Topics*, vol. 193, no. 1, pp. 27–47, 2011.

[19] J. C. Trigeassou, N. Maamri, J. Sabatier, and A. Oustaloup, "A Lyapunov approach to the stability of fractional differential equations," *Signal Processing*, vol. 91, no. 3, pp. 437–445, 2011.

[20] Y. Li, Y. Chen, and I. Podlubny, "Stability of fractional-order nonlinear dynamic systems: lyapunov direct method and generalized Mittag-Leffler stability," *Computers & Mathematics with Applications*, vol. 59, no. 5, pp. 1810–1821, 2010.

[21] J. Yuan, B. Shi, and W. Ji, "Adaptive sliding mode control of a novel class of fractional chaotic systems," *Advances in Mathematical Physics*, vol. 2013, Article ID 576709, 13 pages, 2013.

[22] N. Aguila-Camacho, M. A. Duarte-Mermoud, and J. A. Gallegos, "Lyapunov functions for fractional order systems," *Communications in Nonlinear Science and Numerical Simulation*, vol. 19, no. 9, pp. 2951–2957, 2014.

[23] M. R. Faieghi, H. Delavari, and D. Baleanu, "A note on stability of sliding mode dynamics in suppression of fractional-order chaotic systems," *Computers & Mathematics with Applications*, vol. 66, no. 5, pp. 832–837, 2013.

[24] I. Petráš, *Fractional-Order Nonlinear Systems: Modeling, Analysis and Simulation*, Springer, 2011.

Research Article

Approximated Fractional Order Chebyshev Lowpass Filters

Todd Freeborn,[1] Brent Maundy,[2] and Ahmed S. Elwakil[3]

[1]*Tangent Design Engineering Ltd., 2719 7 Avenue Northeast, Calgary, AB, Canada T2A 2L9*
[2]*Department of Electrical and Computer Engineering, University of Calgary, 2500 University Dr. N. W., Calgary, AB, Canada T2N 1N4*
[3]*Department of Electrical and Computer Engineering, University of Sharjah, P.O. Box 27272, UAE*

Correspondence should be addressed to Todd Freeborn; todd.freeborn@gmail.com

Received 13 June 2014; Accepted 21 August 2014

Academic Editor: Guido Maione

Copyright © 2015 Todd Freeborn et al. This is an open access article distributed under the Creative Commons Attribution License, which permits unrestricted use, distribution, and reproduction in any medium, provided the original work is properly cited.

We propose the use of nonlinear least squares optimization to approximate the passband ripple characteristics of traditional Chebyshev lowpass filters with fractional order steps in the stopband. MATLAB simulations of $(1 + \alpha)$, $(2 + \alpha)$, and $(3 + \alpha)$ order lowpass filters with fractional steps from $\alpha = 0.1$ to $\alpha = 0.9$ are given as examples. SPICE simulations of 1.2, 1.5, and 1.8 order lowpass filters using approximated fractional order capacitors in a Tow-Thomas biquad circuit validate the implementation of these filter circuits.

1. Introduction

Fractional calculus, the branch of mathematics concerning differentiations and integrations to noninteger order, has been steadily migrating from the theoretical realms of mathematicians into many applied and interdisciplinary branches of engineering [1]. From the import of these concepts into electronics for analog signal processing emerged the field of fractional order filter design. This import into filter design has yielded much recent progress in theory [2–6], noise analysis [7], stability analysis [8], implementation [9–13], and applications [14, 15]. These filter circuits have all been designed using the fractional Laplacian operator, s^α, because the algebraic design of transfer functions is much simpler than solving the difficult time domain representations of fractional derivatives. One definition of a fractional derivative of order α is given by the Caputo derivative [16] as

$$ {}_a^C D_t^\alpha f(t) = \frac{1}{\Gamma(\alpha - n)} \int_a^t \frac{f^{(n)}(\tau)\, d\tau}{(t-\tau)^{\alpha+1-n}}, \tag{1} $$

where $\Gamma(\cdot)$ is the gamma function and $n - 1 \leq \alpha \leq n$. The Caputo definition of a fractional derivative is often used over other approaches because the initial conditions for this definition take the same form as the more familiar integer order differential equations. Applying the Laplace transform to the fractional derivative of (1) with lower terminal $a = 0$ yields

$$ \mathscr{L}\left\{ {}_0^C D_t^\alpha f(t) \right\} = s^\alpha F(s) - \sum_{k=0}^{n-1} s^{\alpha-k-1} f^{(k)}(0), \tag{2} $$

where s^α is also referred to as the fractional Laplacian operator. With zero initial conditions (2) can be simplified to

$$ \mathscr{L}\left\{ {}_0^C D_t^\alpha f(t) \right\} = s^\alpha F(s). \tag{3} $$

Therefore it becomes possible to define a general fractance device with impedance proportional to s^α [17], where the traditional circuit elements are special cases of the general device when the order is −1, 0, and 1 for a capacitor, resistor, and inductor, respectively. The expressions of the voltage across a traditional capacitor are defined by integer order integration of the current through it. This element can be expanded to the fractional domain using noninteger order integration which results in the time domain expression for the voltage across the fractional order capacitor given by

$$ v_C^\alpha(t) = \frac{1}{C\Gamma(\alpha)} \int_0^t \frac{i(\tau)}{(t-\tau)^{1-\alpha}} d\tau, \tag{4} $$

where $0 \leq \alpha \leq 1$ is the fractional orders of the capacitor, $i(t)$ is the current through the element, C is the capacitance with units $F/s^{1-\alpha}$, and (s) is a unit of time not to be mistaken with the Laplacian operator. Note that we will refer to the units of these devices as (F) for simplicity.

By applying the Laplace transform to (4) with zero initial conditions the impedance of this fractional order element is given as $Z_C^{\alpha}(s) = 1/s^{\alpha}C$. Using this element in electrical circuits increases the range of responses that can be realized, expanding them from the narrow integer subset to the more general fractional domain. While these devices are not yet commercially available, recent research regarding their manufacture and production shows very promising results [18–20]. Therefore, it is becoming increasingly important to develop the theory behind using these fractional elements so that when they are available their unique characteristics can be fully taken advantage of.

In traditional filter design, ideal filters are approximated using methods that include Butterworth, Chebyshev, Elliptic, and Bessel filters. These filters attempt to approximate the ideal frequency response given by

$$H(\omega) = \begin{cases} 1, & \omega < \omega_c, \\ 0, & \text{elsewhere}, \end{cases} \tag{5}$$

for a lowpass filter that passes all frequencies below the cutoff frequency (ω_c) with no attenuation and removes all frequencies above. A necessary condition for physically realizable filters though is to satisfy the Paley-Wiener criterion [21] which requires a nonzero magnitude response. Hence, ideal filters are not physically realizable because they have a magnitude of zero in a certain frequency range. However, in [21] it was suggested that ideal filters when viewed from the fractional order perspective might not require satisfying the Paley-Wiener criterion to be physically realizable. If fractional order filters do not require satisfying the Paley-Wiener criterion it marks another significant different over their integer order counterparts; which requires further investigation to determine conclusively.

In this work we use a nonlinear least squares optimization routine to determine the coefficients of a fractional order transfer function required to approximate the passband ripple characteristics of traditional Chebyshev lowpass filters. MATLAB simulations of $(1 + \alpha)$, $(2 + \alpha)$, and $(3 + \alpha)$ order lowpass filters with fractional steps from $\alpha = 0.1$ to $\alpha = 0.9$ designed using this process are given as examples. SPICE simulations of 1.2, 1.5, and 1.8 order lowpass filters using approximated fractional order capacitors in a Tow-Thomas biquad circuit validate the implementation of these filter circuits.

1.1. Approximated Chebyshev Response. Fractional order lowpass filters with order $(1 + \alpha)$ have previously been designed in [9, 22] using the transfer function given by

$$H_{\text{LP}}^{1+\alpha}(s) = \frac{a_0}{a_1 s^{1+\alpha} + a_2 s^{\alpha} + 1} \tag{6}$$

and realized using various topologies including a Tow-Thomas biquad [9], fractional $\text{RL}_{\beta}\text{C}_{\alpha}$ circuits, and field programmable analog arrays (FPAAs) [22]. In [22] the coefficients of (6) were selected to approximate the flat passband response of the Butterworth filters. These coefficients were selected using a numerical search that compared the passband of the fractional filter to the Butterworth approximation over the frequency range $\omega = 0.01$ rad/s to 1 rad/s and returned the coefficients that yielded the lowest error over this region.

A similar method can be applied to determine the coefficients of (6) required to approximate the ripple characteristics in the passband of the Chebyshev approximation. Here a nonlinear least squares fitting is used that attempts to solve the problem

$$\begin{aligned} &\min_x \left\| |H(x,\omega)| - |C_n(\omega)| \right\|_2^2 \\ &\quad = \min_x \sum_{i=1}^{k} \left(|H(x,\omega_i)| - |C_n(\omega_i)| \right)^2 \\ &\text{s.t.} \quad x > 0.1, \end{aligned} \tag{7}$$

where x is the vector of filter coefficients, $|H(x)|$ is the magnitude response using (6) calculated using x, $|C_n(j\omega)|$ is the normalized nth order Chebyshev magnitude response, $|H(x,\omega_i)|$ and $|C_n(\omega_i)|$ are the magnitude responses of (6) and nth order Chebyshev approximation at frequency ω_i, and k is the total number of data points in the collected magnitude response. This routine aims to find the coefficients that minimize the error between the magnitude response of (6) and the Chebyshev approximation. The constraint $(x > 0.1)$ is added for this problem because negative coefficients are not physically possible and to return values will be easily realized in hardware. This is not the first application of optimization routines in the field of fractional filters. Previously, optimization routines have been employed in [23] to generate approximations of $1/(s + 1)^{\alpha}$ for simulation and further realization for audio applications.

Applying the nonlinear least squares fitting over the frequency range $\omega = 1 \times 10^{-5}$ rad/s to 1 rad/s using (6) and the second order Chebyshev filter designed with a ripple of 3 dB with transfer function

$$C_2(s) = \frac{0.5012}{s^2 + 0.6449s + 0.7079} \tag{8}$$

yields the coefficients given in Table 1 for orders $\alpha = 0.2$, 0.5, and 0.8. The 3 dB ripple was selected over smaller ripple magnitudes to highlight the difference in ripple size using the fractional order response over the integer order response. The coefficients were determined in MATLAB using the *lsqcurvefit* function to implement the NLSF described by (7). This function uses the trust-region-reflective algorithm [24] with termination tolerances of the function value and the solution set to 10^{-6}.

The magnitude responses using these coefficients, as well as those determined for orders $\alpha = 0.1$ to 0.9 in steps of 0.1, are given in Figure 1(a) as dashed lines. For comparison, the magnitude responses of first and second order Chebyshev lowpass filters with 3 dB ripples are also given. From these responses attenuations with fractional steps between the first

Table 1: Coefficient values for $(1+\alpha)$, $(2+\alpha)$, and $(3+\alpha)$ fractional order transfer functions to approximate Chebyshev passband response.

Order	α	a_0	a_1	a_2	a_3	a_4	a_5	a_6	$\lvert\theta_W\rvert_{\min}$
$1+\alpha$	0.2	0.7495	0.5095	0.1	—	—	—	—	16.5°
	0.5	0.7135	1.215	0.1	—	—	—	—	13.1°
	0.8	0.7107	1.5281	0.5092	—	—	—	—	11.9°
$2+\alpha$	0.2	1.061	2.246	0.1	2.1	0.2577	—	—	12.2°
	0.5	1.013	3.652	0.1	2.912	0.2608	—	—	10.5°
	0.8	1.002	4.252	1.210	3.481	0.1	—	—	10.0°
$3+\alpha$	0.2	0.7339	3.735	0.1	2.464	2.920	0.1	0.1	10.1°
	0.5	0.7146	5.734	0.1	2.878	3.907	0.1	0.3466	9.6°
	0.8	0.7087	6.256	1.246	6.592	0.1	1.894	0.1906	9.2°

and second order Chebyshev responses, with −20 dB/decade and −40 dB/decade attenuations, respectively, are visible above frequencies of 10 rad/s. In the inset highlighting the responses around 1 rad/s the increase in ripple size for increasing order is visible reaching values of −2.5867 dB, −0.8854 dB, and 0.0356 dB for $\alpha = 0.2$, 0.5, and 0.8, respectively. Therefore, using this method filter responses of order $(1+\alpha)$ with both fractional-step attenuation in the stopband and fractional ripple characteristics can be created.

This method can also be applied to create higher order filters with fractional characteristics in both stopband and passband. The fractional transfer function for a $(2+\alpha)$ filter response, developed by combining (6) and a bilinear transfer function, is given below:

$$H_{\mathrm{LP}}^{2+\alpha}(s) = \frac{a_0}{a_1 s^{2+\alpha} + a_2 s^{1+\alpha} + a_3 s + a_4 s^{\alpha} + 1}. \tag{9}$$

Applying (7) from $\omega = 1\times10^{-5}$ rad/s to 1 rad/s using (9) and the third order Chebyshev filter designed with a ripple of 3 dB given by the transfer function

$$C_3(s) = \frac{0.2506}{s^3 + 0.5972s^2 + 0.9283s + 0.2506} \tag{10}$$

yields the parameters given in Table 1 for orders $\alpha = 0.2$, 0.5, and 0.8. The magnitude responses using these parameters, as well as those determined for orders $\alpha = 0.1$ to 0.9 in steps of 0.1, are given in Figure 1(b) as dashed lines. For comparison the magnitude responses of second and third order Chebyshev lowpass filters with 3 dB ripples are also given. Again, fractional steps between the integer order magnitude responses are visible above frequencies of 10 rad/s. Similar to the $(1+\alpha)$ filter, the size of the ripples in the passband increases with the fractional order (α).

This method is further applied to create a $(3+\alpha)$ filter response, developed by combining (6) and a biquadratic transfer function, with transfer function given by

$$H_{\mathrm{LP}}^{3+\alpha}(s) = \frac{a_0}{a_1 s^{3+\alpha} + a_2 s^{2+\alpha} + a_3 s^2 + a_4 s^{1+\alpha} + a_5 s + a_6 s^{\alpha} + 1}. \tag{11}$$

Applying (7) from $\omega = 1\times10^{-5}$ rad/s to 1 rad/s using (11) and the fourth order Chebyshev filter designed with a ripple of 3 dB given by the transfer function

$$C_4(s) = \frac{0.1253}{s^4 + 0.5816s^3 + 1.1691s^2 + 0.4048s + 0.1770} \tag{12}$$

yields the parameters given in Table 1 for orders $\alpha = 0.2$, 0.5, and 0.8. The magnitude responses using these parameters, as well as those determined for orders $\alpha = 0.1$ to 0.9 in steps of 0.1, are given in Figure 1(c) as dashed lines. For comparison the magnitude responses of third and fourth order Chebyshev lowpass filters with 3 dB ripples are given.

While these filters exhibit fractional characteristics in their magnitude response, in the next section we analyze their stability to ensure that these fractional transfer functions are physically realizable.

1.2. Stability. Analyzing the stability of fractional filters requires conversion of the s-domain transfer functions to the W-plane defined in [25]. This transforms the transfer function from fractional order to integer order to be analyzed using traditional integer order analysis methods. The process for this analysis can be done using the following steps.

(1) Convert the fractional transfer function to the W-plane using the transformations $s = W^m$ and $\alpha = k/m$ [25].

(2) Select k and m for the desired α value.

(3) Solve the transformed transfer function for all poles in the W-plane and if any of the absolute pole angles, $\lvert\theta_W\rvert$, are less than $\pi/2m$ rad/s then the system is unstable; otherwise if all $\lvert\theta_W\rvert > \pi/2m$ then the system is stable.

Applying this process to the denominators of (6), (9), and (11) yields the characteristic equations in the W-plane given by

$$0 = a_1 W^{m+k} + a_2 W^k + 1, \tag{13}$$

$$0 = a_1 W^{2m+k} + a_2 W^{k+m} + a_3 W^m + a_4 W^k + 1, \tag{14}$$

$$0 = a_1 W^{3m+k} + a_2 W^{2m+k} + a_3 W^{2m} + a_4 W^{m+k} + a_5 W^k + a_6 W^m + 1. \tag{15}$$

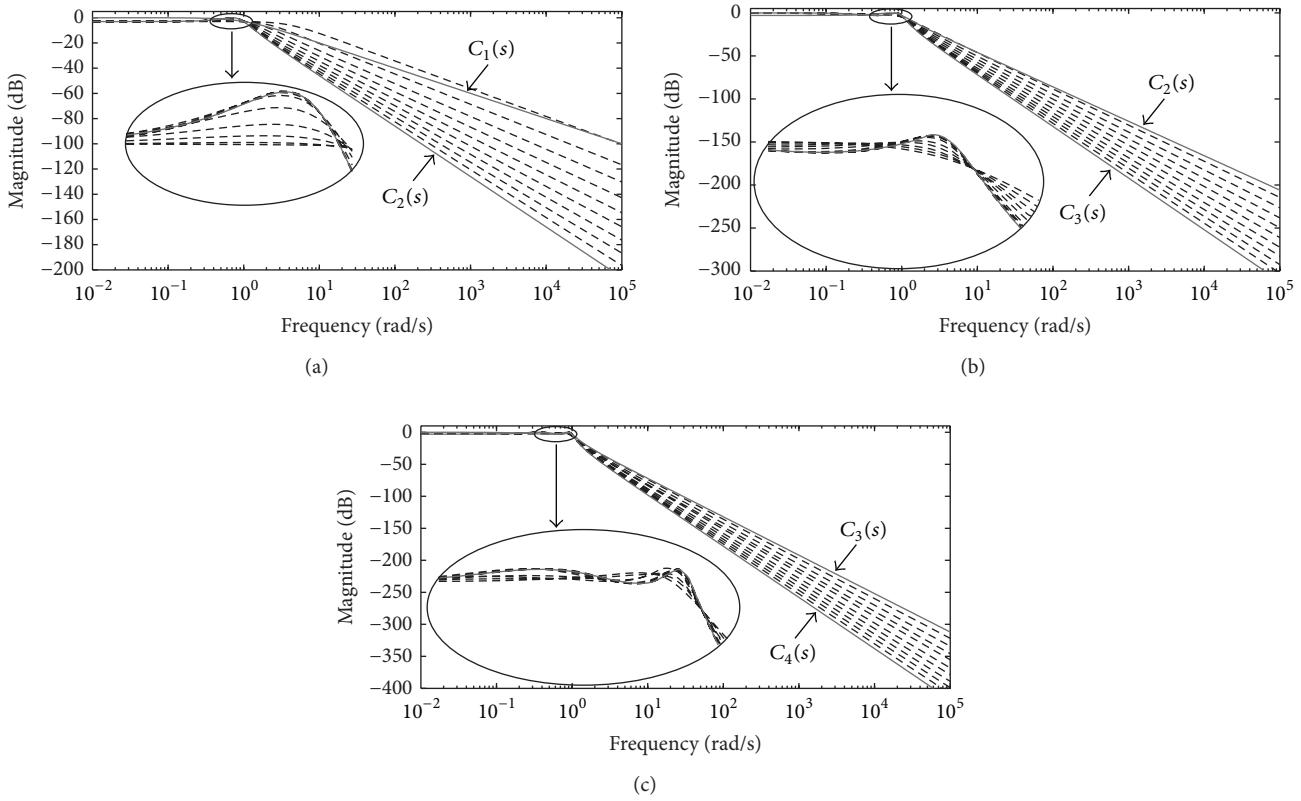

Figure 1: Simulated magnitude responses of (a) $(1 + \alpha)$, (b) $(2 + \alpha)$, and (c) $(3 + \alpha)$ lowpass fractional order filter circuits for $\alpha = 0.1$ to 0.9 in steps of 0.1 with coefficients selected to approximate Chebyshev passband response using nonlinear least squares fitting.

The roots of (13)–(15) for $\alpha = 0.1$, 0.5, and 0.9 were calculated with $k = 1$, 5, and 9, respectively, when $m = 10$. The minimum root angles, $|\theta_W|_{\min}$, for each case are given in Table 1. The angles for each case are greater than the minimum required angle, $|\theta_W| > \pi/2m = 9^\circ$, confirming that each filter using the coefficients in Table 1 is stable and can be physically realized.

2. Circuit Realization

The fractional order transfer function (6) can be realized by the Tow-Thomas biquad, given in Figure 2, when C_2 is replaced with a fractional order capacitor with impedance $Z_{C_2} = 1/s^\alpha C_2$ and $0 \le \alpha \le 1$. This topology was previously employed in [9] to realize fractional order filter circuits with flat passband characteristics and fractional attenuations in the stopband. The transfer function of the fractional order Tow-Thomas biquad at the noninverting lowpass output is given by

$$\frac{V_o(s)}{V_{in}(s)} = \frac{R_3R_5/R_4R_6}{s^{1+\alpha}R_2R_3C_1C_2 + s^\alpha\left(R_2R_3C_2/R_1\right) + 1}. \quad (16)$$

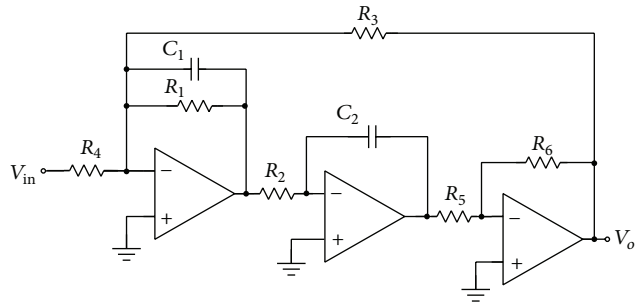

Figure 2: Tow-Thomas biquad topology.

Comparing the coefficients of (16) to (6) yields the following relationships:

$$a_0 = \frac{R_3R_5}{R_4R_6}, \quad (17)$$

$$a_1 = R_2R_3C_1C_2, \quad (18)$$

$$a_2 = \frac{R_2R_3C_2}{R_1}. \quad (19)$$

Table 2: Component values to realize (16) when $\alpha = 0.2$, 0.5, and 0.8.

Component	Values for FLPF of order		
	1.2	1.5	1.8
C_1 (F)		0.159 μ	
C_2 (F)	173.9 μ	12.6 μ	0.915 μ
R_1 (Ω)	5095	12.147 k	3.001 k
R_2 (Ω)	679.8	1702.5	2150.1
R_3 (Ω)	749.5	713.5	710.7
R_4, R_5, R_6 (Ω)		1000	

Using (17) to (19) we have 3 design equations and 8 variables yielding 5 degrees of freedom in our selection of the component values required to realize the desired a_0, a_1, and a_2 values for the approximated fractional Chebyshev magnitude response. Therefore, setting $C_1 = C_2 = 1$ F and $R_4 = R_5 = R_6 = 1\ \Omega$ the design equations for the remaining components become

$$a_0 = R_3, \tag{20}$$

$$a_1 = R_2 R_3, \tag{21}$$

$$a_2 = \frac{R_2 R_3}{R_1}. \tag{22}$$

Solving equations (20) to (22) with the $(1 + \alpha)$ coefficients from Table 1 for R_1, R_2, and R_3 yields the component values in Table 2 to realize the approximated fractional Chebyshev magnitude response, magnitude scaled by a factor of 1000 and frequency shifted to 1 kHz.

2.1. SPICE Simulations. Although there has been much progress towards realizing fractional order capacitors [18–20] there are currently no commercial devices using these processes available to implement these circuits, though their increasing progress towards commercialization highlights the need to research their use in electronic circuits to take advantage of their unique characteristics when they do become available. Until commercial devices with the desired characteristics become available integer order approximations must be used to realize fractional circuits. There are many methods to create an approximation of s^α which include continued fraction expansions (CFEs) as well as rational approximation methods [26]. These methods present a large array of approximations with the accuracy and approximated frequency band increasing as the order of the approximation increases. Here, a CFE method [27] was selected to model the fractional order capacitors for SPICE simulations. Collecting eight terms of the CFE yields a 4th order approximation of the fractional capacitor that can be physically realized using the RC ladder network in Figure 3.

The component values required for the 4th order approximation of the fractional capacitances with values of 173.9 μF, 12.6 μF, and 0.915 μF and orders 0.2, 0.5, and 0.8, respectively, using the RC ladder network in Figure 3, shifted to a center frequency of 1 kHz, are given in Table 3.

Table 3: Component values to realize 4th order approximations of fractional capacitors with values of 173.9 μF, 12.6 μF, and 0.915 μF and orders 0.2, 0.5, and 0.8, respectively. The center frequency is 1 kHz.

Component	Values		
	$C_2 = 173.9\ \mu$F $\alpha = 0.2$	$C_2 = 12.6\ \mu$F $\alpha = 0.5$	$C_2 = 0.915\ \mu$F $\alpha = 0.8$
R_a (Ω)	431.8	111.2	18.4
R_b (Ω)	285.2	251.7	92.8
R_c (Ω)	241.4	378.7	236.2
R_d (Ω)	337.2	888.9	981.6
R_e (Ω)	1020.2	7369.7	53.1 k
C_b (F)	53.5 n	83.7 n	301.3 n
C_c (F)	375.5 n	295.6 n	585.2 n
C_d (F)	1.114 μ	536.5 n	635.3 n
C_e (F)	2.804 μ	693.7 n	273.0 n

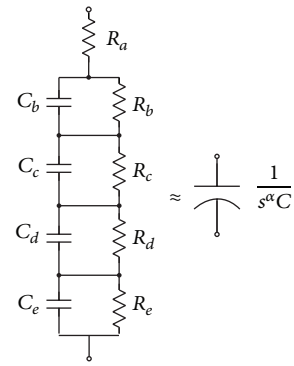

Figure 3: RC ladder structure to realize a 4th order integer approximation of a fractional order capacitor.

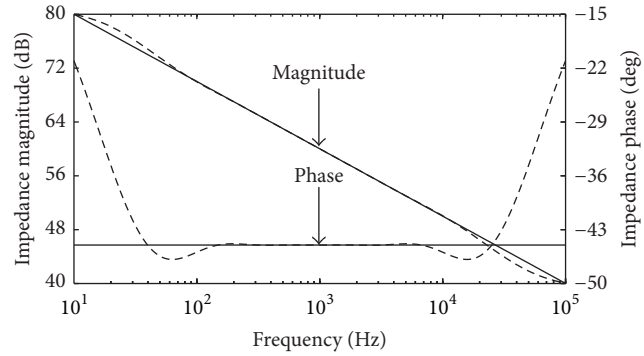

Figure 4: Magnitude and phase response of the approximated fractional order capacitor (dashed) compared to the ideal (solid) with capacitance of 12.6 μF and order 0.5 after scaling to a center frequency of 1 kHz.

The magnitude and phase of the ideal (solid line) and 4th order approximated (dashed) fractional order capacitor with capacitance 12.6 μF and order $\alpha = 0.5$, shifted to a center frequency of 1 kHz, are presented in Figure 4. From this figure we observe that the approximation is very good over almost 4 decades, from 200 Hz to 70 kHz, for the magnitude and

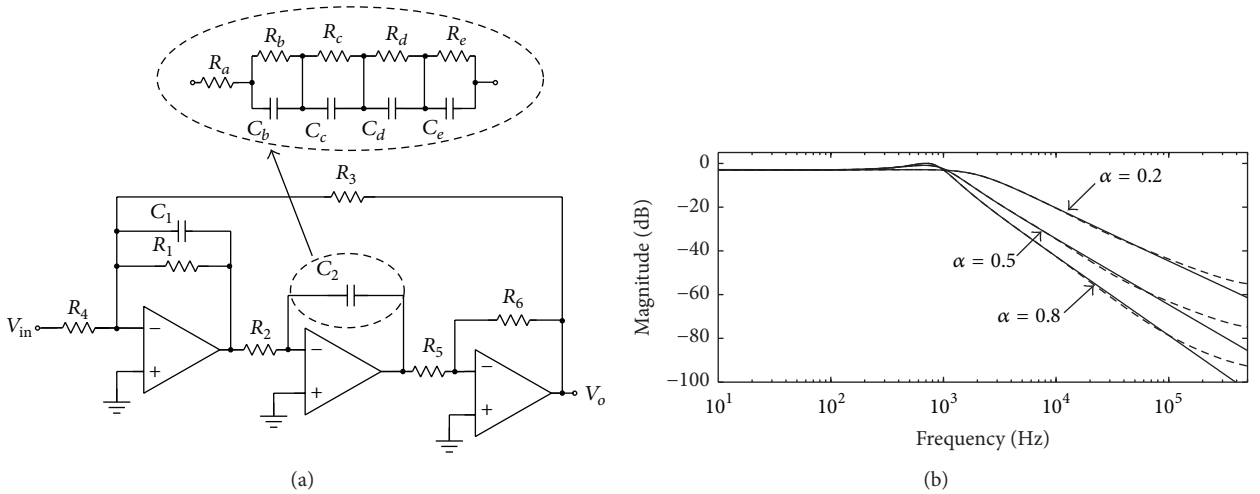

Figure 5: (a) Fractional Tow-Thomas biquad realized using approximated fractional capacitor and (b) SPICE simulated magnitude responses of $(1 + \alpha)$ lowpass fractional order filter circuits for $\alpha = 0.2$, 0.5, and 0.8 using component values from Tables 2 and 3.

almost 2 decades, from 200 Hz to 6 kHz, for the phase. In these regions, the deviation of the approximation from ideal does not exceed 1.23 dB and 0.23° for the magnitude and phase, respectively.

Using the component values in Tables 2 and 3, the approximated fractional Tow-Thomas biquad, shown in Figure 5(a), was simulated in LTSPICE IV using LT1037 op amps to realize responses of order $(1 + \alpha) = 1.2$, 1.5, and 1.8. The SPICE simulated magnitude responses (dashed lines) compared to the ideal responses (solid lines) are shown in Figure 5(b).

The SPICE simulated magnitude responses show very good agreement with the MATLAB simulated ideal responses. The deviations above 20 kHz can be attributed to the approximations of the fractional order capacitors which show significant error from their ideal behaviour above this frequency. These simulations verify that the fractional Tow-Thomas circuit can be used to realize the approximated fractional Chebyshev lowpass filter responses using approximated fractional order capacitors and that the correct selection of coefficients in the fractional order transfer function can yield ripples in the passband of the magnitude response.

3. Conclusion

We have proposed a new method using a nonlinear least squares optimization to determine the coefficients of fractional order transfer functions of order $(1+\alpha)$, $(2+\alpha)$, and $(3+\alpha)$ that will approximate the passband ripple characteristics of Chebyshev lowpass filters. These filter circuits were verified in simulation using approximated fractional order capacitors in a Tow-Thomas biquad circuit. This work has the potential to be applied to filters of any order and to also approximate the other traditional filter approximations using fractional order circuits that give a greater degree of control of the magnitude characteristics.

Conflict of Interests

The authors declare that there is no conflict of interests regarding the publication of this paper.

References

[1] A. S. Elwakil, "Fractional-order circuits and systems: an emerging interdisciplinary research area," *IEEE Circuits and Systems Magazine*, vol. 10, no. 4, pp. 40–50, 2010.

[2] A. G. Radwan, A. S. Elwakil, and A. Soliman, "Fractional-order sinusoidal oscillators: design procedure and practical examples," *IEEE Transactions on Circuits and Systems I: Regular Papers*, vol. 55, no. 7, pp. 2051–2063, 2008.

[3] A. Radwan, A. Elwakil, and A. Soliman, "On the generalization of second-order filters to the fractional order domain," *Journal of Circuits, Systems and Computers*, vol. 18, no. 2, pp. 361–386, 2009.

[4] P. Ahmadi, B. Maundy, A. S. Elwakil, and L. Belostostski, "High-quality factor asymmetric-slope band pass filters: a fractional-order capacitor approach," *IET Circuits, Devices & Systems*, vol. 6, no. 3, pp. 187–197, 2012.

[5] A. Soltan, A. G. Radwan, and A. M. Soliman, "Fractional order filter with two fractional elements of dependant orders," *Microelectronics Journal*, vol. 43, no. 11, pp. 818–827, 2012.

[6] A. G. Radwan and M. E. Fouda, "Optimization of fractional-order RLC filters," *Circuits, Systems, and Signal Processing*, vol. 32, no. 5, pp. 2097–2118, 2013.

[7] A. Lahiri and T. K. Rawat, "Noise analysis of single stage fractional-order low pass filter using stochastic and fractional calculus," *ECTI Transactions on Electronics and Communications*, vol. 7, no. 2, pp. 136–143, 2009.

[8] A. Radwan, "Stability analysis of the fractional-order $RL_\beta C_\alpha$ circuit," *Journal of Fractional Calculus and Applications*, vol. 3, no. 1, pp. 1–15, 2012.

[9] T. J. Freeborn, B. Maundy, and A. S. Elwakil, "Fractional-step Tow-Thomas biquad filters," *Nonlinear Theory and Its Applications, IEICE*, vol. 3, no. 3, pp. 357–374, 2012.

[10] A. S. Ali, A. G. Radwan, and A. M. Soliman, "Fractional order Butterw orth filter: active and passive realizations," *IEEE Journal on Emerging and Selected Topics in Circuits and Systems*, vol. 3, no. 3, pp. 346–354, 2013.

[11] M. C. Tripathy, K. Biswas, and S. Sen, "A design example of a fractional-order Kerwin-Huelsman-Newcomb biquad filter with two fractional capacitors of different order," *Circuits, Systems, and Signal Processing*, vol. 32, no. 4, pp. 1523–1536, 2013.

[12] M. C. Tripathy, D. Mondal, K. Biswas, and S. Sen, "Experimental studi es on realization of fractional inductors and fractionalorder bandpass filters," *International Journal of Circuit Theory and Applications*, 2014.

[13] A. Soltan, A. G. Radwan, and A. M. Soliman, "CCII based fractional filters of different orders," *Journal of Advanced Research*, vol. 5, no. 2, pp. 157–164, 2014.

[14] M. C. Tripathy, D. Mondal, K. Biswas, and S. Sen, "Design and performance study of phase-locked loop using fractional-order loop filter," *International Journal of Circuit Theory and Applications*, 2014.

[15] G. Tsirimokou, C. Laoudias, and C. Psychalinos, "0.5-V fractional-order companding filters," *International Journal of Circuit Theory and Applications*, 2014.

[16] I. Podlubny, *Fractional Differential Equations*, Academic Press, San Diego, Calif, USA, 1999.

[17] M. Nakagawa and K. Sorimachi, "Basic characteristics of a fractance device," *IEICE Transactions on Fundamentals of Electronics, Communications and Computer Sciences*, vol. 75, pp. 1814–1819, 1992.

[18] M. Sivarama Krishna, S. Das, K. Biswas, and B. Goswami, "Fabrication of a fractional order capacitor with desired specifications: a study on process identification and characterization," *IEEE Transactions on Electron Devices*, vol. 58, no. 11, pp. 4067–4073, 2011.

[19] T. Haba, G. Ablart, T. Camps, and F. Olivie, "Influence of the electrical parameters on the input impedance of a fractal structure realised on silicon," *Chaos, Solitons Fractals*, vol. 24, no. 2, pp. 479–490, 2005.

[20] A. M. Elshurafa, M. N. Almadhoun, K. N. Salama, and H. N. Alshareef, "Microscale electrostatic fractional capacitors using reduced graphene oxide percolated polymer composites," *Applied Physics Letters*, vol. 102, no. 23, Article ID 232901, 2013.

[21] R. C. Paley and N. Wiener, *Fourier Transforms in the Complex Domain*, American Mathematical Society Colloquium Publication, New York, NY, USA, 19th edition, 1934.

[22] T. J. Freeborn, B. Maundy, and A. S. Elwakil, "Field programmable an alogue array implementations of fractional step filters," *IET Digital Library: IET Circuits, Devices & Systems*, vol. 4, no. 6, pp. 514–524, 2010.

[23] T. Helie, "Simulation of fractional-order low-pass filters," *IEEE/ACM Transactions on Audio, Speech, and Language Processing*, vol. 22, no. 11, pp. 1636–1647, 2014.

[24] T. F. Coleman and Y. Li, "An interior trust region approach for nonlinear minimization subject to bounds," *SIAM Journal on Optimization*, vol. 6, no. 2, pp. 418–445, 1996.

[25] A. G. Radwan, A. M. Soliman, A. S. Elwakil, and A. Sedeek, "On the stability of linear systems with fractional-order elements," *Chaos, Solitons & Fractals*, vol. 40, no. 5, pp. 2317–2328, 2009.

[26] I. Podlubny, I. Petráš, B. M. Vinagre, P. O'Leary, and L. Dorčák, "Analogue realizations of fractional-order controllers," *Nonlinear Dynamics*, vol. 29, no. 1–4, pp. 281–296, 2002.

[27] B. T. Krishna and K. V. V. S. Reddy, "Active and passive realization of fractance device of order 1/2," *Active and Passive Electronic Components*, vol. 2008, Article ID 369421, 5 pages, 2008.

Research Article

On a Time-Fractional Integrodifferential Equation via Three-Point Boundary Value Conditions

Dumitru Baleanu,[1,2] Shahram Rezapour,[3] Sina Etemad,[3] and Ahmed Alsaedi[4]

[1] *Department of Mathematics, Cankaya University, Ogretmenler Caddesi 14, Balgat, 06530 Ankara, Turkey*
[2] *Institute of Space Sciences, Magurele, Bucharest, Romania*
[3] *Department of Mathematics, Azarbaijan Shahid Madani University, Azarshahr, Tabriz, Iran*
[4] *Department of Mathematics, Faculty of Science, King Abdulaziz University, Jeddah 21589, Saudi Arabia*

Correspondence should be addressed to Dumitru Baleanu; dumitru.baleanu@gmail.com

Received 15 July 2014; Revised 15 October 2014; Accepted 20 October 2014

Academic Editor: Guido Maione

Copyright © 2015 Dumitru Baleanu et al. This is an open access article distributed under the Creative Commons Attribution License, which permits unrestricted use, distribution, and reproduction in any medium, provided the original work is properly cited.

The existence and the uniqueness theorems play a crucial role prior to finding the numerical solutions of the fractional differential equations describing the models corresponding to the real world applications. In this paper, we study the existence of solutions for a time-fractional integrodifferential equation via three-point boundary value conditions.

1. Introduction

There is no doubt that the fractional calculus has various important applications in many fields as mathematics (see the following monographs [1, 2] and the references therein), physics [3], and economics [4], as well as in many other branches of science and engineering [3, 5, 6]. Recently the numerical methods were applied intensively to solve complicated fractional differential equations (FDE) which describe the real world applications. As an example, we mention that several physical processes exhibit fractional order behavior varying with time and/or space [7]. Thus, a class of phenomena can be obtained by analyzing this most general model. A fundamental step is to prove the existence and uniqueness of the proposed fractional nonlinear differential equations for these models. There are many works on fractional differential equations and inclusions. The existence of solutions for integrodifferential equations of fractional order with nonlocal three-point fractional boundary conditions was developed in [8] while the importance of antiperiodic type integral boundary conditions was discussed in [9]. The existence of solutions for fractional differential inclusions in the presence of the separated boundary conditions in Banach space was developed in [10]. We recall that the existence and multiplicity of positive solutions for singular fractional boundary value problems were analyzed in [11]. The existence and multiplicity of positive solutions for singular fractional boundary value problems were the topic debated in [12]. Making use of the fixed point results on cones, the existence and uniqueness of positive solutions for some nonlinear fractional differential equations were developed in [13]. Further results on positive solutions of a boundary value problem for nonlinear fractional differential equations were reported in [14] and new results on the existence results on nonlinear fractional differential equations were reported in [15]. For other related results we suggest for the readers [16, 17] as well as the references therein. We recall that the existence of solutions for some fractional partial differential equations was investigated in [18, 19] and the references therein.

Let n be a natural number, $n-1 < \alpha < n$, $a, b \in \mathbb{R}$, and $u \in C([a,b] \times [a,b], \mathbb{R})$. The Riemann-Liouville time-fractional order integral of the function u is defined by $I^{\alpha}_{*t}u(x,t) = (1/\Gamma(\alpha)) \int_0^t (u(x,\tau)/(t-\tau)^{1-\alpha}) d\tau$ for all $x, t \in [a,b]$ whenever the integral exists (more details regarding the basic definitions of the fractional calculus can be seen in [1]). Also, the Caputo derivative of time-fractional of order

α for the function u is defined by ${}^{c}D^{\alpha}_{*t}u(x,t) = (1/\Gamma(n-\alpha))\int_0^t (t-\tau)^{n-\alpha-1}(\partial^n u(x,\tau)/\partial\tau^n)d\tau$ (see for more details [1]). It has been proved that the general solution of the time-fractional differential equation ${}^{c}D^{\alpha}_{*t}u(x,t) = 0$ is given by $u(x,t) = c_0 + c_1 t + c_2 t^2 + \cdots + c_{n-1}t^{n-1}$, where $c_0, \ldots, c_{n-1}$ are real constants and $n = [\alpha] + 1$ (see [20]). Also, for each $T > 0$ and $u \in C([0,T]\times[0,T])$ we have $I^{\alpha}_{*t}\,{}^{c}D^{\alpha}_{*t}u(x,t) = u(x,t) + c_0 + c_1 t + c_2 t^2 + \cdots + c_{n-1}t^{n-1}$, where $c_0, \ldots, c_{n-1}$ are real constants and $n = [\alpha] + 1$ ([20]). Let M be a bounded set in a metric space (X,d). Then the Kuratowski measure of noncompactness is defined by (see [21])

$$\alpha(M) = \inf\{\epsilon : M \text{ covered by finitely many sets in which the diameter of each set is less than or equal to } \epsilon\}. \tag{1}$$

Let $\Phi : D(\Phi) \subseteq X \to X$ be a bounded and continuous operator on a Banach space X. Then Φ is called a condensing map whenever $\alpha(\Phi(B)) < \alpha(B)$ for all bounded sets $B \subset D(\Phi)$, where α denotes the Kuratowski measure of noncompactness (see [21]).

In this paper, we study the existence of solutions for a time-fractional integrodifferential equation via three-point boundary value conditions under certain conditions. We mention that the investigated equation generalized a huge class of classical ordinary differential equations which can be found in applications in engineering and physics. The boundary conditions used in this paper are as general as possible and for particular cases of the parameters we recover several cases of fractional nonlinear differential equations. In this way, we use the next Lemma and Sadovskii's fixed point theorem for condensing maps (see [22]).

Lemma 1 (see [23]). *Let X be a Banach space, $D \subseteq X$, $k \in [0,1)$, $K : D \to X$ a k-contraction, and $C : D \to X$ a compact operator. Then $K + C$ is a k-set contraction and so a condensing map.*

Theorem 2 (see [22]). *Let B be a convex, bounded, and closed subset of a Banach space X and $\Phi : B \to B$ a condensing map. Then Φ has a fixed point.*

2. Main Results

Suppose that $J = [0,1]\times[0,1]$, $1 \le q < 2$, and $X = \{u : u, (\partial^q/\partial t^q)u \in C(J,\mathbb{R})\}$ endowed via the norm

$$\|u\| = \sup_{(x,t)\in J}|u(x,t)| + \sup_{(x,t)\in J}\left|\frac{\partial^q}{\partial t^q}u(x,t)\right|, \tag{2}$$

where $(\partial^q/\partial t^q)u(x,t)$ denotes the standard Caputo time-fractional derivative. Let $2 \le \alpha < 3$, $0 < \beta < 1$, $1 \le \delta < 2$, $0 \le \eta \le 1$, and $\lambda, \mu \in \mathbb{R}$, and $f : J \times X^2 \to X$ and $g : J \times X \to X$ are continuous functions. We investigate the nonlinear time-fractional integrodifferential equation as follows:

$$-\frac{\partial^\alpha}{\partial t^\alpha}u(x,t) = \lambda f\left(x,t,u(x,t),\frac{\partial^q}{\partial t^q}u(x,t)\right) + \mu I^{\beta}_{*t}g(x,t,u(x,t)) \tag{$*$}$$

via the three-point boundary value conditions $(\partial^{\delta+1}/\partial t^{\delta+1})u(x,0) = (\partial^{\delta+1}/\partial t^{\delta+1})u(x,1)$, $(\partial^\delta/\partial t^\delta)u(x,1) - (\partial^\delta/\partial t^\delta)u(x,\eta) = 0$, and $u(x,0) = 0$. In this way, we give first next result.

Lemma 3. *An element u_0 in X is a solution for the problem $(*)$ via the three-point boundary value conditions if and only if u_0 is a solution for the time-fractional integral equation*

$$u(x,t) = \int_0^1 G_x(t,\tau)\left[\lambda f\left(x,\tau,u(x,\tau),\frac{\partial^q}{\partial\tau^q}u(x,\tau)\right) + \mu I^{\beta}_{*t}g(x,\tau,u(x,\tau))\right]d\tau, \tag{3}$$

where

$$\begin{aligned} G_x(t,\tau) &= -\frac{(t-\tau)^{\alpha-1}}{\Gamma(\alpha)} \\ &\quad + \left(\left[2t\Gamma(2-\delta)\left(1-\eta^{2-\delta}\right) + t^2\left(\eta^{1-\delta}-1\right)\Gamma(3-\delta)\right](1-\tau)^{\alpha-\delta-2}\right) \\ &\quad \times \left(2\Gamma(\alpha-\delta-1)\left[\eta^{1-\delta}(2-\delta)+\eta^{2-\delta}(\delta-1)-1\right]\right)^{-1} \\ &\quad + \frac{\left[t^2(1-\delta)\Gamma(3-\delta) - 2t\Gamma(3-\delta)\right](1-\tau)^{\alpha-\delta-1}}{2\Gamma(\alpha-\delta)\left[\eta^{1-\delta}(2-\delta)+\eta^{2-\delta}(\delta-1)-1\right]} \\ &\quad + \frac{\left[2t\Gamma(3-\delta) - t^2(1-\delta)\Gamma(3-\delta)\right](\eta-\tau)^{\alpha-\delta-1}}{\Gamma(\alpha-\delta)2\left[\eta^{1-\delta}(2-\delta)+\eta^{2-\delta}(\delta-1)-1\right]}, \end{aligned} \tag{4}$$

whenever $0 \le \tau \le \eta \le t \le 1$,

$$\begin{aligned} G_x(t,\tau) &= -\frac{(t-\tau)^{\alpha-1}}{\Gamma(\alpha)} \\ &\quad + \left(\left[2t\Gamma(2-\delta)\left(1-\eta^{2-\delta}\right) + t^2\left(\eta^{1-\delta}-1\right)\Gamma(3-\delta)\right](1-\tau)^{\alpha-\delta-2}\right) \\ &\quad \times \left(2\Gamma(\alpha-\delta-1)\left[\eta^{1-\delta}(2-\delta)+\eta^{2-\delta}(\delta-1)-1\right]\right)^{-1} \\ &\quad + \frac{\left[t^2(1-\delta)\Gamma(3-\delta) - 2t\Gamma(3-\delta)\right](1-\tau)^{\alpha-\delta-1}}{2\Gamma(\alpha-\delta)\left[\eta^{1-\delta}(2-\delta)+\eta^{2-\delta}(\delta-1)-1\right]}, \end{aligned} \tag{5}$$

whenever $0 \le \eta \le \tau \le t \le 1$,

$$\begin{aligned} G_x(t,\tau) &= \left(\left[2t\Gamma(2-\delta)\left(1-\eta^{2-\delta}\right)\right.\right. \\ &\quad \left.\left.+t^2\left(\eta^{1-\delta}-1\right)\Gamma(3-\delta)\right](1-\tau)^{\alpha-\delta-2}\right) \\ &\quad \times\left(2\Gamma(\alpha-\delta-1)\left[\eta^{1-\delta}(2-\delta)+\eta^{2-\delta}(\delta-1)-1\right]\right)^{-1} \\ &\quad +\frac{\left[t^2(1-\delta)\Gamma(3-\delta)-2t\Gamma(3-\delta)\right](1-\tau)^{\alpha-\delta-1}}{2\Gamma(\alpha-\delta)\left[\eta^{1-\delta}(2-\delta)+\eta^{2-\delta}(\delta-1)-1\right]}, \end{aligned} \tag{6}$$

whenever $0 \le \eta \le t \le \tau \le 1$,

$$\begin{aligned} G_x(t,\tau) &= \left(\left[2t\Gamma(2-\delta)\left(1-\eta^{2-\delta}\right)\right.\right. \\ &\quad \left.\left.+t^2\left(\eta^{1-\delta}-1\right)\Gamma(3-\delta)\right](1-\tau)^{\alpha-\delta-2}\right) \\ &\quad \times\left(2\Gamma(\alpha-\delta-1)\left[\eta^{1-\delta}(2-\delta)+\eta^{2-\delta}(\delta-1)-1\right]\right)^{-1} \\ &\quad +\frac{\left[t^2(1-\delta)\Gamma(3-\delta)-2t\Gamma(3-\delta)\right](1-\tau)^{\alpha-\delta-1}}{2\Gamma(\alpha-\delta)\left[\eta^{1-\delta}(2-\delta)+\eta^{2-\delta}(\delta-1)-1\right]}, \end{aligned} \tag{7}$$

whenever $0 \le t \le \eta \le \tau \le 1$,

$$\begin{aligned} G_x(t,\tau) &= \left(\left[2t\Gamma(2-\delta)\left(1-\eta^{2-\delta}\right)\right.\right. \\ &\quad \left.\left.+t^2\left(\eta^{1-\delta}-1\right)\Gamma(3-\delta)\right](1-\tau)^{\alpha-\delta-2}\right) \\ &\quad \times\left(2\Gamma(\alpha-\delta-1)\left[\eta^{1-\delta}(2-\delta)+\eta^{2-\delta}(\delta-1)-1\right]\right)^{-1} \\ &\quad +\frac{\left[t^2(1-\delta)\Gamma(3-\delta)-2t\Gamma(3-\delta)\right](1-\tau)^{\alpha-\delta-1}}{2\Gamma(\alpha-\delta)\left[\eta^{1-\delta}(2-\delta)+\eta^{2-\delta}(\delta-1)-1\right]} \\ &\quad +\frac{\left[2t\Gamma(3-\delta)-t^2(1-\delta)\Gamma(3-\delta)\right](\eta-\tau)^{\alpha-\delta-1}}{\Gamma(\alpha-\delta)2\left[\eta^{1-\delta}(2-\delta)+\eta^{2-\delta}(\delta-1)-1\right]}, \end{aligned} \tag{8}$$

whenever $0 \le t \le \tau \le \eta \le 1$, *and*

$$\begin{aligned} G_x(t,\tau) &= -\frac{(t-\tau)^{\alpha-1}}{\Gamma(\alpha)} \\ &\quad +\left(\left[2t\Gamma(2-\delta)\left(1-\eta^{2-\delta}\right)\right.\right. \\ &\quad \left.\left.+t^2\left(\eta^{1-\delta}-1\right)\Gamma(3-\delta)\right](1-\tau)^{\alpha-\delta-2}\right) \\ &\quad \times\left(2\Gamma(\alpha-\delta-1)\left[\eta^{1-\delta}(2-\delta)+\eta^{2-\delta}(\delta-1)-1\right]\right)^{-1} \\ &\quad +\frac{\left[t^2(1-\delta)\Gamma(3-\delta)-2t\Gamma(3-\delta)\right](1-\tau)^{\alpha-\delta-1}}{2\Gamma(\alpha-\delta)\left[\eta^{1-\delta}(2-\delta)+\eta^{2-\delta}(\delta-1)-1\right]} \\ &\quad +\frac{\left[2t\Gamma(3-\delta)-t^2(1-\delta)\Gamma(3-\delta)\right](\eta-\tau)^{\alpha-\delta-1}}{\Gamma(\alpha-\delta)2\left[\eta^{1-\delta}(2-\delta)+\eta^{2-\delta}(\delta-1)-1\right]}, \end{aligned} \tag{9}$$

whenever $0 \le \tau \le t \le \eta \le 1$.

Proof. Let u_0 be a solution for the time-fractional integrodifferential equation $(*)$ via the boundary value conditions. Put $y_0(x,t) = \lambda f(x,t,u_0(x,t),(\partial^q/\partial t^q)u_0(x,t)) + \mu I^{\beta}_{*t} g(x,t,u_0(x,t))$. Choose $c_0, c_1, c_2 \in \mathbb{R}$ such that $u_0(x,t) = -\int_0^t ((t-\tau)^{\alpha-1}/\Gamma(\alpha))y_0(x,\tau)d\tau + c_0 + c_1 t + c_2 t^2$. Thus, we get

$$\begin{aligned} \frac{\partial^{\delta}}{\partial t^{\delta}}u_0(x,t) &= -\int_0^t \frac{(t-\tau)^{\alpha-\delta-1}}{\Gamma(\alpha-\delta)}y_0(x,\tau)\,d\tau \\ &\quad +c_1\frac{t^{1-\delta}}{\Gamma(2-\delta)}+c_2\frac{2t^{2-\delta}}{\Gamma(3-\delta)} \end{aligned} \tag{10}$$

and $(\partial^{\delta+1}/\partial t^{\delta+1})u_0(x,t) = -\int_0^t ((t-\tau)^{\alpha-\delta-2}/\Gamma(\alpha-\delta-1))y_0(x,\tau)d\tau + c_1(t^{-\delta}/\Gamma(1-\delta)) + c_2(2t^{1-\delta}/\Gamma(2-\delta))$. Now by using the boundary value conditions, we obtain $c_0 = 0$,

$$\begin{aligned} c_1 &= \frac{\Gamma(2-\delta)\left(1-\eta^{2-\delta}\right)}{\left[\eta^{1-\delta}(2-\delta)+\eta^{2-\delta}(\delta-1)-1\right]} \\ &\quad \times\int_0^1 \frac{(1-\tau)^{\alpha-\delta-2}}{\Gamma(\alpha-\delta-1)}y_0(x,\tau)\,d\tau \\ &\quad -\frac{\Gamma(3-\delta)}{\left[\eta^{1-\delta}(2-\delta)+\eta^{2-\delta}(\delta-1)-1\right]} \\ &\quad \times\int_0^1 \frac{(1-\tau)^{\alpha-\delta-1}}{\Gamma(\alpha-\delta)}y_0(x,\tau)\,d\tau \\ &\quad +\frac{\Gamma(3-\delta)}{\left[\eta^{1-\delta}(2-\delta)+\eta^{2-\delta}(\delta-1)-1\right]} \\ &\quad \times\int_0^{\eta} \frac{(\eta-\tau)^{\alpha-\delta-1}}{\Gamma(\alpha-\delta)}y_0(x,\tau)\,d\tau, \\ c_2 &= \frac{(1-\delta)\Gamma(3-\delta)}{2\left[\eta^{1-\delta}(2-\delta)+\eta^{2-\delta}(\delta-1)-1\right]} \\ &\quad \times\int_0^1 \frac{(1-\tau)^{\alpha-\delta-1}}{\Gamma(\alpha-\delta)}y_0(x,\tau)\,d\tau \end{aligned}$$

$$
\begin{aligned}
&- \frac{(1-\delta)\,\Gamma(3-\delta)}{2\left[\eta^{1-\delta}(2-\delta)+\eta^{2-\delta}(\delta-1)-1\right]} \\
&\times \int_0^{\eta} \frac{(\eta-\tau)^{\alpha-\delta-1}}{\Gamma(\alpha-\delta)}\, y_0(x,\tau)\, d\tau \\
&+ \frac{\left(\eta^{1-\delta}-1\right)\Gamma(3-\delta)}{2\left[\eta^{1-\delta}(2-\delta)+\eta^{2-\delta}(\delta-1)-1\right]} \\
&\times \int_0^{1} \frac{(1-\tau)^{\alpha-\delta-2}}{\Gamma(\alpha-\delta-1)}\, y_0(x,\tau)\, d\tau.
\end{aligned} \tag{11}
$$

Hence,

$$
\begin{aligned}
u_0(x,t) &= -\int_0^t \frac{(t-\tau)^{\alpha-1}}{\Gamma(\alpha)}\, y_0(x,\tau)\, d\tau \\
&+ \frac{2t\Gamma(2-\delta)\left(1-\eta^{2-\delta}\right)+t^2\left(\eta^{1-\delta}-1\right)\Gamma(3-\delta)}{2\left[\eta^{1-\delta}(2-\delta)+\eta^{2-\delta}(\delta-1)-1\right]} \\
&\times \int_0^{1} \frac{(1-\tau)^{\alpha-\delta-2}}{\Gamma(\alpha-\delta-1)}\, y_0(x,\tau)\, d\tau \\
&+ \frac{t^2(1-\delta)\,\Gamma(3-\delta)-2t\Gamma(3-\delta)}{2\left[\eta^{1-\delta}(2-\delta)+\eta^{2-\delta}(\delta-1)-1\right]} \\
&\times \int_0^{1} \frac{(1-\tau)^{\alpha-\delta-1}}{\Gamma(\alpha-\delta)}\, y_0(x,\tau)\, d\tau \\
&+ \frac{2t\Gamma(3-\delta)-t^2(1-\delta)\,\Gamma(3-\delta)}{2\left[\eta^{1-\delta}(2-\delta)+\eta^{2-\delta}(\delta-1)-1\right]} \\
&\times \int_0^{\eta} \frac{(\eta-\tau)^{\alpha-\delta-1}}{\Gamma(\alpha-\delta)}\, y_0(x,\tau)\, d\tau \\
&= \int_0^1 G_x(t,\tau)\, y_0(x,\tau)\, d\tau.
\end{aligned} \tag{12}
$$

Thus, u_0 is a solution for the time-fractional integral equation. It is obvious that u_0 is a solution for the time-fractional integrodifferential equation $(*)$ whenever u_0 is a solution for the time-fractional integral equation. This completes the proof. □

By considering the proof of last result, one can get that the solution of the time-fractional integrodifferential equation $(*)$ is in the form

$$
\begin{aligned}
u(x,t) &= -\lambda \int_0^t \frac{(t-\tau)^{\alpha-1}}{\Gamma(\alpha)} f\left(x,\tau,u(x,\tau),\frac{\partial^q}{\partial t^q}u(x,\tau)\right) d\tau \\
&- \mu \int_0^t \frac{(t-\tau)^{\alpha+\beta-1}}{\Gamma(\alpha+\beta)}\, g(x,\tau,u(x,\tau))\, d\tau \\
&+ \frac{tQ+t^2R}{2N}\lambda \\
&\times \int_0^1 \frac{(1-\tau)^{\alpha-\delta-2}}{\Gamma(\alpha-\delta-1)} f\left(x,\tau,u(x,\tau),\frac{\partial^q}{\partial t^q}u(x,\tau)\right) d\tau \\
&+ \frac{tQ+t^2R}{2N}\mu \\
&\times \int_0^1 \frac{(1-\tau)^{\alpha+\beta-\delta-2}}{\Gamma(\alpha+\beta-\delta-1)}\, g(x,\tau,u(x,\tau))\, d\tau \\
&+ \frac{t^2S-tM}{2N}\lambda \\
&\times \int_0^1 \frac{(1-\tau)^{\alpha-\delta-1}}{\Gamma(\alpha-\delta)} f\left(x,\tau,u(x,\tau),\frac{\partial^q}{\partial t^q}u(x,\tau)\right) d\tau \\
&+ \frac{t^2S-tM}{2N}\mu \int_0^1 \frac{(1-\tau)^{\alpha+\beta-\delta-1}}{\Gamma(\alpha+\beta-\delta)}\, g(x,\tau,u(x,\tau))\, d\tau \\
&+ \frac{tM-t^2S}{2N}\lambda \\
&\times \int_0^{\eta} \frac{(\eta-\tau)^{\alpha-\delta-1}}{\Gamma(\alpha-\delta)} f\left(x,\tau,u(x,\tau),\frac{\partial^q}{\partial t^q}u(x,\tau)\right) d\tau \\
&+ \frac{tM-t^2S}{2N}\mu \int_0^{\eta} \frac{(\eta-\tau)^{\alpha+\beta-\delta-1}}{\Gamma(\alpha+\beta-\delta)}\, g(x,\tau,u(x,\tau))\, d\tau,
\end{aligned} \tag{13}
$$

where $Q = 2\Gamma(2-\delta)(1-\eta^{2-\delta})$, $R = (\eta^{1-\delta}-1)\Gamma(3-\delta)$, $S = (1-\delta)\Gamma(3-\delta)$, $M = 2\Gamma(3-\delta)$, and $N = [\eta^{1-\delta}(2-\delta)+\eta^{2-\delta}(\delta-1)-1]$ with $\eta^{1-\delta}, \eta^{2-\delta} \neq 1$.

Theorem 4. *Let $p_1 \in (0,1)$, $p_2 \in (0, \alpha-\delta)$, $p = \min\{p_1, p_2\}$, $L, m \in L_{1/p}([0,1], \mathbb{R}^+)$, and $\psi : \mathbb{R}^+ \to \mathbb{R}^+$ be a nondecreasing bounded function. Suppose that $f : J \times X^2 \to X$ and $g : J \times X \to X$ are continuous functions such that $|f(x,t,u,w) - f(x,t,v,z)| \leq L(t)(|u-v| + |w-z|)$ and $|g(x,t,u(x,t)| \leq m(t)\psi(\|u\|)$ for all $(x,t) \in J$ and $u, v, w, z \in X$. Put*

$$
\begin{aligned}
\gamma := |\lambda| &\left[\frac{1}{\Gamma(\alpha)} \left(\frac{1-p}{\alpha-p}\right)^{1-p} + \frac{1}{\Gamma(\alpha-q)} \left(\frac{1-p}{\alpha-q-p}\right)^{1-p} \right. \\
&+ \left|\frac{Q+R}{2N}\right| \frac{1}{\Gamma(\alpha-\delta-1)} \left(\frac{1-p}{\alpha-\delta-p-1}\right)^{1-p} \\
&+ \left|\frac{(2-q)Q+2R}{2N\Gamma(3-q)}\right| \frac{1}{\Gamma(\alpha-\delta-1)} \\
&\times \left(\frac{1-p}{\alpha-\delta-p-1}\right)^{1-p} \\
&+ \left|\frac{S}{2N}\right| \frac{\left(1+\eta^{\alpha-\delta-p}\right)}{\Gamma(\alpha-\delta)} \left(\frac{1-p}{\alpha-\delta-p}\right)^{1-p} \\
&+ \left|\frac{2S-(2-q)M}{2N\Gamma(3-q)}\right| \frac{\left(1+\eta^{\alpha-\delta-p}\right)}{\Gamma(\alpha-\delta)} \\
&\left. \times \left(\frac{1-p}{\alpha-\delta-p}\right)^{1-p} \right] \|L\|_{1/p}.
\end{aligned} \tag{14}
$$

If $\gamma < 1$, then the time-fractional integrodifferential equation $(*)$ has at least one solution.

Proof. First, put

$$\begin{aligned} w &= |\lambda|\,\sigma + |\mu|\,b \\ &\times \left[\frac{1}{\Gamma(\alpha+\beta)} \left(\frac{1-p}{\alpha+\beta-p} \right)^{1-p} + \frac{1}{\Gamma(\alpha+\beta-q)} \right. \\ &\times \left(\frac{1-p}{\alpha+\beta-q-p} \right)^{1-p} + \left| \frac{Q+R}{2N} \right| \frac{1}{\Gamma(\alpha+\beta-\delta-1)} \\ &\times \left(\frac{1-p}{\alpha+\beta-\delta-p-1} \right)^{1-p} + \left| \frac{(2-q)Q+2R}{2N\Gamma(3-q)} \right| \\ &\times \frac{1}{\Gamma(\alpha+\beta-\delta-1)} \left(\frac{1-p}{\alpha+\beta-\delta-p-1} \right)^{1-p} \\ &+ \left| \frac{S}{2N} \right| \frac{\left(1+\eta^{\alpha+\beta-\delta-p}\right)}{\Gamma(\alpha+\beta-\delta)} \left(\frac{1-p}{\alpha+\beta-\delta-p} \right)^{1-p} \\ &+ \left| \frac{2S-(2-q)M}{2N\Gamma(3-q)} \right| \frac{\left(1+\eta^{\alpha+\beta-\delta-p}\right)}{\Gamma(\alpha+\beta-\delta)} \\ &\times \left. \left(\frac{1-p}{\alpha+\beta-\delta-p} \right)^{1-p} \right] \|m\|_{1/p}, \end{aligned} \tag{15}$$

where

$$\begin{aligned} \sigma = K &\left(\frac{1}{\Gamma(\alpha+1)} + \frac{1}{\Gamma(\alpha-q+1)} \right. \\ &+ \left| \frac{Q+R}{2N} \right| \frac{1}{\Gamma(\alpha-\delta)} + \left| \frac{(2-q)Q+2R}{2N\Gamma(3-q)} \right| \frac{1}{\Gamma(\alpha-\delta)} \\ &+ \left| \frac{S}{2N} \right| \left(\frac{1+\eta^{\alpha-\delta}}{\Gamma(\alpha-\delta+1)} \right) \\ &+ \left. \left| \frac{2S-(2-q)M}{2N\Gamma(3-q)} \right| \left(\frac{1+\eta^{\alpha-\delta}}{\Gamma(\alpha-\delta+1)} \right) \right). \end{aligned} \tag{16}$$

Now, choose $r \geq w/(1-\gamma)$ and consider the closed, convex, and bounded subset $B_r = \{u \in X : \|u\| \leq r\}$ of X. Define the operator $\Phi : B_r \to X$ by

$$\begin{aligned} &(\Phi u)(x,t) \\ &= -\lambda \int_0^t \frac{(t-\tau)^{\alpha-1}}{\Gamma(\alpha)} f\left(x, \tau, u(x,\tau), \frac{\partial^q}{\partial t^q} u(x,\tau) \right) d\tau \\ &- \mu \int_0^t \frac{(t-\tau)^{\alpha+\beta-1}}{\Gamma(\alpha+\beta)} g(x,\tau,u(x,\tau))\,d\tau + \frac{tQ+t^2R}{2N} \\ &\times \left[\lambda \int_0^1 \frac{(1-\tau)^{\alpha-\delta-2}}{\Gamma(\alpha-\delta-1)} f\left(x, \tau, u(x,\tau), \frac{\partial^q}{\partial t^q} u(x,\tau) \right) d\tau \right. \\ &+ \left. \mu \int_0^1 \frac{(1-\tau)^{\alpha+\beta-\delta-2}}{\Gamma(\alpha+\beta-\delta-1)} g(x,\tau,u(x,\tau))\,d\tau \right] \\ &+ \frac{t^2S-tM}{2N} \\ &\times \left[\lambda \int_0^1 \frac{(1-\tau)^{\alpha-\delta-1}}{\Gamma(\alpha-\delta)} f\left(x, \tau, u(x,\tau), \frac{\partial^q}{\partial t^q} u(x,\tau) \right) d\tau \right. \\ &+ \mu \int_0^1 \frac{(1-\tau)^{\alpha+\beta-\delta-1}}{\Gamma(\alpha+\beta-\delta)} g(x,\tau,u(x,\tau))\,d\tau \\ &- \lambda \int_0^\eta \frac{(\eta-\tau)^{\alpha-\delta-1}}{\Gamma(\alpha-\delta)} f\left(x, \tau, u(x,\tau), \frac{\partial^q}{\partial t^q} u(x,\tau) \right) d\tau \\ &- \left. \mu \int_0^\eta \frac{(\eta-\tau)^{\alpha+\beta-\delta-1}}{\Gamma(\alpha+\beta-\delta)} g(x,\tau,u(x,\tau))\,d\tau \right], \end{aligned} \tag{17}$$

for all $(x,t) \in J$. Now, decompose Φ by $\Phi = \Phi_1 + \Phi_2$, where

$$\begin{aligned} &(\Phi_1 u)(x,t) \\ &= -\lambda \int_0^t \frac{(t-\tau)^{\alpha-1}}{\Gamma(\alpha)} f\left(x, \tau, u(x,\tau), \frac{\partial^q}{\partial t^q} u(x,\tau) \right) d\tau \\ &+ \frac{tQ+t^2R}{2N} \lambda \\ &\times \int_0^1 \frac{(1-\tau)^{\alpha-\delta-2}}{\Gamma(\alpha-\delta-1)} f\left(x, \tau, u(x,\tau), \frac{\partial^q}{\partial t^q} u(x,\tau) \right) d\tau \\ &+ \frac{t^2S-tM}{2N} \lambda \\ &\times \left[\int_0^1 \frac{(1-\tau)^{\alpha-\delta-1}}{\Gamma(\alpha-\delta)} f\left(x, \tau, u(x,\tau), \frac{\partial^q}{\partial t^q} u(x,\tau) \right) d\tau \right. \\ &- \left. \int_0^\eta \frac{(\eta-\tau)^{\alpha-\delta-1}}{\Gamma(\alpha-\delta)} f\left(x, \tau, u(x,\tau), \frac{\partial^q}{\partial t^q} u(x,\tau) \right) d\tau \right], \end{aligned}$$

$$\begin{aligned} &(\Phi_2 u)(x,t) \\ &= -\mu \int_0^t \frac{(t-\tau)^{\alpha+\beta-1}}{\Gamma(\alpha+\beta)} g(x,\tau,u(x,\tau))\,d\tau \\ &+ \frac{tQ+t^2R}{2N} \mu \int_0^1 \frac{(1-\tau)^{\alpha+\beta-\delta-2}}{\Gamma(\alpha+\beta-\delta-1)} g(x,\tau,u(x,\tau))\,d\tau \\ &+ \frac{t^2S-tM}{2N} \left[\mu \int_0^1 \frac{(1-\tau)^{\alpha+\beta-\delta-1}}{\Gamma(\alpha+\beta-\delta)} g(x,\tau,u(x,\tau))\,d\tau \right. \\ &- \left. \mu \int_0^\eta \frac{(\eta-\tau)^{\alpha+\beta-\delta-1}}{\Gamma(\alpha+\beta-\delta)} g(x,\tau,u(x,\tau))\,d\tau \right], \end{aligned} \tag{18}$$

for all $(x,t) \in J$. Now, we show that $\Phi(B_r) \subset B_r$. Let $\sup_{x,t\in[0,1]}|f(x,t,0,0)| \le K$, $(x,t) \in J$, and $u \in B_r$. Then, we have

$$
\begin{aligned}
&\left|\Phi_1 u(x,t)\right| \\
&\le |\lambda| \left| \int_0^t \frac{(t-\tau)^{\alpha-1}}{\Gamma(\alpha)} \right. \\
&\qquad \left. \times \left[f\left(x,\tau,u(x,\tau),\frac{\partial^q}{\partial t^q}u(x,\tau)\right) \right. \right. \\
&\qquad \left. \left. - f(x,\tau,0,0) + f(x,\tau,0,0) \right] d\tau \right| \\
&\quad + \left|\frac{Q+R}{2N}\right| |\lambda| \\
&\quad \times \left| \int_0^1 \frac{(1-\tau)^{\alpha-\delta-2}}{\Gamma(\alpha-\delta-1)} \left[f\left(x,\tau,u(x,\tau),\frac{\partial^q}{\partial t^q}u(x,\tau)\right) \right. \right. \\
&\qquad \left. \left. - f(x,\tau,0,0) + f(x,\tau,0,0) \right] d\tau \right| \\
&\quad + \left|\frac{S}{2N}\right| |\lambda| \left| \int_0^1 \frac{(1-\tau)^{\alpha-\delta-1}}{\Gamma(\alpha-\delta)} \right. \\
&\qquad \left. \times \left[f\left(x,\tau,u(x,\tau),\frac{\partial^q}{\partial t^q}u(x,\tau)\right) \right. \right. \\
&\qquad \left. \left. - f(x,\tau,0,0) + f(x,\tau,0,0) \right] d\tau \right| \\
&\quad + \left|\frac{S}{2N}\right| |\lambda| \left| \int_0^\eta \frac{(\eta-\tau)^{\alpha-\delta-1}}{\Gamma(\alpha-\delta)} \right. \\
&\qquad \left. \times \left[f\left(x,\tau,u(x,\tau),\frac{\partial^q}{\partial t^q}u(x,\tau)\right) \right. \right. \\
&\qquad \left. \left. - f(x,\tau,0,0) + f(x,\tau,0,0) \right] d\tau \right| \\
&\le |\lambda| r \left[\int_0^t \frac{(t-\tau)^{\alpha-1}}{\Gamma(\alpha)} L(\tau)\, d\tau \right] + \frac{|\lambda| K}{\Gamma(\alpha+1)} \\
&\quad + \left|\frac{Q+R}{2N}\right| |\lambda| r \left[\int_0^1 \frac{(1-\tau)^{\alpha-\delta-2}}{\Gamma(\alpha-\delta-1)} L(\tau)\, d\tau \right] \\
&\quad + \left|\frac{Q+R}{2N}\right| |\lambda| \frac{K}{\Gamma(\alpha-\delta)} \\
&\quad + \left|\frac{S}{2N}\right| |\lambda| r \left[\int_0^1 \frac{(1-\tau)^{\alpha-\delta-1}}{\Gamma(\alpha-\delta)} L(\tau)\, d\tau \right] \\
&\quad + \left|\frac{S}{2N}\right| |\lambda| \frac{K}{\Gamma(\alpha-\delta+1)} \\
&\quad + \left|\frac{S}{2N}\right| |\lambda| r \left[\int_0^\eta \frac{(\eta-\tau)^{\alpha-\delta-1}}{\Gamma(\alpha-\delta)} L(\tau)\, d\tau \right] \\
&\quad + \left|\frac{S}{2N}\right| |\lambda| \frac{K\eta^{\alpha-\delta}}{\Gamma(\alpha-\delta+1)} \\
&\le \frac{|\lambda| r}{\Gamma(\alpha)} \left(\int_0^t (t-\tau)^{(\alpha-1)/(1-p)}\, d\tau \right)^{1-p} \left(\int_0^1 L^{1/p}(\tau)\, d\tau \right)^p \\
&\quad + \left|\frac{Q+R}{2N}\right| \frac{|\lambda| r}{\Gamma(\alpha-\delta-1)} \left(\int_0^1 (1-\tau)^{(\alpha-\delta-2)/(1-p)}\, d\tau \right)^{1-p} \\
&\quad \times \left(\int_0^1 L^{1/p}(\tau)\, d\tau \right)^p \\
&\quad + \left|\frac{S}{2N}\right| \frac{|\lambda| r}{\Gamma(\alpha-\delta)} \left(\int_0^1 (1-\tau)^{(\alpha-\delta-1)/(1-p)}\, d\tau \right)^{1-p} \\
&\quad \times \left(\int_0^1 L^{1/p}(\tau)\, d\tau \right)^p \\
&\quad + \left|\frac{S}{2N}\right| \frac{|\lambda| r}{\Gamma(\alpha-\delta)} \left(\int_0^\eta (\eta-\tau)^{(\alpha-\delta-1)/(1-p)}\, d\tau \right)^{1-p} \\
&\quad \times \left(\int_0^1 L^{1/p}(\tau)\, d\tau \right)^p \\
&\quad + |\lambda| K \left(\frac{1}{\Gamma(\alpha+1)} + \left|\frac{Q+R}{2N}\right| \frac{1}{\Gamma(\alpha-\delta)} \right. \\
&\qquad \left. + \left|\frac{S}{2N}\right| \left(\frac{1+\eta^{\alpha-\delta}}{\Gamma(\alpha-\delta+1)} \right) \right) \\
&\le |\lambda| r \left[\frac{1}{\Gamma(\alpha)} \left(\frac{1-p}{\alpha-p} \right)^{1-p} \right. \\
&\qquad + \left|\frac{Q+R}{2N}\right| \frac{1}{\Gamma(\alpha-\delta-1)} \left(\frac{1-p}{\alpha-\delta-p-1} \right)^{1-p} \\
&\qquad + \left|\frac{S}{2N}\right| \frac{1}{\Gamma(\alpha-\delta)} \left(\frac{1-p}{\alpha-\delta-p} \right)^{1-p} \\
&\qquad \left. + \left|\frac{S}{2N}\right| \frac{\eta^{\alpha-\delta-p}}{\Gamma(\alpha-\delta)} \left(\frac{1-p}{\alpha-\delta-p} \right)^{1-p} \right] \|L\|_{1/p} \\
&\quad + |\lambda| K \left(\frac{1}{\Gamma(\alpha+1)} + \left|\frac{Q+R}{2N}\right| \frac{1}{\Gamma(\alpha-\delta)} \right. \\
&\qquad \left. + \left|\frac{S}{2N}\right| \left(\frac{1+\eta^{\alpha-\delta}}{\Gamma(\alpha-\delta+1)} \right) \right)
\end{aligned}
\tag{19}
$$

and similarly

$$
\begin{aligned}
&\left|\frac{\partial^q}{\partial t^q}\Phi_1 u(x,t)\right| \\
&\le |\lambda| \left| \int_0^t \frac{(t-\tau)^{\alpha-q-1}}{\Gamma(\alpha-q)} \left[f\left(x,\tau,u(x,\tau),\frac{\partial^q}{\partial t^q}u(x,\tau)\right) \right. \right. \\
&\qquad \left. \left. - f(x,\tau,0,0) + f(x,\tau,0,0) \right] d\tau \right|
\end{aligned}
$$

$$
\begin{aligned}
&+\left|\frac{(2-q)Q+2R}{2N\Gamma(3-q)}\right||\lambda|\\
&\times\left|\int_0^1\frac{(1-\tau)^{\alpha-\delta-2}}{\Gamma(\alpha-\delta-1)}\left[f\left(x,\tau,u(x,\tau),\frac{\partial^q}{\partial t^q}u(x,\tau)\right)\right.\right.\\
&\qquad\left.\left.-f(x,\tau,0,0)+f(x,\tau,0,0)\right]d\tau\right|\\
&+\left|\frac{2S-(2-q)M}{2N\Gamma(3-q)}\right||\lambda|\\
&\times\left|\int_0^1\frac{(1-\tau)^{\alpha-\delta-1}}{\Gamma(\alpha-\delta)}\left[f\left(x,\tau,u(x,\tau),\frac{\partial^q}{\partial t^q}u(x,\tau)\right)\right.\right.\\
&\qquad\left.\left.-f(x,\tau,0,0)+f(x,\tau,0,0)\right]d\tau\right|\\
&+\left|\frac{2S-(2-q)M}{2N\Gamma(3-q)}\right||\lambda|\\
&\times\left|\int_0^\eta\frac{(\eta-\tau)^{\alpha-\delta-1}}{\Gamma(\alpha-\delta)}\left[f\left(x,\tau,u(x,\tau),\frac{\partial^q}{\partial t^q}u(x,\tau)\right)\right.\right.\\
&\qquad\left.\left.-f(x,\tau,0,0)+f(x,\tau,0,0)\right]d\tau\right|\\
&\le\frac{|\lambda|r}{\Gamma(\alpha-q)}\left(\int_0^t(t-\tau)^{(\alpha-q-1)/(1-p)}d\tau\right)^{1-p}\\
&\times\left(\int_0^1L^{1/p}(\tau)\,d\tau\right)^p\\
&+\left|\frac{(2-q)Q+2R}{2N\Gamma(3-q)}\right|\frac{|\lambda|r}{\Gamma(\alpha-\delta-1)}\\
&\times\left(\int_0^1(1-\tau)^{(\alpha-\delta-2)/(1-p)}d\tau\right)^{1-p}\left(\int_0^1L^{1/p}(\tau)\,d\tau\right)^p\\
&+\left|\frac{2S-(2-q)M}{2N\Gamma(3-q)}\right|\frac{|\lambda|r}{\Gamma(\alpha-\delta)}\\
&\times\left(\int_0^1(1-\tau)^{(\alpha-\delta-1)/(1-p)}d\tau\right)^{1-p}\left(\int_0^1L^{1/p}(\tau)\,d\tau\right)^p\\
&+\left|\frac{2S-(2-q)M}{2N\Gamma(3-q)}\right|\frac{|\lambda|r}{\Gamma(\alpha-\delta)}\\
&\times\left(\int_0^\eta(\eta-\tau)^{(\alpha-\delta-1)/(1-p)}d\tau\right)^{1-p}\left(\int_0^1L^{1/p}(\tau)\,d\tau\right)^p\\
&+|\lambda|K\left(\frac{1}{\Gamma(\alpha-q+1)}+\left|\frac{(2-q)Q+2R}{2N\Gamma(3-q)}\right|\frac{1}{\Gamma(\alpha-\delta)}\right.\\
&\qquad\left.+\left|\frac{2S-(2-q)M}{2N\Gamma(3-q)}\right|\left(\frac{1+\eta^{\alpha-\delta}}{\Gamma(\alpha-\delta+1)}\right)\right)\\
&\le|\lambda|r\left[\frac{1}{\Gamma(\alpha-q)}\left(\frac{1-p}{\alpha-q-p}\right)^{1-p}+\left|\frac{(2-q)Q+2R}{2N\Gamma(3-q)}\right|\right.\\
&\qquad\times\frac{1}{\Gamma(\alpha-\delta-1)}\left(\frac{1-p}{\alpha-\delta-p-1}\right)^{1-p}\\
&\qquad+\left|\frac{2S-(2-q)M}{2N\Gamma(3-q)}\right|\frac{1}{\Gamma(\alpha-\delta)}\left(\frac{1-p}{\alpha-\delta-p}\right)^{1-p}\\
&\qquad\left.+\left|\frac{2S-(2-q)M}{2N\Gamma(3-q)}\right|\frac{\eta^{\alpha-\delta-p}}{\Gamma(\alpha-\delta)}\left(\frac{1-p}{\alpha-\delta-p}\right)^{1-p}\right]\\
&\times\|L\|_{1/p}\\
&+|\lambda|K\left(\frac{1}{\Gamma(\alpha-q+1)}+\left|\frac{(2-q)Q+2R}{2N\Gamma(3-q)}\right|\frac{1}{\Gamma(\alpha-\delta)}\right.\\
&\qquad\left.+\left|\frac{2S-(2-q)M}{2N\Gamma(3-q)}\right|\left(\frac{1+\eta^{\alpha-\delta}}{\Gamma(\alpha-\delta+1)}\right)\right).
\end{aligned}
\tag{20}
$$

Thus, we get

$$
\begin{aligned}
&\|\Phi_1u(x,t)\|\\
&\le|\lambda|r\left[\frac{1}{\Gamma(\alpha)}\left(\frac{1-p}{\alpha-p}\right)^{1-p}+\frac{1}{\Gamma(\alpha-q)}\left(\frac{1-p}{\alpha-q-p}\right)^{1-p}\right.\\
&\qquad+\left|\frac{Q+R}{2N}\right|\frac{1}{\Gamma(\alpha-\delta-1)}\left(\frac{1-p}{\alpha-\delta-p-1}\right)^{1-p}\\
&\qquad+\left|\frac{(2-q)Q+2R}{2N\Gamma(3-q)}\right|\frac{1}{\Gamma(\alpha-\delta-1)}\\
&\qquad\times\left(\frac{1-p}{\alpha-\delta-p-1}\right)^{1-p}\\
&\qquad+\left|\frac{S}{2N}\right|\frac{\left(1+\eta^{\alpha-\delta-p}\right)}{\Gamma(\alpha-\delta)}\left(\frac{1-p}{\alpha-\delta-p}\right)^{1-p}\\
&\qquad+\left|\frac{2S-(2-q)M}{2N\Gamma(3-q)}\right|\frac{\left(1+\eta^{\alpha-\delta-p}\right)}{\Gamma(\alpha-\delta)}\\
&\qquad\left.\times\left(\frac{1-p}{\alpha-\delta-p}\right)^{1-p}\right]\|L\|_{1/p}\\
&+|\lambda|K\left(\frac{1}{\Gamma(\alpha+1)}+\frac{1}{\Gamma(\alpha-q+1)}+\left|\frac{Q+R}{2N}\right|\frac{1}{\Gamma(\alpha-\delta)}\right.\\
&\qquad+\left|\frac{(2-q)Q+2R}{2N\Gamma(3-q)}\right|\frac{1}{\Gamma(\alpha-\delta)}\\
&\qquad+\left|\frac{S}{2N}\right|\left(\frac{1+\eta^{\alpha-\delta}}{\Gamma(\alpha-\delta+1)}\right)\\
&\qquad\left.+\left|\frac{2S-(2-q)M}{2N\Gamma(3-q)}\right|\left(\frac{1+\eta^{\alpha-\delta}}{\Gamma(\alpha-\delta+1)}\right)\right).
\end{aligned}
\tag{21}
$$

If $\sup_{u\in X}\psi(\|u\|)\le b$, then we have

$$
\begin{aligned}
&\left|\Phi_2 u(x,t)\right| \\
&\quad\le |\mu|\left|\int_0^t \frac{(t-\tau)^{\alpha+\beta-1}}{\Gamma(\alpha+\beta)} g(x,\tau,u(x,\tau))\,d\tau\right| \\
&\qquad+\left|\frac{Q+R}{2N}\right||\mu|\left|\int_0^1 \frac{(1-\tau)^{\alpha+\beta-\delta-2}}{\Gamma(\alpha+\beta-\delta-1)} g(x,\tau,u(x,\tau))\,d\tau\right| \\
&\qquad+\left|\frac{S}{2N}\right||\mu|\left|\int_0^1 \frac{(1-\tau)^{\alpha+\beta-\delta-1}}{\Gamma(\alpha+\beta-\delta)} g(x,\tau,u(x,\tau))\,d\tau\right| \\
&\qquad+\left|\frac{S}{2N}\right||\mu|\left|\int_0^\eta \frac{(\eta-\tau)^{\alpha+\beta-\delta-1}}{\Gamma(\alpha+\beta-\delta)} g(x,\tau,u(x,\tau))\,d\tau\right| \\
&\quad\le \frac{|\mu|b}{\Gamma(\alpha+\beta)}\left(\int_0^t (t-\tau)^{(\alpha+\beta-1)/(1-p)}\,d\tau\right)^{1-p} \\
&\qquad\times\left(\int_0^1 m^{1/p}(\tau)\,d\tau\right)^p+\left|\frac{Q+R}{2N}\right|\frac{|\mu|b}{\Gamma(\alpha+\beta-\delta-1)} \\
&\qquad\times\left(\int_0^1 (1-\tau)^{(\alpha+\beta-\delta-2)/(1-p)}\,d\tau\right)^{1-p} \\
&\qquad\times\left(\int_0^1 m^{1/p}(\tau)\,d\tau\right)^p \\
&\qquad+\left|\frac{S}{2N}\right|\frac{|\mu|b}{\Gamma(\alpha+\beta-\delta)}\left(\int_0^1 (1-\tau)^{(\alpha+\beta-\delta-1)/(1-p)}\right)^{1-p} \\
&\qquad\times\left(\int_0^1 m^{1/p}(\tau)\,d\tau\right)^p \\
&\qquad+\left|\frac{S}{2N}\right|\frac{|\mu|b}{\Gamma(\alpha+\beta-\delta)}\left(\int_0^\eta (\eta-\tau)^{(\alpha+\beta-\delta-1)/(1-p)}\right)^{1-p} \\
&\qquad\times\left(\int_0^1 m^{1/p}(\tau)\,d\tau\right)^p \\
&\quad\le |\mu|b\left[\frac{1}{\Gamma(\alpha+\beta)}\left(\frac{1-p}{\alpha+\beta-p}\right)^{1-p}+\left|\frac{Q+R}{2N}\right|\right. \\
&\qquad\qquad\times\frac{1}{\Gamma(\alpha+\beta-\delta-1)}\left(\frac{1-p}{\alpha+\beta-\delta-p-1}\right)^{1-p} \\
&\qquad\qquad+\left|\frac{S}{2N}\right|\frac{1}{\Gamma(\alpha+\beta-\delta)}\left(\frac{1-p}{\alpha+\beta-\delta-p}\right)^{1-p} \\
&\qquad\qquad\left.+\left|\frac{S}{2N}\right|\frac{\eta^{\alpha+\beta-\delta-p}}{\Gamma(\alpha+\beta-\delta)}\left(\frac{1-p}{\alpha+\beta-\delta-p}\right)^{1-p}\right] \\
&\qquad\times\|m\|_{1/p}
\end{aligned}
\tag{22}
$$

and similarly

$$
\begin{aligned}
&\left|\frac{\partial^q}{\partial t^q}\Phi_2 u(x,t)\right| \\
&\quad\le |\mu|\left|\int_0^t \frac{(t-\tau)^{\alpha+\beta-q-1}}{\Gamma(\alpha+\beta-q)} g(x,\tau,u(x,\tau))\,d\tau\right| \\
&\qquad+\left|\frac{(2-q)Q+2R}{2N\Gamma(3-q)}\right||\mu| \\
&\qquad\times\left|\int_0^1 \frac{(1-\tau)^{\alpha+\beta-\delta-2}}{\Gamma(\alpha+\beta-\delta-1)} g(x,\tau,u(x,\tau))\,d\tau\right| \\
&\qquad+\left|\frac{2S-(2-q)M}{2N\Gamma(3-q)}\right||\mu| \\
&\qquad\times\left|\int_0^1 \frac{(1-\tau)^{\alpha+\beta-\delta-1}}{\Gamma(\alpha+\beta-\delta)} g(x,\tau,u(x,\tau))\,d\tau\right| \\
&\qquad+\left|\frac{2S-(2-q)M}{2N\Gamma(3-q)}\right||\mu| \\
&\qquad\times\left|\int_0^\eta \frac{(\eta-\tau)^{\alpha+\beta-\delta-1}}{\Gamma(\alpha+\beta-\delta)} g(x,\tau,u(x,\tau))\,d\tau\right| \\
&\quad\le \frac{|\mu|b}{\Gamma(\alpha+\beta-q)}\left(\int_0^t (t-\tau)^{(\alpha+\beta-q-1)/(1-p)}\,d\tau\right)^{1-p} \\
&\qquad\times\left(\int_0^1 m^{1/p}(\tau)\,d\tau\right)^p \\
&\qquad+\left|\frac{(2-q)Q+2R}{2N\Gamma(3-q)}\right|\frac{|\mu|b}{\Gamma(\alpha+\beta-\delta-1)} \\
&\qquad\times\left(\int_0^1 (1-\tau)^{(\alpha+\beta-\delta-2)/(1-p)}\,d\tau\right)^{1-p} \\
&\qquad\times\left(\int_0^1 m^{1/p}(\tau)\,d\tau\right)^p+\left|\frac{2S-(2-q)M}{2N\Gamma(3-q)}\right| \\
&\qquad\times\frac{|\mu|b}{\Gamma(\alpha+\beta-\delta)}\left(\int_0^1 (1-\tau)^{(\alpha+\beta-\delta-1)/(1-p)}\,d\tau\right)^{1-p} \\
&\qquad\times\left(\int_0^1 m^{1/p}(\tau)\,d\tau\right)^p+\left|\frac{2S-(2-q)M}{2N\Gamma(3-q)}\right| \\
&\qquad\times\frac{|\mu|b}{\Gamma(\alpha+\beta-\delta)}\left(\int_0^\eta (\eta-\tau)^{(\alpha+\beta-\delta-1)/(1-p)}\,d\tau\right)^{1-p} \\
&\qquad\times\left(\int_0^1 m^{1/p}(\tau)\,d\tau\right)^p \\
&\quad\le |\mu|b\left[\frac{1}{\Gamma(\alpha+\beta-q)}\left(\frac{1-p}{\alpha+\beta-q-p}\right)^{1-p}\right. \\
&\qquad\qquad\left.+\left|\frac{(2-q)Q+2R}{2N\Gamma(3-q)}\right|\right.
\end{aligned}
$$

$$\times \frac{1}{\Gamma(\alpha+\beta-\delta-1)}\left(\frac{1-p}{\alpha+\beta-\delta-p-1}\right)^{1-p} + \left|\frac{2S-(2-q)M}{2N\Gamma(3-q)}\right| \frac{1}{\Gamma(\alpha+\beta-\delta)} \times \left(\frac{1-p}{\alpha+\beta-\delta-p}\right)^{1-p} + \left|\frac{2S-(2-q)M}{2N\Gamma(3-q)}\right| \times \frac{\eta^{\alpha+\beta-\delta-p}}{\Gamma(\alpha+\beta-\delta)}\left(\frac{1-p}{\alpha+\beta-\delta-p}\right)^{1-p}\Bigg] \|m\|_{1/p}. \tag{23}$$

Hence,

$$\begin{aligned}
&\|\Phi_2 u(x,t)\| \\
&\le |\mu| b \Bigg[\frac{1}{\Gamma(\alpha+\beta)}\left(\frac{1-p}{\alpha+\beta-p}\right)^{1-p} + \frac{1}{\Gamma(\alpha+\beta-q)} \\
&\quad \times \left(\frac{1-p}{\alpha+\beta-q-p}\right)^{1-p} + \left|\frac{Q+R}{2N}\right| \\
&\quad \times \frac{1}{\Gamma(\alpha+\beta-\delta-1)}\left(\frac{1-p}{\alpha+\beta-\delta-p-1}\right)^{1-p} \\
&\quad + \left|\frac{(2-q)Q+2R}{2N\Gamma(3-q)}\right| \frac{1}{\Gamma(\alpha+\beta-\delta-1)} \\
&\quad \times \left(\frac{1-p}{\alpha+\beta-\delta-p-1}\right)^{1-p} + \left|\frac{S}{2N}\right| \\
&\quad \times \frac{\left(1+\eta^{\alpha+\beta-\delta-p}\right)}{\Gamma(\alpha+\beta-\delta)}\left(\frac{1-p}{\alpha+\beta-\delta-p}\right)^{1-p} \\
&\quad + \left|\frac{2S-(2-q)M}{2N\Gamma(3-q)}\right| \frac{\left(1+\eta^{\alpha+\beta-\delta-p}\right)}{\Gamma(\alpha+\beta-\delta)} \\
&\quad \times \left(\frac{1-p}{\alpha+\beta-\delta-p}\right)^{1-p}\Bigg] \|m\|_{1/p}
\end{aligned} \tag{24}$$

and so

$$\begin{aligned}
&\|\Phi u(x,t)\| \\
&\le \|\Phi_1 u(x,t)\| + \|\Phi_2 u(x,t)\| \\
&\le |\lambda| r \Bigg[\frac{1}{\Gamma(\alpha)}\left(\frac{1-p}{\alpha-p}\right)^{1-p} + \frac{1}{\Gamma(\alpha-q)}\left(\frac{1-p}{\alpha-q-p}\right)^{1-p} \\
&\quad + \left|\frac{Q+R}{2N}\right| \frac{1}{\Gamma(\alpha-\delta-1)}\left(\frac{1-p}{\alpha-\delta-p-1}\right)^{1-p} \\
&\quad + \left|\frac{(2-q)Q+2R}{2N\Gamma(3-q)}\right| \frac{1}{\Gamma(\alpha-\delta-1)} \\
&\quad \times \left(\frac{1-p}{\alpha-\delta-p-1}\right)^{1-p} + \left|\frac{S}{2N}\right| \frac{\left(1+\eta^{\alpha-\delta-p}\right)}{\Gamma(\alpha-\delta)} \\
&\quad \times \left(\frac{1-p}{\alpha-\delta-p}\right)^{1-p} + \left|\frac{2S-(2-q)M}{2N\Gamma(3-q)}\right| \\
&\quad \times \frac{\left(1+\eta^{\alpha-\delta-p}\right)}{\Gamma(\alpha-\delta)}\left(\frac{1-p}{\alpha-\delta-p}\right)^{1-p}\Bigg] \|L\|_{1/p} \\
&\quad + |\lambda| K \Bigg(\frac{1}{\Gamma(\alpha+1)} + \frac{1}{\Gamma(\alpha-q+1)} + \left|\frac{Q+R}{2N}\right| \\
&\qquad \times \frac{1}{\Gamma(\alpha-\delta)} + \left|\frac{(2-q)Q+2R}{2N\Gamma(3-q)}\right| \frac{1}{\Gamma(\alpha-\delta)} \\
&\qquad + \left|\frac{S}{2N}\right| \left(\frac{1+\eta^{\alpha-\delta}}{\Gamma(\alpha-\delta+1)}\right) \\
&\qquad + \left|\frac{2S-(2-q)M}{2N\Gamma(3-q)}\right| \left(\frac{1+\eta^{\alpha-\delta}}{\Gamma(\alpha-\delta+1)}\right)\Bigg) \\
&\quad + |\mu| b \Bigg[\frac{1}{\Gamma(\alpha+\beta)}\left(\frac{1-p}{\alpha+\beta-p}\right)^{1-p} + \frac{1}{\Gamma(\alpha+\beta-q)} \\
&\qquad \times \left(\frac{1-p}{\alpha+\beta-q-p}\right)^{1-p} + \left|\frac{Q+R}{2N}\right| \\
&\qquad \times \frac{1}{\Gamma(\alpha+\beta-\delta-1)}\left(\frac{1-p}{\alpha+\beta-\delta-p-1}\right)^{1-p} \\
&\qquad + \left|\frac{(2-q)Q+2R}{2N\Gamma(3-q)}\right| \frac{1}{\Gamma(\alpha+\beta-\delta-1)} \\
&\qquad \times \left(\frac{1-p}{\alpha+\beta-\delta-p-1}\right)^{1-p} + \left|\frac{S}{2N}\right| \\
&\qquad \times \frac{\left(1+\eta^{\alpha+\beta-\delta-p}\right)}{\Gamma(\alpha+\beta-\delta)}\left(\frac{1-p}{\alpha+\beta-\delta-p}\right)^{1-p} \\
&\qquad + \left|\frac{2S-(2-q)M}{2N\Gamma(3-q)}\right| \frac{\left(1+\eta^{\alpha+\beta-\delta-p}\right)}{\Gamma(\alpha+\beta-\delta)} \\
&\qquad \times \left(\frac{1-p}{\alpha+\beta-\delta-p}\right)^{1-p}\Bigg] \|m\|_{1/p} \\
&\le \gamma r + w \le r.
\end{aligned} \tag{25}$$

This implies that $\Phi B_r \subset B_r$. Now, we show that Φ_1 is continuous. Let $x, t \in [0,1]$ and $\{u_n\}$ be a sequence with $u_n \to u$. Then, we have

$$\begin{aligned}
&\|\Phi_1 u_n(x,t) - \Phi_1 u(x,t)\| \\
&\le \Bigg[\frac{|\lambda| \|L\|_{1/p}}{\Gamma(\alpha)}\left(\frac{1-p}{\alpha-p}\right)^{1-p} + \frac{|\lambda| \|L\|_{1/p}}{\Gamma(\alpha-q)}\left(\frac{1-p}{\alpha-q-p}\right)^{1-p} \\
&\quad + \left|\frac{Q+R}{2N}\right| \frac{|\lambda| \|L\|_{1/p}}{\Gamma(\alpha-\delta-1)}\left(\frac{1-p}{\alpha-\delta-p-1}\right)^{1-p}
\end{aligned}$$

$$+\left|\frac{(2-q)Q+2R}{2N\Gamma(3-q)}\right|\frac{|\lambda|\,\|L\|_{1/p}}{\Gamma(\alpha-\delta-1)}\left(\frac{1-p}{\alpha-\delta-p-1}\right)^{1-p}$$
$$+\left|\frac{S}{2N}\right|\frac{|\lambda|\,\|L\|_{1/p}\left(1+\eta^{\alpha-\delta-p}\right)}{\Gamma(\alpha-\delta)}\left(\frac{1-p}{\alpha-\delta-p}\right)^{1-p}$$
$$+\left|\frac{2S-(2-q)M}{2N\Gamma(3-q)}\right|\frac{|\lambda|\,\|L\|_{1/p}\left(1+\eta^{\alpha-\delta-p}\right)}{\Gamma(\alpha-\delta)}$$
$$\times\left(\frac{1-p}{\alpha-\delta-p}\right)^{1-p}\Bigg]\|u_n-u\|. \tag{26}$$

Thus, Φ_1 is continuous. On the other hand, Φ_1 is a γ-contraction because

$$\begin{aligned}
&\|\Phi_1u(x,t)-\Phi_1v(x,t)\|\\
&\le\Bigg[\frac{|\lambda|\,\|L\|_{1/p}}{\Gamma(\alpha)}\left(\frac{1-p}{\alpha-p}\right)^{1-p}+\frac{|\lambda|\,\|L\|_{1/p}}{\Gamma(\alpha-q)}\left(\frac{1-p}{\alpha-q-p}\right)^{1-p}\\
&\quad+\left|\frac{Q+R}{2N}\right|\frac{|\lambda|\,\|L\|_{1/p}}{\Gamma(\alpha-\delta-1)}\left(\frac{1-p}{\alpha-\delta-p-1}\right)^{1-p}\\
&\quad+\left|\frac{(2-q)Q+2R}{2N\Gamma(3-q)}\right|\frac{|\lambda|\,\|L\|_{1/p}}{\Gamma(\alpha-\delta-1)}\left(\frac{1-p}{\alpha-\delta-p-1}\right)^{1-p}\\
&\quad+\left|\frac{S}{2N}\right|\frac{|\lambda|\,\|L\|_{1/p}\left(1+\eta^{\alpha-\delta-p}\right)}{\Gamma(\alpha-\delta)}\left(\frac{1-p}{\alpha-\delta-p}\right)^{1-p}\\
&\quad+\left|\frac{2S-(2-q)M}{2N\Gamma(3-q)}\right|\frac{|\lambda|\,\|L\|_{1/p}\left(1+\eta^{\alpha-\delta-p}\right)}{\Gamma(\alpha-\delta)}\\
&\quad\times\left(\frac{1-p}{\alpha-\delta-p}\right)^{1-p}\Bigg]\|u-v\|,
\end{aligned}\tag{27}$$

for all $u,v\in B_r$. Now, we show that Φ_2 is a compact map. We showed that Φ_2 is uniformly bounded. Now, we show that Φ_2 maps the bounded sets into equicontinuous sets. Let $(x,t_1),(x,t_2)\in J$ such that $t_1<t_2$. Then, we have

$$\begin{aligned}
&|\Phi_2u(x,t_2)-\Phi_2u(x,t_1)|\\
&\le\frac{|\mu|}{\Gamma(\alpha+\beta)}\int_0^{t_1}\left[(t_2-\tau)^{\alpha+\beta-1}-(t_1-\tau)^{\alpha+\beta-1}\right]\\
&\qquad\times|g(x,\tau,u(x,\tau))|\,d\tau\\
&\quad+\frac{|\mu|}{\Gamma(\alpha+\beta)}\int_{t_1}^{t_2}(t_2-\tau)^{\alpha+\beta-1}|g(x,\tau,u(x,\tau))|\,d\tau\\
&\quad+\frac{|t_2-t_1|\,|Q|+\left|t_2^2-t_1^2\right||R|}{|2N|}|\mu|\\
&\quad\times\int_0^1\frac{(1-\tau)^{\alpha+\beta-\delta-2}}{\Gamma(\alpha+\beta-\delta-1)}|g(x,\tau,u(x,\tau))|\,d\tau\\
&\quad+\frac{\left|t_2^2-t_1^2\right||S|-|t_2-t_1|\,|M|}{|2N|}|\mu|\\
&\quad\times\left[\int_0^1\frac{(1-\tau)^{\alpha+\beta-\delta-1}}{\Gamma(\alpha+\beta-\delta)}|g(x,\tau,u(x,\tau))|\,d\tau\right.\\
&\qquad\left.-\int_0^{\eta}\frac{(\eta-\tau)^{\alpha+\beta-\delta-1}}{\Gamma(\alpha+\beta-\delta)}|g(x,\tau,u(x,\tau))|\,d\tau\right]\\
&\le\frac{|\mu|\,b}{\Gamma(\alpha+\beta)}\int_0^{t_1}\left[(t_2-\tau)^{\alpha+\beta-1}-(t_1-\tau)^{\alpha+\beta-1}\right]m(\tau)\,d\tau\\
&\quad+\frac{|\mu|\,b}{\Gamma(\alpha+\beta)}\int_{t_1}^{t_2}(t_2-\tau)^{\alpha+\beta-1}m(\tau)\,d\tau\\
&\quad+\left(\frac{|t_2-t_1|\,|Q|+\left|t_2^2-t_1^2\right||R|}{|2N|}\right)|\mu|\,b\\
&\quad\times\int_0^1\frac{(1-\tau)^{\alpha+\beta-\delta-2}}{\Gamma(\alpha+\beta-\delta-1)}m(\tau)\,d\tau\\
&\quad+\left(\frac{\left|t_2^2-t_1^2\right||S|-|t_2-t_1|\,|M|}{|2N|}\right)|\mu|\,b\\
&\quad\times\left[\int_0^1\frac{(1-\tau)^{\alpha+\beta-\delta-1}}{\Gamma(\alpha+\beta-\delta)}m(\tau)\,d\tau\right.\\
&\qquad\left.-\int_0^{\eta}\frac{(\eta-\tau)^{\alpha+\beta-\delta-1}}{\Gamma(\alpha+\beta-\delta)}m(\tau)\,d\tau\right],\\
&\left|\frac{\partial^q}{\partial t^q}\Phi_2u(x,t_2)-\frac{\partial^q}{\partial t^q}\Phi_2u(x,t_1)\right|\\
&\le\frac{|\mu|\,b}{\Gamma(\alpha+\beta-q)}\\
&\quad\times\int_0^{t_1}\left[(t_2-\tau)^{\alpha+\beta-q-1}-(t_1-\tau)^{\alpha+\beta-q-1}\right]m(\tau)\,d\tau\\
&\quad+\frac{|\mu|\,b}{\Gamma(\alpha+\beta-q)}\int_{t_1}^{t_2}(t_2-\tau)^{\alpha+\beta-q-1}m(\tau)\,d\tau\\
&\quad+\left(\left(\frac{\left|t_2^{1-q}-t_1^{1-q}\right|}{\Gamma(2-q)}|Q|\right.\right.\\
&\qquad\left.\left.+\frac{\left|t_2^{2-q}-t_1^{2-q}\right|}{\Gamma(3-q)}|R|\right)\times|2N|^{-1}\right)|\mu|\,b\\
&\quad\times\int_0^1\frac{(1-\tau)^{\alpha+\beta-\delta-2}}{\Gamma(\alpha+\beta-\delta-1)}m(\tau)\,d\tau\\
&\quad+\left(\left(\frac{2\left|t_2^{2-q}-t_1^{2-q}\right|}{\Gamma(3-q)}|S|\right.\right.\\
&\qquad\left.\left.-\frac{\left|t_2^{1-q}-t_1^{1-q}\right|}{\Gamma(2-q)}|M|\right)\times|2N|^{-1}\right)|\mu|\,b
\end{aligned}$$

$$\times \left[\int_0^1 \frac{(1-\tau)^{\alpha+\beta-\delta-1}}{\Gamma(\alpha+\beta-\delta)} m(\tau)\, d\tau - \int_0^\eta \frac{(\eta-\tau)^{\alpha+\beta-\delta-1}}{\Gamma(\alpha+\beta-\delta)} m(\tau)\, d\tau \right], \tag{28}$$

for all $u \in B_r$. Hence, $\|\Phi_2 u(x,t_2) - \Phi_2 u(x,t_1)\| \to 0$ as $t_2 \to t_1$. By using the Arzela-Ascoli theorem, we get that the operator Φ_2 is completely continuous and so Φ_2 is compact on J. Now by using Lemma 1, the operator $\Phi = \Phi_1 + \Phi_2$ is a condensing map on B_r and so Φ has a fixed point by using Theorem 2. Now by using Lemma 3, it is easy to see that the fixed point of Φ is a solution for the time-fractional integrodifferential equation $(*)$. □

Example 5. Let $\alpha = 5/2$, $\beta = 3/4$, $q = 3/2$, $\delta = 5/4$, $\eta = 2/3$, $\lambda = 1/1000$, $\mu = 1$, and $p = 3/4$. Now, consider the time-fractional integrodifferential equation

$$-\frac{\partial^{5/2}}{\partial t^{5/2}} u(x,t) = \frac{1}{1000}\left(\frac{t|u|}{1+|u|} + \frac{t\left|\left(\partial^{3/2}/\partial t^{3/2}\right)u\right|}{1+\left|\left(\partial^{3/2}/\partial t^{3/2}\right)u\right|} \right) + I_{*t}^{3/4}\left(\frac{t^2|u|^3}{1+|u|^3} \right) \tag{29}$$

via the boundary conditions $u(x,0) = 0$, $(\partial^{9/4}/\partial t^{9/4})u(x,0) = (\partial^{9/4}/\partial t^{9/4})u(x,1)$, and $(\partial^{5/4}/\partial t^{5/4})u(x,1) - (\partial^{5/4}/\partial t^{5/4})u(x,2/3) = 0$. Define the maps $f : J \times X^2 \to X$ by $f(x,t,u(x,t),(\partial^{3/2}/\partial t^{3/2})u(x,t)) = t|u|/(1+|u|) + t|(\partial^{3/2}/\partial t^{3/2})u|/(1+|(\partial^{3/2}/\partial t^{3/2})u|)$ and $g : J \times X \to X$ by $g(x,t,u(x,t)) = t^2|u|^3/(1+|u|^3)$. Define $L(t) = t$ and $m(t) = t^2$ for all t. Then, we have $\|L\|_{1/p} = \|t\|_{4/3} = 0.077$. Define $\psi : \mathbb{R}^+ \to \mathbb{R}^+$ by $\psi(z) = 1$ for all z. It is easy to check that

$$\left| f\left(x,t,u(x,t), \frac{\partial^{3/2}}{\partial t^{3/2}} u(x,t)\right) - f\left(x,t,v(x,t), \frac{\partial^{3/2}}{\partial t^{3/2}} v(x,t)\right)\right| \le L(t)\left(|u-v| + \left| \frac{\partial^{3/2}}{\partial t^{3/2}} u - \frac{\partial^{3/2}}{\partial t^{3/2}} v \right| \right) \tag{30}$$

and $|g(x,t,u(x,t))| \le m(t)\psi(\|u\|)$ for all $u, v \in X$ and t. One can calculate that $\|m\|_{1/p} = \|t^2\|_{4/3} = (3/11)^{3/4}$ and $\gamma \simeq 0.002579$. Now by using Theorem 4, the time-fractional integrodifferential equation has a solution.

3. Conclusion

A time-fractional integrodifferential equation via three-point boundary value conditions was investigated and the existence of the solution was proved for three-point boundary value conditions. One example was studied in detail. For particular forms of the functions f and g and of the investigated equation and for various values of $2 \le \alpha < 3$, $0 < \beta < 1$, $1 \le \delta < 2$, $0 \le \eta \le 1$, λ, and μ we can reobtain the forms of several nonlinear time-fractional differential equations describing the complex phenomena which arise in science and engineering.

Conflict of Interests

The authors declare that there is no conflict of interests regarding the publication of this paper.

Acknowledgment

Research of the authors was supported by Azarbaijan Shahid Madani University.

References

[1] I. Podlubny, *Fractional Differential Equations*, Academic Press, San Diego, Calif, USA, 1999.

[2] S. G. Samko, A. A. Kilbas, and O. I. Marichev, *Fractional Integrals and Derivatives: Theory and Applications*, Gordon and Breach Science Publishers, Yverdon, Switzerland, 1993.

[3] R. Hilfer, *Applications of Fractional Calculus in Physics*, Academic Press, New York, NY, USA, 1999.

[4] W. Wyss, "The fractional Black-Scholes equation," *Fractional Calculus and Applied Analysis*, vol. 3, no. 1, pp. 51–61, 2000.

[5] J. Sabatier, O. P. Agrawal, and J. A. Tenreiro Machado, *Advances in Fractional Calculus: Theoretical Developments and Applications in Physics and Engineering*, Springer, 2007.

[6] G. Maione, "On the Laguerre rational approximation to fractional discrete derivative and integral operators," *IEEE Transactions on Automatic Control*, vol. 58, no. 6, pp. 1579–1585, 2013.

[7] H. Zhang, F. Liu, P. Zhuang, I. Turner, and V. Anh, "Numerical analysis of a new space-time variable fractional order advection-dispersion equation," *Applied Mathematics and Computation*, vol. 242, pp. 541–550, 2014.

[8] R. P. Agarwal, S. K. Ntouyas, B. Ahmad, and M. S. Alhothuali, "Existence of solutions for integro-differential equations of fractional order with nonlocal three-point fractional boundary conditions," *Advances in Difference Equations*, vol. 2013, article 128, 2013.

[9] B. Ahmad, S. K. Ntouyas, and A. Alsaedi, "On fractional differential inclusions with anti-periodic type integral boundary conditions," *Boundary Value Problems*, vol. 2013, article 82, 2013.

[10] A. Alsaedi, S. K. Ntouyas, and B. Ahmad, "Existence results for Langevin fractional differential inclusions involving two fractional orders with four-point multiterm fractional integral boundary conditions," *Abstract and Applied Analysis*, vol. 2013, Article ID 869837, 17 pages, 2013.

[11] Z. Bai and W. Sun, "Existence and multiplicity of positive solutions for singular fractional boundary value problems," *Computers & Mathematics with Applications*, vol. 63, no. 9, pp. 1369–1381, 2012.

[12] D. Baleanu, R. P. Agarwal, H. Mohammadi, and S. Rezapour, "Some existence results for a nonlinear fractional differential equation on partially ordered Banach spaces," *Boundary Value Problems*, vol. 2013, article 112, 2013.

[13] D. Baleanu, H. Mohammadi, and S. Rezapour, "The existence of solutions for a nonlinear mixed problem of singular fractional differential equations," *Advances in Difference Equations*, vol. 2013, article 359, 2013.

[14] D. Baleanu, H. Mohammadi, and S. Rezapour, "Positive solutions of an initial value problem for nonlinear fractional differential equations," *Abstract and Applied Analysis*, vol. 2012, Article ID 837437, 7 pages, 2012.

[15] D. Baleanu, S. Rezapour, and H. Mohammadi, "Some existence results on nonlinear fractional differential equations," *Philosophical Transactions of the Royal Society of London*, vol. 371, Article ID 20120144, 2013.

[16] X. Liu and Z. Liu, "Existence results for fractional differential inclusions with multivalued term depending on lower-order derivative," *Abstract and Applied Analysis*, vol. 2012, Article ID 423796, 24 pages, 2012.

[17] P. D. Phung and L. X. Truong, "On a fractional differential inclusion with integral boundary conditions in Banach space," *Fractional Calculus and Applied Analysis*, vol. 16, no. 3, pp. 538–558, 2013.

[18] L. Debnath and D. D. Bhatta, "Solutions to few linear fractional inhomogeneous partial differential equations in fluid mechanics," *Fractional Calculus and Applied Analysis*, vol. 7, no. 1, pp. 21–36, 2004.

[19] F. Huang and F. Liu, "The fundamental solution of the space-time fractional advection-dispersion equation," *Journal of Applied Mathematics and Computing*, vol. 18, no. 1-2, pp. 339–350, 2005.

[20] K. S. Miller and B. Ross, *An Introduction to the Fractional Calculus and Fractional Differential Equations*, John Wiley & Sons, New York, NY, USA, 1993.

[21] A. Granas and J. Dugundji, *Fixed Point Theory*, Springer, New York, NY, USA, 2003.

[22] B. N. Sadovskii, "A fixed-point principle," *Functional Analysis and Its Applications*, vol. 1, no. 2, pp. 151–153, 1967.

[23] E. Zeidler, *Nonlinear Functional Analysis and its Application: Fixed Point-Theorems*, Springer, 1986.

Review Article

Computational Challenge of Fractional Differential Equations and the Potential Solutions: A Survey

Chunye Gong,[1,2,3] Weimin Bao,[1,2] Guojian Tang,[1] Yuewen Jiang,[4] and Jie Liu[3]

[1] *College of Aerospace Science and Engineering, National University of Defense Technology, Changsha 410073, China*
[2] *Science and Technology on Space Physics Laboratory, Beijing 100076, China*
[3] *School of Computer Science, National University of Defense Technology, Changsha 410073, China*
[4] *Department of Engineering Science, University of Oxford, Oxford OX2 0ES, UK*

Correspondence should be addressed to Chunye Gong; gongchunye@gmail.com

Received 13 June 2014; Revised 6 August 2014; Accepted 9 September 2014

Academic Editor: Guido Maione

Copyright © 2015 Chunye Gong et al. This is an open access article distributed under the Creative Commons Attribution License, which permits unrestricted use, distribution, and reproduction in any medium, provided the original work is properly cited.

We present a survey of fractional differential equations and in particular of the computational cost for their numerical solutions from the view of computer science. The computational complexities of time fractional, space fractional, and space-time fractional equations are $O(N^2M)$, $O(NM^2)$, and $O(NM(M+N))$ compared with $O(MN)$ for the classical partial differential equations with finite difference methods, where M, N are the number of space grid points and time steps. The potential solutions for this challenge include, but are not limited to, parallel computing, memory access optimization (fractional precomputing operator), short memory principle, fast Fourier transform (FFT) based solutions, alternating direction implicit method, multigrid method, and preconditioner technology. The relationships of these solutions for both space fractional derivative and time fractional derivative are discussed. The authors pointed out that the technologies of parallel computing should be regarded as a basic method to overcome this challenge, and some attention should be paid to the fractional killer applications, high performance iteration methods, high order schemes, and Monte Carlo methods. Since the computation of fractional equations with high dimension and variable order is even heavier, the researchers from the area of mathematics and computer science have opportunity to invent cornerstones in the area of fractional calculus.

1. Introduction

The idea of fractional is natural. If $\partial u/\partial x$ and $\partial^2 u/\partial x^2$ exist, $\partial^{1.5} u/\partial x^{1.5}$ maybe exists too. Fractional equations can be used to describe some physical phenomena more accurately than the classical integer order differential equation [1]. Fractional differential equations (FDEs) provide a powerful instrument for the description of memory and hereditary properties of different substances. The fractional diffusion equations play an important role in dynamical systems of semiconductor research, hydrogeology, bioinformatics, finance [2], and other research areas [3–6]. Rajeev and Kushwaha [7] presented a mathematical model describing the time fractional anomalous diffusion process of a generalized Stefan problem which is a limiting case of a shoreline problem. Space fractional advection-diffusion equations arise when velocity variations are heavy tailed and describe particle motion that account for variation in the flow field over the entire system [8]. FDEs may be divided into two fundamental types: time fractional differential equations and space fractional differential equations. For the fractional ordinary equations and fractional order control systems are also studied [9, 10]. The stability of fractional order control systems attracts many attentions [11, 12]. For example, Laguerre continued fraction expansion of the Tustin fractional discrete-time operator was investigated by Maione [13].

Some analytical methods were proposed for fractional differential equation [14, 15]. Saha Ray [16] presented the analytical solutions of the space fractional diffusion equations by two-step Adomian decomposition method. Momani and Odibat [17] gave a comparison between the homotopy perturbation method and the variational iteration method for linear fractional partial differential equations. By using initial conditions, the explicit solutions of the equations have

been presented in the closed form and then their solutions have been represented graphically. Because most of fractional problems cannot be solved analytically, more and more works focus on their numerical solutions. There are many numerical solutions proposed for fractional equations [18], such as finite difference method (FDM) [18]. FDM is intuitive to understand and easy to learn for inexperienced researcher from the areas rather than mathematics. So this survey focuses on FDM for fractional equations.

For the numerical solutions of different differential equations, the area of mathematics pays much attention to approximating the equation more accurately and faster (accuracy and speed). The area of computer science mainly focuses on the runtime (speed) and code reuse (software). The numerical methods (mathematic area) have eternal value and may exist along with the existence of human culture [19–21]. The implementations (computer area) are closer to the human society and the real applications but vary quickly along with the computer architecture [22–28]. The computational cost of the numerical solutions for fractional equations is much heavier than that for the traditional integer order equations. In the near future, the fractional problems with high dimension, long time iterations, and huge grid points will need to be solved. These problems are real challenge for today's computer technologies and algorithms.

2. Fractional Differential Equations

2.1. Origins. In 1695, L'Hopital wrote to Leibniz asking him about a particular notation he had used in his publications for the nth-derivative of the linear function $f(x) = x$, $D^n x/Dx^n$ [29, 30]. L'Hopital's posed the question to Leibniz: what would the result be if $n = 1/2$? Leibniz's response was "An apparent paradox, from which one day useful consequences will be drawn." In these words fractional calculus was born [31]. Later, Fourier, Euler, and Laplace dabbled with fractional calculus [32].

2.2. A Short Summary of FDE. There are mainly three kinds of FDEs:

(1) time fractional [33, 34],

(2) space fractional [35],

(3) space-time fractional [36].

One of the main challenges in fractional differential equation is the nonlocality of the fractional operator. In the case of a time fractional derivative, one needs to store all the history, whereas in the case of a space fractional derivative, one needs to deal with almost-dense matrices.

The partial differential equations (PDEs) mainly have three categories: parabolic, hyperbolic, and elliptic. There are corresponding FDEs to deal with the fractional conditions. There are various FDEs listed below:

(1) the parabolic, widely studied fractional diffusion equation [37, 38],

(2) the hyperbolic Telegraph equation [39],

(3) the elliptic fractional Laplace equation [40],

(4) fractional Black-Scholes equation in computational finance [41],

(5) fractional wave equation for sound, light, and water waves [42],

(6) fractional Fokker-Planck equations describing the time evolution of the probability density function of the velocity of a particle [43],

(7) fractional Euler equations and fractional Navier-Stokes equations [44] for fluid dynamics [45],

(8) fractional kinetic equations for motion of objects [46],

(9) the perfect, fractional Maxwell's equations for electrodynamics [47],

(10) fractional Boltzmann equations for particle transport [48].

We can suppose that *if there is a PDE, there will be a FDE*. The reason is that replacing the integer derivative with fractional derivative and solving the FDE with different numerical methods is not a hard job.

The numerical schemes [49] for these FDEs are listed below:

(1) finite difference method (FDM) [18, 50, 51],

(2) finite element method [52–54],

(3) finite volume method [55–57],

(4) Adomian decomposition method [58],

(5) Fourier transform method [59],

(6) spectral method [60],

(7) meshless method [61–63],

(8) exponential difference method [64, 65],

(9) Monte Carlo method [66].

The Monte Carlo (MC) method, which uses repeated random sampling to obtain numerical results, belongs to undetermined computational methods.

2.3. A Hot Topic in Recent Years. Machado et al. [29] collected 20 special issues on fractional calculus. In 2011 and 2012, there are about 7 special issues on this topic. There are more special issues in the nearby four years (2011–2014) than those of 1999 to 2010 [29]. And there are additional 20 special issues in the years of 2013 and 2014. So the researches on fractional calculus can be regarded as a collective revelry.

3. Computational Challenge

3.1. A Classical Partial Differential Equation (PDE)

3.1.1. Heat Equation/Diffusion Equation. The heat equation is a parabolic PDE which describes the distribution of heat (or variation in temperature) in a given region over time,

shown in (1). This equation is also known as the diffusion equation:

$$\begin{aligned} &\frac{\partial u(x,t)}{\partial t} = d(x)\frac{\partial^2 u(x,t)}{\partial x^2} + f(x,t), \\ &u(x,0) = \phi(x), \quad x \in [x_L, x_R], \\ &u(x_L,t) = \varphi(t), \quad t \in [0,T], \\ &u(x_R,t) = \psi(t), \quad t \in [0,T], \end{aligned} \tag{1}$$

where the $d(x)$ is the diffusion constant.

3.1.2. Numerical Method. Define $t_n = n\tau$, $x_i = ih$ for $0 \le n \le N$, $0 \le i \le M$, where M and N are positive integer and $\tau = T/N$, $h = (x_R - x_L)/M$ are time step size and space step size, respectively. Define u_i^n, f_i^n, d_i as the numerical approximation to $u(x_i, t_n)$, $f(x_i, t_n)$, and $d(x_i)$. Using a forward difference at time t_n and a second-order central difference for the space derivative at position x_i, we get the explicit finite difference approximation for the one-dimensional heat equation:

$$\frac{u_i^{n+1} - u_i^n}{\tau} = d_i \frac{u_{i+1}^n - 2u_i^n + u_{i-1}^n}{h^2} + f_i^n. \tag{2}$$

The u_i^{n+1} can be obtained by this way:

$$u_i^{n+1} = a_1 u_{i+1}^n + a_2 u_i^n + a_3 u_{i-1}^n + \tau f_i^n, \tag{3}$$

where $a_1 = a_3 = -d_i\tau/h^2$ and $a_2 = 1 - 2d_i\tau/h^2$.

If we use the backward difference at time t_{n+1} and a second-order central difference for the space derivative at position x_i we get the explicit finite difference approximation for (1):

$$\frac{u_i^{n+1} - u_i^n}{\tau} = d_i \frac{u_{i+1}^{n+1} - 2u_i^{n+1} + u_{i-1}^{n+1}}{h^2} + f_i^{n+1}. \tag{4}$$

The u_i^{n+1} can be obtained by this way:

$$a_1 u_{i+1}^{n+1} + a_2 u_i^{n+1} + a_3 u_{i-1}^{n+1} = u_i^n + \tau f_i^n, \tag{5}$$

where $a_1 = a_3 = d_i\tau/h^2$ and $a_2 = 1 + 2d_i\tau/h^2$.

The classical PDE is used to compare the fractional equations. For convenience, there are several hypotheses for this paper.

(1) We just focus on the explicit FDM of (3), because these kinds of comparisons between fractional equations and classical equations are straightforward. The comparison between implicit FDE of (5) and implicit schemes of fractional equations is more complex [67].

(2) The computational cost of diffusion coefficient d_i and source f_i^n (or f_i^{n+1}) is ignored, because they only need compute once. And they are different with different equations and make the comparison complicated.

3.1.3. Computational Cost. Each grid point of time step t_{n+1} needs 4 multiplications and 3 additions. There are $M - 1$ grid points in each time step. So each time step needs $7(M - 1)$ arithmetic logic operations. There are about N time steps. So the total computational cost is about $7N(M - 1)$. The computational cost will vary linearly along the number of time steps and grid points.

3.2. Time Fractional Diffusion Equation

3.2.1. Numerical Method. Liu et al. [63] developed an implicit radial basis function (RBF) meshless approach for time fractional diffusion equations and found that the presented meshless formulation is very effective for modeling and simulation of fractional differential equations. Murillo and Yuste developed an explicit difference method for solving fractional diffusion with Caputo form [68]:

$$\begin{aligned} &\frac{\partial^\alpha u(x,t)}{\partial^\alpha t} = \frac{\partial^2 u(x,t)}{\partial x^2} \quad (0 < \alpha < 1), \\ &u(x,0) = g(x), \quad x \in (0, x_R), \\ &u(0,t) = u(x_R,t) = 0 \end{aligned} \tag{6}$$

on a finite domain $0 < x < x_R$ and $0 \le t \le T$.

The explicit finite difference approximation for (6) is described as follows [69]:

$$\tau^{-\alpha} \sum_{i=0}^{n+1} w_i \left(u_j^{n+1-i} - u_j^0\right) = \frac{1}{h^2}\left(u_{j+1}^n - 2u_j^n + u_{j-1}^n\right), \tag{7}$$

where w_i is the normalized Grünwald weight defined with

$$w_i = (-1)^i \binom{\alpha}{i}. \tag{8}$$

Define $\mu = \tau^\alpha/h^2$, $b_n = \sum_{i=0}^{n-1} w_i$, and $U^n = (u_1^n, u_2^n, \ldots, u_{M-1}^n)^T$; we can get

$$U^{n+1} = b_{n+1}U^0 - \sum_{i=1}^{n+1} w_i U^{n+1-i} + \mu A U^n, \tag{9}$$

where matrix A is a tridiagonal matrix, defined by

$$A_{M-1\times M-1} = \begin{pmatrix} -2 & 1 & & & \\ 1 & -2 & 1 & & \\ & \bullet & \bullet & & \\ & & \bullet & \bullet & 1 \\ & & & 1 & -2 \end{pmatrix}. \tag{10}$$

3.2.2. Computational Cost. In order to get U^{n+1}, the right-sided computation of (9) should be performed. There are mainly one tridiagonal matrix-vector multiplication, many constant-vector multiplications, and many vector-vector additions in the right-sided computation.

(1) The tridiagonal matrix-vector multiplication is AU^n and a new vector $U^{n+1} = AU^n$ is got.

(2) The constant-vector multiplications are $V^{'} = b_{n+1}U^0$, $V'' = \mu V^1$, $V^i = w_i U^{n+1-i}$.

(3) The vector-vector additions are $U^{n+1} = U^{n+1} + V^{'} + V'' - \sum_{i=1}^{n+1} V^i$.

There are about $5(M-1)$ operations for tridiagonal matrix-vector multiplication. For time step t_{n+1} needs $(n+8)(M-1)$ arithmetic logic operations with $n = 1 \to N$. So the total computational cost for (9) is about

$$\begin{aligned} &8N(M-1) + (1+2+\cdots+N-1)(M-1) \\ &\quad = 8N(M-1) + \frac{N(N-1)(M-1)}{2} \\ &\quad = N\left(\frac{N}{2} + 7.5\right)(M-1). \end{aligned} \tag{11}$$

The computational cost varies linearly along the number of grid points but squares with the number of time steps.

3.3. Space Fractional Diffusion Equation

3.3.1. Numerical Method. A classical numerical scheme for the space fractional diffusion equation is the second-order fractional Crank-Nicolson method proposed by Tadjeran et al. [38, 70], where the Richardson extrapolation technique is used to the first order shift Grünwald formula for space fractional derivative. Tadjeran et al. [70] presented a practical numerical method in time and space to solve a class of initial-boundary value with variable coefficients on a finite domain for

$$\frac{\partial u(x,t)}{\partial t} = d(x)\frac{\partial^\alpha u(x,t)}{\partial x^\alpha} + q(x,t) \tag{12}$$

on a finite domain $x_L < x < x_R$ with $1 < \alpha < 2$ and $0 \le t \le T$. The case of $1 < \alpha < 2$ models a super-diffusive flow in which a cloud of diffusing particles spreads at a faster rate than the classical diffusion model predictions [71, 72].

The explicit finite difference approximation for (12) is

$$\frac{u_i^{n+1} - u_i^n}{\tau} = \frac{d_i}{h^\alpha}\left(\sum_{k=0}^{i+1} g_{\alpha,k} u_{i-k+1}^n\right) + q_i^n, \tag{13}$$

where $u_i^n = u(x_i, t_n)$, $d_i = d(x_i)$, and $q_i^n = q(x_i, t_n)$. The $g_{\alpha,k}$ is the normalized Grünwald weight [70, 73]:

$$g_{\alpha,k} = \frac{\Gamma(k-\alpha)}{\Gamma(-\alpha)\Gamma(k+1)}. \tag{14}$$

These normalized weights only depend on the order α and the index k. The resulting equation can be explicitly solved for u_i^{n+1} to give

$$u_i^{n+1} = u_i^n + \frac{d_i \tau}{h^\alpha}\left(\sum_{k=0}^{i+1} g_{\alpha,k} u_{i-k+1}^n\right) + \tau q_i^n. \tag{15}$$

3.3.2. Computational Cost. The ith grid point of time step t_{n+1} needs $i+6$ multiplication, addition, and division. There are $M-1$ grid points in each time step. So each time step needs $(M-1)6 + (1+2+\cdots+M-1) = (M-1)((M/2)+6)$ arithmetic logic operations. There are about N time steps. So the total computational cost is about $N(M-1)((M/2)+6)$.

3.4. Riesz Space Fractional Diffusion Equation

3.4.1. Numerical Method. Shen et al. [74] investigated the Green function and a discrete random walk model for Riesz fractional advection-dispersion equation on infinite domain with an initial condition and also presented implicit and explicit finite differences to this problem on a finite domain. Çelik and Duman [75] applied the Crank-Nicolson method to a fractional diffusion equation which has the Riesz fractional derivative and obtained that the method is unconditionally stable and convergent. The Riesz space fractional reaction-diffusion equation [76, 77] is

$$\begin{aligned} &\frac{\partial u(x,t)}{\partial t} = -u(x,t) + {}_xD_0^\alpha u(x,t) + q(x,t), \\ &u(x,0) = g(x), \quad x \in (x_L, x_R), \\ &u(x_L,t) = u(x_R,t) = 0 \end{aligned} \tag{16}$$

with $1 < \alpha \le 2$ and $0 \le t \le T$. Both $u(x,t)$ and $g(x)$ are real valued and sufficiently well-behaved function. ${}_xD_0^\alpha u(x,t)$ is the Riesz space fractional derivative.

With adopting an Euler approximation in time, the explicit difference approximation can be got:

$$\begin{aligned} \frac{u_i^{n+1} - u_i^n}{\tau} &= -u_i^n - \frac{1}{ch^\alpha} \\ &\quad \times \left[\sum_{k=0}^{i+1} g_k u_{i+1-k}^n + \sum_{k=0}^{M-i+1} g_k u_{i-1+k}^n\right] + f_i^n, \end{aligned} \tag{17}$$

where $g_0 = 1$, $g_k = (-1)^k \alpha(\alpha-1)\cdots(\alpha-k+1)/k!$, $k = 1, 2, 3, \ldots$ is the normalized Grünwald weight, $c = 1/2\cos(\alpha\pi/2)$, and $f_i^n = q(x_i, t_n)$.

Equation (17) results in a linear system of equations

$$U^{n+1} = AU^n + Q^n, \tag{18}$$

where $U^n = (u_1^n, u_2^n, \ldots, u_{M-1}^n)^T$, $Q^n = (\tau f_1^n, \tau f_2^n, \ldots, \tau f_{M-1}^n)^T$ with $q_i^n = \tau f_i^n$ $(1 \le i < M-1)$, and $A = (a_{ij})_{(M-1)\times(M-1)}$ is a matrix of coefficient. A is defined by

$$a_{i,j} = \begin{cases} -\dfrac{\tau}{ch^\alpha} g_{i+1-j}, & \text{for } 1 \le j < i-1, \\ -\dfrac{\tau}{ch^\alpha}(g_0 + g_2), & \text{for } j = i-1, \\ (1-\tau) - 2\dfrac{\tau}{ch^\alpha} g_1, & \text{for } j = i, \\ -\dfrac{\tau}{ch^\alpha}(g_0 + g_2), & \text{for } j = i+1, \\ -\dfrac{\tau}{ch^\alpha} g_{j-i+1}, & \text{for } i+1 < j < M-1. \end{cases} \tag{19}$$

3.4.2. Computational Cost. From (18), the $M-1$ results are produced by AU^n for each time step. The inner product of vectors v^1 and v^2 with size m has m multiplications and $m-1$ additions. AU^n for each time step needs $(M-1)(2M-3)$ operations. Assuming τf_i^n is pre-performed, each time step needs $(M-1)(2M-2)$ arithmetic logic operations. There are about N time steps. So the total computational cost is about $N(M-1)(2M-2)$. The computational cost will vary linearly along the number of time steps but square with the number of grid points. From analytical view, the computation of (18) is about four times heavier than that of (15).

3.5. Space-Time Riesz-Caputo Fractional Convection-Diffusion Equation. The fractional advection-diffusion (dispersion) equation has been applied to many problems. Fractional advection-dispersion equations are used in groundwater hydrology to model the transport of passive tracers carried out by fluid flow in a porous medium [78]. Shen et al. [79] presented an explicit difference approximation and an implicit difference approximation for the space-time Riesz-Caputo fractional advection-diffusion equation with initial and boundary conditions in a finite domain. They proved that the implicit difference approximation is unconditionally stable and convergent, but the explicit difference approximation is conditionally stable and convergent. Liu et al. [80] proposed an implicit difference method and an explicit difference method to solve the space-time fractional advection-diffusion equation and discussed the stability and convergence of the method.

3.5.1. Numerical Method. We consider the following space-time Riesz-Caputo fractional advection-diffusion equation (STRCFADE) studied by Shen et al. [79]. This equation is obtained by replacing the space-derivative in the advection-diffusion equation with a generalized derivative of order β_1, β_2 with $0 < \beta_1 < 1$, $1 < \beta_2 < 2$ and time-derivative with a generalized derivative of order α with $0 < \alpha < 1$. We consider

$$
\begin{aligned}
{}_0D_t^{\alpha} u(x,t) &= B_1 \frac{\partial^{\beta_1} u(x,t)}{\partial |x|^{\beta_1}} + B_2 \frac{\partial^{\beta_2} u(x,t)}{\partial |x|^{\beta_2}} + f(x,t), \\
u(x,0) &= \phi(x), \quad x \in [0, x_R], \\
u(0,t) &= u(x_R,t) = 0, \quad t \in [0,T]
\end{aligned}
\tag{20}
$$

on a finite domain $0 \le x \le x_R$ and $0 \le t \le T$. The coefficients B_1 and B_2 are both positive constants and represent the diffusion (dispersion) coefficient and the average fluid velocity. The $\partial^{\beta_1} u(x,t)/\partial|x|^{\beta_1}$ and $\partial^{\beta_2} u(x,t)/\partial|x|^{\beta_2}$ are Riesz space fractional derivatives of order β_1 and β_2, respectively. Then we can get the explicit finite differential approximation for (20) [79]:

$$
\begin{aligned}
u_i^{n+1} &= \sum_{j=0}^{n-1} \left(b_j - b_{j+1}\right) u_i^{n-j} + b_n u_i^0 + B_1 \mu_1 \left(\sum_{k=-i}^{N-i} \omega_k^{\beta_1} u_{i+k}^n \right) \\
&\quad + B_2 \mu_2 \left(\sum_{k=-i}^{N-i} \omega_k^{\beta_2} u_{i+k}^n \right) + \mu_0 \varphi_i^n, \quad i = 1, \ldots, N-1,
\end{aligned}
$$

$$
\begin{aligned}
u_0^{n+1} &= u_N^{n+1} = 0, \\
u_i^0 &= \phi_i,
\end{aligned}
\tag{21}
$$

where $\mu_0 = \tau^{\alpha}\Gamma(2-\alpha)$, $\mu_1 = \mu_0/h^{\beta_1}$, and $\mu_2 = \mu_0/h^{\beta_2}$. More information can be referred to in [79].

3.5.2. Computational Cost. From Section 3.4.2, we know that the computational cost of $B_1\mu_1(\sum_{k=-i}^{N-i} \omega_k^{\beta_1} u_{i+k}^n) + B_2\mu_2(\sum_{k=-i}^{N-i} \omega_k^{\beta_2} u_{i+k}^n) + \mu_0\varphi_i^n$ of N time steps is about $N(M-1)(2M-2)$ operations. From Section 3.2.2, we know that the computational cost of $\sum_{j=0}^{n-1}(b_j - b_{j+1})u_i^{n-j} + b_n u_i^0$ of N time steps with n ranging from 1 to N is about $N(N/2)(M-1)$. So the total computational cost is about $N(M-1)(2M-2+(N/2))$. The computational cost varies quadratically with the number of time steps or the number of grid points.

For fixed $M = 4097$, the comparison between the computational costs of the numerical solution among classical PDE, time fractional, space fractional, Riesz space fractional, and space-time Riesz-Caputo fractional equations is shown in Figure 1. For fixed $N = 2048$, the computational cost is shown in Figure 2.

3.6. More Challenges. There are more computational challenges listed below:

(1) high dimensional problems [55, 81],

(2) implicit schemes [67, 82],

(3) high order schemes [33, 83],

(4) variable order problems [84],

(5) huge memory space requirement.

The high dimensional problems are more computation expensive [55, 81, 85, 86]. For example, the two-dimensional time fractional diffusion equation (2D-TFDE) [67, 87] is

$$
\begin{aligned}
{}_0D_t^{\alpha} u(x,y,t) &= a(x,y,t) \frac{\partial^2 u(x,y,t)}{\partial x^2} \\
&\quad + a(x,y,t) \frac{\partial^2 u(x,y,t)}{\partial y^2} + f(x,y,t), \\
u(x,y,0) &= \phi(x,y), \quad (x,y) \in \Omega, \\
u(x,y,t)|_{\partial\Omega} &= 0, \quad t \in [0,T],
\end{aligned}
\tag{22}
$$

where $\Omega = \{(x,y) \mid 0 \le x \le L_1, 0 \le y \le L_2, a(x,y,t) > 0,$ and $b(x,y,t) > 0\}$.

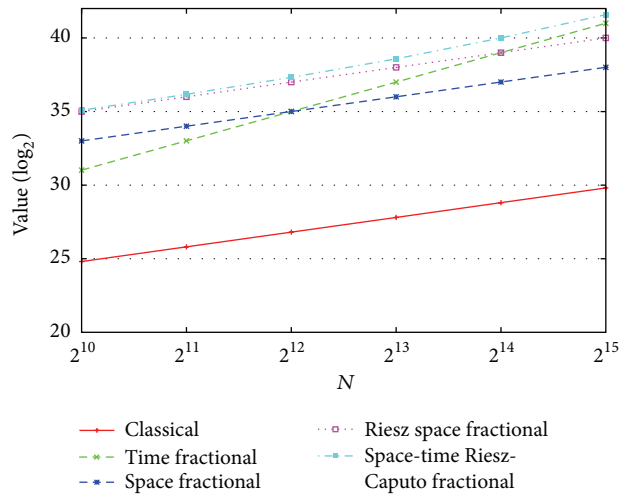

Figure 1: Comparison of the computational cost with different grid points for fixed $M = 4097$ among classical, time fractional, space fractional, Riesz space fractional, and space-time Riesz-Caputo fractional equations.

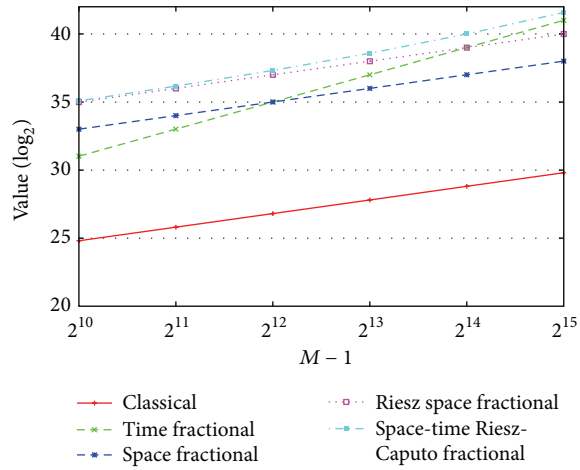

Figure 2: Comparison of the computational cost with different time step for fixed $N = 2048$ among classical, time fractional, space fractional, Riesz space fractional, and space-time Riesz-Caputo fractional equations.

The approximating scheme is [87]

$$\begin{aligned} u_{i,j}^{n+1} - u_{i,j}^{n} + \sum_{s=1}^{n} (b_s) \left(u_{i,j}^{n+1-s} - u_{i,j}^{n-s}\right) \\ = \mu_1 \Gamma(2-\alpha)\, a_{i,j}^{n} \left(u_{i+1,j}^{n} - 2u_{i,j}^{n} + u_{i-1,j}^{n}\right) \\ + \mu_2 \Gamma(2-\alpha)\, b_{i,j}^{n} \left(u_{i,j+1}^{n} - 2u_{i,j}^{n} + u_{i,j-1}^{n}\right) \\ + \tau^{\alpha} \Gamma(2-\alpha)\, f_{i,j}^{n}, \end{aligned} \tag{23}$$

where $\mu_1 = \tau^{\alpha}/h_x^2$ and $\mu_2 = \tau^{\alpha}/h_y^2$. The h_x and h_y are the step size along X and Y directions. The computational complexity is about $O(N^2M^2)$, which is much bigger than the computational complexity of one-dimensional problems when the number of grid points is bigger enough.

The direct Gauss elimination for implicit scheme of FDE is not convenient. Solving unsteady FDE with implicit schemes relies on the iteration method at each time step. The variable order problems [84, 88] have complex coefficients, which need more arithmetic logic operations. The high order schemes [33, 38, 70] need more arithmetic logic operations too.

The memory usage belongs to the computing resources. So the huge memory requirement of FDE is a kind of computational challenge in the broader sense. This is especially true for time fractional problems. Ignoring the memory usage of the coefficients and source terms, the one-dimensional equation (9) needs $8(M-1)N$ bytes of memory space and the two-dimensional equation (23) needs $8M^2N$ bytes of memory space. For three-dimensional problems, the memory usage is $8M^3N$ at least. It needs 15.625 PB (1 PB = 1024^5 bytes) memory space with $M = 10240$, $N = 2048$ for three-dimensional problems. Maybe only the most powerful supercomputer [89] can satisfy the huge memory requirement.

4. Potential Solutions

There are several ways which can be used to overcome the computational challenge of FDEs.

4.1. Parallel Computing. Large scale applications and algorithms in science and engineering such as neutron transport [90–92], light transport [93], computational fluid dynamics [94, 95], molecular dynamics [96], and computational finance and different numerical methods [97] rely on parallel computing [98, 99].

Gong et al. [77] present a parallel algorithm for Riesz space fractional diffusion equation based on MPI parallel programming model at the first time. The parallel algorithm is as accurate as the serial algorithm and achieves 79.39% parallel efficiency compared with 8 processes on a distributed memory cluster system. The parallel implicit iterative algorithm was studied for two-dimensional time fractional problem and a task distribution model is shown in Figure 3 [67]. M_x, M_y, P_x, P_y stand for the discrete grid points, parallel processes along X, Y directions.

Domain decomposition method is regarded as the basic mathematical background for many parallel applications [100–102]. A domain decomposition algorithm for time fractional reaction-diffusion equation with implicit finite difference method was proposed [103]. The domain decomposition algorithm keeps the same parallelism as Jacobi iteration but needs much fewer iterations.

Diethelm [104] implemented the fractional version of the second-order Adams-Bashforth-Moulton method on a parallel computer and discussed the precise nature of the parallelization concept. Parallel computing has already appeared in some studies on FDEs, but until today their power for approximating fractional derivatives and solving FDEs has not been fully recognized.

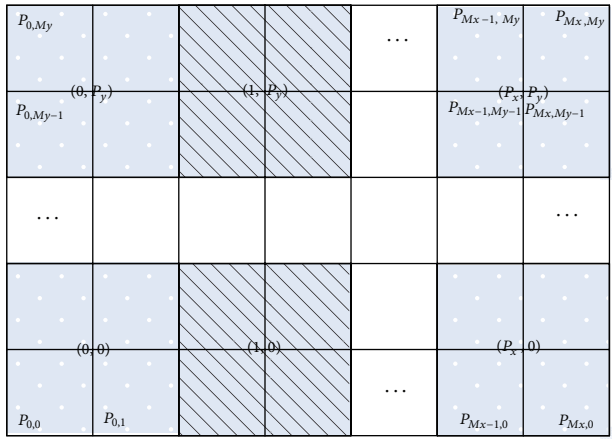

Figure 3: The two-dimensional task distribution model for 2D-TFDE.

4.2. Memory Access Optimization (Fractional Precomputing Operator). Memory access optimization is generally regarded as a technology of computer architecture. It is also useful from the view of applications. One feature of the modern computer architecture is multilayer memory. For example, the traditional CPU has fast cache and slow main memory. The new graphics processing unit (GPU) has fast shared memory and slow memory. Reusing the data in shared memory is a key point to improve the performance of GPU applications [105–109]. A very useful optimization is presented for fractional derivative [69, 110]. We can name this fractional precomputing operator, which will be a very basic and useful optimizing technology for the implementation of fractional algorithms and applications. The example of fractional precomputing operator can refer to Algorithms 4 and 5 in reference [69].

On CPU platform, an optimization of the sum of constant vector multiplication is presented and 2-time speedup can be got for both serial and parallel algorithm for the time fractional equation [69]. The key technology is reusing the data in cache through loop unrolling. Zhang et al. [110] presented code optimization for fractional Adams-Bashforth-Moulton method by loop fusion and loop unrolling.

On GPU platform, Liu et al. [111] presented an optimized CUDA kernel for the numerical solution of time fractional equation and 1.2–2.7-time performance improvement is achieved.

4.3. Short Memory Principle. The short memory principle [3] means the unknown grid points only rely on the recent past (in time) or near neighbors (in space). This principle has been proved to be an easy and powerful way for various kinds of fractional differential equations [112, 113]. The short memory principle is also called fixed memory principle or logarithmic memory principle. The idea of short memory principle is simple. Taking time fractional equation as an example in Section 3.2.1, the value of w_i becomes smaller while i is increasing. In (9), the accumulation of $\sum_{i=1}^{n+1} w_i U^{n+1-i}$ is replaced with $\sum_{i=\min\{1,n+1-K\}}^{n+1} w_i U^{n+1-i}$. K is a positive integer, which means if n is very big, the computation of the accumulation is fixed.

Based on short memory principle, some principles with better balance of computation speed and computation accuracy are presented. The logarithmic memory principle is developed with a good approximation to the true solution at reasonable computational cost [114]. Another principle is equal-weight memory principle, in which an equal-weight is applied to all past data in history, and the result is reserved instead of being discarded [115]. The equal-weight memory principle is an interesting and useful approximation method to fractional derivative.

4.4. FFT Based Solution. Because of the nonlocal property of fractional differential operators, the numerical methods have full coefficient matrices which require computational cost of $O(M^3)$ for implicit scheme per time step, where M is the number of grid points. Ford and Simpson [114] developed a faster scheme for the calculation of fractional integrals. A reduction in the amount of computational work can be achieved by using a graded mesh, thereby making the $O(N^2)$ method to a $O(N \log N)$ method. The underlying idea is based on the fact that the fractional integral possesses a fundamental scaling property that can be exploited in a natural way [114].

Wang et al. [116, 117] developed a fast finite difference method for fractional diffusion equations, which only requires computational cost of $O(N\log_2 N)$ while retaining the same accuracy and approximation property as the regular finite difference method. Numerical experiments show that the fast method has a significant reduction of CPU time [86]. The fast method should have a banded coefficient matrix instead of the full matrix. The properties of Toeplitz and circulant matrices, fast Fourier transform (FFT), and inverse FFT are used to reduce the computational cost. The method is also called superfast-preconditioned iterative method for steady-state space fractional diffusion equations [118].

An efficient iteration method for Toeplitz-plus-band triangular systems, which may produced by fractional ordinary differential equations, was developed. Some methods such as matrix splitting, FFT, compress memory storage, and adjustable matrix bandwidth are used in the presented solution. The interesting technologies are the adjustable matrix bandwidth and solving fractional ordinary differential equations with iteration method. The experimental results show that the presented efficient iteration method is 4.25 times faster than the regular solution [10].

4.5. Alternating Direction Implicit Method. The alternating direction implicit (ADI) method is a finite difference method for solving traditional PDEs. The approximation methods for fractional equations result in a very complicated set of equations in multiple dimensions, which are hard to solve [67, 81, 85]. So the ADI method is developed for high dimensional problems [33, 117]. The advantage of the fractional ADI method is that the equations that have to be solved in each step have a simpler structure. The time fractional problems

can be solved efficiently with the tridiagonal matrix algorithm [33]. The space fractional problems can use the FFT to accelerate the computation [117].

4.6. Multigrid Method. The multigrid method is usually exploited for solving ill-conditioned systems. The main idea of multigrid is to accelerate the convergence of a basic iterative method by global correction form, accomplished by solving a coarse problem. Pang and Sun [119] proposed a multigrid method to solve the initial-boundary value problem of a fractional diffusion equation. The experimental results show that the multigrid + FFT method runs hundred times faster than Gaussian elimination method and the conjugate gradient normal residual (CGNR) method. A full V-cycle multigrid method is proposed for the stationary fractional advection dispersion equation [120] and ten-time performance improvement is achieved.

4.7. Preconditioning Technology. Preconditioning is typically related to reducing a condition number of the problem with iterative methods. It shows that both the average number of iterations and the CPU time by the PCGNR (preconditioner CGNR) method with circulant preconditioners are much less than those by the CGNR method and less than that by the multigrid method [121]. The circulant preconditioner [121], banded preconditioner [122], fast Poisson preconditioners [123], and preconditioned conjugate gradient squared method plus FFT [118] are developed for different FDEs.

4.8. Relationships among These Potential Solutions. The potential solutions for the computational challenge of FDE are investigated above. Many people will be curious about these relationships: can we combine these methods to develop a fastest solution for FDEs? The answer is still unknown. The performance of these solutions varies from different FDE applications. Their relationships are shown in Table 1. The PC, MAO, SMP, FFT, ADI, MGM, and PT stand for parallel computing, memory access optimization, short memory principle, FFT based solution, alternating direction implicit method, multigrid method, and preconditioning technology. The score means the degrees of the two solutions are harmonious. Higher score means using two solutions can achieve better performance.

For time fractional derivative [124], only memory access optimization [69, 111] and short memory principle [3] are useful. Here, the time fractional derivative is different from time fractional problems. For example, the one- and two-dimensional FDEs are parallelized by Gong et al. [67, 69]. These parallel algorithms are based on the partition of space not time.

Table 1: Relationships among the potential solutions for space fractional derivative.

	PC	MAO	SMP	FFT	ADI	MGM	FT
PC	—	3	3	2[a]	3	2[a]	2[a]
MAO		—	3	1[b]	3	3	3
SMP			—	1[c]	3	3	3
FFT				—	3	3	3
ADI					—	3	3
MGM						—	2[d]
PT							—

[a]The parallel efficiency of FFT, multigrid, preconditioner is limiting.
[b]It is hard to use MAO within FFT.
[c]Because of the Toeplitz structure, FFT cannot use short memory principle.
[d]The philosophy of multigrid and preconditioning technology are different. But there are some multigrid preconditioners.

5. Future Directions

5.1. Fractional Killer Applications. Killer application is a kind of application that is so necessary or desirable that it proves the core value of some larger technology. A killer application is something like Project Apollo in space technology, the IBM 360 in personal computer industry, and the IPhone in the smart phone industry. The fractional research still lacks these kinds of killer applications. It needs fractional applications to solve scientific or engineering problems in physical world, such as the fractional flow/control of hypersonic vehicle, not only the academical problems. The fractional killer application should be proved that it is more useful than the traditional classical application. Solving real problems in physical world will build an economic foundation for fractional researches.

5.2. Parallel Computing. The technologies of parallel computing should be regarded as a basic method to overcome the computational challenge for FDEs. There are three potential solutions for the computational challenge of FDEs. The short memory principle is an experimental method, which is useful in real fractional applications. The $O(N \log N)$ methods [117] used the property of Toeplitz matrices and FFT technology. Parallel computing is a foundational technology for scientific and engineering computation. Fortunately, the short memory principle and $O(N \log N)$ methods are compatible with parallel computing. So it is interesting to develop algorithms which is faster than $O(N \log N)$ methods. The numerical methods of space fractional equations with global dependence are much harder to be parallelized than that of the time fractional equations. So the task distribution model, load balance of the parallel algorithm for space fractional equations should be paid attention to.

5.3. High Performance Iteration Methods. Different kind of numerical methods is very easily found for FDEs. The direct methods such as Gauss elimination are not suitable for large scale fractional applications. The iterative methods for these numerical methods are not fully studied and very few works can be found [118, 125]. We think that different iterative methods, such as Jacobi method and Gauss-Seidel and Krylov subspace method, are effective for fractional linear systems which are produced from FDEs. Does the coefficient matrix of FDEs have some other special properties or not? The answer is still unknown. The convergence and stability of these iterative methods should be proved as well.

5.4. High Order Schemes for Fractional Derivatives. The traditional partial derivatives have many high order schemes. For time fractional equation, the high order schemes for traditional integer derivative are not hard to build. But for fractional derivatives, the high order schemes are under developing [70, 126–128]. High order schemes will be used in the numerical solutions of FDEs where high accuracy is required in the presence of shocks or discontinuities.

5.5. Monte Carlo Method. The Monte Carlo method has advantage in solving nonlinear, high dimensional, complex geometry problems. In order to get the approximation of a small domain, the determined methods, such as FDM, must resolve the total definition domain with boundary conditions. The Monte Carlo method only focuses on the small domain. This property is very useful if we are only interested in this small domain. The Monte Carlo method is easy to be parallelized and needs much less memory space than determined methods. The fractional equations are a kind of nonlinear problem and their high dimensional problems are very computation intensive. So Monte Carlo method for FDEs needs to be studied in the future. Because of the high nonlinear and nonlocal property of FDEs, the sampling efficiency will be the key point of Monte Carlo method for FDEs.

6. Conclusions

In this paper, we give a comprehensive review of FDEs and its computational challenge. This kind of challenge will become an incoming problem for the computer industry if the real fractional problems need to be approximated. We reviewed a wide range of computational costs that come from different kinds of fractional equations. While we have collected several potential solutions on this challenge, we believe that the long-term legacy of solutions will allow the real world scientific and engineering applications come true.

Conflict of Interests

The authors declare that there is no conflict of interests regarding the publication of this paper.

Acknowledgments

This research work is supported in part by the National Natural Science Foundation of China under Grants no. 61402039, no. 61303265, and no. 60970033, in part by Specialized Research Fund for the Doctoral Program of Higher Education under Grant no. 20114307110001, and in part by 973 Program of China under Grants no. 2014CB430205 and no. 61312701001. The authors would like to thank the anonymous reviewers for their helpful comments as well.

References

[1] R. Klages, G. Radons, and I. Sokolov, *Anomalous Transport: Foundations and Applications*, Wiley-VCH, Weinheim, Germany, 2008.

[2] R. R. Nigmatullin, T. Omay, and D. Baleanu, "On fractional filtering versus conventional filtering in economics," *Communications in Nonlinear Science and Numerical Simulation*, vol. 15, no. 4, pp. 979–986, 2010.

[3] I. Podlubny, *Fractional Differential Equations*, Academic Press, San Diego, Calif, USA, 1999.

[4] G. Maione and A. Punzi, "Combining differential evolution and particle swarm optimization to tune and realize fractional-order controllers," *Mathematical and Computer Modelling of Dynamical Systems*, vol. 19, no. 3, pp. 277–299, 2013.

[5] D. Baleanu, A. K. Golmankhaneh, R. Nigmatullin, and A. K. Golmankhaneh, "Fractional Newtonian mechanics," *Central European Journal of Physics*, vol. 8, no. 1, pp. 120–125, 2010.

[6] C. Farges, M. Moze, and J. Sabatier, "Pseudo-state feedback stabilization of commensurate fractional order systems," *Automatica*, vol. 46, no. 10, pp. 1730–1734, 2010.

[7] Rajeev and M. Kushwaha, "Homotopy perturbation method for a limit case Stefan problem governed by fractional diffusion equation," *Applied Mathematical Modelling*, vol. 37, no. 5, pp. 3589–3599, 2013.

[8] R. Schumer, M. M. Meerschaert, and B. Baeumer, "Fractional advectiondispersion equations for modeling transport at the Earth surface," *Journal of Geophysical Research: Earth Surface*, vol. 114, no. 4, Article ID F00A07, 2009.

[9] G. Maione, "High-speed digital realizations of fractional operators in the delta domain," *IEEE Transactions on Automatic Control*, vol. 56, no. 3, pp. 697–702, 2011.

[10] C. Gong, W. Bao, G. Tang, C. Min, and J. Liu, "An efficient iteration method for toeplitz -plus-band triangular systems generated from fractional ordinary differential equation," *Mathematical Problems in Engineering*, vol. 2014, Article ID 194249, 5 pages, 2014.

[11] J. C. Trigeassou, N. Maamri, J. Sabatier, and A. Oustaloup, "A Lyapunov approach to the stability of fractional differential equations," *Signal Processing*, vol. 91, no. 3, pp. 437–445, 2011.

[12] J. Sabatier, M. Moze, and C. Farges, "LMI stability conditions for fractional order systems," *Computers and Mathematics with Applications*, vol. 59, no. 5, pp. 1594–1609, 2010.

[13] G. Maione, "On the Laguerre rational approximation to fractional discrete derivative and integral operators," *IEEE Transactions on Automatic Control*, vol. 58, no. 6, pp. 1579–1585, 2013.

[14] H. Jiang, F. Liu, I. Turner, and K. Burrage, "Analytical solutions for the multi-term time-fractional diffusion-wave/diffusion equations in a finite domain," *Computers and Mathematics with Applications*, vol. 64, no. 10, pp. 3377–3388, 2012.

[15] M. Alipour and D. Baleanu, "Approximate analytical solution for nonlinear system of fractional differential equations by BPs operational matrices," *Advances in Mathematical Physics*, vol. 2013, Article ID 954015, 9 pages, 2013.

[16] S. Saha Ray, "Analytical solution for the space fractional diffusion equation by two-step adomian decomposition method," *Communications in Nonlinear Science and Numerical Simulation*, vol. 14, no. 4, pp. 1295–1306, 2009.

[17] S. Momani and Z. Odibat, "Comparison between the homotopy perturbation method and the variational iteration method for linear fractional partial differential equations," *Computers and Mathematics with Applications*, vol. 54, no. 7-8, pp. 910–919, 2007.

[18] S. Chen, F. Liu, and V. Anh, "A novel implicit finite difference method for the one-dimensional fractional percolation equation," *Numerical Algorithms*, vol. 56, no. 4, pp. 517–535, 2011.

[19] J. Yan, G.-M. Tan, and N.-H. Sun, "Optimizing parallel Sn sweeps on unstructured grids for multi-core clusters," *Journal of Computer Science and Technology*, vol. 28, no. 4, pp. 657–670, 2013.

[20] H. Yang and X.-C. Cai, "Parallel fully implicit two-grid methods for distributed control of unsteady incompressible flows," *International Journal for Numerical Methods in Fluids*, vol. 72, no. 1, pp. 1–21, 2013.

[21] X. Liu, T. Gu, X. Hang, and Z. Sheng, "A parallel version of QMRCGSTAB method for large linear systems in distributed parallel environments," *Applied Mathematics and Computation*, vol. 172, no. 2, pp. 744–752, 2006.

[22] D. Ming, "A parallel Attainable Region construction method suitable for implementation on a graphics processing unit (GPU)," *Computers and Chemical Engineering*, vol. 67, pp. 103–120, 2014.

[23] X. Liao, L. Xiao, C. Yang, and Y. Lu, "Milkyway-2 supercomputer: system and application," *Frontiers of Computer Science*, vol. 8, no. 3, pp. 345–356, 2014.

[24] W. Xu, Y. Lu, Q. Li et al., "Hybrid hierarchy storage system in MilkyWay-2 supercomputer," *Frontiers of Computer Science*, vol. 8, no. 3, pp. 367–377, 2014.

[25] F. Aquotte and A. F. da Silva, "PSIM: a modular particle system on graphics processing unit," *IEEE Latin America Transactions*, vol. 12, no. 2, pp. 321–329, 2014.

[26] S. J. Pennycook, S. D. Hammond, S. A. Jarvis, and G. R. Mudalige, "Performance analysis of a hybrid MPI/CUDA implementation of the NASLU benchmark," *ACM SIGMETRICS Performance Evaluation Review*, vol. 38, no. 4, pp. 23–29, 2011.

[27] D. Mu, P. Chen, and L. Wang, "Accelerating the discontinuous Galerkin method for seismic wave propagation simulations using the graphic processing unit (GPU)-single-GPU implementation," *Computers and Geosciences*, vol. 51, pp. 282–292, 2013.

[28] S. Mauger, G. C. de Verdière, L. Bergé, and S. Skupin, "GPU accelerated fully space and time resolved numerical simulations of self-focusing laser beams in SBS-active media," *Journal of Computational Physics*, vol. 235, pp. 606–625, 2013.

[29] J. T. Machado, V. Kiryakova, and F. Mainardi, "Recent history of fractional calculus," *Communications in Nonlinear Science and Numerical Simulation*, vol. 16, no. 3, pp. 1140–1153, 2011.

[30] J. A. Tenreiro Machado, V. Kiryakova, and F. Mainardi, "A poster about the recent history of fractional calculus," *Fractional Calculus & Applied Analysis*, vol. 13, no. 3, pp. 329–334, 2010.

[31] A. Loverro, "Fractional calculus: history, definitions and applications for the engineer," Tech. Rep. 46556, Department of Aerospace and Mechanical Engineering, Notre Dame, Ind, USA, 2004.

[32] K. Nishimoto, *An Essence of Nishimoto's Fractional Calculus (Calculus in the 21st Century): Integrations and Differentiations of Arbitrary Order*, Descartes Press Company, 1991.

[33] M. Cui, "Compact alternating direction implicit method for two-dimensional time fractional diffusion equation," *Journal of Computational Physics*, vol. 231, no. 6, pp. 2621–2633, 2012.

[34] W. Zhang, X. Cai, and S. Holm, "Time-fractional heat equations and negative absolute temperatures," *Computers and Mathematics with Applications*, vol. 67, no. 1, pp. 164–171, 2014.

[35] Q. Yang, F. Liu, and I. Turner, "Numerical methods for fractional partial differential equations with Riesz space fractional derivatives," *Applied Mathematical Modelling: Simulation and Computation for Engineering and Environmental Systems*, vol. 34, no. 1, pp. 200–218, 2010.

[36] J. Zhao, J. Xiao, and Y. Xu, "A finite element method for the multiterm time-space Riesz fractional advection-diffusion equations in finite domain," *Abstract and Applied Analysis*, vol. 2013, Article ID 868035, 15 pages, 2013.

[37] Y. Lin and C. Xu, "Finite difference/spectral approximations for the time-fractional diffusion equation," *Journal of Computational Physics*, vol. 225, no. 2, pp. 1533–1552, 2007.

[38] C. Tadjeran and M. M. Meerschaert, "A second-order accurate numerical method for the two-dimensional fractional diffusion equation," *Journal of Computational Physics*, vol. 220, no. 2, pp. 813–823, 2007.

[39] N. J. Ford, J. Xiao, and Y. Yan, "Stability of a numerical method for a space-time-fractional telegraph equation," *Computational Methods in Applied Mathematics*, vol. 12, no. 3, pp. 273–288, 2012.

[40] T. Chang, "Boundary integral operator for the fractional laplace equation in a bounded lipschitz domain," *Integral Equations and Operator Theory*, vol. 72, no. 3, pp. 345–361, 2012.

[41] G. Jumarie, "Derivation and solutions of some fractional Black-Scholes equations in coarse-grained space and time. Application to Merton's optimal portfolio," *Computers & Mathematics with Applications*, vol. 59, no. 3, pp. 1142–1164, 2010.

[42] P. Straka, M. M. Meerschaert, R. J. McGough, and Y. Zhou, "Fractional wave equations with attenuation," *Fractional Calculus and Applied Analysis*, vol. 16, no. 1, pp. 262–272, 2013.

[43] W. Deng, "Finite element method for the space and time fractional Fokker-Planck equation," *SIAM Journal on Numerical Analysis*, vol. 47, no. 1, pp. 204–226, 2008.

[44] S. Momani and Z. Odibat, "Analytical solution of a time-fractional Navier-Stokes equation by Adomian decomposition method," *Applied Mathematics and Computation*, vol. 177, no. 2, pp. 488–494, 2006.

[45] M. A. Herzallah and D. Baleanu, "Fractional Euler-Lagrange equations revisited," *Nonlinear Dynamics*, vol. 69, no. 3, pp. 977–982, 2012.

[46] A. I. Saichev and G. M. Zaslavsky, "Fractional kinetic equations: solutions and applications," *Chaos*, vol. 7, no. 4, pp. 753–764, 1997.

[47] T. Wenchang, P. Wenxiao, and X. Mingyu, "A note on unsteady flows of a viscoelastic fluid with the fractional Maxwell model between two parallel plates," *International Journal of Non-Linear Mechanics*, vol. 38, no. 5, pp. 645–650, 2003.

[48] R. A. El-Nabulsi, "The fractional Boltzmann transport equation," *Computers and Mathematics with Applications*, vol. 62, no. 3, pp. 1568–1575, 2011.

[49] K. Diethelm, "An investigation of some nonclassical methods for the numerical approximation of Caputo-type fractional derivatives," *Numerical Algorithms*, vol. 47, no. 4, pp. 361–390, 2008.

[50] K. Diethelm, N. J. Ford, and A. D. Freed, "A predictor-corrector approach for the numerical solution of fractional differential equations," *Nonlinear Dynamics*, vol. 29, no. 1–4, pp. 3–22, 2002.

[51] M. Cui, "Compact finite difference method for the fractional diffusion equation," *Journal of Computational Physics*, vol. 228, no. 20, pp. 7792–7804, 2009.

[52] N. J. Ford, J. Xiao, and Y. Yan, "A finite element method for time fractional partial differential equations," *Fractional Calculus and Applied Analysis*, vol. 14, no. 3, pp. 454–474, 2011.

[53] X. Zhang, J. Liu, J. Wen, B. Tang, and Y. He, "Analysis for one-dimensional time-fractional Tricomi-type equations by LDG methods," *Numerical Algorithms*, vol. 63, no. 1, pp. 143–164, 2013.

[54] K. Mustapha and W. McLean, "Uniform convergence for a discontinuous Galerkin, time-stepping method applied to a fractional diffusion equation," *IMA Journal of Numerical Analysis*, vol. 32, no. 3, pp. 906–925, 2012.

[55] Q. Yang, I. Turner, F. Liu, and M. Ilić, "Novel numerical methods for solving the time-space fractional diffusion equation in two dimensions," *SIAM Journal on Scientific Computing*, vol. 33, no. 3, pp. 1159–1180, 2011.

[56] H. Hejazi, T. Moroney, and F. Liu, "A finite volume method for solving the two-sided time-space fractional advection-dispersion equation," *Central European Journal of Physics*, vol. 11, no. 10, pp. 1275–1283, 2013.

[57] H. Hejazi, T. Moroney, and F. Liu, "Stability and convergence of a finite volume method for the space fractional advection-dispersion equation," *Journal of Computational and Applied Mathematics*, vol. 255, pp. 684–697, 2014.

[58] S. Momani, "An explicit and numerical solutions of the fractional KdV equation," *Mathematics and Computers in Simulation*, vol. 70, no. 2, pp. 110–118, 2005.

[59] B. Tang, C. Jiang, and H. Zhu, "Fractional fourier transform for confluent hypergeometric beams," *Physics Letters A*, vol. 376, no. 38-39, pp. 2627–2631, 2012.

[60] A. R. Carella and C. A. Dorao, "Least-squares spectral method for the solution of a fractional advection-dispersion equation," *Journal of Computational Physics*, vol. 232, pp. 33–45, 2013.

[61] A. Shirzadi, L. Ling, and S. Abbasbandy, "Meshless simulations of the two-dimensional fractional-time convection-diffusion-reaction equations," *Engineering Analysis with Boundary Elements*, vol. 36, no. 11, pp. 1522–1527, 2012.

[62] Q. Liu, F. Liu, I. Turner, V. Anh, and Y. T. Gu, "A RBF meshless approach for modeling a fractal mobile/immobile transport model," *Applied Mathematics and Computation*, vol. 226, pp. 336–347, 2014.

[63] Q. Liu, Y. T. Gu, P. Zhuang, F. Liu, and Y. F. Nie, "An implicit RBF meshless approach for time fractional diffusion equations," *Computational Mechanics*, vol. 48, no. 1, pp. 1–12, 2011.

[64] R. Garrappa, "A family of Adams exponential integrators for fractional linear systems," *Computers and Mathematics with Applications*, vol. 66, no. 5, pp. 717–727, 2013.

[65] R. Garrappa and M. Popolizio, "Generalized exponential time differencing methods for fractional order problems," *Computers & Mathematics with Applications*, vol. 62, no. 3, pp. 876–890, 2011.

[66] D. Fulger, E. Scalas, and G. Germano, "Monte Carlo simulation of uncoupled continuous-time random walks yielding a stochastic solution of the space-time fractional diffusion equation," *Physical Review E*, vol. 77, no. 2, Article ID 021122, 2008.

[67] C. Gong, W. Bao, G. Tang, Y. Jiang, and J. Liu, "A parallel algorithm for the two-dimensional time fractional diffusion equation with implicit difference method," *The Scientific World Journal*, vol. 2014, Article ID 219580, 8 pages, 2014.

[68] J. Q. Murillo and S. B. Yuste, "An explicit difference method for solving fractional diffusion and diffusion-wave equations in the caputo form," *Journal of Computational and Nonlinear Dynamics*, vol. 6, no. 2, Article ID 021014, 2011.

[69] C. Gong, W. Bao, G. Tang, B. Yang, and J. Liu, "An efficient parallel solution for Caputo fractional reaction-diffusion equation," *Journal of Supercomputing*, vol. 68, no. 3, pp. 1521–1537, 2014.

[70] C. Tadjeran, M. M. Meerschaert, and H. P. Scheffler, "A second-order accurate numerical approximation for the fractional diffusion equation," *Journal of Computational Physics*, vol. 213, no. 1, pp. 205–213, 2006, http://dx.doi.org/10.1016/j.jcp.2005.08.008.

[71] M. M. Meerschaert, D. A. Benson, H.-P. Scheffler, and P. Becker-Kern, "Governing equations and solutions of anomalous random walk limits," *Physical Review E*, vol. 66, no. 6, Article ID 060102, 2002.

[72] R. Metzler and J. Klafter, "The restaurant at the end of the random walk: recent developments in the description of anomalous transport by fractional dynamics," *Journal of Physics A: Mathematical and General*, vol. 37, no. 31, pp. R161–R208, 2004.

[73] K. S. Miller and B. Ross, *An Introduction to the Fractional Calculus and Fractional Differential Equations*, John Wiley & Sons, New York, NY, USA, 1993.

[74] S. Shen, F. Liu, V. Anh, and I. Turner, "The fundamental solution and numerical solution of the Riesz fractional advection-dispersion equation," *IMA Journal of Applied Mathematics*, vol. 73, no. 6, pp. 850–872, 2008.

[75] C. Çelik and M. Duman, "Crank-Nicolson method for the fractional diffusion equation with the Riesz fractional derivative," *Journal of Computational Physics*, vol. 231, no. 4, pp. 1743–1750, 2012.

[76] J. Chen and F. Liu, "Analysis of stability and convergence of numerical approximation for the Riesz fractional reaction-dispersion equation," *Journal of Xiamen University*, vol. 45, no. 4, pp. 466–469, 2006 (Chinese).

[77] C. Gong, W. Bao, and G. Tang, "A parallel algorithm for the Riesz fractional reaction-diffusion equation with explicit finite difference method," *Fractional Calculus and Applied Analysis*, vol. 16, no. 3, pp. 654–669, 2013.

[78] A. Yildirim and H. Koçak, "Homotopy perturbation method for solving the space-time fractional advection-dispersion equation," *Advances in Water Resources*, vol. 32, no. 12, pp. 1711–1716, 2009.

[79] S. Shen, F. Liu, and V. Anh, "Numerical approximations and solution techniques for the space-time Riesz-Caputo fractional advection-diffusion equation," *Numerical Algorithms*, vol. 56, no. 3, pp. 383–403, 2011.

[80] F. Liu, P. Zhuang, V. Anh, I. Turner, and K. Burrage, "Stability and convergence of the difference methods for the space-time fractional advection-diffusion equation," *Applied Mathematics and Computation*, vol. 191, no. 1, pp. 12–20, 2007.

[81] C.-M. Chen and F. Liu, "A numerical approximation method for solving a three-dimensional space Galilei invariant fractional advection-diffusion equation," *Journal of Applied Mathematics and Computing*, vol. 30, no. 1-2, pp. 219–236, 2009.

[82] K. Mustapha, "An implicit finite-difference time-stepping method for a sub-diffusion equation, with spatial discretization by finite elements," *IMA Journal of Numerical Analysis*, vol. 31, no. 2, pp. 719–739, 2011.

[83] J. Huang, N. Nie, and Y. Tang, "A second order finite difference-spectral method for space fractional diffusion equations," *Science China Mathematics*, vol. 57, no. 6, pp. 1303–1317, 2014.

[84] P. Zhuang, F. Liu, V. Anh, and I. Turner, "Numerical methods for the variable-order fractional advection-diffusion equation with a nonlinear source term," *SIAM Journal on Numerical Analysis*, vol. 47, no. 3, pp. 1760–1781, 2009.

[85] M. Cui, "Convergence analysis of high-order compact alternating direction implicit schemes for the two-dimensional time fractional diffusion equation," *Numerical Algorithms*, vol. 62, no. 3, pp. 383–409, 2013.

[86] H. Wang and T. S. Basu, "A fast finite difference method for two-dimensional space-fractional diffusion equations," *SIAM Journal on Scientific Computing*, vol. 34, no. 5, pp. A2444–A2458, 2012.

[87] P. Zhuang and F. Liu, "Finite difference approximation for two-dimensional time fractional diffusion equation," *Journal of Algorithms & Computational Technology*, vol. 1, no. 1, pp. 1–15, 2007.

[88] H. Sun, W. Chen, and Y. Chen, "Variable-order fractional differential operators in anomalous diffusion modeling," *Physica A: Statistical Mechanics and Its Applications*, vol. 388, no. 21, pp. 4586–4592, 2009.

[89] X. Liao, "MilkyWay-2: back to the world Top 1," *Frontiers of Computer Science*, vol. 8, no. 3, pp. 343–344, 2014.

[90] S. J. Pennycook, S. D. Hammond, G. R. Mudalige, S. A. Wright, and S. A. Jarvis, "On the acceleration of wavefront applications using distributed many-core architectures," *Computer Journal*, vol. 55, no. 2, pp. 138–153, 2012.

[91] Q. Xu, G.-L. Yu, K. Wang, and J.-L. Sun, "Research on gpu-accelerated algorithm in 3d finite difference neutro n diffusion calculation method," *Nuclear Science and Techniques*, vol. 25, no. 1, Article ID 010501, 2014.

[92] M. Rosa, J. S. Warsa, and M. Perks, "A cellwise block-gauss-seidel iterative method for multigroup S_N transport on a hybrid parallel computer architecture," *Nuclear Science and Engineering*, vol. 174, no. 3, pp. 209–226, 2013.

[93] A. K. Jha, M. A. Kupinski, H. H. Barrett, E. Clarkson, and J. H. Hartman, "Three-dimensional Neumann-series approach to model light transport in nonuniform media," *Journal of the Optical Society of America A*, vol. 29, no. 9, pp. 1885–1899, 2012.

[94] C. Xu, X. Deng, L. Zhang et al., "Parallelizing a high-order CFD software for 3D, multi-block, structural grids on the TianHe-1A supercomputer," in *Supercomputing*, vol. 7905 of *Lecture Notes in Computer Science*, Springer, Berlin, Germany, 2013.

[95] Y.-X. Wang, L.-L. Zhang, W. Liu et al., "Efficient parallel implementation of large scale 3D structured grid CFD applications on the Tianhe-1A supercomputer," *Computers & Fluids*, vol. 80, no. 1, pp. 244–250, 2013.

[96] Q. Wu, C. Yang, T. Tang, and L. Xiao, "Exploiting hierarchy parallelism for molecular dynamics on a petascale heterogeneous system," *Journal of Parallel and Distributed Computing*, vol. 73, no. 12, pp. 1592–1604, 2013.

[97] F. Chen and J. Shen, "A GPU parallelized spectral method for elliptic equations in rectangular domains," *Journal of Computational Physics*, vol. 250, pp. 555–564, 2013.

[98] Z. Mo, A. Zhang, X. Cao et al., "JASMIN: a parallel software infrastructure for scientific computing," *Frontiers of Computer Science in China*, vol. 4, no. 4, pp. 480–488, 2010.

[99] C. Xu, X. Deng, L. Zhang et al., "Collaborating CPU and GPU for large scale high-order CFD for simulations with complex grids on the tianhe-1A supercom puter," *Journal of Computational Physics*, vol. 278, pp. 275–297, 2014.

[100] R. Chen, Y. Wu, Z. Yan, Y. Zhao, and X.-C. Cai, "A parallel domain decomposition method for 3D unsteady incompressible flows at high reynolds number," *Journal of Scientific Computing*, vol. 58, no. 2, pp. 275–289, 2014.

[101] H. Yang, C. Yang, and X.-C. Cai, "Parallel domain decomposition methods with mixed order discretization for fully implicit solution of tracer transport problems on the cubed-sphere," *Journal of Scientific Computing*, 2014.

[102] C. Yang, J. Cao, and X. C. Cai, "A fully implicit domain decomposition algorithm for shallow water equations on the cubed-sphere," *SIAM Journal on Scientific Computing*, vol. 32, no. 1, pp. 418–438, 2010.

[103] C. Gong, W. Bao, G. Tang, Y. Jiang, and J. Liu, "A domain decomposition method for time fractional reaction-diffusion equation," *The Scientific World Journal*, vol. 2014, Article ID 681707, 5 pages, 2014.

[104] K. Diethelm, "An efficient parallel algorithm for the numerical solution of fractional differential equations," *Fractional Calculus and Applied Analysis*, vol. 14, no. 3, pp. 475–490, 2011.

[105] C. Gong, J. Liu, L. Chi, H. Huang, J. Fang, and Z. Gong, "GPU accelerated simulations of 3D deterministic particle transport using discrete ordinates method," *Journal of Computational Physics*, vol. 230, no. 15, pp. 6010–6022, 2011.

[106] C. Gong, J. Liu, Z. Gong, J. Qin, and J. Xie, "Optimizing Sweep3D for graphic processor unit," in *Algorithms and Architectures for Parallel Processing*, C.-H. Hsu, L. Yang, J. Park, and S.-S. Yeo, Eds., vol. 6081 of *Lecture Notes in Computer Science*, pp. 416–426, Springer, Berlin, Germany, 2010.

[107] X. Gan, C. Liu, Z. Wang et al., "Accelerating GOR algorithm using CUDA," *Applied Mathematics and Information Sciences*, vol. 7, no. 2, pp. 563–567, 2013.

[108] C. Gong, J. Liu, H. Huang, and Z. Gong, "Particle transport with unstructured grid on GPU," *Computer Physics Communications*, vol. 183, no. 3, pp. 588–593, 2012.

[109] X. Gan, Z. Wang, L. Shen, and Q. Zhu, "Data layout pruning on GPU," *Applied Mathematics & Information Sciences*, vol. 5, no. 2, pp. 129–138, 2011.

[110] W. Zhang, W. Wei, and X. Cai, "Performance modeling of serial and parallel implementations of the fractional Adams-Bashforth-Moulton method," *Fractional Calculus and Applied Analysis*, vol. 17, no. 3, pp. 617–637, 2014.

[111] J. Liu, C. Gong, W. Bao, G. Tang, and Y. Jiang, "Solving the Caputo fractional reaction-diffusion equation on GPU," *Discrete Dynamics in Nature and Society*, vol. 2014, Article ID 820162, 2014.

[112] Y. Xu and Z. He, "The short memory principle for solving Abel differential equation of fractional order," *Computers and Mathematics with Applications*, vol. 62, no. 12, pp. 4796–4805, 2011.

[113] W. Deng, "Short memory principle and a predictor-corrector approach for fractional differential equations," *Journal of Computational and Applied Mathematics*, vol. 206, no. 1, pp. 174–188, 2007.

[114] N. J. Ford and A. C. Simpson, "The numerical solution of fractional differential equations: speed versus accuracy," *Numerical Algorithms*, vol. 26, no. 4, pp. 333–346, 2001.

[115] H.-L. Cao, X. Li, Z.-H. Deng, and Y. Qin, "Control-oriented fast numerical approaches of fractional-order models," *Control Theory and Applications*, vol. 28, no. 5, pp. 715–721, 2011 (Chinese).

[116] H. Wang, K. Wang, and T. Sircar, "A direct $O(N\log^2 N)$ finite difference method for fractional diffusion equations," *Journal of Computational Physics*, vol. 229, no. 21, pp. 8095–8104, 2010.

[117] H. Wang and K. Wang, "An $O(N\log^2 N)$ alternating-direction finite difference method for two-dimensional fractional diffusion equations," *Journal of Computational Physics*, vol. 230, no. 21, pp. 7830–7839, 2011.

[118] H. Wang and N. Du, "A superfast-preconditioned iterative method for steady-state space-fractional diffusion equations," *Journal of Computational Physics*, vol. 240, pp. 49–57, 2013.

[119] H.-K. Pang and H.-W. Sun, "Multigrid method for fractional diffusion equations," *Journal of Computational Physics*, vol. 231, no. 2, pp. 693–703, 2012.

[120] Z. Zhou and H. Wu, "Finite element multigrid method for the boundary value problem of fractional advection dispersion equation," *Journal of Applied Mathematics*, vol. 2013, Article ID 385403, 8 pages, 2013.

[121] S.-L. Lei and H.-W. Sun, "A circulant preconditioner for fractional diffusion equations," *Journal of Computational Physics*, vol. 242, pp. 715–725, 2013.

[122] T. Moroney and Q. Yang, "A banded preconditioner for the two-sided, nonlinear space-fractional diffusion equation," *Computers and Mathematics with Applications*, vol. 66, no. 5, pp. 659–667, 2013.

[123] T. Moroney and Q. Yang, "Efficient solution of two-sided nonlinear space-fractional diffusion equations using fast poisson preconditioners," *Journal of Computational Physics*, vol. 246, pp. 304–317, 2013.

[124] J. A. Tenreiro Machado, "Fractional derivatives: probability interpretation and frequency response of rational approximations," *Communications in Nonlinear Science and Numerical Simulation*, vol. 14, no. 9-10, pp. 3492–3497, 2009.

[125] F.-R. Lin, S.-W. Yang, and X.-Q. Jin, "Preconditioned iterative methods for fractional diffusion equation," *Journal of Computational Physics*, vol. 256, pp. 109–117, 2014.

[126] W. Deng, S. Du, and Y. Wu, "High order finite difference WENO schemes for fractional differential equations," *Applied Mathematics Letters*, vol. 26, no. 3, pp. 362–366, 2013.

[127] H. Zhou, W. Tian, and W. Deng, "Quasi-compact finite difference schemes for space fractional diffusion equations," *Journal of Scientific Computing*, vol. 56, no. 1, pp. 45–66, 2013.

[128] C. Lubich, "Discretized fractional calculus," *SIAM Journal on Mathematical Analysis*, vol. 17, no. 3, pp. 704–719, 1986.

Research Article

Hybrid Prediction and Fractal Hyperspectral Image Compression

Shiping Zhu,[1] Dongyu Zhao,[1] and Fengchao Wang[2]

[1] *Department of Measurement Control and Information Technology, School of Instrumentation Science and Optoelectronics Engineering, Beihang University, Beijing 100191, China*
[2] *CSR Qingdao Sifang Locomotive and Rolling Stock Co., Ltd., No. 88 Jinhong East Road, Chengyang District, Qingdao 266111, China*

Correspondence should be addressed to Shiping Zhu; spzhu@163.com

Received 16 July 2014; Revised 20 October 2014; Accepted 21 October 2014

Academic Editor: J. A. Tenreiro Machado

Copyright © 2015 Shiping Zhu et al. This is an open access article distributed under the Creative Commons Attribution License, which permits unrestricted use, distribution, and reproduction in any medium, provided the original work is properly cited.

The data size of hyperspectral image is too large for storage and transmission, and it has become a bottleneck restricting its applications. So it is necessary to study a high efficiency compression method for hyperspectral image. Prediction encoding is easy to realize and has been studied widely in the hyperspectral image compression field. Fractal coding has the advantages of high compression ratio, resolution independence, and a fast decoding speed, but its application in the hyperspectral image compression field is not popular. In this paper, we propose a novel algorithm for hyperspectral image compression based on hybrid prediction and fractal. Intraband prediction is implemented to the first band and all the remaining bands are encoded by modified fractal coding algorithm. The proposed algorithm can effectively exploit the spectral correlation in hyperspectral image, since each range block is approximated by the domain block in the adjacent band, which is of the same size as the range block. Experimental results indicate that the proposed algorithm provides very promising performance at low bitrate. Compared to other algorithms, the encoding complexity is lower, the decoding quality has a great enhancement, and the PSNR can be increased by about 5 dB to 10 dB.

1. Introduction

Hyperspectral imaging technology is a major innovation in the course of development of remote sensing technology, which combines ground target spectra determined by material composition and the image reflecting ground target existing layout completely, and provides spectral information of dozens to hundreds of narrow bands while obtaining target spatial information for each pixel, thereby achieving a unity of image and spectra [1]. Hyperspectral remote sensing has been successfully applied in many areas such as geology, ecology, atmospheric study, and soil study and is playing an increasingly important role [2].

Hyperspectral image adds 3D spectral information based on 2D information about ground image. Hyperspectral data is a cube of a spectral image, whose spatial image dimension reflects the 2D spatial distribution of ground target features and whose spectral dimension reflects the spectral curve features. Spatial correlation exists in the spatial image dimension of hyperspectral image data and spectral correlation exists in the spectral dimension [3]. Accordingly, the difference between hyperspectral image compression and ordinary image compression is to remove both the spatial redundancies and the spectral redundancies. At present, the commonly used hyperspectral image compression methods include prediction-based, transformation-based, and vector quantization-based methods. For example, [4] used median prediction algorithm for hyperspectral intraband prediction and then used linear prediction and context prediction mixed algorithm for hyperspectral interband prediction, thereby implementing lossless compression of hyperspectral images. Penna et al. [5] used point extraction strategy to reduce the calculated amount of KLT and applied this improved KLT to the decorrelation of hyperspectral images, without having a significant impact on reconstructed image quality. Qian [6] proposed a fast vector quantization algorithm to improve the

generation efficiency of codebook, which did not require full search, thereby greatly reducing the complexity.

In addition to the above conventional coding methods, fractal coding method characterized by its innovative ideas, high compression ratio, and resolution independence is considered as one of the most promising second-generation compression coding methods. Our previous studies of fractal video compression [7, 8] also demonstrate its good compression performance. Fractal coding techniques are based on the theory of iterated function systems (IFS) and are further developed by Barnsley in the early 1980s [9, 10]. The IFS theory is based on Banach's contraction mapping principle, which states that a contractive transformation, defined on a complete metric space, possesses a unique fixed point or attractor. For the purpose of image compression, this idea translates into finding an optimal contractive transformation whose attractor closely approximates a given target image. This problem is widely known as the inverse problem in the fractal image coding literature. But this must involve manual intervention and it is extremely hard to find a contractive transformation with an attractor approximating the whole image. In the late 1980s, Jacquin developed a block-based fractal image compression scheme exploiting local self-similarities that are inherent in many real-world images [11] and made fractal image compression become automatic. In his scheme, the image is subdivided into a pair of simple and uniform partitions: a domain partition of larger subblocks, also known as parent subblocks, and a range partition of smaller subblocks, also known as child subblocks. A parent subblock is mapped into its corresponding child subblock using a geometric mapping, followed by a simple affine transformation, known as the gray-level map. Therefore, a digitized image can be stored as a collection of the position of the corresponding parent subblock and transformation coefficients for each child subblock. This generally requires much less memory, resulting in data compression.

We observe that there exist strong similarities between adjacent bands of hyperspectral images, so that we guess that fractal coding will be suitable for hyperspectral image compression. In this paper, we make a try to combine prediction and fractal coding for hyperspectral image compression. The algorithm first carries out intraband prediction for the first band which is treated as the basic band, and we extend the block-based fractal image compression scheme to two adjacent bands, which is to say each range block is approximated by the domain block in the adjacent band, which is of the same size as the range block to remove the spectral redundancies. The experimental results with AVIRIS (airborne visible infrared imaging spectrometer) hyperspectral remote sensing images indicate that the algorithm provides very promising performance at low bitrate.

The rest of the paper is organized as follows. The basis of fractal image coding is summarized in Section 2. The proposed hybrid prediction and fractal hyperspectral image compression algorithm is presented in Section 3. The experimental results are presented in Section 4. And finally the conclusions are outlined in Section 5.

2. Fractal Image Coding Basis

2.1. Fractal Image Coding Theory. The fundamental principle of fractal coding consists of the representation of an image by a contractive transform of which the fixed point is close to that image [12]. The image space is accepted as a complete metric space. By the contractive mapping theorem and collage theorem, the contractive transform is always possible within certain threshold. Original approach with IFS tries to find a number of affine mappings on the entire image, which is rather slow in terms of searching the contractive map function. Jacquin's partitioned iteration function system (PIFS) [13] takes a different approach by finding the individual mappings for subsets of the images. Each PIFS contains a complete metric space (X, d) and a series of contraction mapping $\omega_i : X \to X$ as defined in this space. Fractal image coding just uses a PIFS to represent an original image so that the image after iterative decoding closely approximates the attractor of this PIFS as well as the original image. The contraction mapping coefficients constitute the fractal code of the original image.

The attractor theorem is as follows.

Attractor Theorem. Assuming $\{X : \omega_1, \omega_2, \omega_3, \ldots, \omega_n\}$ is an IFS in the completely metric space (X, d), then we have the following.

(1) Transformation $W : H(x) \to H(x)$ defined by the following equation:

$$W(B) = \bigcup_{i=1}^{n} \omega_n(B), \quad \forall B \in H(x), \tag{1}$$

is the contraction mapping of complete metric space $(H(x), h)$, whose contractive factor is

$$\begin{aligned} s &= \max(s_1, s_2, \ldots, s_n), \\ h(W(B), W(C)) &\le s \times h(B, C), \quad \forall B, C \in H(x), \end{aligned} \tag{2}$$

where h represents the Hausdorff metric.

(2) Compression transformation W has a unique fixed point $\overline{A} \in H(x)$, so that it satisfies the following equation:

$$\overline{A} = W\left(\overline{A}\right) = \bigcup_{i=1}^{n} \omega_i\left(\overline{A}\right). \tag{3}$$

And the fixed point can be obtained by iteration, namely:

$$\overline{A} = \lim_{n \to \infty} W^n(B), \quad \forall B \in H(x), \tag{4}$$

where

$$W^0(B) = W(B), \qquad W^n(B) = W\left(W^{n-1}(B)\right). \tag{5}$$

Fixed point $\overline{A} \in H(x)$ is called the attractor of IFS.

That is to say, for any set B, iterative sequence $W^n(B)$ converges to the attractor of PIFS. Its inverse problem takes the given original image as the attractor to solve its contraction mapping. It is very difficult to solve the inverse problem accurately, but collage theorem gives out a possible

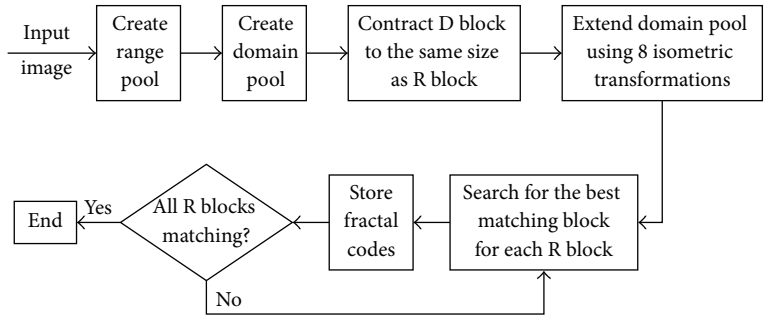

Figure 1: Flow chart of the basic block-based fractal image compression.

solution to this problem. That is, approximately minimize the distance $d(\mu_{\text{org}}, \mu_{\text{fix}})$ between original image μ_{org} and attractor image μ_{fix} by minimizing the distance $d(\mu_{\text{org}}, W\mu_{\text{org}})$ between original image μ_{org} and its collage image $W\mu_{\text{org}}$.

The collage theorem is as follows.

Collage Theorem. Assuming (X, d) is a complete metric space, given a set $L \in H(x)$ and a number $\varepsilon > 0$, if we can find a IFS$\{X; \omega_1, \omega_2, \omega_3, \ldots, \omega_n; s\}$ $(0 \le s < 1)$, which makes

$$h\left(L, \bigcup_{i=1}^{n} \omega_i(L)\right) \le \varepsilon, \tag{6}$$

then

$$h\left(L, \overline{A}\right) \le \frac{h\left(L, \bigcup_{i=1}^{n} \omega_i(L)\right)}{1-s} \le \frac{\varepsilon}{1-s}, \tag{7}$$

where h is Hausdorff metric and $\overline{A}$ is attractor of this IFS.

2.2. Fractal Image Coding Implementation. The basic block-based fractal image coding algorithm flow chart is shown in Figure 1.

Firstly, divide the original input image into nonoverlapping R blocks to form R block set $\{R\}$ and overlapped D blocks to form D block set $\{D\}$, with size of each R block at $N \times N$ and that of each D block at $2N \times 2N$. R blocks and D blocks are usually obtained by sliding window method.

Then, contract all D blocks to the size of $N \times N$, that is, the same size as R blocks, usually by downsampling or averaging the intensities of its four neighboring pixels,

$$\begin{aligned} d(x, y) &= \big(d(2x, 2y) + d(2x+1, 2y) + d(2x, 2y+1) \\ &\quad + d(2x+1, 2y+1)\big) \times \frac{1}{4}, \end{aligned} \tag{8}$$

where $d(x, y)$ represents the intensity of D block at position (x, y).

Afterwards, contracted D block is extended through 8 isometric transformations (including identical transformation; rotations by 90°, 180°, and 270° about the block center; symmetric reflections about vertical central axis, horizontal central axis, leading diagonal, and secondary diagonal). The extended domain pool is defined as $\{\widetilde{D}\}$.

In order to find the best matching block for each R block, contraction mapping transformation $\{W_i\}$ is defined as

$$W_i \begin{bmatrix} x \\ y \\ z \end{bmatrix} = \begin{bmatrix} a_i & b_i & 0 \\ c_i & d_i & 0 \\ 0 & 0 & s_i \end{bmatrix} \begin{bmatrix} x \\ y \\ z \end{bmatrix} + \begin{bmatrix} e_i \\ f_i \\ o_i \end{bmatrix}, \tag{9}$$

where x and y represent spatial coordinates; z represents pixel value; a_i, b_i, c_i, and d_i define one of the 8 isometric transformations; s_i represents brightness adjustment factor with its absolute value smaller than 1; o_i represents brightness offset factor.

Searching for matching block is a process of minimizing the following equation:

$$E\left(R, \widetilde{D}\right) = \left\| R - \left(s \cdot \widetilde{D} + o \cdot I\right) \right\|, \tag{10}$$

where $\| \cdot \|$ represents vector 2-norm.

Finally, use (9) and (10) to find the best matching block from the extended domain pool $\{\widetilde{D}\}$ for each R block and store the sequence number of isometric transformation, location of the best matching D block, and corresponding brightness scale factor s and offset factor o. After fractal parameters of all R blocks are stored, the total fractal encoding process is completed.

Fractal image decoding process is very simple, which can be completed by only inputting an arbitrary initial image (initial size of the image should be equal to that of its original image as required) and then iteratively applying the corresponding transformation to initial image based on the stored fractal parameters. Decoding process can be expressed as follows:

$$\begin{aligned} R_i^{(k)} &= s_i \cdot t_l \circ S\left(D_{m(i)}^{(k-1)}\right) + o_i \cdot I, \\ \mu^{(k)} &= \bigcup_i R_i^{(k)}, \end{aligned} \tag{11}$$

where $R_i^{(k)}$ represents the ith R block of image $\mu^{(k)}$ after k times' iterations; $D_{m(i)}^{(k-1)}$ represents the best matching block of $R_i^{(k)}$ and is derived from image $\mu^{(k-1)}$ after $k-1$ times' iterations; $D_{m(i)}^{(0)}$ is derived from the best matching D block of

the initial image; s_i and o_i represent the corresponding optimum brightness adjustment factor and offset factor, respectively; S and t_l represent spatial contraction transformation and isometric transformation, respectively. The symbol $\circ$ is the composition operator.

If k reaches a predetermined number of iterations N (generally less than 10), then stop iteration and output image $\mu^{(N)}$. This is the decoded image, namely, approximation of the image to be encoded.

3. Hybrid Prediction and Fractal Hyperspectral Image Compression

Because each band of a hyperspectral image corresponds to the same location on the earth, hyperspectral data cube has a strong spectral correlation, whose spatial correlation is relatively weak. The basic fractal image coding algorithm does not use spectral correlation, which therefore cannot be directly used for compressing hyperspectral images. In order to take full advantage of spatial and spectral correlations of hyperspectral image, we propose a method for lossy compression of hyperspectral image based on hybrid prediction and fractal. The first band is intraband prediction encoded, and the remaining bands are interband fractal encoded. The difference is that each range block is approximated by the domain block in the adjacent decoded band, which is of the same size as the range block to exploit the spectral correlation. Then the prediction errors as well as fractal residual are further transformed, quantified, and entropy encoded, and the fractal parameters are also entropy encoded to improve the compression efficiency. The compression scheme divides each band into range blocks with the size of 16×16. The block diagram for this scheme is shown in Figure 2.

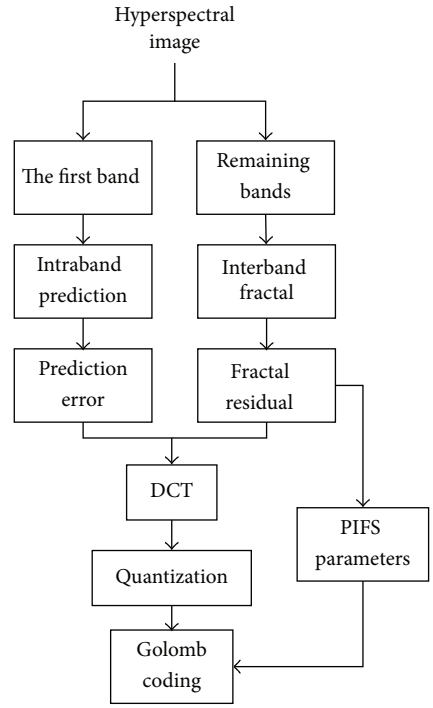

Figure 2: Block diagram of the proposed scheme.

3.1. Intraband Prediction. Linear prediction has been studied in hyperspectral image compression [14–16]. In this section, we describe the intraband prediction design of our scheme. The main purpose is to remove spatial correlation as well as obtaining a high quality decoded reference band.

Hyperspectral images are usually texture abundant. For example, Figure 3(a) shows a simulated color IR view of an airborne hyperspectral data flight line over the "Washington DC Mall," which has much detail. The sensor system used in this case measured pixel response in 210 bands in the 0.4 to 2.4 μm region of the visible and infrared spectrum. Bands in the 0.9 and 1.4 μm region where the atmosphere is opaque have been omitted from the dataset, leaving 191 bands. The dataset contains 1208 scan lines with 307 pixels in each scan line. The color image is made using bands 60, 27, and 17 for the red, green, and blue colors, respectively. Figure 3(b) is the first band of the hyperspectral image.

To predict more precisely, we design 9 linear predictors with different prediction directions, as shown in Figure 4. Eight prediction modes, as shown in Figure 4(a), are utilized for more suitably predicting textures with structures in the respective directions. The 16 samples of the 4×4 block, which is labeled as a–p, are predicted using the prior decoded neighboring pixels in the corresponding directions in the adjacent blocks labeled as A–Q, which is shown in Figure 4(b). In addition, the DC mode is used to predict smooth area, and each pixel in the shadowed block is predicted using the mean value of the neighboring pixels labeled as A–D and I–L, which is shown in Figure 4(c).

The prediction mode with the minimum sum of squared difference (SSD) is chosen as the final prediction mode. The SSD is calculated as follows:

$$\mathrm{SSD}(s,c) = \sum_{x=1}^{4}\sum_{y=1}^{4}\left(s(x,y) - c(x,y)\right)^2, \tag{12}$$

where $s(x, y)$ represents the source signal at position (x, y); $c(x, y)$ represents the reconstruction signal at position (x, y) using the corresponding prediction mode.

3.2. Interband Fractal Coding. In order to remove the existing spectral redundancy in hyperspectral image, we have made some modifications to the basic block-based fractal image compression scheme. In our scheme, each range block is approximated by the domain block in the adjacent band, which is of the same size as the range block. And considering that the adjacent bands have similar spatial topology structures, as shown in Figure 5, thus isometric transformation process can be omitted. Statistics also show that the best matching D block appears near R block with a large probability [17], so it is not necessary to use full search. In our scheme, the search range of block matching is reduced to a small region centering the corresponding position of R block, as shown in Figure 6. In addition, we adopt an adaptive block size instead of the original fixed size block partition method.

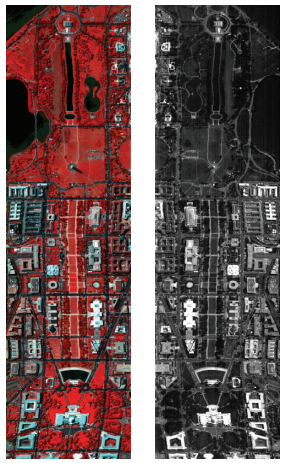

(a) The simulated color view with bands 60, 27, and 17

(b) The first band image

Figure 3: Hyperspectral data of the "Washington DC Mall."

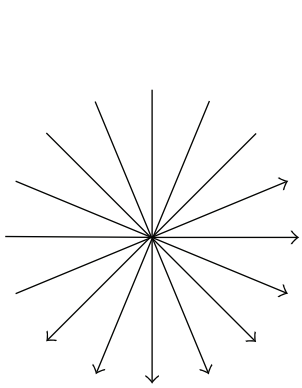

(a) 8 prediction directions

Q	A	B	C	D	E	F	G	H
I	a	b	c	d				
J	e	f	g	h				
K	i	j	k	l				
L	m	n	o	p				

(b) Directional prediction

	A	B	C	D
I				
J		Mean (A~D, I~L)		
K				
L				

(c) DC prediction

Figure 4: Predictors for intraband prediction.

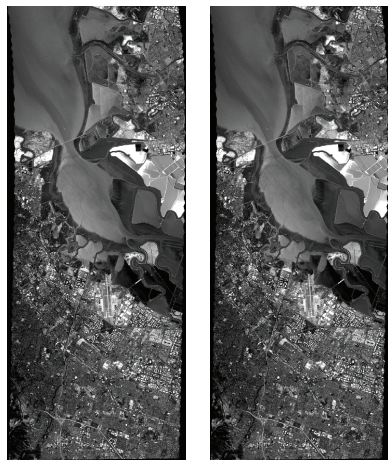

(a) The 25th band

(b) The 26th band

Figure 5: Two adjacent bands of hyperspectral image "Moffett Field."

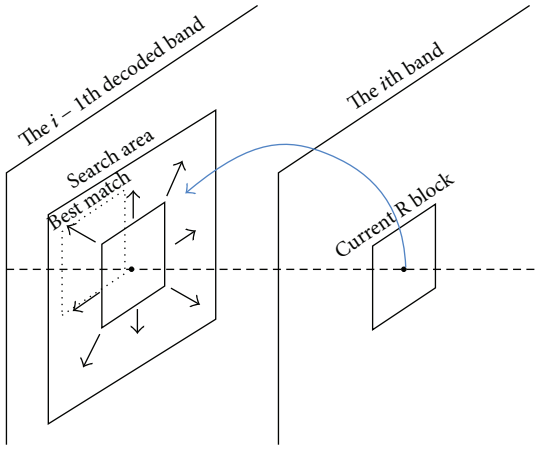

Figure 6: Sketch map of block matching.

The specific steps for interband fractal coding are as follows.

Step 1. The current hyperspectral band image is divided into nonoverlapping R blocks with the size of 16×16, and all R blocks can cover the whole band image.

Step 2. Encode each R block in turn.

(1) The searching area is located in the adjacent decoded band, and with the same coordinate of the current R block as the center, move 7 pixels (a variable parameter determined at the encoder) upward, downward, and towards left and right, to form the rectangular search area, as shown in Figure 6. Search the best matching D block in the search area, with the MSE (mean square error) as the matching criterion:

$$\mathrm{MSE}(s,o) = \frac{1}{N}\sum_{i=1}^{N}\left[r_i - (s \cdot d_i + o)\right]^2, \tag{13}$$

where r_i represents the pixel value of the current R block, d_i represents the pixel value of the corresponding matching block, N represents the number of pixels of the current R block, s is the scale factor, and o is the offset factor. s and o are obtained as follows.

Solving the equation for MSE(s, o),

$$\frac{\partial \mathrm{MSE}(s,o)}{\partial s} = \frac{1}{N}\sum_{i=1}^{N} 2\left(s \cdot d_i + o - r_i\right) \cdot d_i. \tag{14}$$

Setting to 0,

$$\begin{aligned} 0 &= s\sum_{i=1}^{N} d_i^2 + o\sum_{i=1}^{N} d_i - \sum_{i=1}^{N} r_i \cdot d_i, \\ o &= \frac{1}{\sum_{i=1}^{N} d_i}\left(\sum_{i=1}^{N} r_i \cdot d_i - s\sum_{i=1}^{N} d_i^2\right). \end{aligned} \tag{15}$$

Similarly,

$$\frac{\partial \mathrm{MSE}(s,o)}{\partial o} = \frac{1}{N}\sum_{i=1}^{N} 2\left(s \cdot d_i + o - r_i\right) \cdot 1. \tag{16}$$

Setting to 0,

$$\begin{aligned} 0 &= s\sum_{i=1}^{N} d_i + \sum_{i=1}^{N} o - \sum_{i=1}^{N} r_i, \\ s\sum_{i=1}^{N} d_i &= \sum_{i=1}^{N} r_i - N \cdot o. \end{aligned} \tag{17}$$

Substituting,

$$\begin{aligned} s &= \frac{N\left(\sum_{i=1}^{N} r_i \cdot d_i\right) - \sum_{i=1}^{N} r_i \sum_{i=1}^{N} d_i}{N\sum_{i=1}^{N} d_i^2 - \left(\sum_{i=1}^{N} d_i\right)^2}, \\ o &= \frac{1}{N}\left(\sum_{i=1}^{N} r_i - s\sum_{i=1}^{N} d_i\right). \end{aligned} \tag{18}$$

If the minimum MSE is less than T_16 (here is 10.5), the domain block can be considered as well-matched, and we can record the current IFS coefficients and continue to the next R block; otherwise, go to (2).

(2) The R block is divided into two 16×8 R subblocks. Search the best matching block for each 16×8 R subblock, respectively, in the domain pool, and the size of searched matching block is 16×8. If the minimum MSEs of the two 16×8 R subblocks are both smaller than T_16, the domain block can be considered as well-matched, and we can record the IFS coefficients of the two 16×8 R subblocks and continue to the next R block; otherwise, go to (3).

(3) The R block is divided into two 8×16 R subblocks. Search the best matching block for each 8×16 R subblock, respectively, in the search area, and the size of searched matching block is 8×16. If the minimum MSEs of the two 8×16 R subblocks are both smaller than T_16, the domain block can be considered as well-matched, and we can record the IFS coefficients of the two 16×8 R subblocks and continue to the next R block; otherwise, go to (4).

(4) This R block is divided into four 8×8 R subblocks for which, respectively, search for the best matching block also in the size of 8×8 in the search area, and if the minimum MSEs of all four 8×8 R subblocks are smaller than T_8 (here is 8.0), we can record the IFS coefficients of the four 8×8 R subblocks and continue to the next R block; otherwise, we can further divide the 8×8 R subblock which is not well matched into two 8×4 R sub-subblocks or two 4×8 R sub-subblocks or four 4×4 sub-subblocks just in the same way.

Step 3. Repeat Step 2 until all R blocks of the current hyperspectral band have found the best matching blocks.

The flowchart is shown in Figure 7.

3.3. Residual Image and Fractal Parameters Encoding. In a general prediction encoding system, once the prediction is formed, it is subtracted from the original band, and the residual is usually further compressed using transformation encoding and entropy encoding. In our scheme, the residual image of the first hyperspectral band is obtained through subtracting the predicted band image by the original band

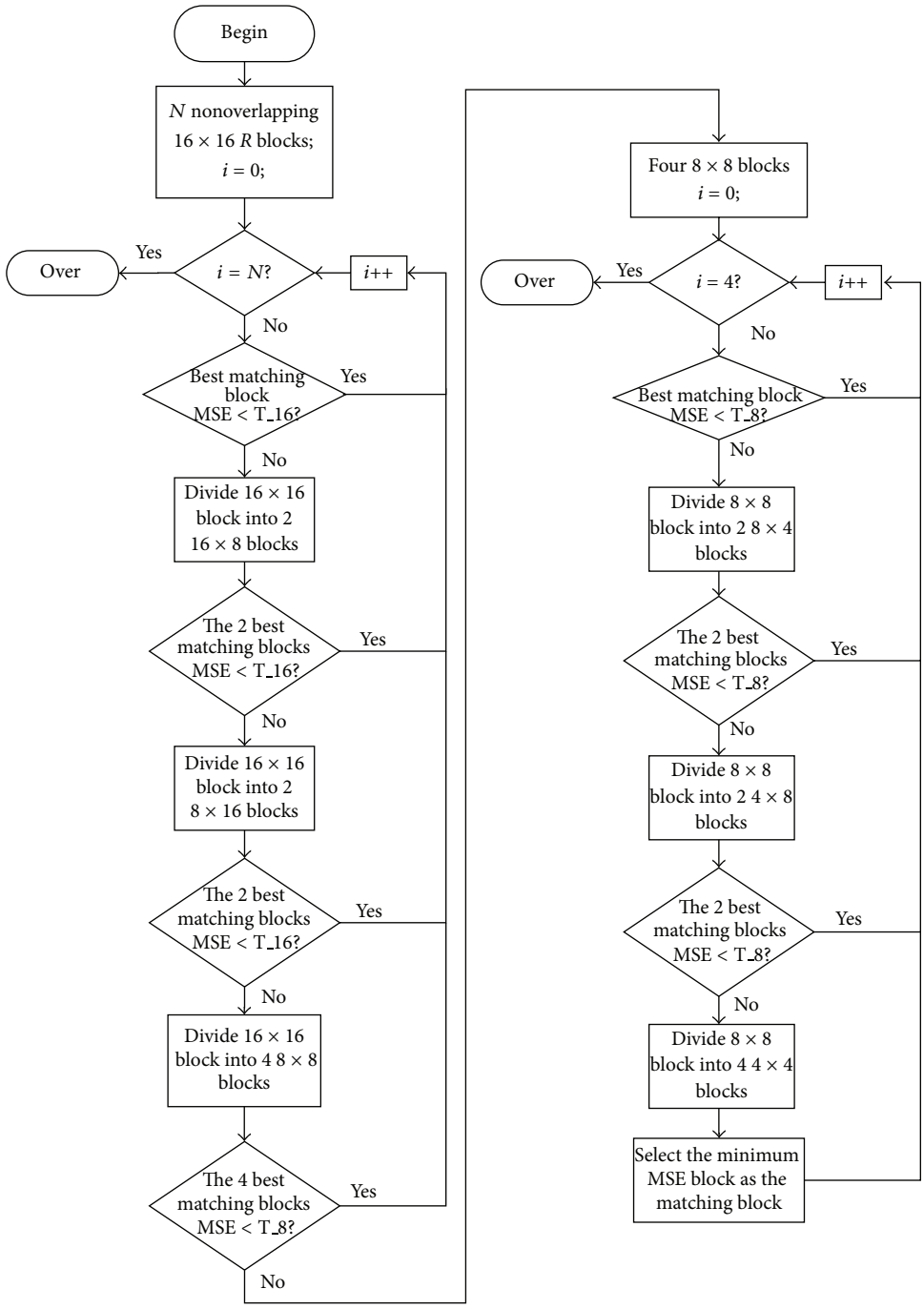

Figure 7: Flowchart of block matching process.

image. In addition, the residual of fractal encoding is also processed in the same way, while it is ignored in the basic fractal encoding algorithm and most fractal literatures. The residual image of the fractal encoding is formed by

$$\text{residual} = \sum \left(r_i - \left(s \cdot d_i + o\right)\right). \tag{19}$$

The residual image is DCT transformed, quantized, and Golomb entropy encoded. In parallel, the quantized data are rescaled and inverse transformed and added to the prediction band to reconstruct a coded version of the band which is stored for later interband fractal encoding. The fractal parameters are also Golomb entropy encoded.

4. Experimental Result

Two AVIRIS [18] hyperspectral data cubes, "Cuprite" and "Low Altitude," derived from JPL are used. The size of the data cubes was originally 512 lines × 614 pixels with 224 spectral bands and 1087 lines × 614 pixels with 224 spectral bands,

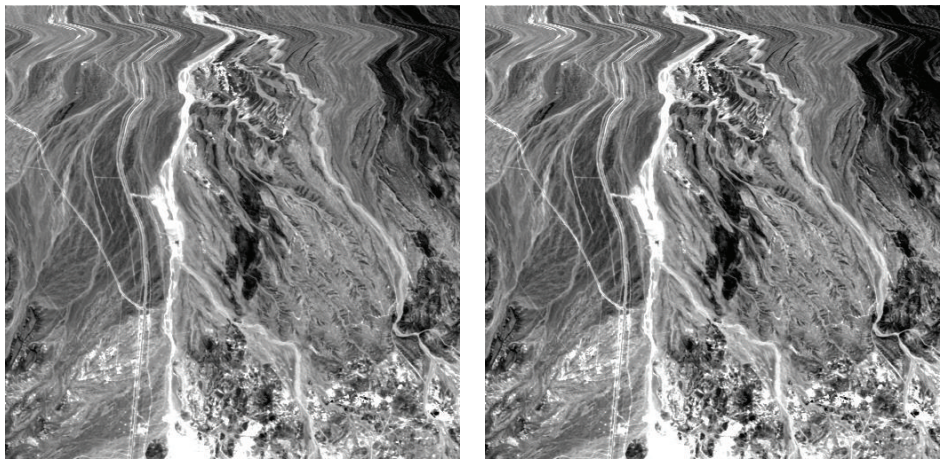

(a) Original image (b) Decoded image

Figure 8: The 17th band subimage of "Cuprite."

respectively. In this paper, a subset of them with 512 lines × 512 pixels with all 224 bands was tested. The experiments were performed on a computer with an Intel Core 2 Quad Q9300 @ 2.50 GHz CPU and 4 GB RAM. PSNR is used to measure the quality of the compression data. It is defined as follows:

$$\text{PSNR} = 10 \log_{10} \frac{\text{Peaksignal}^2}{\text{MSE}}, \quad (20)$$

where Peaksignal is the maximum value in the data cube and MSE is calculated as

$$\text{MSE} = \frac{1}{n_x n_y n_b} \sum_{x=1}^{n_x} \sum_{y=1}^{n_y} \sum_{b=1}^{n_b} \left[O(x, y, b) - D(x, y, b) \right], \quad (21)$$

where $O(x, y, b)$ and $D(x, y, b)$ are, respectively, the pixel values of the original and the reconstructed data of band b at location (x, y), n_y is the total number of lines in the data cube, n_x is the total number of pixels per line, and n_b is the total number of bands in the data cube.

Figure 8(a) shows the 17th band of "Cuprite" truncated from the original data cube for the experiment, and Figure 8(b) shows the decoded result image at 0.1 bpppb. As seen in Figure 8, there is almost no difference of subjective quality between the compressed image and the original image.

Figure 9 shows the PSNR comparison of "Low Altitude" encoded by the 3D-SPIHT [21] and the proposed algorithm. 3D-SPIHT coding is the three-dimensional extension version of the set partitioning in hierarchical trees (SPIHT) coding, which is based on the concentrative energy of wavelet coefficients, to exhibit symmetric branching in all three dimensions. More details can be found in [21]. It can be seen from Figure 9 that the PSNR of the first band by the algorithm of the article is higher than every other band, indicating that the prediction algorithm adopted obtains high encoding quality. The PSNRs of all bands of "Low Altitude" compressed by the proposed algorithm are higher than those in the 3D-SPIHT algorithm. It is calculated that the average value of

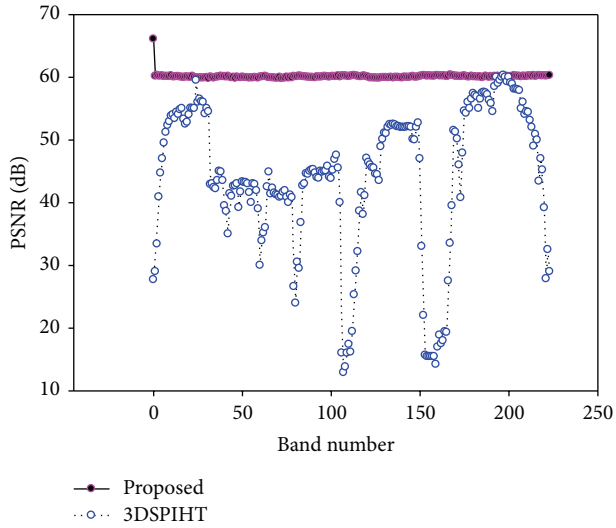

Figure 9: PSNR comparison of each band for "Low Altitude" at the compression ratio of 32 : 1.

PSNRs of all bands of "Low Altitude" compressed by the proposed algorithm is 60.07 dB, which is 15.91 dB higher than that of the 3D-SPIHT algorithm.

The PSNR comparison results at different bitrates are as shown in Tables 1 and 2. The AT-3DSPIHT [19] algorithm in Tables 1 and 2 is an improvement of 3D-SPIHT algorithm by means of asymmetric structure, having a longer tree along the wavelet axis than that of the traditional tree structure, and the PSNR performance of AT-3DSPIHT for hyperspectral image is better than 3D-SPIHT. More details can be found in [19]. Experimental results show that the PSNR of "Low Altitude" compressed by the proposed algorithm is slightly lower than that of AT-3DSPIHT at 0.1 bpppb, except that they are all higher than the contrast algorithms. In comprehensive consideration of all bitrates, compared with AT-3DSPIHT algorithm, the PSNR of the proposed algorithm is increased

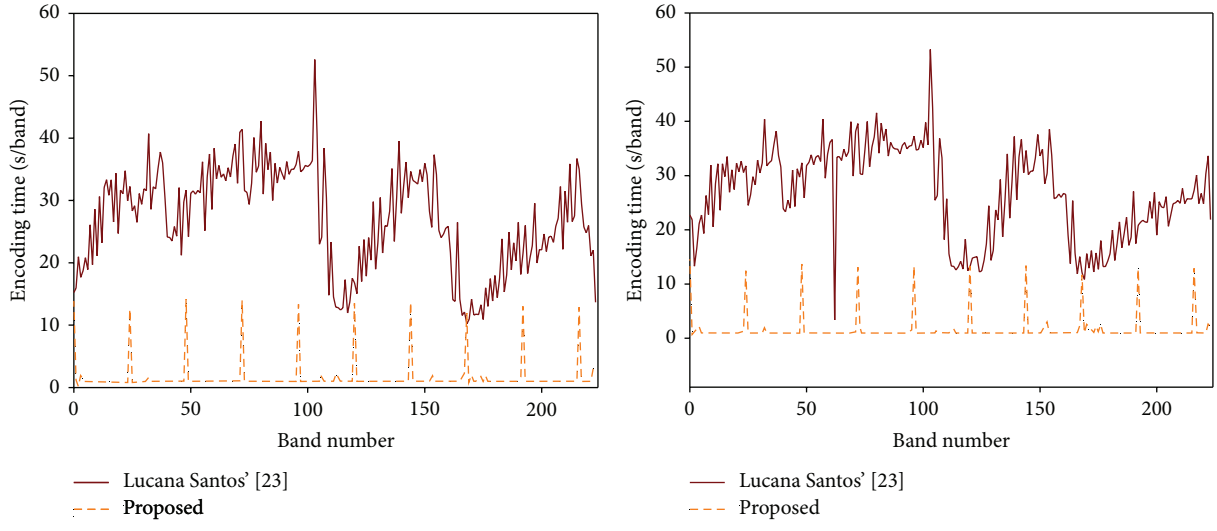

(a) Yellowstone_sc0 (b) Yellowstone_sc3

Figure 10: Encoding time comparison.

Table 1: PSNR comparison for "Low Altitude" at different bitrates (unit: dB).

	Code rate (bpp)			
	0.1	0.15	0.2	0.25
AT-3DSPIHT [19]	47.50	49.51	51.50	52.61
F. Zhao et al. [20]	41.62	43.33	44.95	46.08
Proposed	46.50	54.37	57.21	60.07

Table 2: PSNR comparison for "Cuprite" at different bitrates (unit: dB).

	Code rate (bpp)			
	0.05	0.1	0.15	0.2
AT-3DSPIHT [19]	44.25	45.47	46.72	48.05
F. Zhao et al. [20]	48.09	48.88	49.60	50.31
Proposed	49.44	60.08	66.51	67.65

by 9.53 dB averagely, and compared with the algorithm in [20], it is averagely increased by 11.12 dB.

In [22], a compression algorithm of hyperspectral remote sensing image based on 3D wavelet transform and 3D fractal is proposed. The classical eight kinds of affine transformations in 2D fractal image compression are generalized to nineteen for the 3D fractal image compression. When the compression ratio on the Earth Observation-1 (EO-1) satellite hyperspectral image of China Dongting Lake area is 80 : 1, the PSNR is 36.78 dB, while the PSNR of our proposed scheme at the same compression ratio is 41.78 dB. We can achieve a compression quality improvement of 5 dB.

To evaluate the encoding complexity of the proposed algorithm, we compare the encoding time of the proposed algorithm with that of Lucana Santos' [23]. The corresponding encoding time by the two schemes for "Yellowstone_sc0" and "Yellowstone_sc3" is recorded in Figure 10, which is displayed in seconds/band. Both scenes have the size of 512 lines × 680 pixels with 224 bands. From these results, we can see that the proposed algorithm has lower complexity and our scheme saves total 94.1% encoding time on average.

5. Conclusion

A lossy compression algorithm of hyperspectral image based on hybrid prediction and fractal is proposed. Intraband predictors with different directions are designed to remove the spatial correlation of the first band, and a high decoding quality can be obtained, which provides a good basic band for the following fractal encoding. The remaining bands are encoded by interband fractal encoding. The spectral redundancy can be removed since each range block is approximated by the domain block in the adjacent band, which is of the same size as the range block. Adaptive block partitions as well as a local search are also adopted in the fractal encoding. Finally, the residuals of prediction and fractal encoding are DCT transformed and Golomb entropy encoded. The fractal parameters are also Golomb entropy encoded.

Experimental results show that the algorithm achieves effective compression of hyperspectral image at low bitrate. The decoded quality is greatly improved, and the PSNR performance is increased by about 5 to 10 dB. Besides, the encoding complexity also has a great advantage. The proposed hybrid prediction and fractal hyperspectral image compression algorithm is a breakthrough to the traditional algorithm framework of hyperspectral image compression, providing a commendable solution for lossy compression of hyperspectral image.

Conflict of Interests

The authors declare that there is no conflict of interests regarding the publication of this paper.

Acknowledgments

This project is funded by the National Natural Science Foundation of China (NSFC) under Grants nos. 61375025, 61075011, and 60675018 and also by the Scientific Research Foundation for the Returned Overseas Chinese Scholars from the State Education Ministry of China. The authors would also like to express their appreciations to the reviewers for their thorough review and very helpful comments, which help in improving this paper.

References

[1] Q. Du, N. Raksuntorn, S. Cai, and R. J. Moorhead, "Color display for hyperspectral imagery," *IEEE Transactions on Geoscience and Remote Sensing*, vol. 46, no. 6, pp. 1858–1866, 2008.

[2] N. R. M. Noor and T. Vladimirova, "Investigation into lossless hyperspectral image compression for satellite remote sensing," *International Journal of Remote Sensing*, vol. 34, no. 14, pp. 5072–5104, 2013.

[3] A. Karami, M. Yazdi, and G. Mercier, "Compression of hyperspectral images using discerete wavelet transform and tucker decomposition," *IEEE Journal of Selected Topics in Applied Earth Observations and Remote Sensing*, vol. 5, no. 2, pp. 444–450, 2012.

[4] Y. Liang, J. Li, and K. Guo, "Lossless compression of hyperspectral images using hybrid context prediction," *Optics Express*, vol. 20, no. 7, pp. 8199–8206, 2012.

[5] B. Penna, T. Tillo, E. Magli, and G. Olmo, "Transform coding techniques for lossy hyperspectral data compression," *IEEE Transactions on Geoscience and Remote Sensing*, vol. 45, no. 5, pp. 1408–1421, 2007.

[6] S.-E. Qian, "Hyperspectral data compression using a fast vector quantization algorithm," *IEEE Transactions on Geoscience and Remote Sensing*, vol. 42, no. 8, pp. 1791–1798, 2004.

[7] S. Zhu, Y. Hou, Z. Wang, and K. Belloulata, "Fractal video sequences coding with region-based functionality," *Applied Mathematical Modelling*, vol. 36, no. 11, pp. 5633–5641, 2012.

[8] S. Zhu, L. Li, J. Chen, and K. Belloulata, "An automatic region-based video sequence codec based on fractal compression," *AEU—International Journal of Electronics and Communications*, vol. 68, no. 8, pp. 795–805, 2014.

[9] M. F. Barnsley, *Fractals Everywhere*, Academic Press, Boston, Mass, USA, 1988.

[10] M. F. Barnsley and S. Demko, "Iterated function systems and the global construction of fractals," *Proceedings of the Royal Society A*, vol. 399, no. 1817, pp. 243–275, 1985.

[11] A. E. Jacquin, "Image coding based on a fractal theory of iterated contractive image transformations," *IEEE Transactions of Image Processing*, vol. 1, no. 1, pp. 18–30, 1992.

[12] B. Wohlberg and G. de Jager, "A review of the fractal image coding literature," *IEEE Transactions on Image Processing*, vol. 8, no. 12, pp. 1716–1729, 1999.

[13] Y. Fisher, *Fractal Image Compression-Theory and Application*, Springer, New York, NY, USA, 1994.

[14] R. E. Roger and M. C. Cavenor, "Lossless compression of AVIRIS images," *IEEE Transactions on Image Processing*, vol. 5, no. 5, pp. 713–719, 1996.

[15] A. C. Miguel, R. E. Ladner, and E. A. Riskiny, *Predictive Coding of Hyperspectral Images*, Springer, New York, NY, USA, 2006.

[16] Y. Zhang and M. D. Desai, "Hyperspectral image compression based on adaptive recursive bidirection prediction/JPEG," *Pattern Recognition*, vol. 33, no. 11, pp. 1851–1861, 2000.

[17] H. Hartenstein, M. Ruhl, and D. Saupe, "Region-based fractal image compression," *IEEE Transactions on Image Processing*, vol. 9, no. 7, pp. 1171–1184, 2000.

[18] http://aviris.jpl.nasa.gov/.

[19] X. Tang, S. Cho, and W. A. Pearlman, "3D set partitioning coding methods in hyperspectral image compression," in *Proceedings of the International Conference on Image Processing (ICIP '03)*, pp. 239–242, Barcelona, Spain, September 2003.

[20] F. Zhao, G. Liu, and X. Wang, "An efficient macroblock-based diverse and flexible prediction modes selection for hyperspectral images coding," *Signal Processing: Image Communication*, vol. 25, no. 9, pp. 697–708, 2010.

[21] S. Lim, K. Sohn, and C. Lee, "Compression for hyperspectral images using three dimensional wavelet transform," in *Proceedings of the IEEE International Geoscience and Remote Sensing Symposium (IGARSS '01)*, pp. 109–111, July 2001.

[22] W. Pan, Y. Zou, and L. Ao, "A compression algorithm of hyperspectral remote sensing image based on 3-D wavelet transform and fractal," in *Proceedings of 3rd International Conference on Intelligent System and Knowledge Engineering (ISKE '08)*, pp. 1237–1241, November 2008.

[23] L. Santos, S. López, G. M. Callicó, J. F. López, and R. Sarmiento, "Performance evaluation of the H.264/AVC video coding standard for lossy hyperspectral image compression," *IEEE Journal of Selected Topics in Applied Earth Observations and Remote Sensing*, vol. 5, no. 2, pp. 451–461, 2012.

Research Article

A Novel High Efficiency Fractal Multiview Video Codec

Shiping Zhu, Dongyu Zhao, and Ling Zhang

Department of Measurement Control and Information Technology, School of Instrumentation Science and Optoelectronics Engineering, Beihang University, Beijing 100191, China

Correspondence should be addressed to Shiping Zhu; spzhu@163.com

Received 17 July 2014; Accepted 15 September 2014

Academic Editor: Guido Maione

Copyright © 2015 Shiping Zhu et al. This is an open access article distributed under the Creative Commons Attribution License, which permits unrestricted use, distribution, and reproduction in any medium, provided the original work is properly cited.

Multiview video which is one of the main types of three-dimensional (3D) video signals, captured by a set of video cameras from various viewpoints, has attracted much interest recently. Data compression for multiview video has become a major issue. In this paper, a novel high efficiency fractal multiview video codec is proposed. Firstly, intraframe algorithm based on the H.264/AVC intraprediction modes and combining fractal and motion compensation (CFMC) algorithm in which range blocks are predicted by domain blocks in the previously decoded frame using translational motion with gray value transformation is proposed for compressing the anchor viewpoint video. Then temporal-spatial prediction structure and fast disparity estimation algorithm exploiting parallax distribution constraints are designed to compress the multiview video data. The proposed fractal multiview video codec can exploit temporal and spatial correlations adequately. Experimental results show that it can obtain about 0.36 dB increase in the decoding quality and 36.21% decrease in encoding bitrate compared with JMVC8.5, and the encoding time is saved by 95.71%. The rate-distortion comparisons with other multiview video coding methods also demonstrate the superiority of the proposed scheme.

1. Introduction

In recent years, multiview video (MVV) is attracting considerable attention. This is because MVV can provide consumers with depth sense to the observed scene as if it really exists in front of consumers, allow consumers to freely change views, and interactively modify the properties of a scene. This type of video may be offered in the future home electronics devices, such as immersive teleconference, 3DTV [1], 3 D mobile phone, and home video camcorder. For example, in immersive teleconference, there is an interaction between consumers. Participants at different geographical sites meet virtually and see each other in either free viewpoint or 3DTV style. The immersiveness provides a more natural way of communications. However, in such a low bit rate communication channel such as the wireless mobile network, owing to the insufficient bit budget, MVV compression will cause the heavy loss of visual detail information.

MVV contains a large amount of statistical dependencies since it is a collection of multiple videos simultaneously captured in a scene at different camera locations. Therefore, efficient compression techniques are required for the above consumer electronic applications [2].

Fractal compression, which has the advantages of high compression ratio, resolution independence, and fast decoding speed, is considered as one of the most promising compression methods. The basic idea of fractal image coding is to find a contractive mapping whose unique attractor approximates the original image. For the decoding, an arbitrary image with the same size of the original image is input into the decoder, and, after several times of iteratively applying the recorded contractive mappings to the input image, the reconstructed image will be obtained. Much effort [3–5] has been made to the fractal still image compression after Jacquin's fractal block coding algorithm [6]. However, a little work has been reported on the fractal video compression, let alone the fractal multiview video compression [7]. For fractal video compression, there are two extensions of still image compression, which are cube-based compression [8] and frame-based compression [9]. In the former method, video sequences are partitioned into nonoverlapping 3D range blocks and overlapping 3D domain blocks with larger size

than range blocks. Then the key issue turns to find the best matching domain cuboid and the corresponding contractive mapping for every range cuboid, which is very complicated. In the latter method, each frame is encoded using the previous frame as a domain pool except the first frame which is encoded using a still image fractal scheme or some other methods. The main advantage of the frame-based algorithm is that decoding a frame consists of just one application of mapping so that iteration is not required at the decoder. However, the temporal correlation between the frames may not be effectively exploited, since the size of the domain block is larger than that of the range block [10].

In this paper, a novel highly efficient fractal multiview video codec by combined temporal/interview prediction is proposed. The anchor viewpoint video is encoded by improved frame-based fractal video compression approach, which combines the fractal coder with the well-known motion compensation (MC) technique. The other viewpoint videos are not only predicted from temporally neighboring images but also from the corresponding images in adjacent views.

This paper is organized as follows. The fractal compression theory and mathematical background is summarized in Section 2. The anchor viewpoint video compression algorithm is presented in Section 3 and then the proposed high efficiency fractal multiview video codec is presented in Section 4. The experimental results are shown in Section 5. Finally the conclusions are outlined in Section 6.

2. The Fractal Compression Theory and Mathematical Background

2.1. Mathematical Background. The mathematical background of fractal coding technique is the contraction mapping theorem and the collage theorem [11].

For the complete metric space (X, d), where X is a set and d is a metric on X, the mapping, $\omega : X \to X$ is said to be contractive if and only if

$$d\left(\omega\left(x\right), \omega\left(y\right)\right) \leq \alpha \cdot d\left(x, y\right), \quad 0 \leq \alpha < 1, \ \forall x, y \in X, \tag{1}$$

where α is called the contractivity factor of the contractive mapping.

For a contractive mapping $\omega : X \to X$ on (X, d); then there exists a unique point, $x_f \in X$, such that, for any point $x \in X$,

$$x_f = \omega\left(x_f\right) = \lim_{n \to \infty} \omega^n\left(x\right). \tag{2}$$

Such a point x_f is called a fixed point or the attractor of the mapping $\omega : X \to X$, where $\omega^n(x)$ represents the nth iteration application of ω to x. This is the famous Banach's fixed point theorem or contractive mapping theorem [11].

For the fractal image coding, if the encoder can find a contractive mapping whose attractor is the original image, then we only need to store the mapping with less bits instead of the original pixel values. But in the practical implementation, it is impossible to find a contractive mapping whose attractor is exactly the original image. Instead, the fractal encoder attempts to find the contractive mapping whose collage is close to the original image.

The collage theorem is as follows.

For the complete metric space (X, d), α is the contractivity factor of contractive mapping $\omega : X \to X$; then the fixed point x_f of the contractive mapping ω satisfies

$$d\left(x, x_f\right) \leq \frac{1}{1-\alpha} d\left(x, w\left(x\right)\right). \tag{3}$$

This means that the decoded attractor x_f is close to the original image x, if the collage $w(x)$ is close to the original image x. Therefore it converts to the minimization problem of the collage error.

2.2. Fractal Image Coding. In the practical implementation of the fractal image encoding process, the original image is firstly partitioned into nonoverlapping range blocks, covering the whole image, and overlapping domain blocks, usually twice the size of the range blocks in both width and height. For each range block the goal is to find a domain block and a contractive mapping that jointly minimize a dissimilarity (distortion) criterion. Usually the RMS (root mean square) metric is used. The contractive mapping applied to the domain block classically consists of the following parts [12]:

(i) geometrical contraction (usually by downsampling the domain block to the same size of the range block),

(ii) affine transformation (modeled by the 8 isometric transformations which contain the identity, rotation by 90°, 180°, and 270° and reflection about the midhorizontal axis, the midvertical axis, the first diagonal, and the second diagonal),

(iii) gray value transformation (a least square optimization is performed in order to compute the best values for the parameters s and o which are scaling factor and offset factor, resp.).

Here, s and o can be computed by minimizing the following equation:

$$E\left(s, o\right) = \sum_{i=1}^{n} \sum_{j=1}^{m} \left(s \cdot d_{ij} + o - r_{ij}\right)^2, \tag{4}$$

where $\{d_{ij} \ (i = 1, 2, \ldots, n; \ j = 1, 2, \ldots, m)\}$ is the pixel value of the domain block after geometrical contraction and affine transformation and $\{r_{ij} \ (i = 1, 2, \ldots, n; \ j = 1, 2, \ldots, m)\}$ is the pixel value of the range block.

Then s and o can be obtained by making $\partial E(s, o)/\partial s$ and $\partial E(s, o)/\partial s$ equal to zero. So that

$$\begin{aligned} s &= \frac{nm \sum_{i=1}^{n} \sum_{j=1}^{m} d_{ij} r_{ij} - \sum_{i=1}^{n} \sum_{j=1}^{m} d_{ij} \sum_{i=1}^{n} \sum_{j=1}^{m} r_{ij}}{nm \sum_{i=1}^{n} \sum_{j=1}^{m} d_{ij}^2 - \left(\sum_{i=1}^{n} \sum_{j=1}^{m} d_{ij}\right)^2}, \\ o &= \frac{\sum_{i=1}^{n} \sum_{j=1}^{m} r_{ij} - s \cdot \sum_{i=1}^{n} \sum_{j=1}^{m} d_{ij}}{nm}. \end{aligned} \tag{5}$$

The fractal encoding process can be finished by storing all the data necessary for each range block including the location

of the corresponding domain block, the index of the applied isometric transformation, and the values s and o. The decoding process is to iteratively apply the stored transformations to an arbitrary initial image.

3. The Anchor Viewpoint Video Compression

The most well-known fractal video codec is a hybrid fractal coder of circular prediction mapping (CPM) and noncontractive interframe mapping (NCIM) [13], in which the first four frames are encoded by CPM and the remaining frames are encoded by NCIM. In both the CPM and the NCIM, each range block is motion compensated by a domain block in the adjacent frame, which is of the same size as the range block. The main difference between the CPM and the NCIM is that the CPM should be contractive and the decoding process needs iteration, while the NCIM need not be contractive. The simulation results show better performance for the NCIM-coded frames than that for the CPM-coded frames.

Different from the abovementioned approach, in our proposed scheme, we first partition the video sequences into groups of frames (GOFs) to avoid error propagation. Every first frame in each GOF is encoded by intraframe prediction without depending on the previous frames, and the remaining frames in each GOF are encoded by combining fractal with the motion compensation (CFMC) as shown in Figure 1. In CFMC, each range block is motion compensated by a domain block in the adjacent previously predicted frame rather than the previous source frame, which is of the same size as the range block.

3.1. Intraframe Prediction. The intraframe prediction in our scheme uses for reference the intraprediction modes of international video coding standard H.264/AVC [14]. We make some modifications to make it appropriate to the overall fractal video compression scheme. Firstly, we partition each frame into range blocks of maximum size 16 × 16 and minimum size 4 × 4, using the quadtree structure [15], while H.264 only has two kinds of sizes of blocks which are 4×4 and 16×16, respectively, and does not use the quadtree structure. Secondly, H.264 specifies 9 intraprediction modes for 4 × 4 luma blocks and 4 intraprediction modes for 16 × 16 luma blocks as shown in Figures 2 and 3, respectively, while we use the 9 modes in Figure 2 for range blocks in the bottom level of the quadtree and the 4 modes in Figure 3 for range blocks in other levels of the quadtree. Thirdly, H.264 chooses the best mode using Lagrangian rate distortion optimization (RDO) technique [16] by traversing all the possible block sizes and prediction modes which is very time consuming, while for simplification, in our scheme, subdivision of the range block is performed only when the prediction error is still above a prescribed threshold and the minimum allowable partition is not reached.

A prediction frame is generated and subtracted from the original frame to form an error-frame, which is further transformed, quantized, and entropy encoded. In parallel, the quantized data are rescaled and inverse transformed and added to the prediction frame to reconstruct a coded version of the frame which is stored for later predictions. In the decoder, the bitstreams are entropy decoded, rescaled, and inverse transformed to form a decoded error-frame. The decoder generates the same prediction that is created at the encoder and adds this to the decoded error-frame to produce a reconstructed frame.

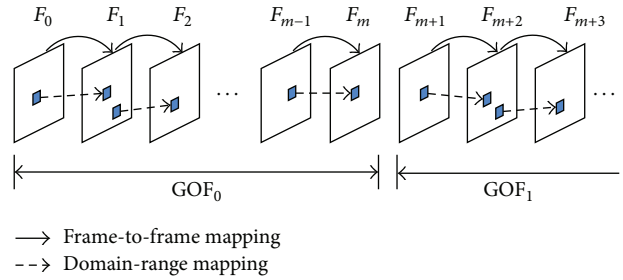

Figure 1: The structure of anchor viewpoint video coding.

3.2. Combining Fractal with Motion Compensation. Traditional motion compensation technique making use of block matching is based on the assumptions of locally translational motion and conservation of image intensity, whereas we may relax these assumptions when applying motion compensation technique used in our fractal video compression. The assumption of translation is replaced by an affine motion and the assumption of conservation of image intensity is replaced by the concept of linearly changing image intensity.

We investigate and compare the following four schemes:

S0: traditional (translational motion and conservation of image intensity) block matching,

S1: translational motion with gray value transformation,

S2: affine block matching using 8 isometric transformations,

S3: affine block matching using 8 isometric transformations with gray value transformation.

Exhaustive search in a search window which is formed by extending the collocated domain block by ±7 pixels in four directions is used for a range block as shown in Figure 4, where F_m represents the current frame to be encoded and F'_{m-1} represents the adjacent coded version.

Figure 5(a) compares the PSNR performance of the different schemes on the "Ballroom" video. Clearly the gray value transformation leads to significant PSNR gain, whereas the gain for affine transformation is only moderate. Figure 5(b) compares the encoding time of the different schemes. Obviously, the schemes without affine transformation (S0 and S1) are much faster compared to schemes using the affine motion model (S2 and S3), while gray value transformation is compu-tationally not very expensive. Test results on other video sequences such as "Race" and "Flamenco" show the same trends.

Considering the tradeoff between computational complexity and quality gain, we finally adopt S1 in our CFMC

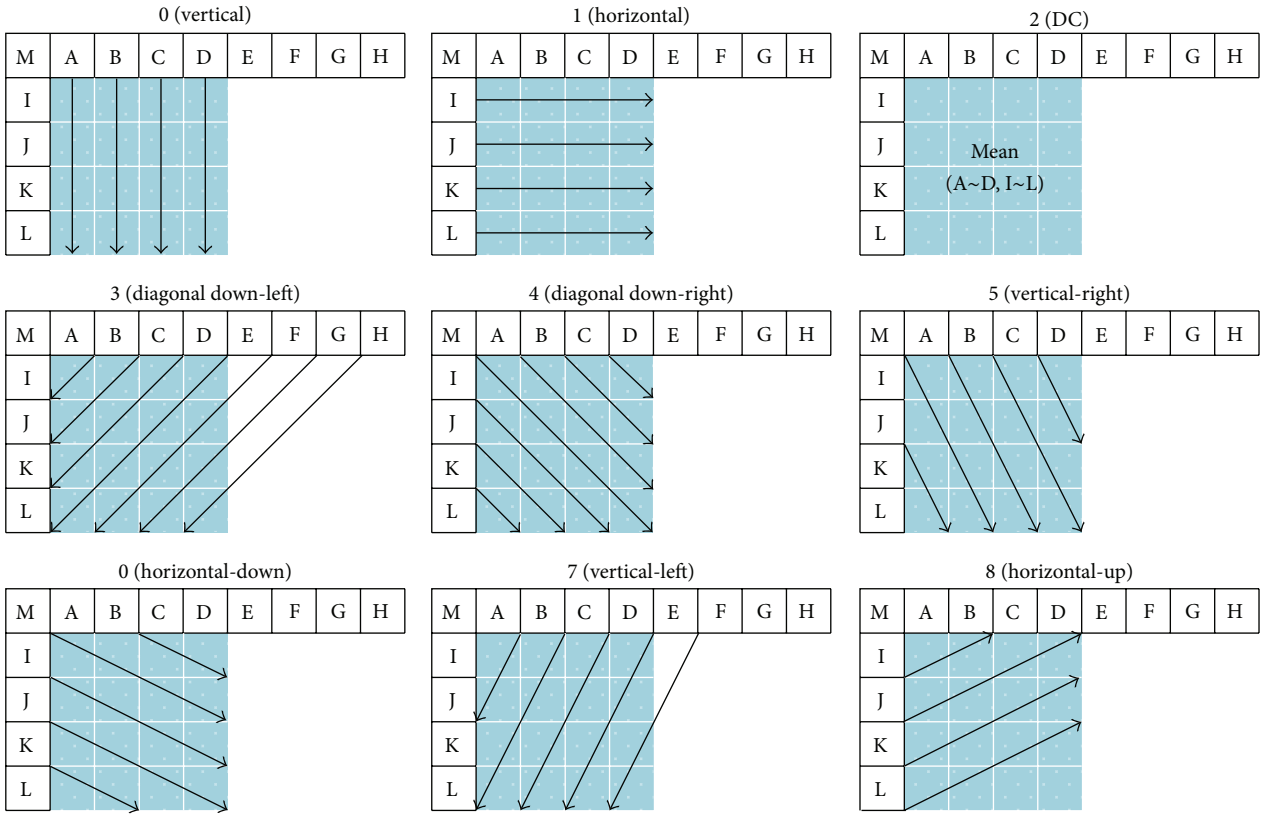

Figure 2: Nine intraprediction modes.

algorithm. Namely, range blocks in the current frame are predicted by domain blocks of the reference-frame using translational motion with gray value transformation.

To achieve better quality, the prediction frame is subtracted from the original frame to form an error-frame, which is transformed, quantized, and entropy encoded. In parallel, the quantized data are rescaled and inverse transformed and added to the prediction frame to reconstruct a coded version of the frame which is stored for later predictions, and the CFMC data including the positions of corresponding domain blocks, scale factors, and offset factors are entropy encoded. In the decoder, the bitstreams of error-frame are entropy decoded, rescaled, and inverse transformed to form a decoded error-frame. The bitstreams of CFMC data are entropy decoded and generate the prediction frame by applying corresponding translational motion with gray value transformation only once without iteration. Then a reconstructed frame is produced by adding the prediction frame to the decoded error-frame. This contrasts to 2D fractal video coding schemes which do not consider the coding of error-frames at all.

4. Fractal Multiview Video Compression Scheme

The coding structure between different views needs to be considered when extending single view fractal video coding to multiview video coding. Therefore, we propose the temporal-spatial prediction structure and fast disparity estimation algorithm.

4.1. Temporal-Spatial Prediction Structure. Multiview video sequences are captured by several cameras at the same time and there exists a high degree of correlation between interviews and intraviews. So we propose a temporal-spatial prediction structure based on view center and view distance. When processing the multiview video signal, disparity compensation and CFMC are combined to reduce the number of intraframe coded frames and improve the view compensation efficiency.

The proposed new prediction structure is shown in Figure 6 which contains 3 views. The center viewpoint video is the anchor video coded with the intraframe prediction and CFMC algorithm in Section 3 and the other viewpoint videos are coded based on disparity compensation and CFMC.

Figure 7 is the geometric schematic diagram of temporal-spatial prediction. Disparity estimation and CFMC are used for prediction to reduce data redundancy adequately.

4.2. Fast Disparity Estimation Algorithm. Geometric constraints between neighboring frames in multiview video sequences can be used to eliminate spatial redundancies. Parallax distribution constraints, which contain epipolar constraint, directional constraint, and spatial-time domain correlation, are used in the proposed fast disparity estimation algorithm.

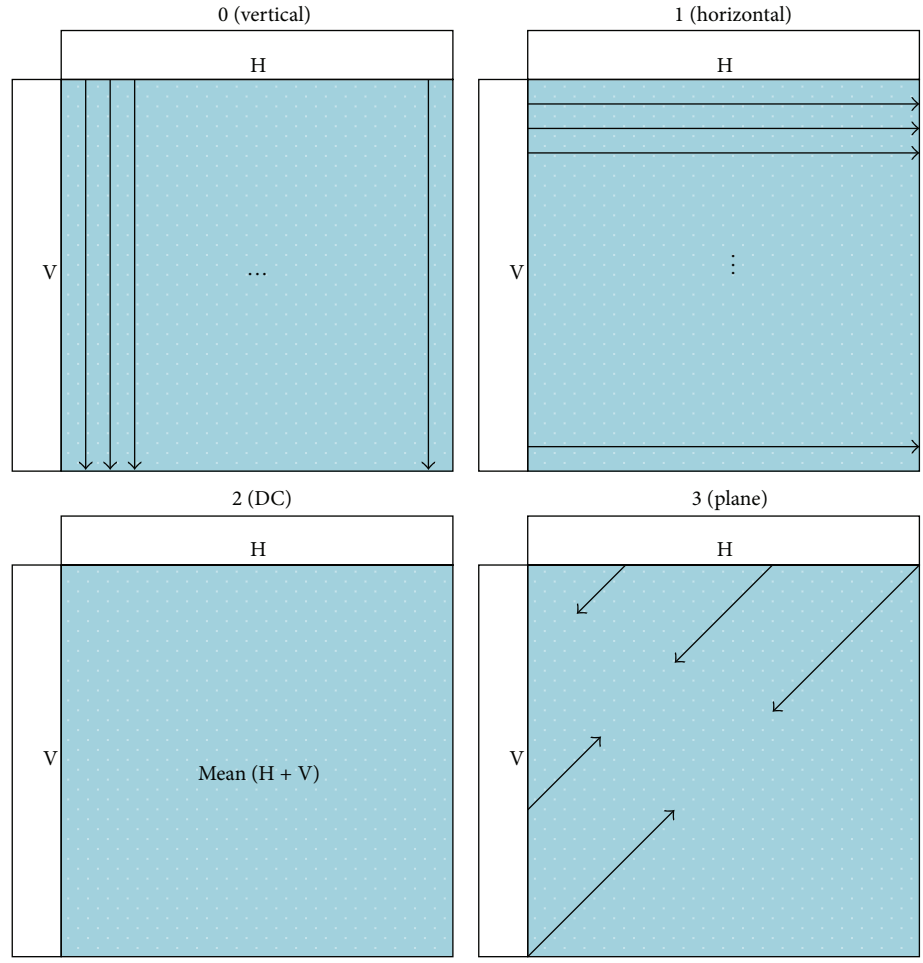

Figure 3: Four intraprediction modes.

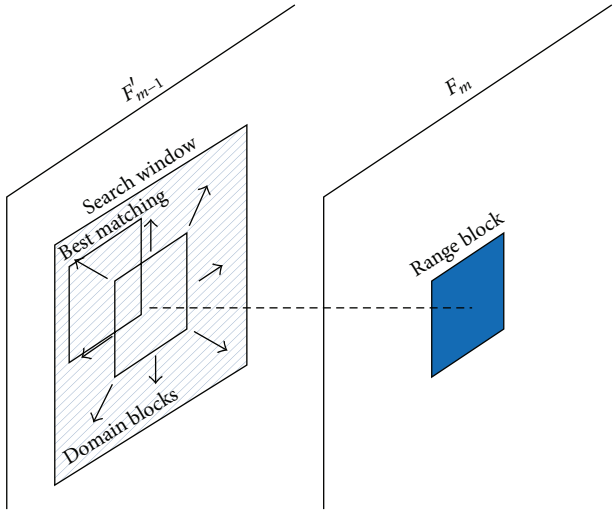

Figure 4: Search window for range block.

Epipolar constraint: the epipolar geometry is the intrinsic projective geometry between two views. Epipolar line can be found in the right image for a point of left image, on which the corresponding point can be searched. For parallel systems, only the search of x direction is needed just along the scan line. In other words, traditional two-dimensional search can be simplified to one-dimensional search along the scan line.

Directional constraint: in parallel systems, the vertical component of disparity vector is always equal to zero. The horizontal component is determined by the following formula:

$$d_x(x, y, z) = \frac{FB}{z}, \tag{6}$$

where $d_x(x, y, z)$ represents the horizontal component of disparity vector corresponding to the point (x, y, z). F represents the camera's focal length. B represents the baseline distance between the two cameras. We can see from formula (6) that the horizontal component of disparity vector is always positive; that is, for the same scene, the left perspective projection image always moves slightly left relative to the right image. Therefore, searching only in one direction instead of two directions is enough.

The spatial-time domain correlation: the disparity vector in the same frame has a strong correlation. For two adjacent frames, only a few pixels move and the positions of most

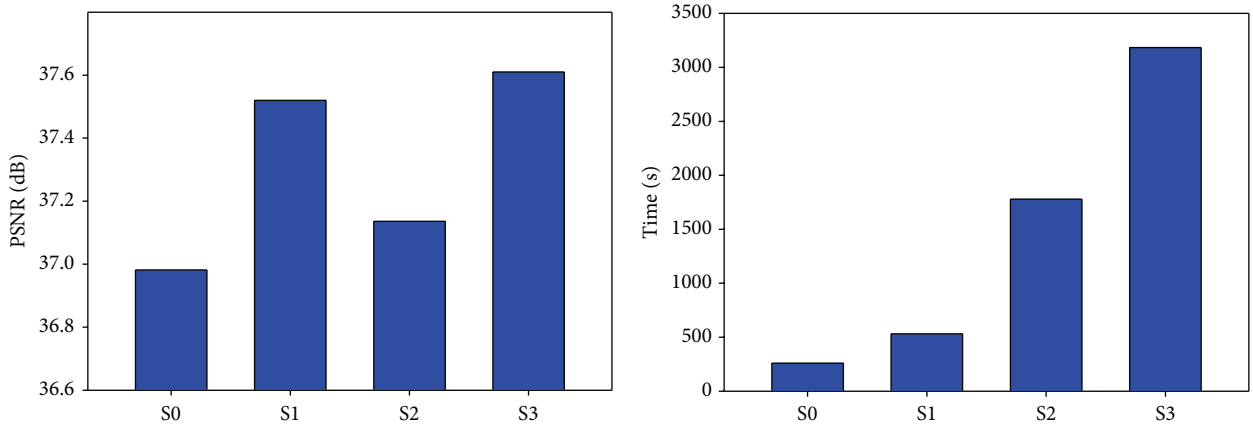

(a) PSNR comparisons (b) Encoding time comparisons

Figure 5: Performance comparisons of the four schemes.

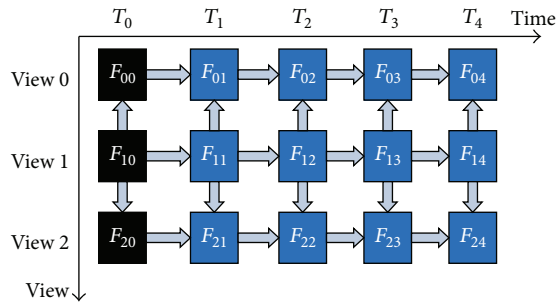

Figure 6: The proposed temporal-spatial prediction structure.

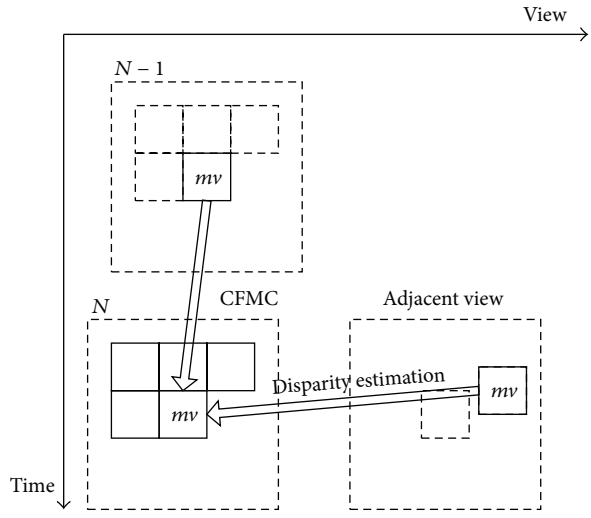

Figure 7: Disparity estimation and CFMC.

pixels have not changed. The disparities of these pixels whose positions have not changed keep basically unchanged. Therefore, corresponding disparity vectors of the neighboring range blocks can be considered as the starting point for a small area search to find the actual disparity vector quickly.

From the three constraints above, we can summarize our fast disparity estimation algorithm as follows. Firstly, search between the disparity vectors of the previously encoded neighboring range blocks to find one with the minimum RMS error as the starting search point. Then search in the horizontal to the right direction within several pixels distance to find the final disparity vector with the minimum RMS error.

Fast disparity estimation algorithm is helpful to reduce the number of search candidates and further to decrease the disparity estimation time. It can greatly improve the coding efficiency, which makes full use of the correlation between left and right views and can find the best matching block more quickly.

4.3. Fractal Multiview Video Compression Process. The overall coding process of the proposed fractal multiview video codec is shown in Figure 8.

Step 1. Partition the video sequences into GOFs.

Step 2. Encode the first frame of GOF in the anchor view using intraframe prediction and process the error-frame.

Step 3. Encode the first frame of GOF in the nonanchor views using fast disparity estimation from collocated frame in the adjacent view and process the error-frame.

Step 4. Encode the remaining frames of GOF in the anchor view using CFMC from the previous decoded frame and process the error-frames.

Step 5. Encode the remaining frames of GOF in the nonanchor views using CFMC from the previous decoded frame and then encode them using fast disparity estimation from collocated frames in the adjacent view. Choose the one with the minimum RMS and process the error-frames.

Step 6. Encode the next GOF using Step 2 to Step 5 until all the frames have been finished.

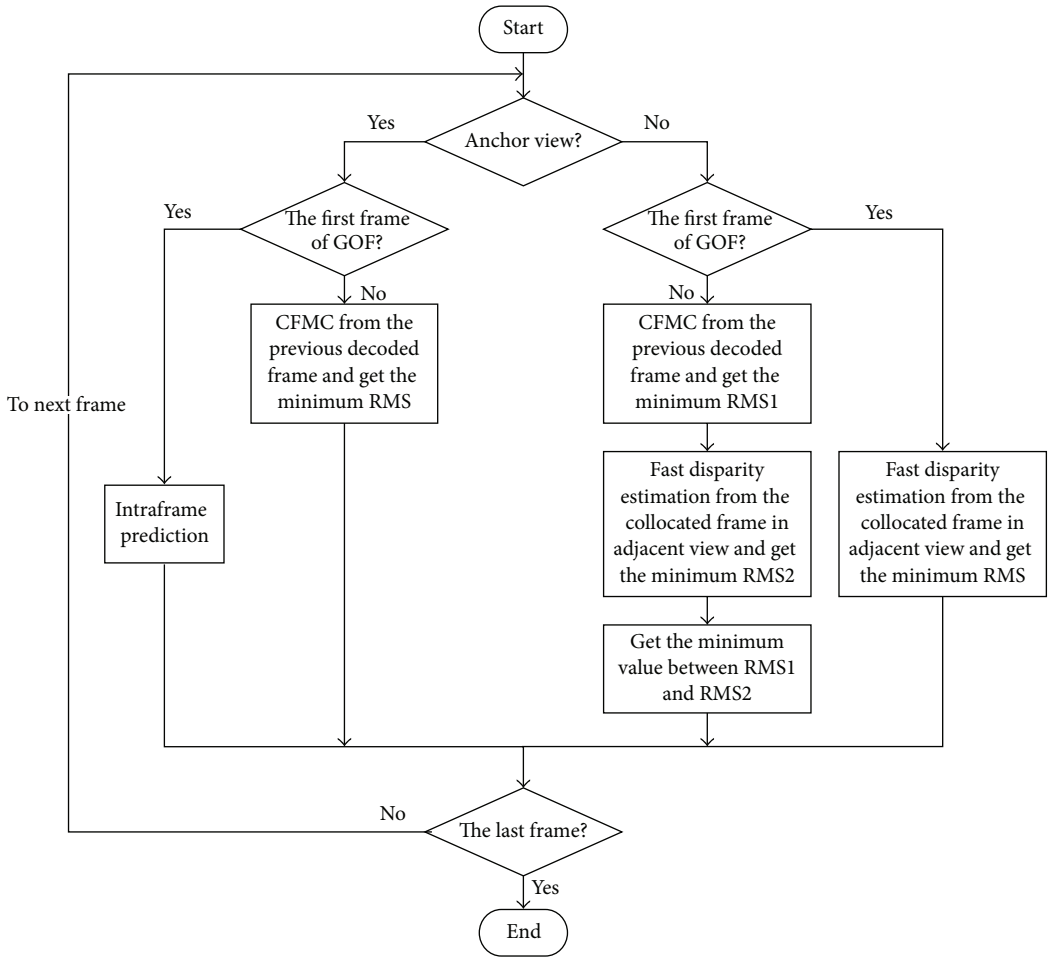

Figure 8: The encoding process block diagram of the proposed system.

5. Experimental Results

To verify the performance of the proposed fractal multiview video codec, three multiview video sequences "Ballroom" (250 frames), "Race" (300 frames), and "Flamenco" (300 frames) are tested. The quadtree structure we used contains three levels and the sizes of range blocks are 16×16, 8×8, and 4×4, respectively. Frame filtering is also applied. The simulations are run on a PC with Intel Core i7 quad 3.4 GHz CPU and 8 GB DDR RAM. The proposed method is implemented and compared with the state-of-the-art multiview video coding (MVC) reference software JMVC8.5 [20]. The configuration settings of the JMVC8.5 simulation environment are shown in Table 1.

Table 2 shows the PSNR, bit number, and encoding time comparisons between the proposed codec and JMVC8.5 using the simulation conditions given above. The numerical results are obtained by computing the average value of all the encoded frames. Overall, average time savings of about 95.71%, bit number savings of about 36.21%, and PSNR gains of 0.36 dB can be observed. Apparently, there is a great improvement on encoding time, bitrate, and PSNR compared to the JMVC8.5.

Table 1: Configuration settings of the JMVC8.5 simulation environment.

NumViewsMinusOne	2
ViewOrder	0-2-1
NumberReferenceFrames	2
GOP size	12
IntraPeriod	12
SearchMode	0: BlockSearch
Frames to be encoded	all frames
QP of all frames	28
SearchRange	±7 pixels
Motion estimation	Full search
SymbolMode	CAVLC

Figures 9(a)–9(c) show the PSNR comparisons of the "Ballroom" left, center, and right view, respectively, between the proposed fractal multiview video codec and JMVC8.5. Figures 10(a)–10(c) show the coding bit number comparisons of the "Ballroom" left, center, and right view, respectively.

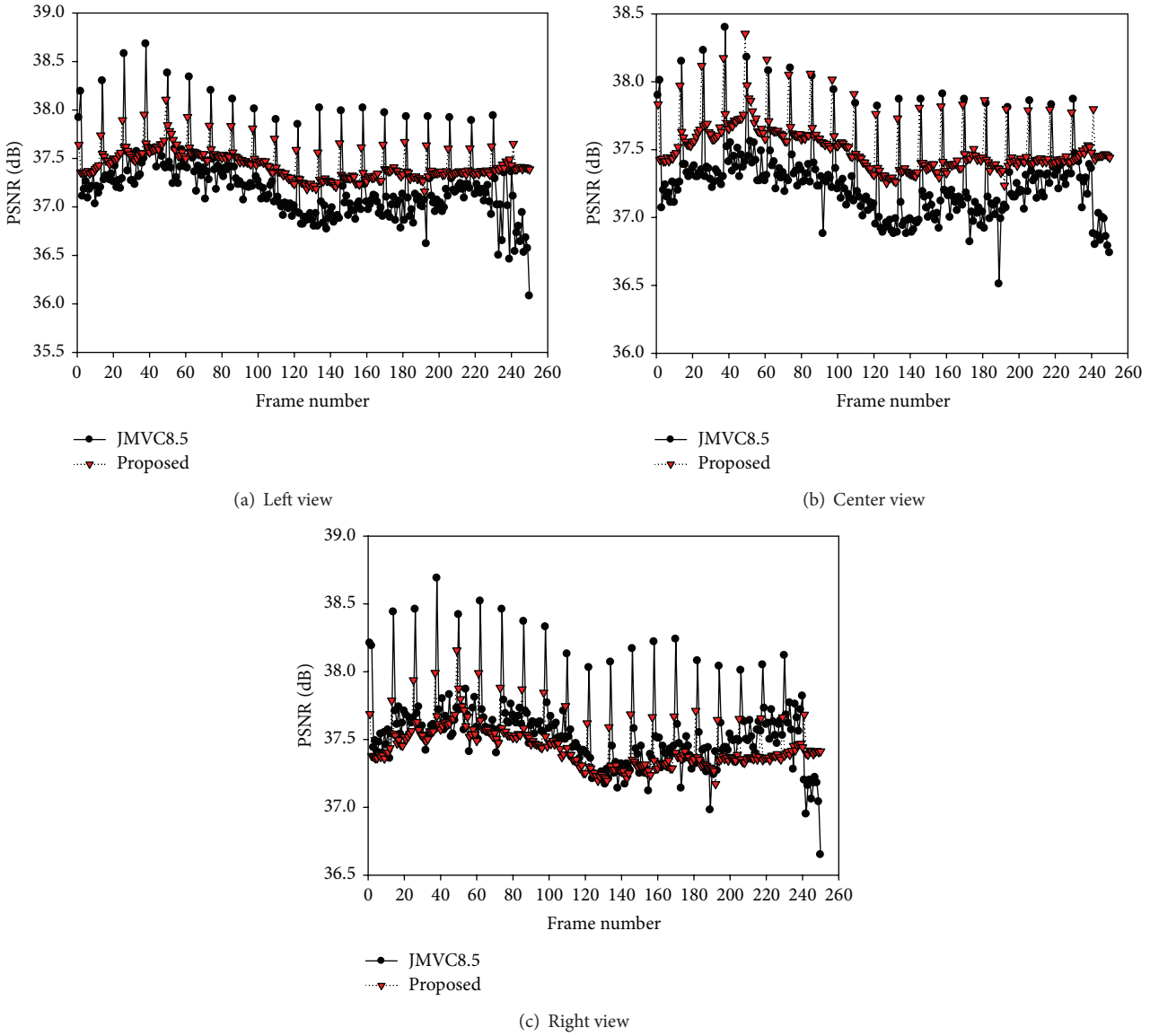

Figure 9: PSNR comparisons of "Ballroom."

Table 2: Performance comparisons between the proposed codec with JMVC8.5.

Video sequences		PSNR (dB)		Bit number (bits/frame)		Time (ms/frame)	
		JMVC8.5	Proposed	JMVC8.5	Proposed	JMVC8.5	Proposed
Ballroom	Left	37.22	**37.44**	46275	**20924**	22976	**632**
	Center	37.25	**37.52**	35635	**47503**	36595	**2127**
	Right	37.55	**37.45**	41230	**25627**	23384	**632**
Race	Left	37.35	**37.98**	91580	**22545**	21055	**661**
	Center	37.63	**38.12**	57711	**85537**	35543	**2226**
	Right	37.46	**37.99**	89584	**31300**	21438	**661**
Flamenco	Left	39.54	**40.06**	59219	**21883**	20665	**606**
	Center	40.31	**40.25**	39659	**51859**	34552	**2048**
	Right	39.34	**40.07**	63750	**27508**	21949	**610**
Average		38.18	**38.54**	58294	**37187**	26462	**1134**

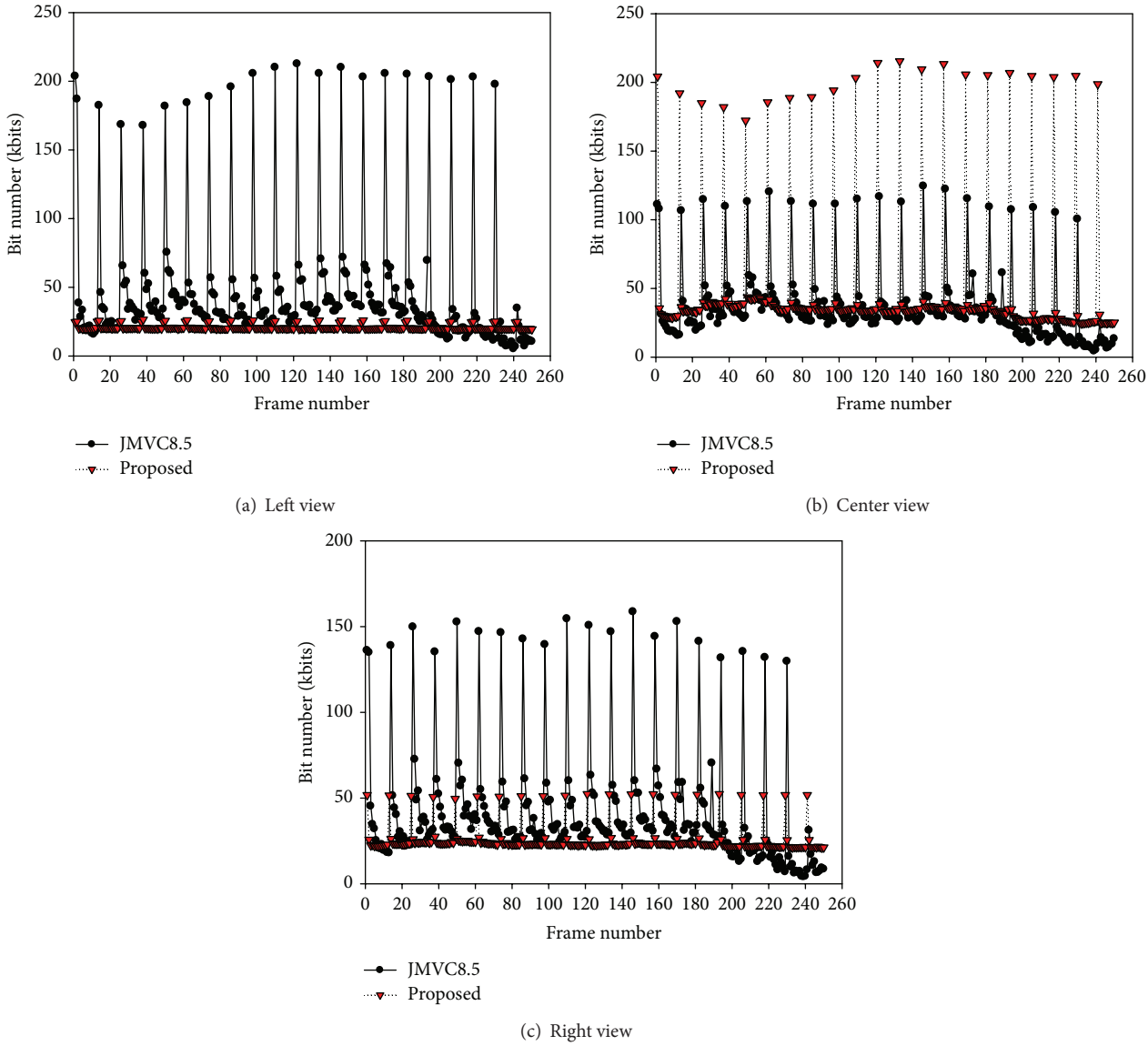

Figure 10: Bit number comparisons of "Ballroom."

Figures 11(a)–11(c) show the encoding time comparisons of the "Ballroom" left, center, and right view.

From Figures 9–11, we can conclude that the proposed fractal multiview video codec reduces the encoding time and improves coding efficiency greatly, which leads to more real-time applications. Figure 12 shows the 18th frame original and decoded images of "Race" resulted from JMVC8.5 and the proposed method.

To verify the good performance of the proposed method, Figure 13 illustrates the rate-distortion comparisons of "Flamenco" among the proposed method, color correction preprocessing method [17], histogram-matching method [18], illumination compensation method [19], no correction method [17], fractal method proposed in [7], and JMVC8.5 [20]. In order to facilitate the comparison, the average performance comparisons of "Flamenco" between the proposed codec and the other schemes computed with the Bjontegaard metric [21] are shown in Table 3.

From Figure 13 and Table 3, we can see that, with the bitrate increasing, the proposed fractal multiview video codec performs better, and the overall encoding performance of the proposed codec is superior to that of algorithms in the references.

6. Conclusion

In this paper, a novel high efficiency fractal multiview video codec is presented to improve the encoding performance.

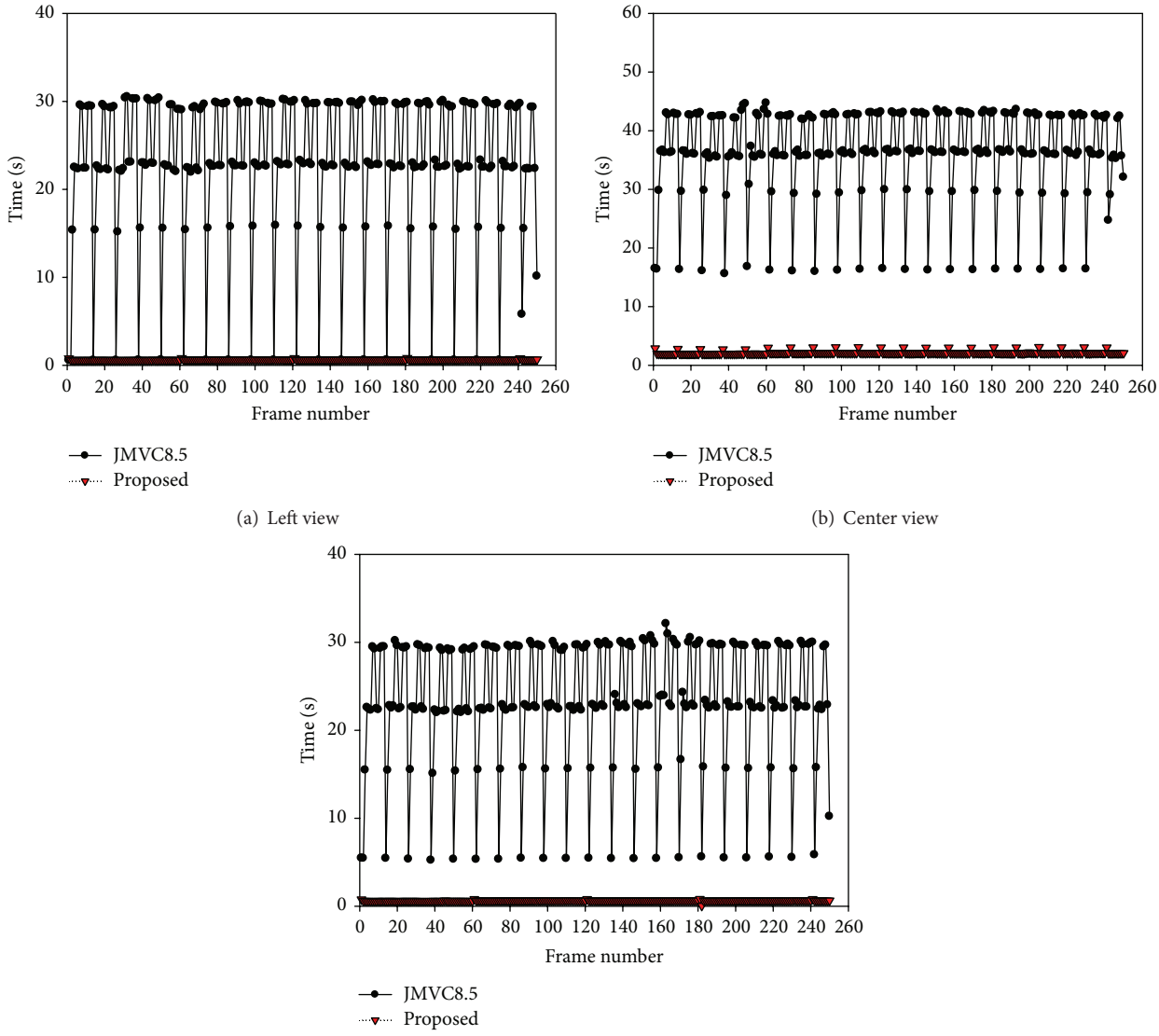

Figure 11: Encoding time comparisons of "Ballroom."

Table 3: Average performance comparisons of "Flamenco" between the proposed codec and the other schemes computed with the Bjontegaard metric.

Schemes	BDPSNR (dB)	BDBR (%)
Color correction preprocessing [17]	1.06	−7.8
Histogram-matching [18]	1.29	−4.3
Illumination compensation [19]	1.43	−5.7
No correction method [17]	1.64	−7.5
Fractal [7]	0.06	−0.4
JMVC8.5	2.35	−17.8

The video sequences are firstly partitioned into GOFs to avoid error propagation. Then, we improve the intraframe prediction to make it suitable for fractal encoding and propose the CFMC algorithm to get better performance of the anchor view. In addition, temporal-spatial prediction structure and fast disparity estimation algorithm are applied to further raise the compression efficiency.

Experimental results show that the proposed fractal multiview video codec spends less encoding time and achieves higher compression ratio with better decoding image quality. An average encoding time saving of about 95.71%, a bitrate saving of about 36.21%, and a PSNR gain of 0.36 dB can be achieved compared with JMVC8.5. In addition, it also shows superiority compared with color correction preprocessing method, histogram-matching method, illumination

(a) Original image

(b) Decoded image with JMVC 8.5

(c) Decoded image with the proposed method

Figure 12: The decoded image results of 18th frame of "Race."

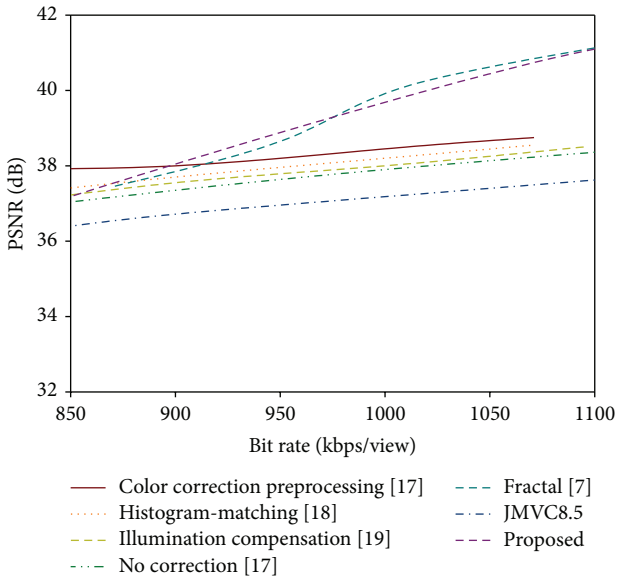

Figure 13: Rate-distortion comparisons of "Flamenco."

compensation method, and no correction method. It has built a good foundation for the further research of multiview fractal video coding and other related coding methods.

Conflict of Interests

The authors declare that there is no conflict of interests regarding the publication of this paper.

Acknowledgments

This project is funded by the National Natural Science Foundation of China (NSFC) under Grants nos. 61375025, 61075-011, and 60675018 and also the Scientific Research Foundation for the Returned Overseas Chinese Scholars from the State Education Ministry of China. The authors would also like to express their appreciations to the reviewers for their thorough review and very helpful comments, which help improve this paper.

References

[1] H. M. Ozaktas and L. Onural, *Three-Dimensional Television: Capture, Transmission, Display*, Springer, New York, NY, USA, 2007.

[2] P. Merkle, A. Smolic, K. Müller, and T. Wiegand, "Efficient prediction structures for multiview video coding," *IEEE Transactions on Circuits and Systems for Video Technology*, vol. 17, no. 11, pp. 1461–1473, 2007.

[3] T. K. Truong, C. M. Kung, J. H. Jeng, and M. L. Hsieh, "Fast fractal image compression using spatial correlation," *Chaos, Solitons and Fractals*, vol. 22, no. 5, pp. 1071–1076, 2004.

[4] C.-C. Wang and C.-H. Hsieh, "An efficient fractal image-coding method using interblock correlation search," *IEEE Transactions on Circuits and Systems for Video Technology*, vol. 11, no. 2, pp. 257–261, 2001.

[5] Y. Iano, F. S. da Silva, and A. L. M. Cruz, "A fast and efficient hybrid fractal-wavelet image coder," *IEEE Transactions on Image Processing*, vol. 15, no. 1, pp. 98–105, 2006.

[6] A. E. Jacquin, "Image coding based on a fractal theory of iterated contractive image transformations," *IEEE Transactions of Image Processing*, vol. 1, no. 1, pp. 18–30, 1992.

[7] S. Zhu, L. Li, and Z. Wang, "A novel fractal monocular and stereo video codec with object-based functionality," *EURASIP Journal on Advances in Signal Processing*, vol. 2012, no. 1, article 227, 14 pages, 2012.

[8] M. S. Lazar and L. T. Bruton, "Fractal block coding of digital video," *IEEE Transactions on Circuits and Systems for Video Technology*, vol. 4, no. 3, pp. 297–308, 1994.

[9] Y. Fisher, D. Rogovin, and T. P. Shen, "Fractal (self-VQ) encoding of video sequences," in *Visual Communications and Image Processing (VCIP '94)*, vol. 2308 of *Proceedings of SPIE*, pp. 1359–1370, Chicago, Ill, USA, September 1994.

[10] C.-S. Kim and S.-U. Lee, "Fractal coding of video sequence by circular prediction mapping," *Fractals*, vol. 5, no. 1, pp. 75–88, 1997.

[11] M. Barnsley, *Fractals Everywhere*, Academic Press, New York, NY, USA, 1988.

[12] A. Pommer, C. Hufnagl, and A. Uhl, "Fractal motion compensation," in *Proceedings of the Visual Communications and Image Processing*, pp. 1050–1061, San Jose, Calif, USA, January 1998.

[13] C.-S. Kim, R.-C. Kim, and S.-U. Lee, "Fractal coding of video sequence using circular prediction mapping and noncontractive interframe mapping," *IEEE Transactions on Image Processing*, vol. 7, no. 4, pp. 601–605, 1998.

[14] T. Wiegand, G. J. Sullivan, G. Bjøntegaard, and A. Luthra, "Overview of the H.264/AVC video coding standard," *IEEE Transactions on Circuits and Systems for Video Technology*, vol. 13, no. 7, pp. 560–576, 2003.

[15] Y. Fisher, *Fractal Image Compression-Theory and Application*, Springer, New York, NY, USA, 1995.

[16] G. J. Sullivan and T. Wiegand, "Rate-distortion optimization for video compression," *IEEE Signal Processing Magazine*, vol. 15, no. 6, pp. 74–90, 1998.

[17] C. Doutre and P. Nasiopoulos, "Color correction preprocessing for multiview video coding," *IEEE Transactions on Circuits and Systems for Video Technology*, vol. 19, no. 9, pp. 1400–1405, 2009.

[18] U. Fecker, M. Barkowsky, and A. Kaup, "Histogram-based prefiltering for luminance and chrominance compensation of multiview video," *IEEE Transactions on Circuits and Systems for Video Technology*, vol. 18, no. 9, pp. 1258–1267, 2008.

[19] A. Vetro, P. Pandit, H. Kimata, A. Smolic, and Y. K. Wang, "Joint Multiview Video Model (JMVM) 8.0," ISO/IEC JTC1/SC29/WG11 and ITU-T Q6/SG16, Doc. JVT-AA207, April 2008.

[20] Joint Video Team of ITU-T VCEG and ISOIEC MPEG, "WD 1 Reference software for MVC (JMVC8.5)," March 2011.

[21] G. Bjontegaard, "Calculation of average PSNR differences between RD curves," in *Proceedings of the 13th VCEG-M33 Meeting*, Austin, Tex, USA, April 2001.

Research Article

Algorithms of Finite Difference for Pricing American Options under Fractional Diffusion Models

Jun Xi,[1,2] Yanqing Chen,[3] and Jianwen Cao[1]

[1] *Laboratory of Parallel Software and Computational Science of Software, Institute of Software Chinese Academy of Sciences, Beijing 100190, China*
[2] *University of Chinese Academy of Sciences, Beijing 100049, China*
[3] *Shandong University of Finance and Economics, Jinan, Shandong 250014, China*

Correspondence should be addressed to Jianwen Cao; isfrom79@gmail.com

Received 11 June 2014; Revised 9 August 2014; Accepted 9 September 2014; Published 30 September 2014

Academic Editor: Guido Maione

Copyright © 2014 Jun Xi et al. This is an open access article distributed under the Creative Commons Attribution License, which permits unrestricted use, distribution, and reproduction in any medium, provided the original work is properly cited.

It is well known that linear complementarity problem (LCP) involving partial integro differential equation (PIDE) arises from pricing American options under Lévy Models. In the case of infinite activity process, the integral part of the PIDE has a singularity, which is generally approximated by a small Brownian component plus a compound Poisson process, in the neighborhood of origin. The PIDE can be reformulated as a fractional partial differential equation (FPDE) under fractional diffusion models, including FMLS (finite moment log stable), CGMY (Carr-Madan-Geman-Yor), and KoBol (Koponen-Boyarchenko-Levendorskii). In this paper, we first present a stable iterative algorithm, which is based on the fractional difference approach and penalty method, to avoid the singularity problem and obtain numerical approximations of first-order accuracy. Then, on the basis of the first-order accurate algorithm, spatial extrapolation is employed to obtain second-order accurate numerical estimates. Numerical tests are performed to demonstrate the effectiveness of the algorithm and the extrapolation method. We believe that this can be used as necessary tools by the engineers in research.

1. Introduction

The holder of American options has the right to exercise at any date prior to maturity and not only at the expiry date, while the holder of European options can exercise his right only at the expiry date. Thus, American options give the holder more freedom; hence, the price of American put is always greater or equal to the price of its European counterpart. There are two types of American options: put option and call option. The put option is a contract that the owner has the right but not the obligation to sell, while the holder of a call option has the right but not the obligation to buy.

Black and Scholes [1] and Merton [2] proposed the classic option pricing model called Black-Scholes model in 1973. In order to fit observed empirical market data better, many modifications to the Black-Scholes model have been proposed to build new models like jump-diffusion models proposed by Kou in [3] and Merton in [4] and infinite jump activity models such as KoBol [5, 6] and CGMY [7]. More general jump-diffusion models with stochastic volatility are considered in [8].

Compared with the jump-diffusion models, infinite activity models like KoBol and CGMY [7, 9] are more flexible to characterize the price process and give a more realistic description of the price process at various time scales. Both time-series and option data indicate that market indices lack a diffusion component and confirm the value of the infinite activity Lévy model [7].

Due to the optimal stopping problem, pricing American options lead to a a linear complementarity problem (LCP) or a variational inequality, which involves a partial integrodifferential equation (PIDE) in the case of models with jumps. Merton et al. [10] proposed a finite difference method for this type of formulation in 1977 under Black-Scholes model. More solutions to the LCP, such as the operator splitting method (OS) [11] under the Black-Scholes model, the PSOR method under the Black-Scholes model, the penalty method [12] under the jump-diffusion models, and the Lagrange

multiplier method [13] under the Black-Scholes model, have been studied as well. Generally second-order accurate finite differences are used to discretize the PDE of the LCP for option pricing. In [14–16], fourth-order accurate finite difference methods have been considered for American options.

As we know, pricing American options are a free boundary problem [6]; hence, the free boundary and the price of an option must be solved simultaneously. If the models satisfy the smooth pasting principle, we can use two types of methods to find the moving location of free boundary: front tracking [17–19] and front fixing [20–22]. However smooth pasting principle does not always hold under models with jumps unless the models satisfy certain conditions.

In the case of pricing American options under the infinite activity jump models, how to deal with the integral part of the PIDE is important because it has a singularity in the neighborhood of origin. Almendral [23] approximates the pure-jump process with a compound Poisson process plus a small Brownian component and accelerates the computation by FFT. An integration by parts technique for rewriting the integrodifferential operator in terms of Volterra operators with a weakly singular kernel is proposed. These methods achieve second-order accuracy.

Fractional derivatives provide a more delicate instrument to capture the characteristics of processes or materials in comparison with the integer-order derivatives, which proves to be very useful in many fields [24]. Under certain conditions, the Grünwald-Letnikov definition of fractional derivative is equivalent to the Riemann-Liouville definition of fractional derivative; hence, the Grünwald-Letnikov definition, which is convenient for numerical valuation, is often used for discretization of the fractional derivatives. Due to the instability caused by standard Grünwald-Letnikov estimates, a shifted Grünwald-Letnikov definition, which is unconditionally stable, is proposed [25].

Cartea and del-Castillo-Negrete [26] presented the fractional partial differential equation (FPDE) under some infinite activity Lévy models (FMLS, KoBol, and CGMY) as a generalization to PIDE and gave a finite difference method using the numerical valuation of fractional derivatives. The numerical solutions of three fractional partial differential equations have been compared by Marom and Momoniat [27]. Their methods are of first-order accuracy and are only for evaluation of European options. Second-order accurate approximation schemes for fractional derivatives have been proposed in [28, 29]. The approach in [28] is based on the classical Crank-Nicholson method combined with spatial extrapolation to obtain temporally and spatially second-order accurate numerical estimates for fractional diffusion equation. By using proper shifting parameter, the generalized shifted Grünwald-Letnikov definition has been proven to be second-order accurate [29].

In this paper, our study focuses on the discretization of fractional derivatives, spatial extrapolation, and design of stable iterative algorithms for pricing American options in the scheme of FPDE. We first present a stable iterative algorithm, which is based on the fractional difference approach and penalty method, to avoid the singularity problem and obtain numerical approximations of first-order accuracy. On the basis of the first-order accurate algorithm, spatial extrapolation is employed to obtain second-order accurate numerical estimates. Discretization of Fractional derivatives results in dense matrices which make the computation expensive, so the fast Fourier transform (FFT) method can be employed to decrease the computation cost to gain an almost linear complexity $O(N \log N)$ from $O(N^2)$ using direct solution.

The outline of this paper is as follows. In Section 2, linear complementarity problem and FPDE arising from pricing American options are introduced. In Section 3, we present the finite difference time and space discretization method. Section 4 describes our method used to solve the systems of linear equations and linear complementarity problems for American options. Numerical experiments are given in Section 5, and finally Section 6 contains conclusions. The main contributions of this paper are the discretization method in Section 3, the algorithm proposed in Section 4, and the numerical experiments in Section 5.

2. Mathematical Model for American Options

Because the value of an American call on an asset paying no dividends is equal to the value of the European call with same strike and maturity [2], only American put options are considered here.

To introduce the mathematical model, let us first recall the Riemann-Liouville definition [26] which is the most widely known definition of the fractional derivatives:

$$
\begin{aligned}
{}_aD_x^{\gamma} f(x) &= \frac{1}{\Gamma(n-\gamma)}\left(\frac{\partial}{\partial x}\right)^n \int_a^x (x-y)^{n-\gamma-1} f(y)\, dy, \\
&\qquad n-1 \le \gamma \le n, \\
{}_xD_a^{\gamma} f(x) &= \frac{1}{\Gamma(n-\gamma)}\left(-\frac{\partial}{\partial x}\right)^n \int_x^a (y-x)^{n-\gamma-1} f(y)\, dy, \\
&\qquad n-1 \le \gamma \le n,
\end{aligned} \tag{1}
$$

where γ is an arbitrary order, n is a positive integer, and a is the boundary.

Under certain conditions, Grünwald-Letnikov definition is equivalent to the Riemann-Liouville definition; hence, we can use Grünwald-Letnikov definition to evaluate the Riemann-Liouville derivatives of the LCP for pricing American options. Grünwald-Letnikov definition [24] is more convenient for numerical valuation than the Riemann-Liouville definition.

Using the known definition of the binomial coefficients

$$
\binom{\gamma}{r} = \frac{\gamma(\gamma-1)(\gamma-2)\cdots(\gamma-r+1)}{r!}, \tag{2}
$$

we have the Grünwald-Letnikov definitions of fractional derivatives

$$
\begin{aligned}
{}_aD_x^\gamma f(x) &= \lim_{\substack{h\to 0\\ nh=x-a}} h^{-\gamma}\sum_{r=0}^{n}(-1)^r\binom{\gamma}{r} f(x-rh),\\
{}_xD_a^\gamma f(x) &= \lim_{\substack{h\to 0\\ nh=a-x}} h^{-\gamma}\sum_{r=0}^{n}(-1)^r\binom{\gamma}{r} f(x+rh),
\end{aligned}
\tag{3}
$$

where γ is an arbitrary order and a is the boundary.

It has been proved that the standard Grünwald-Letnikov definition has stability problem if being used to approximate fractional derivate in the space-fractional advection-dispersion equation. Consider the following:

$$
\frac{\partial c(x,t)}{\partial t} = -v(r)\frac{\partial c(r,t)}{\partial r} + d(r)\frac{\partial^\gamma c(r,t)}{\partial r^\gamma} + f(r,t), \quad \text{where } 1<\gamma\leqslant 2.
\tag{4}
$$

So the shifted Grünwald-Letnikov definition was proposed to approximate Liouville fractional derivative $Af(x) = d^\gamma f(x)/dx^\gamma$:

$$
A_h f(x) = \frac{1}{\Gamma(-\gamma)}\frac{1}{h^\gamma}\sum_{k=0}^{\infty}\frac{\Gamma(k-\gamma)}{\Gamma(k+1)} f(x-(k-p)h),
\tag{5}
$$

where p is a nonnegative integer. $A_h f(x)$ is of first-order accuracy.

Generally, p is set to 1. We have shifted Grünwald-Letnikov definitions for the left and right fractional derivatives:

$$
\begin{aligned}
{}_aD_x^\gamma f(x) &= \lim_{\substack{h\to 0\\ nh=x-a}} h^{-\gamma}\sum_{r=0}^{n}(-1)^r\binom{\gamma}{r} f(x-rh+h),\\
{}_xD_a^\gamma f(x) &= \lim_{\substack{h\to 0\\ nh=a-x}} h^{-\gamma}\sum_{r=0}^{n}(-1)^r\binom{\gamma}{r} f(x+rh-h),
\end{aligned}
\tag{6}
$$

where γ is an arbitrary order and a is the boundary.

In the following, a LCP involving FPDE for pricing American put options under fractional diffusion model is given. We denote the value of American put option by V, the exercise price by K, the expiry time by T, the risk free interest rate by r, and the underlying asset price by e^x. The solution of the following LCP with additional constraints gives the price V of the option.

Using the fractional partial differential equation (FPDE) given in [26] for pricing European options

$$
\begin{aligned}
&\frac{\partial V(x,t)}{\partial t} + A\frac{\partial V(x,t)}{\partial x} + B(x)\,{}_xD_\infty^\gamma\left(b(x)V(x,t)\right)\\
&\quad + C(x)\,{}_{-\infty}D_x^\gamma\left(c(x)V(x,t)\right) + DV(x,t) = 0,
\end{aligned}
\tag{7}
$$

we have the following LCP for pricing American options:

$$
\begin{aligned}
g(x) &= \max\left(K-e^x,0\right), \quad x\in R,\\
V-g(x) &\geq 0, \quad x\in R,\\
\mathfrak{L}V\times\left[V-g(x)\right] &= 0, \quad x\in R,\ t\in[0,T],\\
\mathfrak{L}V &= 0, \quad e^x > f(t),\ t\in[0,T],\\
V-g(x) &= 0, \quad e^x \leq f(t),\ t\in[0,T],\\
\mathfrak{L}V &= 0, \quad e^x > f(t),\ t\in[0,T],\\
V &\longrightarrow K, \quad x\longrightarrow -\infty,\ t\in[0,T],\\
V &\longrightarrow 0, \quad x\longrightarrow \infty,\ t\in[0,T],\\
V(x,T) &= g(x), \quad x\in R,
\end{aligned}
\tag{8}
$$

where

$$
\begin{aligned}
\mathfrak{L}V = &\frac{\partial V(x,t)}{\partial t} + A\frac{\partial V(x,t)}{\partial x} + B(x)\,{}_xD_\infty^\gamma\left(b(x)V(x,t)\right)\\
&+ C(x)\,{}_{-\infty}D_x^\gamma\left(c(x)V(x,t)\right) + DV(x,t)
\end{aligned}
\tag{9}
$$

and γ is the fractional order.

For KoBol model, we have

$$
\begin{aligned}
\mathfrak{L}V = &\frac{\partial V(x,t)}{\partial t} + \left(r-v-\lambda^{\alpha-1}(q-p)\right)\frac{\partial V(x,t)}{\partial x}\\
&+\frac{1}{2}\sigma^\alpha\left[pe^{\lambda x}\,{}_xD_\infty^\alpha\left(e^{-\lambda x}V(x,t)\right)\right.\\
&\left.\quad +qe^{-\lambda x}\,{}_{-\infty}D_x^\alpha\left(e^{\lambda x}V(x,t)\right)\right]\\
&-\left(r+\frac{1}{2}\sigma^\alpha\lambda^\alpha\right)V(x,t),
\end{aligned}
\tag{10}
$$

where

$$
\begin{aligned}
v &= \frac{1}{2}\sigma^\alpha\left\{p(\lambda-1)^\alpha + q(\lambda+1)^\alpha - \lambda^\alpha\right\}, \quad 0<\alpha<1,\\
v &= \frac{1}{2}\sigma^\alpha\left\{p(\lambda-1)^\alpha + q(\lambda+1)^\alpha - \lambda^\alpha - \alpha\lambda^{\alpha-1}(q-p)\right\}, \quad 1<\alpha<2.
\end{aligned}
\tag{11}
$$

For CGMY model, we have

$$
\begin{aligned}
\mathfrak{L}V = &\frac{\partial V(x,t)}{\partial t} + (r-d)\frac{\partial V(x,t)}{\partial x}\\
&+ C\Gamma(-Y)e^{Mx}\,{}_xD_\infty^Y\left(e^{-Mx}V(x,t)\right)\\
&+ C\Gamma(-Y)e^{-Gx}\,{}_{-\infty}D_x^Y\left(e^{Gx}V(x,t)\right)\\
&-\left(r+C\Gamma(-Y)\left(M^Y+G^Y\right)\right)V(x,t),
\end{aligned}
\tag{12}
$$

where

$$
d = C\Gamma(Y)(M-1)^Y - M^Y + (G+1)^Y - G^Y.
\tag{13}
$$

The final value V is given by $V(x,T) = g(x)$, where $g(x)$ is the payoff function for the option contract. For a put option, it is $g(x) = \max(K - e^x, 0)$. We should note that the function $f(t)$ is the free boundary which divides R into two parts. If $x \le f(t)$, then we have the equation $V(x,t) - g(x) = 0$, which means that the price V of the option is the exercise price. If $x > f(t)$, then equation $\mathfrak{L}V = 0$ means that the price V is the solution of the above FPDE.

3. Space and Time Discretization

The above mathematical model involving the fractional derivatives assumes an infinite domain, $x \in (-\infty, +\infty)$. In order to apply finite difference methods, we will need to discretize and truncate the domain of $V(x,t)$. For $L \le x \le R$ and finite time interval $[0,T]$, the terminal condition is given by $V(x,T) = g(x)$. Further, the boundary conditions are $V(L,t) = K$ and $V(R,t) = 0$. By previous work in the field [11, 30], we take e^R at four times the exercise price of the option to ensure that the errors generated by the truncation are small enough so as to be negligible. In fact, the choice of L is simpler than that of R because it is easy to choose proper L so as to keep e^L far from the moving free boundary, hence, the errors caused by the left truncation are small enough too.

For the space discretization, we use a uniform grid on interval $[L,R]$ with $n+1$ grid points. The grid step size is denoted by h. Let $i = 0, 1, 2, \ldots, n$. Then we denote space grid point by $x_i = L + ih$. Analogous to the space discretization, a uniform time step Δt is used to get $m+1$ gird points on interval $[0,T]$. Let $j = 0, 1, 2, \ldots, m$. We denote time grid point by $t_j = j\Delta t$. In order to perform a finite difference approximation of the partial derivatives, we introduce a simplifying piece of notation along with the discrete approximation

$$V\left(x_i, t_j\right) = V\left(L + ih, j\Delta t\right) \approx V_{i,j}. \tag{14}$$

3.1. Singularity of the Fractional Derivatives. Using the above truncation, we actually assume that ${}_{-\infty}D_x^\gamma f(x) \approx {}_LD_x^\gamma f(x)$ and ${}_xD_{+\infty}^\gamma f(x) \approx {}_xD_R^\gamma f(x)$. As we know, ${}_LD_x^\gamma f(x)$ is singular at the lower, $x = L$, boundary and ${}_xD_R^\gamma f(x)$ is singular at the upper, $x = R$, boundary. To understand the nature of the singularity, we take the left fractional derivative ${}_aD_x^\gamma f(x)$ as an example.

Expanding in Taylor series around $x = a$, we have

$$\begin{aligned} &{}_aD_x^\gamma f(x) \\ &= \sum_{k=0}^{m} \frac{f^k(a)(x-a)^{-\gamma+k}}{\Gamma(-\gamma+k+1)} \\ &\quad + \frac{1}{\Gamma(-\gamma+m+1)} \int_a^x (x-\tau)^{m-p} f^{(m+1)}(\tau)\, d\tau. \end{aligned} \tag{15}$$

For $\gamma > 0$, at least, the first term on the right-hand side is singular. Truncation of domain is a must for discretization; so singularity is an important problem that we will clarify in the following discussion on left and right fractional derivatives seperately.

The LCP (8) has a function $f(t)$ which is the free boundary at time t. Generally, the free boundary $f(t)$ is far from the lower, $x = L$, boundary. The price of American option $V(x,t)$ is equal to $g(x)$, when $x \le f(t)$, so we only need to deal with those fractional derivatives which satisfy the condition $x \ge f(t) > L$; hence, no singularity problems exist for left fractional derivatives.

As to the right fractional derivatives, the singularity exists at the upper, $x = R$, boundary if we try to discretize the derivative. Taking into account the boundary condition $V(R,t) = 0$ and the assumption $V(x > R, t) = 0$, the equality ${}_xD_{+\infty}^\gamma f(x) = {}_xD_R^\gamma f(x)$ holds in such a case.

3.2. First-Order Approximation for the Fractional Derivatives. Using the shifted Grünwald-Letnikov definition of fractional derivatives

$$\begin{aligned} {}_aD_x^\gamma f(x) &= \lim_{\substack{h\to 0 \\ nh = x-a}} h^{-\gamma} \sum_{r=0}^{n} (-1)^r \binom{\gamma}{r} f(x - rh + h), \\ {}_xD_a^\gamma f(x) &= \lim_{\substack{h\to 0 \\ nh = a-x}} h^{-\gamma} \sum_{r=0}^{n} (-1)^r \binom{\gamma}{r} f(x + rh - h), \end{aligned} \tag{16}$$

we have for $x = nh$

$${}_aD_x^\gamma f(x) \approx {}_a\Delta_x^\gamma f(x) = h^{-\gamma} \sum_{r=0}^{n} (-1)^r \binom{\gamma}{r} f(x - rh + h), \tag{17}$$

$${}_xD_a^\gamma f(x) \approx {}_x\Delta_a^\gamma f(x) = h^{-\gamma} \sum_{r=0}^{n} (-1)^r \binom{\gamma}{r} f(x + rh - h), \tag{18}$$

which give the first-order accurate approximations.

3.3. First-Order Approximation for the Integer-Order Derivatives. There is a first-order space derivative $\partial V(x,t)/\partial x$ in the LCP (8) to be approximated and we have many choices to use to obtain approximation of order 1 or the higher.

For first-order approximation, we have the forward difference

$$\frac{\partial V_{i,j}}{\partial x} = \frac{V_{i+1,j} - V_{i,j}}{h} + O(h) \tag{19}$$

or the backward difference

$$\frac{\partial V_{i,j}}{\partial x} = \frac{V_{i,j} - V_{i-1,j}}{h} + O(h). \tag{20}$$

In this paper, we choose the backward difference method.

3.4. Crank-Nicolson Discretization. Assuming R is the matrix arising from the finite difference scheme, a general time stepping scheme for pricing American options is

$$\begin{aligned} &\frac{V_{i,j} - V_{i,j+1}}{\Delta t} + \Theta R V_{i,j} + (1-\Theta) R V_{i,j+1} = 0, \quad x_i > f\left(t_j\right), \\ &V_{i,j} = K - e^{x_i}, \quad x_i \le f\left(t_j\right), \end{aligned} \tag{21}$$

where $j = 0, 1, \ldots, m-1$ and $f(t_j)$ is the free boundary at time step t_j. For above $\Theta = 1$ we recover the explicit forward Euler

scheme. $\Theta = 0$ gives the implicit backward Euler method. We have the Crank-Nicolson method when $\Theta = 1/2$.

3.5. Matrix Formulation. Using (18), (20), and (21), we can now have the discretization of the full FPDE (7):

$$\begin{aligned}
&\frac{V_{i,j} - V_{i,j+1}}{\Delta t} \\
&\quad + \Theta \left[A \frac{V_{i,j} - V_{i-1,j}}{h} + B_i h^{-\gamma} \sum_{r=0}^{n-i+1} w_r b_{i+r-1} V_{i+r-1,j} \right. \\
&\qquad \left. + C_i h^{-\gamma} \sum_{r=0}^{i+1} w_r c_{i-r+1} V_{i-r+1,j} + D V_{i,j} \right] \\
&\quad + (1 - \Theta) \left[A \frac{V_{i,j+1} - V_{i-1,j+1}}{h} \right. \\
&\qquad + B_i h^{-\gamma} \sum_{r=0}^{n-i+1} w_r b_{i+r-1} V_{i+r-1,j+1} \\
&\qquad \left. + C_i h^{-\gamma} \sum_{r=0}^{i+1} w_r c_{i-r+1} V_{i-r+1,j+1} + D V_{i,j+1} \right], \\
&\qquad\qquad i = 1, 2, 3, \ldots, n-1,
\end{aligned} \tag{22}$$

where

$$w_r = \frac{1}{2\pi} \int_0^{2\pi} \left(1 - e^{-i\psi}\right)^{\gamma} e^{ir\psi} d\psi, \tag{23}$$

which can be efficiently computed by FFT.

Define matrices G, E, and F such that

$$\begin{aligned}
\left[GV^j\right]_i &= \left(\frac{A * \Delta t}{h} + D * \Delta t \right) V_{i,j} - \frac{A * \Delta t}{h} V_{i-1,j}, \\
\left[EV^j\right]_i &= \Delta t B_i h^{-\gamma} \sum_{r=0}^{i+1} w_r b_{i-r+1} V_{i-r+1,j+1}, \\
\left[FV^j\right]_i &= \Delta t C_i h^{-\gamma} \sum_{r=0}^{n-i+1} w_r c_{i+r-1} V_{i+r-1,j+1}.
\end{aligned} \tag{24}$$

Equation (22) then can be rewritten in matrix form as follows:

$$\begin{aligned}
&[I - (1 - \Theta) G] V^{j+1} \\
&\quad = [I + \Theta G] V^j + (1 - \Theta) [E + F] V^{j+1} + \Theta [E + F] V^j.
\end{aligned} \tag{25}$$

If Θ is set to $1/2$, this fractional Crank-Nicholson discretization approach will produce a method with a local truncation error, that is, $O(\Delta t^2) + O(h)$.

3.6. Spatially Second-Order Approximation Obtained by Extrapolation. In numerical analysis, extrapolation is used to improve the rate of convergence of a sequence. Based on the spatially first-order accurate numerical approximation in 3.5, extrapolation can be employed to improve the low order of spatial convergence. First, we state below the result obtained in [28].

Proposition 1. *Let $1 \le \alpha \le 2$, $f \in C^{n+3}(R)$ such that all derivatives of f up to order $n + 3$ belong to $L^1(R)$. For any integer $p \ge 0$, define the shifted Grünwald operator by*

$$\Delta_{h,p}^{\alpha} f(x) = \sum_{j=0}^{\infty} (-1)^j \binom{\alpha}{j} f\left(x - (j - p) h\right). \tag{26}$$

Then, one has for some constants a_l independent of h, f, and x the fact that

$$h^{-\alpha} \Delta_{h,p}^{\alpha} f(x) = \frac{d^{\alpha}}{dx^{\alpha}} f(x) + \sum_{l=1}^{n-1} \left(a_l \frac{d^{\alpha+l}}{dx^{\alpha+l}} f(x) \right) h^l + O\left(h^n\right) \tag{27}$$

uniformly in $x \in R$.

Writing (27) as

$$h^{-\alpha} \Delta_{h,p}^{\alpha} f(x) = \frac{d^{\alpha}}{dx^{\alpha}} f(x) + c_1 h + c_2 h^2 + O\left(h^3\right), \tag{28}$$

where c_1 and c_2 are independent of h, and (28) shows that the truncation error in the shifted Grünwald finite difference approximation is $c_1 h + c_2 h^2 + O(h^3)$. Now, one can use the Richardson extrapolation method in the following way. First, the Crank-Nicholson method is applied for grid size h and again for grid size $h/2$. This gives two solutions of first-order accuracy for the spatial dimension. We denote by V_h the solution of grid size h and by $V_{h/2}$ the solution of gird size $h/2$. Then, one has

$$\begin{aligned}
V_h &= V + b_1 h + b_2 h^2 + O\left(h^3\right), \\
V_{h/2} &= V + b_1 \frac{h}{2} + b_2 \frac{h^2}{4} + O\left(h^3\right),
\end{aligned} \tag{29}$$

where b_1 and b_2 are real numbers. Taking $V = 2 * V_{h/2} - V_h$, it is obvious that V is spatially 2nd-order accurate.

Based on the classical Crank-Nicholson method combined with spatial extrapolation, we obtain a solution with local truncation error $O(\Delta t^2) + O(h^2)$.

The extrapolation method can be used at each time step before the maturity of options; because we can obtain two solutions of first-order estimates for diffenent spatial grid size at each time step, then second-order approximation can be computed at each time step.

4. The Penalty Method

In order to apply penalty method, we need to replace the following equation in LCP:

$$\mathfrak{L} V \times [V - g(x)] = 0 \tag{30}$$

Table 1: First-order numerical estimates computed by iterative algorithm and second-order estimates obtained by extrapolation.

m	First-order approximation V_h				First-order approximation $V_{h/2}$				Second-order $V = 2V_{h/2} - V_h$	
	n	itns	Value	Change	n	itns	Value	Change	Value	Change
25	128	5.92	0.5386		256	8.00	0.5267		0.5148	
50	256	6.04	0.5275	0.0111	512	8.94	0.5199	0.0068	0.5123	0.0025
100	512	6.18	0.5203	0.0072	1024	9.90	0.5167	0.0032	0.5131	0.0008
200	1024	6.63	0.5169	0.0034	2048	11.03	0.5149	0.0018	0.5129	0.0002
400	2048	7.20	0.5150	0.0019	4096	12.24	0.5139	0.0010	0.5128	0.0001

"itns" is the average number of iterations per time step. m is the number of time steps. n is the number of spatial points. "value" is a sample of the put option values.

(1) Let $(V^{j+1})^0 = V^j$
(2) Let $\widehat{V}^k = (V^{j+1})^k$
(3) Let $\widehat{P}^k = P((V^{j+1})^k)$
(4) For $k = 0, 1, 2, \ldots,$ *until convergence do*
(5) Solve $[I - (1/2)\,G + \widehat{P}^k]\widehat{V}^{k+1} = (1/2)\,[G + E + F]V^j + (1/2)\,[E + F]\widehat{V}^k + \widehat{P}^k V^*$
(6) if $\max_i \left(|\widehat{V}^{k+1} - \widehat{V}^k| / \max(1, |\widehat{V}^{k+1}|)\right) <$ *tolerance then*
(7) Quit
(8) end if
(9) end for

Algorithm 1: Fixed point iteration at each timestep.

with

$$\begin{aligned}\mathfrak{L}V &= \frac{\partial V(x,t)}{\partial t} + A\frac{\partial V(x,t)}{\partial x} + B(x)_x D_\infty^\gamma \left(b(x)\,V(x,t)\right) \\ &\quad + C(x)_{-\infty} D_x^\gamma \left(c(x)\,V(x,t)\right) + DV(x,t) \\ &= \rho \max\left(V(x)^* - V(x,t), 0\right),\end{aligned} \tag{31}$$

where $V(x)^*$ is the payoff upon the exercise and in the limit as the penalty parameter $\rho \to \infty$, the solution satisfies $V(x,t) \geq V(x)^*$. Let P be the matrix given by the above penalty item. Consider the following:

$$P\left(V^{j+1}\right)_{ii} = \begin{cases} \text{large number} & \text{when } V_{i,j+1} < V_i^* \\ 0 & \text{other case.} \end{cases} \tag{32}$$

Then the matrix form for the penalty method is obtained using ((25), (31), (32)). Consider the following:

$$\begin{aligned}&\left[I - (1-\Theta)\,G + P\left(V^{j+1}\right)\right] V^{j+1} \\ &\quad = [I + \Theta G]\,V^j + (1-\Theta)\,[E+F]\,V^{j+1} \\ &\qquad + \Theta\,[E+F]\,V^j + P\left(V^{j+1}\right)V^*.\end{aligned} \tag{33}$$

4.1. Iterative Algorithm. At each time step, we need to solve (33) to obtain the valuation of American options at grid points of $x_i > f(t_j)$. Option values at grid points of $x_i \leq f(t_j)$ are given by payoff function $g(x_i)$. Iterative methods are introduced in Algorithm 1.

5. Numerical Results

In this section, we consider an American put option. A series of tests were carried out to study the effectiveness of our method under KoBol model.

In Table 1, column "change" shows the convergence of our approximations along with the temporal and spatial grid getting finer. Convergence rates of second-order estimates obtained by extrapolation $V = 2V_{h/2} - V_h$ are significantly improved, compared with those of first-order approximations. Hence, the test results confirm the effectiveness of our method.

Figure 1 is an example of first- and second-order approximations under same model conditions.

Figure 2 gives the evolution of pricing process for second-order approximation at all time steps.

6. Conclusions

In this paper, starting from the LCP involving FPDE, we first present the algorithms of first-order approximations for American options under fractional diffusion models. Then, on the basis of the first-order accurate algorithm, spatial extrapolation is employed to obtain second-order accurate numerical estimates. Numerical results in Section 6 prove that the algorithm is feasible and the extrapolation method is effective.

Using the Richardson extrapolation method, we even can obtain numerical approximations of higher order. Hence,

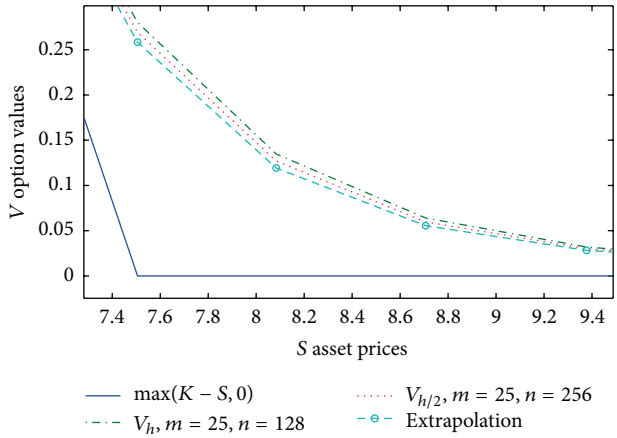

FIGURE 1: Option values for first-order approximations computed by iterative algorithm and second-order estimates obtained by extrapolation with $T = 0.5$, $\lambda = 2$, $\alpha = 1.5$, $\sigma = 0.32$, $K = e^2$, and $r = 0.08$.

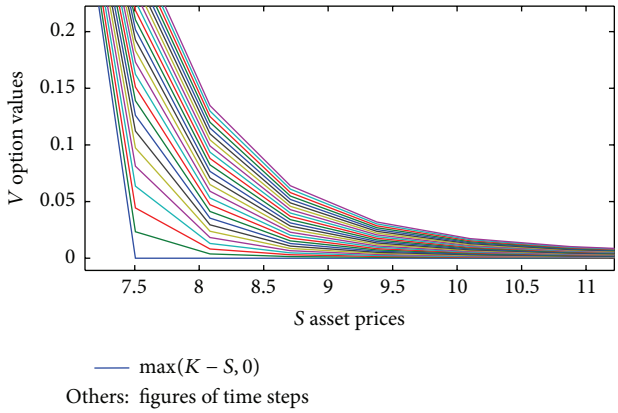

FIGURE 2: Option values for second-order approximations at all timesteps with $m = 25$, $n = 128$, $T = 0.5$, $\lambda = 2$, $\alpha = 1.5$, $\sigma = 0.32$, $K = e^2$, and $r = 0.08$.

the algorithm and extrapolation method form a useful tool box for the engineer. The use of fractional derivatives discretization conveniently avoids the singularity problem in the integral part of the PIDE. With the development of the fractional derivatives, we could see more possibilities of its application in finance.

Finally, as for American options, how to extend our method to other models and get combined with other existing methods might be interesting topics. In order to improve computation performance, new technology like parallel computing or new iterative algorithm having quicker convergence rate are important in further study.

Conflict of Interests

The authors declare that there is no conflict of interests regarding the publication of this paper.

Acknowledgment

This work was funded by Chinese NSF (Grant no. 91230109).

References

[1] F. Black and M. Scholes, "The pricing of options and corporate liabilities," *The Journal of Political Economy*, vol. 81, no. 3, pp. 637–654, 1973.

[2] R. C. Merton, "Theory of rational option pricing," *The Rand Journal of Economics*, vol. 4, pp. 141–183, 1973.

[3] S. G. Kou, "A jump-diffusion model for option pricing," *Management Science*, vol. 48, no. 8, pp. 1086–1101, 2002.

[4] R. C. Merton, "Option pricing when underlying stock returns are discontinuous," *Journal of Financial Economics*, vol. 3, no. 1-2, pp. 125–144, 1976.

[5] I. Koponen, "Analytic approach to the problem of convergence of truncated Lévy flights towards the Gaussian stochastic process," *Physical Review E*, vol. 52, no. 1, pp. 1197–1199, 1995.

[6] S. I. Boyarchenko and S. Z. Levendorskii, *Non-Gaussian Merton-Black-Scholes Theory*, vol. 9, World Scientific, Singapore, 2002.

[7] P. Carr, H. Geman, D. B. Madan, and M. Vor, "The fine structure of asset returns: an empirical investigation," *Journal of Business*, vol. 75, no. 2, pp. 305–332, 2002.

[8] B. Eraker, M. Johannes, and N. Polson, "The impact of jumps in volatility and returns," *Journal of Finance*, vol. 58, no. 3, pp. 1269–1300, 2003.

[9] R. Cont and P. Tankov, *Financial Modelling with Jump Processes*, CRC Press, Boca Raton, Fla, USA, 2004.

[10] R. C. Merton, M. J. Brennan, and E. S. Schwartz, "The valuation of American put options," *The Journal of Finance*, vol. 32, no. 2, pp. 449–462, 1977.

[11] S. Ikonen and J. Toivanen, "Operator splitting methods for American option pricing," *Applied Mathematics Letters*, vol. 17, no. 7, pp. 809–814, 2004.

[12] Y. d'Halluin, P. A. Forsyth, and G. Labahn, "A penalty method for American options with jump diffusion processes," *Numerische Mathematik*, vol. 97, no. 2, pp. 321–352, 2004.

[13] K. Ito and K. Kunisch, "Parabolic variational inequalities: the Lagrange multiplier approach," *Journal de Mathmatiques Pures et Appliques*, vol. 85, no. 3, pp. 415–449, 2006.

[14] C. W. Oosterlee, C. C. W. Leentvaar, and X. Huang, "Accurate American option pricing by grid stretching and high order finite differences," Working Papers, DIAM, Delft University of Technology, Delft, The Netherlands, 2005.

[15] J. Toivanen, "A high-order front-tracking finite difference method for pricing American options under jump-diffusion models," *Journal of Computational Finance*, vol. 13, no. 3, pp. 61–79, 2010.

[16] D. Y. Tangman, A. Gopaul, and M. Bhuruth, "Numerical pricing of options using high-order compact finite difference schemes," *Journal of Computational and Applied Mathematics*, vol. 218, no. 2, pp. 270–280, 2008.

[17] H. Han and X. Wu, "A fast numerical method for the Black-Scholes equation of American options," *SIAM Journal on Numerical Analysis*, vol. 41, no. 6, pp. 2081–2095, 2003.

[18] K. N. Pantazopoulos, E. N. Houstis, and S. Kortesis, "Front-tracking finite difference methods for the valuation of American options," *Computational Economics*, vol. 12, no. 3, pp. 255–273, 1998.

[19] D. Y. Tangman, A. Gopaul, and M. Bhuruth, "A fast high-order finite difference algorithm for pricing American options," *Journal of Computational and Applied Mathematics*, vol. 222, no. 1, pp. 17–29, 2008.

[20] L. Wu and Y. K. Kwok, "A front-fixing finite difference method for the valuation of American options," *Journal of Financial Engineering*, vol. 6, no. 4, pp. 83–97, 1997.

[21] A. D. Holmes and H. Yang, "A front-fixing finite element method for the valuation of American options," *SIAM Journal on Scientific Computing*, vol. 30, no. 4, pp. 2158–2180, 2008.

[22] B. F. Nielsen, O. Skavhaug, and A. Tveito, "Penalty methods for the numerical solution of American multi-asset option problems," *Journal of Computational and Applied Mathematics*, vol. 222, no. 1, pp. 3–16, 2008.

[23] A. Almendral, "Numerical valuation of American options under the CGMY process," in *Exotic Option Pricing and Advanced Lvy Models*, Wiley, Chichester, UK, 2005.

[24] I. Podlubny, *Fractional Differential Equations: An Introduction to Fractional Derivatives, Fractional Differential Equations, to Methods of Their Solution and Some of Their Applications*, Academic Press, New York, NY, USA, 1998.

[25] M. M. Meerschaert and C. Tadjeran, "Finite difference approximations for fractional advection-dispersion flow equations," *Journal of Computational and Applied Mathematics*, vol. 172, no. 1, pp. 65–77, 2004.

[26] Á. Cartea and D. del-Castillo-Negrete, "Fractional diffusion models of option prices in markets with jumps," *Physica A: Statistical Mechanics and Its Applications*, vol. 374, no. 2, pp. 749–763, 2007.

[27] O. Marom and E. Momoniat, "A comparison of numerical solutions of fractional diffusion models in finance," *Nonlinear Analysis: Real World Applications*, vol. 10, no. 6, pp. 3435–3442, 2009.

[28] C. Tadjeran, M. M. Meerschaert, and H. Scheffler, "A second-order accurate numerical approximation for the fractional diffusion equation," *Journal of Computational Physics*, vol. 213, no. 1, pp. 205–213, 2006.

[29] M. H. Nasir, L. K. B. Gunawardana, and H. Abeyrathna, "A second order finite difference approximation for the fractional siffusion equation," *International Journal of Applied Physics and Mathematics*, vol. 3, pp. 237–243, 2013.

[30] P. Tankov, *Financial Modelling with Jump Processes*, CRC Press, 2003.

Research Article

On Fractional Order Dengue Epidemic Model

Hamed Al-Sulami,[1] Moustafa El-Shahed,[1,2] Juan J. Nieto,[1,3] and Wafa Shammakh[1]

[1] *Department of Mathematics, Faculty of Science, King Abdulaziz University, P.O. Box 80203, Jeddah 21589, Saudi Arabia*
[2] *Department of Mathematics, Faculty of Art and Sciences, Qassim University, P.O. Box 3771, Unaizah-Qassim 51911, Saudi Arabia*
[3] *Departamento de Analisis Mateatico, Facultad de Matematicas, Universidad de Santiago de Compostela, 15782 Santiago de Compostela, Spain*

Correspondence should be addressed to Hamed Al-Sulami; hamed9@hotmail.com

Received 17 April 2014; Accepted 23 June 2014; Published 18 August 2014

Academic Editor: J. A. Tenreiro Machado

Copyright © 2014 Hamed Al-Sulami et al. This is an open access article distributed under the Creative Commons Attribution License, which permits unrestricted use, distribution, and reproduction in any medium, provided the original work is properly cited.

This paper deals with the fractional order dengue epidemic model. The stability of disease-free and positive fixed points is studied. Adams-Bashforth-Moulton algorithm has been used to solve and simulate the system of differential equations.

1. Introduction

Dengue is a major public health problem in tropical and subtropical countries. It is a vector-borne disease transmitted by *Aedes aegypti* and *Aedes albopictus* mosquitoes. Four different serotypes can cause dengue fever. A human infected by one serotype, when recovers, gains total immunity to that serotype and only partial and transient immunity with respect to the other three.

Dengue can vary from mild to severe. The more severe forms of dengue include shock syndrome and dengue hemorrhagic fever (DHF). Patients who develop these more serious forms of dengue fever usually need to be hospitalized. The full life cycle of dengue fever virus involves the role of the mosquito as a transmitter (or vector) and humans as the main victim and source of infection. Preventing or reducing dengue virus transmission depends entirely on the control of mosquito vectors or interruption of human vector contact [1, 2].

In this paper we study the fractional order dengue epidemic model. The stability of equilibrium points is studied. Numerical solutions of this model are given. We like to argue that fractional order equations are more suitable than integer order ones in modeling biological, economic, and social systems (generally complex adaptive systems) where memory effects are important. Adams-Bashforth-Moulton algorithm has been used to solve and simulate the system of differential equations.

2. Model Derivation

Esteva and Vargas [3] developed a dengue fever transmission model by assuming that, once a person recovers from the disease, he or she will not be reinfected by the disease. The model also assumes that the host population N_h is constant, that is, the death rate and the birth rate equal μ_H. The host-vector model for the dengue transmission of Esteva and Vargas [3] is as follows:

$$\begin{aligned}
\frac{dS_h}{dt} &= A - \frac{\beta_h b}{N_h} S_h I_v - \mu_h S_h, \\
\frac{dI_h}{dt} &= \frac{\beta_h b}{N_h} S_h I_v - (\mu_h + \gamma) I_h, \\
\frac{dR_h}{dt} &= \gamma I_h - \mu_h R_h, \\
\frac{dS_v}{dt} &= B - \frac{\beta_v b}{N_h} S_v I_h - \mu_v S_v, \\
\frac{dI_v}{dt} &= \frac{\beta_v b}{N_h} S_v I_h - \mu_v I_v,
\end{aligned} \tag{1}$$

where

A is the recruitment rate of the host population,

B is the recruitment rate of the vector population,

S_h is the number of susceptible in the host population,

I_h is the number of infective in the host population,

R_h is the number of immunes in the host population,

N_v is the vector population,

S_v is the number of susceptible in the vector population,

I_v is the number of infective in the vector population,

μ_v is the death rate in the vector population,

β_h is the transmission probability from vector to host,

β_v is the transmission probability from host to vector,

γ is the recovery rate in the host population,

b is the biting rate of the vector.

The notion of fractional calculus was anticipated by Leibniz, one of the founders of standard calculus, in a letter written in 1695. Recently great considerations have been made to the models of FDEs in different aria of researches. The most essential property of these models is their nonlocal property which does not exist in the integer order differential operators. We mean by this property that the next state of a model depends not only upon its current state but also upon all of its historical states. There are many definitions of fractional derivatives [4, 5]. Perhaps the best-known is the Riemann-Liouvile definition. The Riemann-Liouville derivative of order α is defined as

$$ {}_{\mathrm{RL}}D_{0+}^{\alpha} f(t) = \frac{1}{\Gamma(n-\alpha)} \left(\frac{d}{dt}\right)^{n} \int_0^t \frac{f(s)}{(t-s)^{\alpha-n+1}} ds, \quad n = [\alpha] + 1, \tag{2} $$

where $\Gamma()$ is the gamma function and n is an integer. An alternative definition was introduced by Caputo as follows, which is a sort of regularization of the Riemann-Liouville derivative:

$$ D_t^{\alpha} f(t) = \frac{1}{\Gamma(n-\alpha)} \int_0^t \frac{f^{(n)}(s)}{(t-s)^{\alpha-n+1}} ds. \tag{3} $$

Pooseh et al. [6] introduced the notion of fractional derivative in the sense of Riemann-Liouville to reformulate the dynamics of the classical model (1) in terms of fractional derivatives. They applied a recent approximate technique to obtain numerical solutions to the fractional model. The system in this paper will be in the sense of Caputo fractional derivative by the following set of fractional order differential equations:

$$ \begin{aligned} D_t^{\alpha} S_h &= A - \frac{\beta_h b}{N_h} S_h I_v - \mu_h S_h, \\ D_t^{\alpha} I_h &= \frac{\beta_h b}{N_h} S_h I_v - (\mu_h + \gamma) I_h, \\ D_t^{\alpha} R_h &= \gamma I_h - \mu_h R_h, \\ D_t^{\alpha} S_v &= B - \frac{\beta_v b}{N_h} S_v I_h - \mu_v S_v, \\ D_t^{\alpha} I_v &= \frac{\beta_v b}{N_h} S_v I_h - \mu_v I_v. \end{aligned} \tag{4} $$

Because model (4) monitors the dynamics of human populations, all the parameters are assumed to be nonnegative. Furthermore, it can be shown that all state variables of the model are nonnegative for all time $t \geq 0$ (see, for instance, [7–9]).

Lemma 1. *The closed set* $\Omega = \{(S_h, I_h, R_h, S_v, I_v) \in R_+^5 : S_h + I_h + R_h = A/\mu_h, S_v + I_v = B/\mu_v\}$ *is positively invariant with respect to model* (4).

Proof. The fractional derivative of the total population, obtained by adding all the equations of model (4), is given by

$$ D_t^{\alpha} N_h(t) = A - \mu_h N_h(t). \tag{5} $$

The solution to (5) is given by $N_h(t) = N_h(0) E_{\alpha,1}(-\mu_h t^{\alpha}) + A t^{\alpha} E_{\alpha,\alpha+1}(-\mu_h t^{\alpha})$, where $E_{\alpha,\beta}$ is the Mittag-Leffler function. Considering the fact that the Mittag-Leffler function has an asymptotic behavior [4, 10],

$$ E_{\alpha,\beta}(z) \sim -\sum_{k=1}^{\omega} \frac{z^{-k}}{\Gamma(\beta - \alpha k)} + O\left(|z|^{-1-\omega}\right), \quad \left(|z| \longrightarrow \infty, \frac{\alpha\pi}{2} < |\arg(z)| \leq \pi\right). \tag{6} $$

One can observe that $N_h(t) \to A/\mu_h$ as $t \to \infty$. The proof of vector population case is completely similar to that of host population and is therefore omitted. One can observe that $N_v(t) \to B/\mu_v$. Therefore, all solutions of the model with initial conditions in Ω remain in Ω for all $t > 0$. Thus, region Ω is positively invariant with respect to model (4). □

In the following, we will study the dynamics of system (4).

3. Equilibrium Points and Stability

To evaluate the equilibrium points let

$$ D_t^{\alpha} S_h = 0, \quad D_t^{\alpha} I_h = 0, \quad D_t^{\alpha} R_h = 0, \quad D_t^{\alpha} S_v = 0, \quad D_t^{\alpha} I_v = 0. \tag{7} $$

Then $E_0 = (A/\mu_h, 0, 0, (B/\mu_v)\ 0)$. By (4), a positive equilibrium $E_1 = (S_h^1, I_h^1, R_h^1, S_v^1, I_v^1)$ satisfies

$$\begin{aligned}
S_h^1 &= \frac{N_h\mu_v\left(Ab\beta_v + N_h\left(\gamma+\mu_h\right)\mu_v\right)}{b\beta_v\left(bB\beta_h + N_h\mu_h\mu_v\right)},\\
I_h^1 &= \frac{Ab^2B\beta_h\beta_v - N_h^2\mu_h\left(\gamma+\mu_h\right)\mu_v^2}{b\beta_v\left(\gamma+\mu_h\right)\left(bB\beta_h + N_h\mu_h\mu_v\right)},\\
R_h^1 &= \frac{Ab^2B\gamma\beta_h\beta_v - \gamma N_h^2\mu_h\left(\gamma+\mu_h\right)\mu_v^2}{b\beta_v\mu_h\left(\gamma+\mu_h\right)\left(bB\beta_h + N_h\mu_h\mu_v\right)},\\
S_v^1 &= \frac{N_h\left(\gamma+\mu_h\right)\left(bB\beta_h + N_h\mu_h\mu_v\right)}{b\beta_h\left(Ab\beta_v + N_h\left(\gamma+\mu_h\right)\mu_v\right)},\\
I_v^1 &= \frac{Ab^2B\beta_h\beta_v - N_h^2\mu_h\left(\gamma+\mu_h\right)\mu_v^2}{b\beta_h\mu_v\left(Ab\beta_v + N_h\left(\gamma+\mu_h\right)\mu_v\right)}.
\end{aligned} \tag{8}$$

The Jacobian matrix $J(E_0)$ for the system given in (4) evaluated at the disease-free equilibrium is as follows:

$$J\left(E_0\right) = \begin{pmatrix}
-\mu_h & 0 & 0 & 0 & -\dfrac{Ab\beta_h}{N_h\mu_h}\\
0 & -\gamma-\mu_h & 0 & 0 & \dfrac{Ab\beta_h}{N_h\mu_h}\\
0 & \gamma & -\mu_h & 0 & 0\\
0 & -\dfrac{bB\beta_v}{N_h\mu_v} & 0 & -\mu_v & 0\\
0 & \dfrac{bB\beta_v}{N_h\mu_v} & 0 & 0 & -\mu_v
\end{pmatrix}. \tag{9}$$

Theorem 2. *The disease-free equilibrium E_0 is locally asymptotically stable if $R_0 < 1$ and is unstable if $R_0 > 1$.*

Proof. The disease-free equilibrium is locally asymptotically stable if all the eigenvalues, λ_i, $i = 1, 2, 3, 4, 5$ of the Jacobian matrix $J(E_0)$ satisfy the following condition [11–14]:

$$\left|\arg\left(\lambda_i\right)\right| > \frac{\alpha\pi}{2}. \tag{10}$$

The eigenvalues of the Jacobian matrix $J(E_0)$ are $\lambda_1 = -\mu_h$, $\lambda_2 = -\mu_h$, and $\lambda_3 = -\mu_v$; the other two roots are determined by the quadratic equation

$$\lambda^2 + \lambda\left(\gamma+\mu_h+\mu_v\right) + \mu_v\left(\gamma+\mu_h\right)\left(1-R_0\right) = 0, \tag{11}$$

where $R_0 = (ABb^2\beta_h\beta_v)/(\mu_h\ \mu_v^2\ N_h^2(\gamma+\mu_h))$. Hence E_0 is locally asymptotically stable if $R_0 < 1$ and is unstable if $R_0 > 1$.

The quantity $R_0^* = \sqrt{R_0}$ is called the basic reproductive number of the disease, since it represents the average number of secondary cases that one case can produce if introduced into a susceptible population. □

We now discuss the asymptotic stability of the endemic (positive) equilibrium of the system given by (4). The Jacobian matrix $J(E_1)$ evaluated at the endemic equilibrium is given as

$$J\left(E_1\right)\begin{pmatrix}
-\dfrac{b\beta_hI_v^1}{N_h} - \mu_h & 0 & 0 & 0 & -\dfrac{bS_h^1\beta_h}{N_h}\\
\dfrac{b\beta_hI_v^1}{N_h} & -\gamma-\mu_h & 0 & 0 & \dfrac{bS_h^1\beta_h}{N_h}\\
0 & \gamma & -\mu_h & 0 & 0\\
0 & -\dfrac{bS_h^1\beta_v}{N_h} & 0 & -\dfrac{b\beta_vI_h^1}{N_h} - \mu_v & 0\\
0 & \dfrac{bS_v^1\beta_v}{N_h} & 0 & \dfrac{b\beta_vI_h^1}{N_h} & -\mu_v
\end{pmatrix}. \tag{12}$$

The characteristic equation of $J(E_1)$ is

$$\left(\lambda+\mu_h\right)\left(\lambda+\mu_v\right)\left(\lambda^3 + a_1\lambda^2 + a_2\lambda + a_3\right) = 0, \tag{13}$$

where

$$\begin{aligned}
a_1 &= \gamma + \mu_v + \frac{M_2\left(K\theta + M_1\mu_v\right)}{K\theta M_1N_h\mu_v},\\
a_2 &= \left(M_2^2 + K\theta M_1N_h^2\mu_h\mu_v\left(\theta+\mu_v\right)\right.\\
&\quad \left.+M_2N_h\left(K\theta^2 + \left(K\theta + M_1\left(\theta+\mu_h\right)\right)\mu_v\right)\right)\\
&\quad \times\left(K\theta M_1N_h^2\mu_v\right)^{-1},\\
a_3 &= \frac{M_2\left(M_2 + N_h\left(K\theta + M_1\mu_h\right)\mu_v\right)}{KM_1N_h^2\mu_v},\\
M_1 &= Ab^2B\beta_h\beta_v - N_h^2\mu_h\left(\gamma+\mu_h\right)\mu_v^2,\\
M_2 &= Ab\beta_v + N_h\left(\gamma+\mu_h\right)\mu_v,\\
K &= bB\beta_h + N_h\mu_h\mu_v,\\
\theta &= \gamma + \mu_h.
\end{aligned} \tag{14}$$

If $p(x) = x^3 + a_1x^2 + a_2x + a_3$. Let $D(p)$ denote the discriminant of a polynomial $p(x)$; then

$$\begin{aligned}
D\left(p\right) &= -\begin{vmatrix}
1 & a_1 & a_2 & a_3 & 0\\
0 & 1 & a_1 & a_2 & a_3\\
3 & 2a_1 & a_2 & 0 & 0\\
0 & 3 & a_1 & a_2 & 0\\
0 & 0 & 3 & 2a_1 & a_2
\end{vmatrix}\\
&= 18a_1a_2a_3 + \left(a_1a_2\right)^2 - 4a_3a_1^3 - 4a_2^3 - 27a_3^2.
\end{aligned} \tag{15}$$

Following [14–18], we have Proposition 3.

Proposition 3. *One assumes that E_1 exists in R_+^3.*

(i) *If the discriminant of $p(x)$, $D(p)$, is positive and Routh-Hurwitz are satisfied, that is, $D(p) > 0$, $a_1 > 0$, $a_3 > 0$, and $a_1a_2 > a_3$, then E_1 is locally asymptotically stable.*

(ii) *If* $D(p) < 0$, $a_1 > 0$, $a_2 > 0$, $a_1 a_2 = a_3$, *and* $\alpha \in [0, 1)$, *then* E_1 *is locally asymptotically stable.*

(iii) *If* $D(p) < 0$, $a_1 < 0$, $a_2 < 0$, *and* $\alpha > 2/3$, *then* E_1 *is unstable.*

(iv) *The necessary condition for the equilibrium point* E_1, *to be locally asymptotically stable, is* $a_3 > 0$.

4. Numerical Methods and Simulations

Since most of the fractional order differential equations do not have exact analytic solutions, so approximation and numerical techniques must be used. Several analytical and numerical methods have been proposed to solve the fractional order differential equations. For numerical solutions of the system (4) one can use the generalized Adams-Bashforth-Moulton method. To give the approximate solution by means of this algorithm, consider the following nonlinear fractional differential equation [19]:

$$D_t^{\alpha} y(t) = f(t, y(t)), \quad 0 \le t \le T,$$
$$y^{(k)}(0) = y_0^k, \quad k = 0, 1, 2, \ldots, m-1, \quad \text{where } m = [\alpha]. \tag{16}$$

This equation is equivalent to Volterra integral equation:

$$y(t) = \sum_{k=0}^{m-1} y_0^{(k)} \frac{t^k}{k!} + \frac{1}{\Gamma(\alpha)} \int_0^t (t-s)^{\alpha-1} f(s, y(s))\, ds. \tag{17}$$

Diethelm et al. used the predictor-correctors scheme [15, 16, 20] based on the Adams-Bashforth-Moulton algorithm to integrate (17). By applying this scheme to the fractional order dengue epidemic model and setting $h = T/N$, $t_n = nh$, and $n = 0, 1, 2, , \ldots, N \in Z^+$, (17) can be discretized as follows [19]:

$$\begin{aligned}
S_{n+1} &= S_0 + \frac{h^{\alpha}}{\Gamma(\alpha+2)} \left(A - \frac{\beta_h b_h}{N_h} S_{n+1}^p Y_{n+1}^p - \mu_h S_{n+1}^p \right) \\
&\quad + \frac{h^{\alpha}}{\Gamma(\alpha+2)} \sum_{j=0}^{n} a_{j,n+1} \left(A - \frac{\beta_h b_h}{N_h} S_j Y_j - \mu_h S_j \right), \\
I_{n+1} &= I_0 + \frac{h^{\alpha}}{\Gamma(\alpha+2)} \left(\frac{\beta_h b_h}{N_h} S_{n+1}^p Y_{n+1}^p - (\mu_h + \gamma) I_{n+1}^p \right) \\
&\quad + \frac{h^{\alpha}}{\Gamma(\alpha+2)} \sum_{j=0}^{n} a_{j,n+1} \left(\frac{\beta_h b_h}{N_h} S_j Y_j - (\mu_h + \gamma) I_j \right), \\
R_{n+1} &= R_0 + \frac{h^{\alpha}}{\Gamma(\alpha+2)} \left(\gamma I_{n+1}^p - \mu_h R_{n+1}^p \right) \\
&\quad + \frac{h^{\alpha}}{\Gamma(\alpha+2)} \sum_{j=0}^{n} a_{j,n+1} \left(\gamma I_j - \mu_h R_j \right), \\
X_{n+1} &= X_0 + \frac{h^{\alpha}}{\Gamma(\alpha+2)} \left(B - \frac{\beta_v b_h}{N_h} X_{n+1}^p I_{n+1}^p - \mu_h X_{n+1}^p \right) \\
&\quad + \frac{h^{\alpha}}{\Gamma(\alpha+2)} \sum_{j=0}^{n} a_{j,n+1} \left(B - \frac{\beta_v b_h}{N_h} X_j I_j - \mu_v X_j \right), \\
Y_{n+1} &= Y_0 + \frac{h^{\alpha}}{\Gamma(\alpha+2)} \left(\frac{\beta_v b_h}{N_h} X_{n+1}^p I_{n+1}^p - \mu_h Y_{n+1}^p \right) \\
&\quad + \frac{h^{\alpha}}{\Gamma(\alpha+2)} \sum_{j=0}^{n} a_{j,n+1} \left(\frac{\beta_v b_h}{N_h} X_j I_j - \mu_v Y_j \right),
\end{aligned} \tag{18}$$

where

$$\begin{aligned}
S_{n+1}^p &= S_0 + \frac{1}{\Gamma(\alpha)} \sum_{j=0}^{n} b_{j,n+1} \left(A - \frac{\beta_h b_h}{N_h} S_j Y_j - \mu_h S_j \right), \\
I_{n+1}^p &= I_0 + \frac{1}{\Gamma(\alpha)} \sum_{j=0}^{n} b_{j,n+1} \left(\frac{\beta_h b_h}{N_h} S_j Y_j - (\mu_h + \gamma) I_j \right), \\
R_{n+1}^p &= R_0 + \frac{1}{\Gamma(\alpha)} \sum_{j=0}^{n} b_{j,n+1} \left(\gamma I_j - \mu_h R_j \right), \\
X_{n+1}^p &= X_0 + \frac{1}{\Gamma(\alpha)} \sum_{j=0}^{n} b_{j,n+1} \left(B - \frac{\beta_v b_h}{N_h} X_j I_j - \mu_v X_j \right), \\
Y_{n+1}^p &= Y_0 + \frac{1}{\Gamma(\alpha)} \sum_{j=0}^{n} b_{j,n+1} \left(\frac{\beta_v b_h}{N_h} X_j I_j - \mu_v Y_j \right),
\end{aligned} \tag{19}$$

$$a_{j,n+1} = \begin{cases} n^{\alpha+1} - (n-\alpha)(n+1), & j = 0, \\ (n-j+2)^{\alpha+1} + (n-j)^{\alpha+1} & \\ \quad -2(n-j+1)^{\alpha+1}, & 1 \le j \le n, \\ 1, & j = n+1, \end{cases}$$

$$b_{j,n+1} = \frac{h^{\alpha}}{\alpha} \left((n-j+1)^{\alpha} - (n-j)^{\alpha} \right), \quad 0 \le j \le n.$$

5. Discussion

In this paper, we have considered a fractional calculus model for dengue disease. Following [21], Figure 1 shows that S_h drops significantly in a relatively small period of time. Both I_h and I_v increase significantly during the period of 30 days and then eventually oscillate around the endemic state (0.09529, 0.0.00029, and 0.00058). This seems unrealistic in the nature. With constant population of mosquitoes, this fluctuation (in a short period of time) cannot be shown to happen in the nature [21]. As mentioned by [6], Figures 2 and 3 show that even a simple fractional model may give surprisingly good results. However, the transformation of a classical model into a fractional one makes it very sensitive to the order of differentiation α: a small change in α may result in a big change in the final result. From the numerical results in Figures 2 and 3, it is clear that the approximate solutions depend continuously on the fractional derivative α.

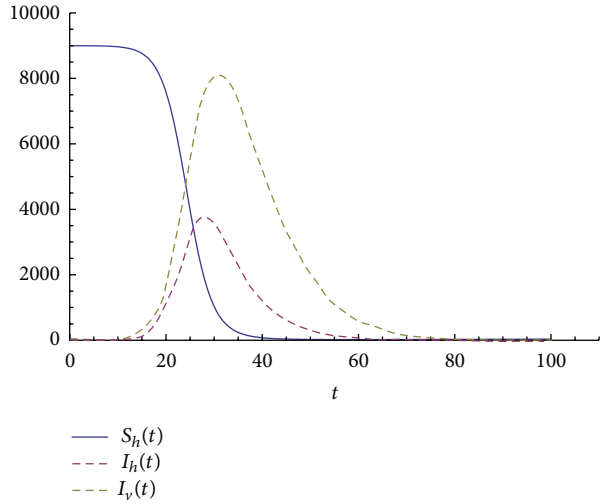

FIGURE 1: $S_h(t)$, $I_h(t)$, and $I_v(t)$ for $\alpha = 1$ and $\mu_h = 0.0000457$; $\mu_v = 0.25$; $b = 0.5$; $\beta_h = 0.75$; $\beta_v = 1$; $\gamma = 0.1428$; $N_h = 10000$; $B = 5000$.

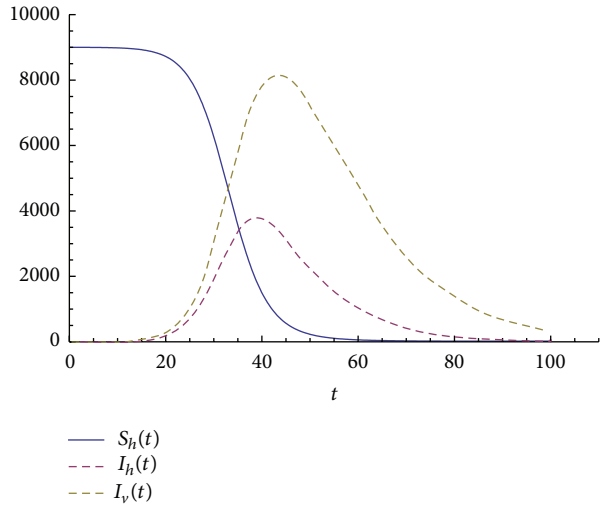

FIGURE 2: $S_h(t)$, $I_h(t)$, and $I_v(t)$ for $\alpha = 0.9$ and $\mu_h = 0.0000457$; $\mu_v = 0.25$; $b = 0.5$; $\beta_h = 0.75$; $\beta_v = 1$; $\gamma = 0.1428$; $N_h = 10000$; $B = 5000$.

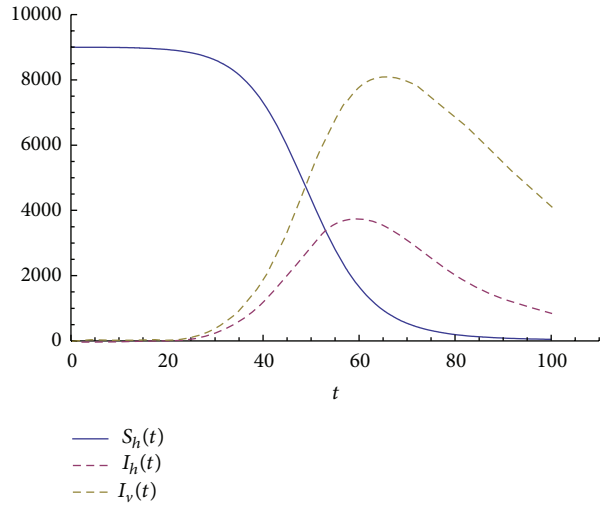

FIGURE 3: $S_h(t)$, $I_h(t)$, and $I_v(t)$ for $\alpha = 0.8$ and $\mu_h = 0.0000457$; $\mu_v = 0.25$; $b = 0.5$; $\beta_h = 0.75$; $\beta_v = 1$; $\gamma = 0.1428$; $N_h = 10000$; $B = 5000$.

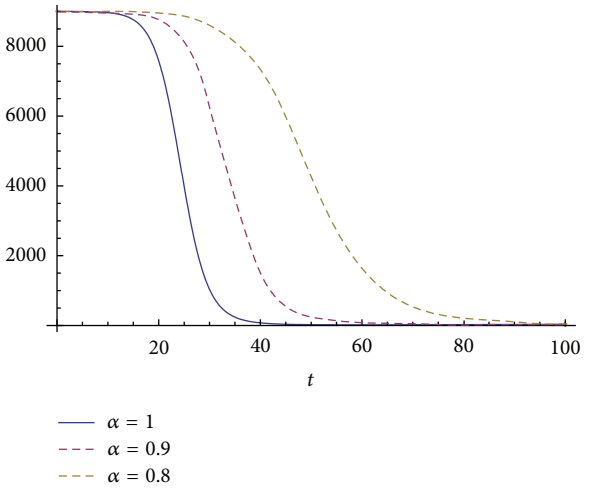

FIGURE 4: $S_h(t)$ for $\alpha = 1, 0.9, 0.8$ and $\mu_h = 0.0000457$; $\mu_v = 0.25$; $b = 0.5$; $\beta_h = 0.75$; $\beta_v = 1$; $\gamma = 0.1428$; $N_h = 10000$; $B = 5000$.

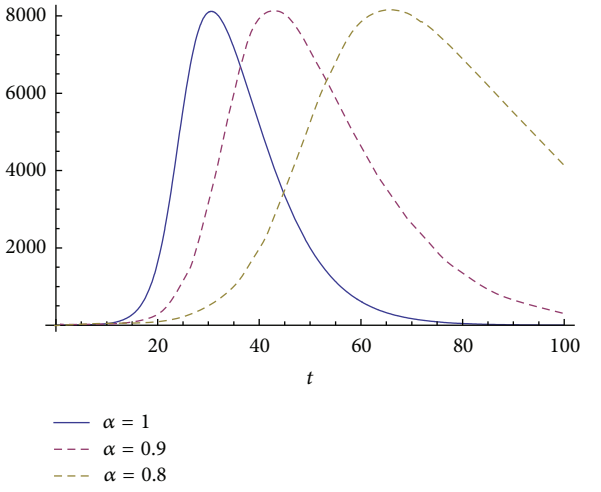

FIGURE 5: $I_h(t)$ for $\alpha = 1, 0.9, 0.8$, $\mu_h = 0.0000457$; $\mu_v = 0.25$; $b = 0.5$; $\beta_h = 0.75$; $\beta_v = 1$; $\gamma = 0.1428$; $N_h = 10000$; $B = 5000$.

The approximate solutions $S_h(t)$, $I_h(t)$, and $I_v(t)$ are displayed in Figures 4 and 5 with different values of α. In each figure three different values of α are considered. When $\alpha = 1$, system (4) is the classical integer-order system (1). In Figure 4, the variation of $S_h(t)$ versus time t is shown for different values of $\alpha = 1, 0.9, 0.8$ by fixing other parameters. It is revealed that S_h does not drop significantly in a relatively small period of time for small values. Figure 5 depicts $I_h(t)$ versus time t. As mentioned by [22, 23], one should note that although the equilibrium points are the same for both integer order and fractional order models the solution of the fractional order model tends to the fixed point over a longer period of time. One also needs to mention that when dealing with real life problems, the order of the system can be determined by using the collected data.

Conflict of Interests

The authors declare that there is no conflict of interests regarding the publication of this paper.

Acknowledgments

This project was funded by the Deanship of Scientific Research (DSR), King Abdulaziz University, under Grant no. 3-130/1433HiCi. The authors, therefore, acknowledge with thanks DSR technical and financial support.

References

[1] H. S. Rodrigues, M. T. Monteiro, and D. F. M. Torres, "Sensitivity analysis in a dengue epidemiological model," *Conference Papers in Mathematics*, vol. 2013, Article ID 721406, 7 pages, 2013.

[2] WHO, *Dengue: Guidelines for Diagnosis, Treatment, Prevention and Control*, World Health Organization, Geneva, Switzerland, 2nd edition, 2009.

[3] L. Esteva and C. Vargas, "Analysis of a dengue disease transmission model," *Mathematical Biosciences*, vol. 150, no. 2, pp. 131–151, 1998.

[4] A. A. Kilbas, H. M. Srivastava, and J. J. Trujillo, *Theory and Application Fractional Differential Equations*, Elseviesr, Amsterdam, The Netherlands, 2006.

[5] I. Podlubny, *Fractional Differential Equations*, Academic Press, New York, NY, USA, 1999.

[6] S. Pooseh, H. S. Rodrigues, and D. F. M. Torres, "Fractional derivatives in dengue epidemics," in *Proceedings of the International Conference on Numerical Analysis and Applied Mathematics: Numerical Analysis and Applied Mathematics (ICNAAM '11)*, pp. 739–742, September 2011.

[7] R. Anderson and R. May, *Infectious Disease of Humans, Dynamics and Control*, Oxford University Press, Oxford, UK, 1995.

[8] E. H. Elbasha, C. N. Podder, and A. B. Gumel, "Analyzing the dynamics of an SIRS vaccination model with waning natural and vaccine-induced immunity," *Nonlinear Analysis: Real World Applications*, vol. 12, no. 5, pp. 2692–2705, 2011.

[9] H. Hethcote, M. Zhien, and L. Shengbing, "Effects of quarantine in six endemic models for infectious diseases," *Mathematical Biosciences*, vol. 180, pp. 141–160, 2002.

[10] R. Gorenflo, J. Loutschko, and Y. Luchko, "Computation of the Mittag-Lefflerfunction $E_{\alpha,\beta}(z)$ and its derivatives," *Fractional Calculus and Applied Analysis*, vol. 5, pp. 491–518, 2002.

[11] E. Ahmed, A. M. A. El-Sayed, A. E. M. El-Mesiry, and H. A. A. El-Saka, "Numerical solution for the fractional replicator equation," *International Journal of Modern Physics C*, vol. 16, no. 7, pp. 1017–1025, 2005.

[12] E. Ahmed, A. M. A. El-Sayed, and H. A. A. El-Saka, "On some Routh-Hurwitz conditions for fractional order differential equations and their applications in Lorenz, Rössler, Chua and Chen systems," *Physics Letters A: General, Atomic and Solid State Physics*, vol. 358, no. 1, pp. 1–4, 2006.

[13] E. Ahmed, A. M. A. El-Sayed, and H. A. A. El-Saka, "Equilibrium points, stability and numerical solutions of fractional-order predator-prey and rabies models," *Journal of Mathematical Analysis and Applications*, vol. 325, no. 1, pp. 542–553, 2007.

[14] D. Matignon, "Stability results for fractional differential equations with applications to control processing," in *Proceedings of the Computational Engineering in Systems Applications*, vol. 2, pp. 963–968, Lille, France, 1996.

[15] K. Diethelm, "An algorithm for the numerical solution of differential equations of fractional order," *Electronic Transactions on Numerical Analysis*, vol. 5, pp. 1–6, 1997.

[16] K. Diethelm and N. J. Ford, "Analysis of fractional differential equations," *Journal of Mathematical Analysis and Applications*, vol. 265, no. 2, pp. 229–248, 2002.

[17] Y. Ding and H. Ye, "A fractional-order differential equation model of HIV infection of CD4+ T-cells," *Mathematical and Computer Modelling*, vol. 50, no. 3-4, pp. 386–392, 2009.

[18] H. Ye and Y. Ding, "Nonlinear dynamics and chaos in a fractional-order HIV model," *Mathematical Problems in Engineering*, vol. 2009, Article ID 378614, 12 pages, 2009.

[19] C. Li and C. Tao, "On the fractional Adams method," *Computers and Mathematics with Applications*, vol. 58, no. 8, pp. 1573–1588, 2009.

[20] K. Diethelm, N. J. Ford, and A. D. Freed, "A predictor-corrector approach for the numerical solution of fractional differential equations," *Nonlinear Dynamics*, vol. 29, no. 1–4, pp. 3–22, 2002.

[21] E. Soewono and A. K. Supriatna, "A Two-dimensional model for transmission of dengue fever disease," *Bulletin of the Malaysian Mathematical Sciences Society*, vol. 24, pp. 48–57, 2001.

[22] E. Demirci, A. Unal, and N. Özalp, "A fractional order SEIR model with density dependent death rate," *Hacettepe Journal of Mathematics and Statistics*, vol. 40, no. 2, pp. 287–295, 2011.

[23] N. Özalp and E. Demiörciö, "A fractional order SEIR model with vertical transmission," *Mathematical and Computer Modelling*, vol. 54, no. 1-2, pp. 1–6, 2011.

Research Article

Fractional Dynamics of Computer Virus Propagation

Carla M. A. Pinto[1] and J. A. Tenreiro Machado[2]

[1] *School of Engineering, Polytechnic of Porto, Center of Mathematics of the University of Porto, Rua Dr. António Bernardino de Almeida 431, 4200-072 Porto, Portugal*
[2] *School of Engineering, Polytechnic of Porto, Rua Dr. António Bernardino de Almeida 431, 4200-072 Porto, Portugal*

Correspondence should be addressed to J. A. Tenreiro Machado; jtenreiromachado@gmail.com

Received 9 April 2014; Accepted 19 May 2014; Published 3 June 2014

Academic Editor: Guido Maione

Copyright © 2014 C. M. A. Pinto and J. A. Tenreiro Machado. This is an open access article distributed under the Creative Commons Attribution License, which permits unrestricted use, distribution, and reproduction in any medium, provided the original work is properly cited.

We propose a fractional model for computer virus propagation. The model includes the interaction between computers and removable devices. We simulate numerically the model for distinct values of the order of the fractional derivative and for two sets of initial conditions adopted in the literature. We conclude that fractional order systems reveal richer dynamics than the classical integer order counterpart. Therefore, fractional dynamics leads to time responses with super-fast transients and super-slow evolutions towards the steady-state, effects not easily captured by the integer order models.

1. Introduction

The global information world in what we live has brought numerous advantages into our lives. Daily commodities like making traveling arrangements, checking bank accounts, buying online books, groceries, and souvenirs, and other important tasks in our lives, such as working, are readily available at the click of a button. Nevertheless, this easy way into the internet has also some disadvantages, namely, in what concerns computer virus propagation. Computer viruses spread and cause huge money losses to companies and customers. Annually, millions of dollars are lost due to virus infections [1].

During the last few years, authors have applied mathematical models for epidemics to computer virus propagation. Computer virus and biological virus have very similar behavioral patterns [2–4]. Based on this observation, some biological epidemic models, such as the susceptible-infected-susceptible (SI/SIS) or the susceptible-infected-recovered (SIR) models, were applied in modeling the epidemic behavior of computer virus patterns [5–12].

In [5, 8], authors study the propagation of viruses and worms in distinct network topologies. In 2005, Zou et al. [6] propose an Internet worm monitoring system that detects a worm in its early propagation stage, using Kalman filter estimation. Moreover, the model can also predict the vulnerable susceptible computer population and estimate the infected computers for uniform-scan worms, such as Code Red. Feng et al. [9] propose a modified SIRS model for computer virus propagation, with dual delays and multistate antivirus measures. Some of the measures may be cleaning, patching, and filtering. Authors use the central manifold theorem and normal form theory to establish explicit formulas for determining the stability and direction of periodic solutions produced by the model. The appearance of periodic solutions is an aggressive state in a computer network, since it means the virus prevalence will not be constant (i.e., will not be easier to combat). A way to control this phenomenon is to combine bifurcation control and reduce virus prevalence strategies, such as using distinct topological network structures. Mishra and Jha [7] develop an SIRS model that includes temporary immunity. The latter is observed when an antivirus software is run in a computer network, after a node gets affected by a malicious object. The authors observe that the endemic equilibrium of the model might be unstable, leading to new outcomes of an SIRS model. Zhu et al. [10] use optimal control methods to fight computer virus propagation. They consider a controlled delayed model and then apply an optimal control strategy, assuming a tradeoff between the control costs and the effects. Ren et al. [11]

study a computer virus propagation model, where the effect of antivirus ability is considered. The ability of an antivirus software can be measured by the number of computers recovered, from infected computers, per unit time, due to running the antivirus software. The ability of an antivirus software is usually proportional to its cost. Backward and Hopf bifurcations can be found in the model, for variation of the antivirus ability. Authors also show the existence of bistable states. Zhu et al. [12] propose a model for computer virus propagation, where the interaction between computers and external removable devices is taken into account. Authors assume reasonable assumptions for this interaction and prove that the state without virus is globally asymptotically stable for a value of the reproduction number, $R_0 < 1$. They also prove that the epidemic state is globally asymptotically stable for values of $R_0 > 1$. Thus, a good strategy to control computer virus transmission is to develop measures such that $R_0 < 1$.

In this paper, we analyze the fractional order version of the integer order model proposed by Zhu et al. [12], for computer and removable devices virus propagation. We simulate numerically the model for different values of the order of the fractional derivative α. In this line of thought, the paper is organized as follows. In Section 3, we describe the model proposed for computer viruses propagation. In Section 4, we analyze several simulations of the model, for distinct values of the fractional derivative, and discuss implications of the results. In the last section, we present the main conclusions and outline some future research topics.

2. Fractional Calculus: A Review

The generalization of the derivative operator $D^{\alpha} f(x)$ to fractional values of α, the order of the derivative, started with the theory of differential calculus, namely, when Leibniz wrote about $D^{1/2} f(x)$. The development of the fractional calculus (FC) is due to many contributions of mathematicians such as Euler, Liouville, Riemann, and Letnikov [13–16]. In the fields of physics and engineering, FC is presently associated with long term memory effects [17–21]. This research is still giving its first steps and new areas of application of FC, such as the modelling of dynamical systems, are emerging [22].

Several definitions of fractional derivatives were proposed. The most used definitions of a fractional derivative of order α are the Riemann-Liouville (RL), Grünwald-Letnikov (GL), and Caputo (C) formulations. GL is defined as

$$ {}_{a}^{\mathrm{GL}}D_{t}^{\alpha} f(t) = \lim_{h \to 0} \frac{1}{h^{\alpha}} \sum_{k=0}^{[(t-a)/h]} (-1)^{k} \binom{\alpha}{k} f(t - kh), \quad t > a, \ \alpha > 0, \tag{1} $$

where $\Gamma(\cdot)$ is Euler's gamma function, $[x]$ means the integer part of x, and h is the step time increment.

These expressions capture the history of the past dynamics, contrary to the integer counterpart that is a "local" operator. This property was recognized in several phenomena and their modelling becomes easier using the FC formalism, while integer order models are often much more complicated.

The GL definition inspired a discrete-time calculation algorithm, based on the approximation of the time increment h by means of the sampling period T, yielding the equation in the z domain:

$$ \frac{\mathcal{Z}\{D^{\alpha} f(t)\}}{\mathcal{Z}\{f(t)\}} = \frac{1}{T^{\alpha}} \sum_{k=0}^{\infty} \frac{(-1)^{k} \Gamma(\alpha+1)}{k!\ \Gamma(\alpha-k+1)} z^{-k} = \left(\frac{1 - z^{-1}}{T} \right)^{\alpha}, \tag{2} $$

where $\mathcal{Z}$ denotes the Z-transform operator.

One implementation of (2) is accomplished by means of a r-term truncated series:

$$ \frac{\mathcal{Z}\{D^{\alpha} f(t)\}}{\mathcal{Z}\{f(t)\}} = \frac{1}{T^{\alpha}} \sum_{k=0}^{r} \frac{(-1)^{k} \Gamma(\alpha+1)}{k!\ \Gamma(\alpha-k+1)} z^{-k}, \tag{3} $$

where, in order to have good approximations, a large r and a small value of T are required.

Expression (3) represents the Euler, or first backward difference, approximation in the so-called $s \to z$ conversion scheme. Another possibility consists in the Tustin conversion rule. The Euler and Tustin rational expressions, $\psi_0(z^{-1}) = ((1 - z^{-1})/T)$ and $\psi_1(z^{-1}) = (2/T)((1 - z^{-1})/(1 + z^{-1}))$, are called generating approximants of zero and first order, respectively. Therefore, the generalization of these conversion methods leads to the noninteger order α results [23]:

$$ s^{\alpha} \approx \left(\frac{1 - z^{-1}}{T} \right)^{\alpha}, \qquad s^{\alpha} \approx \left(\frac{2}{T} \frac{1 - z^{-1}}{1 + z^{-1}} \right)^{\alpha}. \tag{4} $$

The expression $\psi_0^{\alpha}(z^{-1}) = [\psi_0(z^{-1})]^{\alpha}$ and $\psi_1^{\alpha}(z^{-1}) = [\psi_1(z^{-1})]^{\alpha}$ weighted by the factors p and $1 - p$ generate a family of fractional differentiator:

$$ \psi_{av}^{\alpha}\left(z^{-1}\right) = p\psi_0^{\alpha}\left(z^{-1}\right) + (1-p)\,\psi_1^{\alpha}\left(z^{-1}\right). \tag{5} $$

In order to get a rational expression, the final approximation corresponds to a truncated Taylor series or a rational fraction expansion. The arithmetic mean (5) motivates the study of an averaging method [22] based on the generalized formula of averages (often called average of order $q \in \mathbb{R}$):

$$ \psi_{av}^{\alpha}\left(z^{-1}\right) = \left\{ p\left[\psi_0^{\alpha}\left(z^{-1}\right)\right]^{q} + (1-p)\left[\psi_1^{\alpha}\left(z^{-1}\right)\right]^{q} \right\}^{1/q}, \tag{6} $$

where (p, q) are two tuning degrees of freedom, corresponding q to the order of the averaging expression and p to the weighting factor. For example, when $q = \{-1, 0, 1\}$, in expression (6), we get the well-known expressions for the {harmonic, geometric, arithmetic} averages.

3. The Model

The fractional model considered here for computer viruses propagation consists of one SIR (susceptible-infected-recovered) and one SI (susceptible-infected) coupled models.

It is derived as follows. We consider that the entire computer and removable devices population is divided into five classes, the susceptible computers, S, the infected computers, I, the immune (protected with effective antivirus) computers, R, the susceptible removable devices, R_S, and the infected removable devices, R_I. The first system SIR is for computer virus modeling and the second system SI is for removable devices viruses propagation.

Computers are connected to the network at a rate λ_1. Susceptible computers can be infected by other computers, at a rate $\beta_1 SI$, or by a removable device, at a rate $\beta_2(R_I/R_N)S$, and, after that, move to the infected class, I. Parameters β_1 and β_2 are the contact infective forces between susceptible and infective computers and between computers and removable devices, respectively. Infected computers can be repaired at a rate $\sigma_1 I$ and move to the immune class, R, where σ_1 is the recovery rate of infected computers, due to antivirus software. Every computer can be disconnected from the network, at a rate μ_1, in all classes.

The removable devices are recruited, at a rate λ_2, to the susceptible class, R_S. They are infected by the computers at a rate $\beta_2(I/N)R_S$ and then move to the infected removable class, R_I. These infected devices may recover at a rate $\sigma_2(R/N)R_I$ and after they move back to the susceptible class, R_S. Parameter σ_2 is the recovery rate of removable devices, due to antivirus software. All removable devices may break down at a rate μ_2 in all classes.

The model assumes that the antivirus software provides protection of computers, for all times. This is not a realistic assumption, but it simplifies the model at this stage. Future work will consider adding temporary immunity to computers; that is, the model will assume, more realistically, that antivirus software must be updated (i.e., immunity is temporary).

In Figure 1, we depict the schematic diagram of the model.

The system of fractional nonlinear ordinary differential equations, for the proposed model, is given by

$$\begin{aligned}
\frac{dS^\alpha}{dt} &= \lambda_1 - \beta_1 SI - \beta_2 S\frac{R_I}{R_N} - \mu_1 S,\\
\frac{dI^\alpha}{dt} &= \beta_1 SI + \beta_2 S\frac{R_I}{R_N} - (\mu_1 + \sigma_1) I,\\
\frac{dR^\alpha}{dt} &= \sigma_1 I - \mu_1 R,\\
\frac{dR_I^\alpha}{dt} &= \lambda_2 - \beta_2 R_S\frac{I}{N} + \sigma_2 R_I\frac{R}{N} - \mu_2 R_S,\\
\frac{dR_S^\alpha}{dt} &= \beta_2 R_S\frac{I}{N} - \sigma_2 R_I\frac{R}{N} - \mu_2 R_I,
\end{aligned} \tag{7}$$

where $\alpha \in]0, 1]$ is the order of the fractional derivative.

The derivation of model (7) including fractional orders, in a pure mathematical way, embodies some criticism. In fact, it derives from a classical integer order expression and assumes, by including a new degree of freedom, that we can have a better fit between real-world data and theoretical formulation. Furthermore, possibly, the definition of different fractional orders can lead to slight better models but at cost of an increased complexity. Therefore, the proposed methodology follows recent studies [24–26] where fractional models constitute merely an abstract conjecture that needs to be validated in the future, in the presence of real data. In what concerns the meaning of α, while the abstract interpretation can be related solely to "anomalous" or "super-slow" dynamics, its clinical significance remains to be investigated. Possible research directions point to DNA relationship [27, 28].

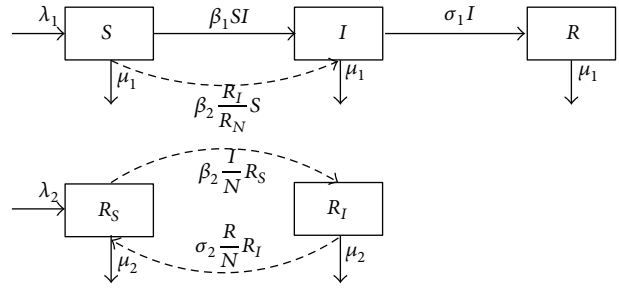

Figure 1: Schematic diagram of the fractional order model (7) for computer viruses propagation [12].

The basic reproduction number, R_0, of the integer order model ($\alpha = 1$) is computed in [12] to be

$$R_0 = \frac{\beta_2^2 + \mu_2\beta_1(\lambda_1/\mu_1)}{\mu_2(\mu_1 + \sigma_1)}. \tag{8}$$

The basic reproduction number, R_0, is defined as the number of secondary infections due to a single infection in a completely susceptible population. For $R_0 < 1$ the disease-free equilibrium is globally asymptotically stable. If $R_0 > 1$, the endemic equilibrium is globally asymptotically stable [12].

4. Numerical Results

In this section we develop several numerical simulations of the new fractional order model (7). The dynamical behavior of the model is studied numerically for variation of the noninteger order derivative α. Initial conditions used in the simulations are found in Table 1 and parameter values in Table 2. For integrating the differential equations of the type $D^\alpha x_i = \varphi_i(x_1, \ldots, x_n)$ a standard integration of order 1 followed by a differentiation of order $1 - \alpha$, approximated by means of (3), was implemented. Furthermore, the numerical calculations adopt the values $r = 10^3$ and $T = 2.5 \cdot 10^{-4}$ year.

In Figure 2, we plot the dynamics of the number of susceptible computers, S, versus time, t, of model (7), for different values of order of the fractional derivative; namely, $\alpha \in \{0.1, \ldots, 1\}$. Initial conditions and parameter values are those of Case 1. For these parameter values, the integer order system has reproduction number $R_0 \simeq 0.84 < 1$ [12].

In Figures 3 and 4 we plot, respectively, the dynamics of the number of infected computers, I, and immune computers, R, versus time t, of model (7), for $\alpha \in \{0.1, \ldots, 1\}$. Initial conditions and parameters are those of Case 1.

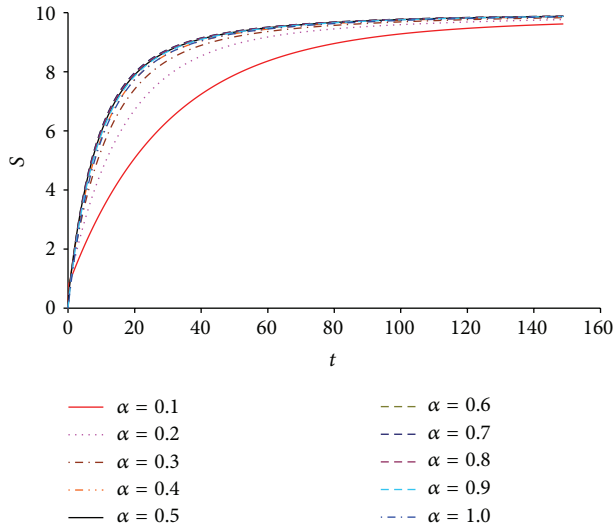

Figure 2: Dynamics of the susceptible computers S versus time t, of system (7), for $\alpha \in \{0.1, \ldots, 1\}$. Parameter values and initial conditions are those of Case 1.

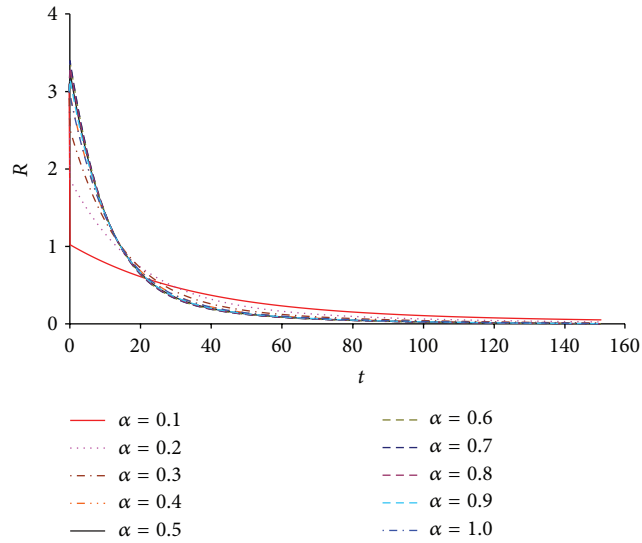

Figure 4: Dynamics of the immune computers R versus time t, of system (7), for $\alpha \in \{0.1, \ldots, 1\}$. Parameter values and initial conditions are those of Case 1.

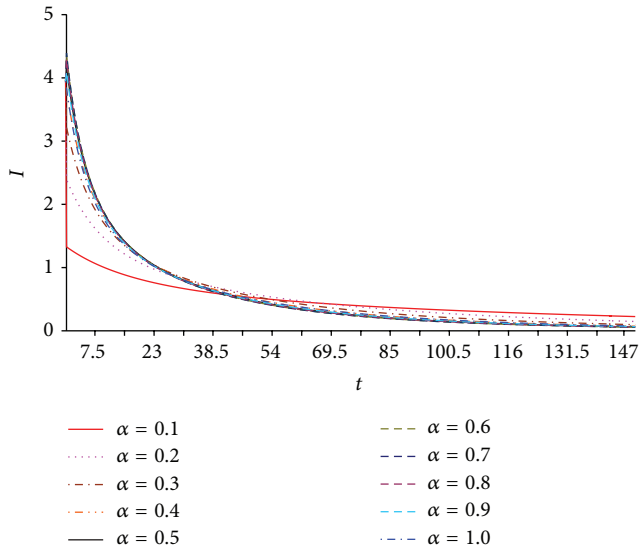

Figure 3: Dynamics of the infected computers I versus time t, of system (7), for $\alpha \in \{0.1, \ldots, 1\}$. Parameter values and initial conditions are those of Case 1.

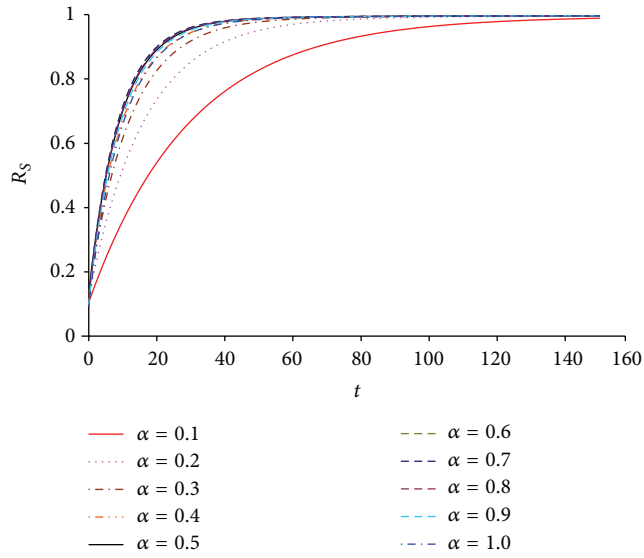

Figure 5: Dynamics of the susceptible removable devices R_S versus time t, of system (7), for $\alpha \in \{0.1, \ldots, 1\}$. Parameter values and initial conditions are those of Case 1.

Table 1: Initial conditions used in the numerical simulations of model (7).

Variable	S	I	R	R_S	R_I
Case 1	0.0	4.0	3.0	0.1	0.5
Case 2	5.0	1.0	0.0	0.5	0.1

In Figures 5 and 6, we plot, respectively, the values of the susceptible removable devices, R_S, and of the infected removable devices, R_I, versus time, t, respectively, for distinct values of the fractional derivative α. Initial conditions are those of Case 1.

From Figures 2–6, we observe that by varying α, we get a smooth variation of the dynamics. It is important to note that we can vary not only the "velocity" of the initial transient but also the evolution towards the steady-state. This effect is typical in fractional dynamical systems, where we can have a super-fast initial transient, followed by a super-slow convergence to the final value. Moreover, we verify also that for $\alpha = 0.1$ we have the slowest evolution, while $\alpha = 0.7$ yields the fastest transient.

In Figures 7–11, we consider initial conditions and parameter values as in Case 2 and vary the fractional derivative α. We increase the values of the contact infective forces to be

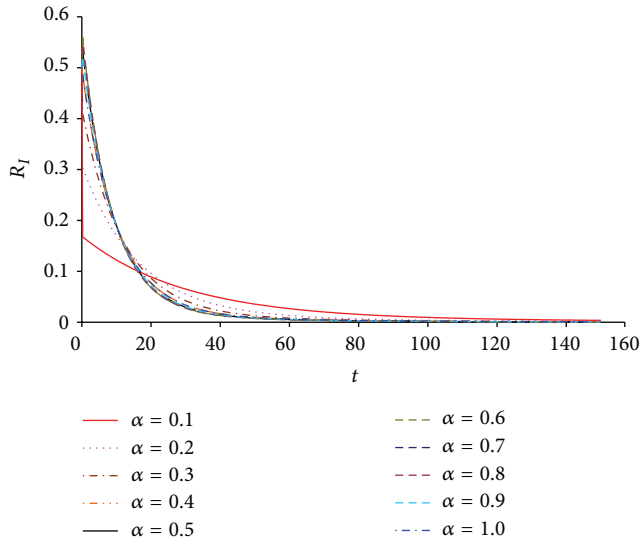

FIGURE 6: Dynamics of the infected removable devices R_I versus time t, of system (7), for $\alpha \in \{0.1, \ldots, 1\}$. Parameter values and initial conditions are those of Case 1.

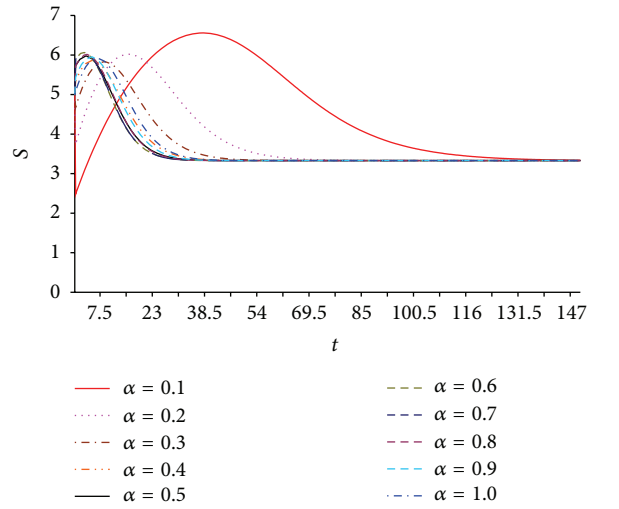

FIGURE 7: Dynamics of the susceptible computers S versus time t, of system (7), $\alpha \in \{0.1, \ldots, 1\}$. Parameter values and initial conditions are as in Case 2, except for $\beta_1 = \beta_2 = 0.035$.

TABLE 2: Parameters used in the numerical simulations of model (7).

Parameter	Case 1	Case 2
λ_1	1	1
λ_2	0.1	0.1
β_1	0.01	0.035
β_2	0.01	0.035
σ_1	0.02	0.02
σ_2	0.005	0.005
μ_1	0.1	0.1
μ_2	0.1	0.1

$\beta_1 = \beta_2 = 0.035$. For these parameter values, the integer order system has reproduction number $R_0 \simeq 3.02 > 1$ [12].

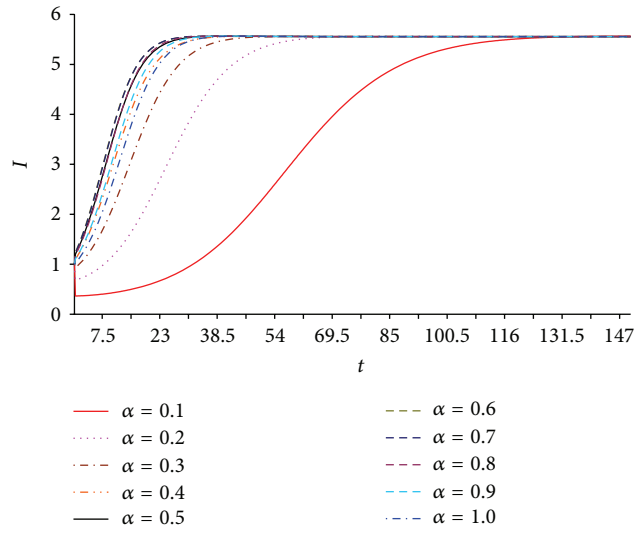

FIGURE 8: Dynamics of the infected computers I versus time t, of system (7), for $\alpha \in \{0.1, \ldots, 1\}$. Parameter values and initial conditions are as in Case 2, except for $\beta_1 = \beta_2 = 0.035$.

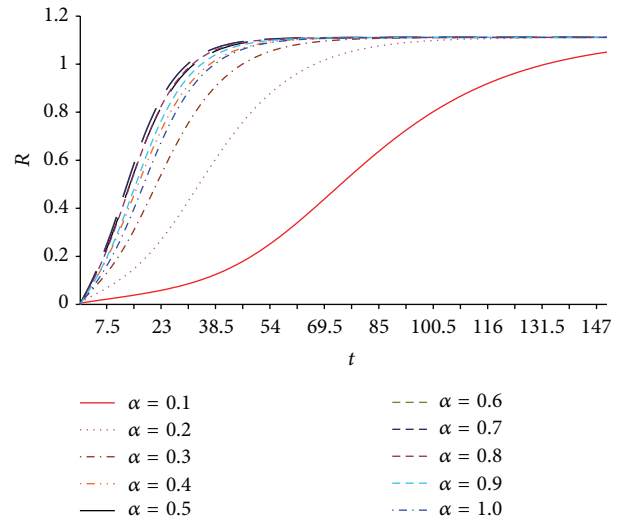

FIGURE 9: Dynamics of the immune computers R versus time t, of system (7), for $\alpha \in \{0.1, \ldots, 1\}$. Parameter values and initial conditions are as in Case 2, except for $\beta_1 = \beta_2 = 0.035$.

In Figure 7, we plot the dynamics of the number of susceptible computers, S, versus time, t, of model (7), for $\alpha \in \{0.1, \ldots, 1\}$.

In Figures 8 and 9, we plot, respectively, the dynamics of the number of infected computers, I, and of immune computers, R, versus time t, of model (7), for $\alpha \in \{0.1, \ldots, 1\}$.

In Figures 10 and 11, we plot, respectively, the values of the susceptible removable devices, R_S, and of the infected removable devices, R_I, versus time t, for $\alpha \in \{0.1, \ldots, 1\}$.

These charts reveal that Case 2 leads to much richer dynamics than Case 1. From Figures 7–11, we observe that by varying α, we can tune the dynamics of the transient. Furthermore, we verify again that for $\alpha = 0.1$, we have

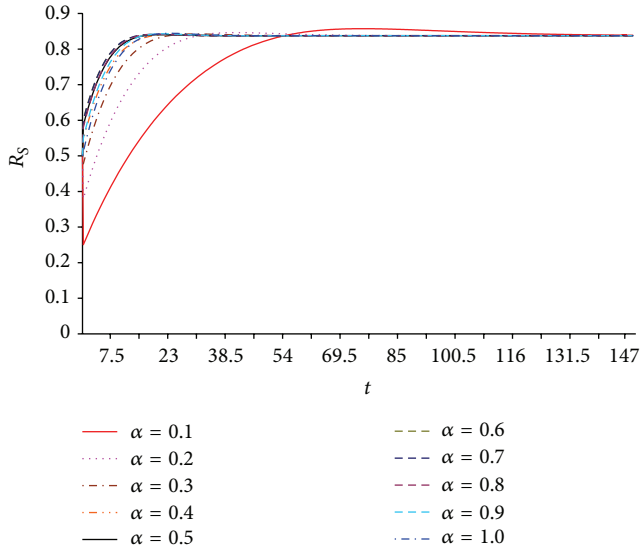

FIGURE 10: Dynamics of the susceptible removable devices R_S versus time t, of system (7), $\alpha \in \{0.1, \ldots, 1\}$. Parameter values and initial conditions are as in Case 2, except for $\beta_1 = \beta_2 = 0.035$.

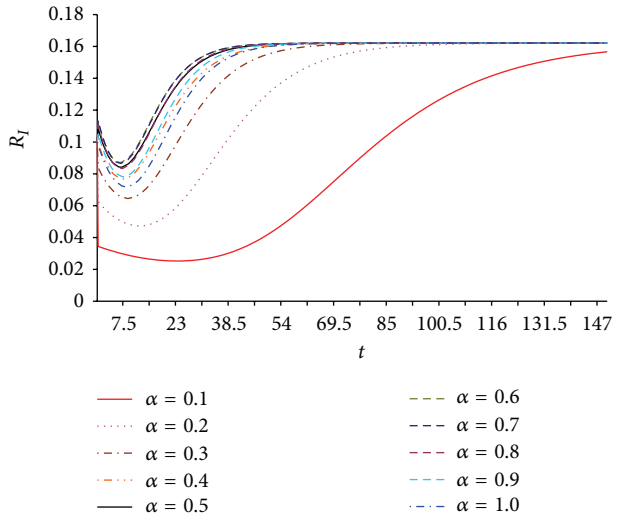

FIGURE 11: Dynamics of the infected removable devices R_I versus time t, of system (7), for $\alpha \in \{0.1, \ldots, 1\}$. Parameter values and initial conditions are as in Case 2, except for $\beta_1 = \beta_2 = 0.035$.

the slowest evolution, whereas for $\alpha = 0.7$, the transient is the fastest. Moreover, from Figure 7, we conclude that the overshoots for different values of α remain globally almost invariant. Even so, for $\alpha = 0.3$, we get the smallest amplitude of the overshoots. As for the transients of the other charts, the fastest dynamics is at $\alpha = 0.7$; therefore, the smaller peak time occurs for $\alpha = 0.7$ and the larger one for $\alpha = 0.1$. It is interesting to note a slight overshoot for the number of susceptible removable devices, R_S, for $\alpha = \{0.1, 0.2, 0.3\}$.

5. Conclusions

We proposed a fractional order model for computer virus propagation, where the interaction of computers and removable devices is included. We simulated the system for distinct values of the order α of the fractional derivative and two sets of initial conditions. We conclude that we can tackle a family of distinct dynamical responses, including very fast transients and super-slow responses, usual in systems with long range memory. The set of initial conditions denoted as Case 1 produces a set of monotonous family of responses, while Case 2 presents more complex patterns. In both cases, the fractional orders $\alpha = 0.1$ and $\alpha = 0.7$ are those that lead to the slowest final evolution and the fastest transients, respectively. Globally, we note that fractional calculus is a mathematical tool well suited to model dynamical systems including important memory phenomena.

Conflict of Interests

The authors declare that there is no conflict of interests regarding the publication of this paper.

Acknowledgments

Authors wish to thank Fundação Gulbenkian, through Prémio Gulbenkian de Apoio à Investigação 2003, and the Polytechnic of Porto, through the PAPRE Programa de Apoio à Publicação em Revistas Científicas de Elevada Qualidade, for financial support.

References

[1] L. A. Gordon, M. P. Loeb, W. Lucyshyn, and R. Richardson, "2005 CSI/FBI crime and security survey," Computer Security Institute, 2005.

[2] S. Datta and W. Hui, "The effectiveness of vaccinations on the spread of email-borne computer viruses," in *Proceedings of the IEEE Canadian Conference on Electrical and Computer Engineering (CCECE '05)*, pp. 219–223, IEEE, Saskatoon, Canada, May 2005.

[3] J. O. Kephart and S. R. White, "Directed-graph epidemiological models of computer viruses," in *Proceedings of the IEEE Computer Society Symposium on Research in Security and Privacy*, pp. 343–358, May 1991.

[4] J. O. Kephart and S. R. White, "Measuring and modeling computer virus prevalence," in *Proceedings of the IEEE Computer Society Symposium on Research in Security and Privacy*, pp. 2–15, May 1993.

[5] M. Garetto, W. Gong, and D. Towsley, "Modeling malware spreading dynamics," in *Proceedings of the 22nd Annual Joint Conference on the IEEE Computer and Communications Societies*, pp. 1869–1879, April 2003.

[6] C. C. Zou, W. Gong, D. Towsley, and L. Gao, "The monitoring and early detection of internet worms," *IEEE/ACM Transactions on Networking*, vol. 13, no. 5, pp. 961–974, 2005.

[7] B. K. Mishra and N. Jha, "Fixed period of temporary immunity after run of anti-malicious software on computer nodes," *Applied Mathematics and Computation*, vol. 190, no. 2, pp. 1207–1212, 2007.

[8] P. De, Y. Liu, and S. K. Das, "An epidemic theoretic framework for vulnerability analysis of broadcast protocols in wireless sensor networks," *IEEE Transactions on Mobile Computing*, vol. 8, no. 3, pp. 413–425, 2009.

[9] L. Feng, X. Liao, H. Li, and Q. Han, "Hopf bifurcation analysis of a delayed viral infection model in computer networks," *Mathematical and Computer Modelling*, vol. 56, no. 7-8, pp. 167–179, 2012.

[10] Q. Zhu, X. Yang, L.-X. Yang, and C. Zhang, "Optimal control of computer virus under a delayed model," *Applied Mathematics and Computation*, vol. 218, no. 23, pp. 11613–11619, 2012.

[11] J. Ren, X. Yang, Q. Zhu, L.-X. Yang, and C. Zhang, "A novel computer virus model and its dynamics," *Nonlinear Analysis: Real World Applications*, vol. 13, no. 1, pp. 376–384, 2012.

[12] Q. Zhu, X. Yang, and J. Ren, "Modeling and analysis of the spread of computer virus," *Communications in Nonlinear Science and Numerical Simulation*, vol. 17, no. 12, pp. 5117–5124, 2012.

[13] K. B. Oldham and J. Spanier, *The Fractional Calculus: Theory and Application of Differentiation and Integration to Arbitrary Order*, Academic Press, New York, NY, USA, 1974.

[14] S. G. Samko, A. A. Kilbas, and O. I. Marichev, *Fractional Integrals and Derivatives: Theory and Applications*, Gordon and Breach Science Publishers, New York, NY, USA, 1993.

[15] K. S. Miller and B. Ross, *An Introduction to the Fractional Calculus and Fractional Differential Equations*, John Wiley & Sons, New York, NY, USA, 1993.

[16] A. A. Kilbas, H. M. Srivastava, and J. J. Trujillo, *Theory and Applications of Fractional Differential Equations*, vol. 204 of *North-Holland Mathematics Studies*, Elsevier, Amsterdam, The Netherlands, 2006.

[17] I. Podlubny, *Fractional Differential Equations: An Introduction to Fractional Derivatives, Fractional Differential Equations, to Methods of Their Solution*, vol. 198 of *Mathematics in Science and Engineering*, Academic Press, San Diego, Calif, USA, 1998.

[18] F. Mainardi, *Fractional Calculus and Waves in Linear Viscoelasticity: An Introduction to Mathematical Models*, Imperial College Press, London, UK, 2010.

[19] V. E. Tarasov, *Fractional Dynamics: Applications of Fractional Calculus to Dynamics of Particles, Fields and Media*, Springer, New York, NY, USA, 2010.

[20] D. Baleanu, K. Diethelm, E. Scalas, and J. J. Trujillo, *Fractional Calculus: Models and Numerical Methods*, Series on Complexity, Nonlinearity and Chaos, World Scientific Publishing, Singapore, 2012.

[21] C. M. Ionescu, *The Human Respiratory System: An Analysis of the Interplay between Anatomy, Structure, Breathing and Fractal Dynamics*, Series in BioEngineering, Springer, London, UK, 2013.

[22] J. A. Tenreiro Machado, A. M. Galhano, A. M. Oliveira, and J. K. Tar, "Approximating fractional derivatives through the generalized mean," *Communications in Nonlinear Science and Numerical Simulation*, vol. 14, no. 11, pp. 3723–3730, 2009.

[23] J. A. T. Machado, "Analysis and design of fractional-order digital control systems," *Systems Analysis Modelling Simulation*, vol. 27, no. 2-3, pp. 107–122, 1997.

[24] A. A. M. Arafa, S. Z. Rida, and M. Khalil, "A fractional-order model of HIV infection with drug therapy effect," *Journal of the Egyptian Mathematical Society*, 2013.

[25] Y. Ding and H. Ye, "A fractional-order differential equation model of HIV infection of $CD4^+$ T-cells," *Mathematical and Computer Modelling*, vol. 50, no. 3-4, pp. 386–392, 2009.

[26] E. J. Solteiro Pires, J. A. Tenreiro Machado, and P. B. de Moura Oliveira, "Fractional order dynamics in a GA planner," *Signal Processing*, vol. 83, no. 11, pp. 2377–2386, 2003.

[27] J. A. Tenreiro Machado, A. C. Costa, and M. D. Quelhas, "Fractional dynamics in DNA," *Communications in Nonlinear Science and Numerical Simulation*, vol. 16, no. 8, pp. 2963–2969, 2011.

[28] J. A. T. Machado, A. C. Costa, and M. D. Quelhas, "Wavelet analysis of human DNA," *Genomics*, vol. 98, no. 3, pp. 155–163, 2011.